# Chapter A.3
# Thermal Evaluation

## TABLE OF CONTENTS

## LIST OF TABLES

## LIST OF FIGURES

# Chapter A.3
# Thermal Evaluation

NOTE: References in this Chapter are shown as [1], [2], etc. and refer to the reference list in Section A.3.5.

This chapter presents the thermal evaluations which demonstrate that the MP197HB transport cask (TC) meets thermal requirements of 10 CFR 71 [6] for transportation of BWR and PWR spent fuel assemblies (FA) within the following DSCs: 69BTH, 61BTH Type 1 and Type 2, 61BT, 37PTH, 32PTH, 32PTH Type 1, 32PTH1 Type 1 and Type 2, 32PT, 24PTH-S, 24PTH-L, 24PTH-S-LC, 24PT4, 61BTHF, and 24PTHF.

The maximum heat load per DSC allowed for transportation in MP197HB TC varies for different DSC types from 18.3 kW to 32 kW. The table below summarizes the maximum heat load per DSC for transportation in comparison with maximums allowed for storage.

**Maximum Heat Load per DSC**

| DSC type | Max. Heat Load for Transport (kW) | Max. Heat Load for Storage (kW) |
|---|---|---|
| 69BTH | 26.0 | N/A |
| | 29.2 | N/A |
| | 32.0 | N/A |
| 61BTH Type 1 | 22.0 | 22.0 [3] |
| 61BTH Type 2 | 24.0 | 31.2 [3] |
| 61BT | 18.3 | 18.3 [1] |
| 37PTH | 22.0 | N/A |
| 32PTH / 32PTH Type 1 | 26.0 | 34.8 [4] |
| 32PTH1 Type 1 | 26.0 | 40.8 [3] |
| 32PTH1 Type 2 | 24.0 | 31.2 [3] |
| 32PT | 24.0 | 24.0 [1] |
| 24PTH-S or -L (w/ Al inserts) | 26.0 | 40.8 [1] |
| 24PTH-S or –L (w/o Al inserts) | 26.0 | 31.2 [1] |
| 24PTH-S-LC | 24.0 | 24.0 [1] |
| 24PT4 | 24.0 | 24.0 [2] |

For all DSC types, this evaluation demonstrates that DSC component temperatures are within material temperature limits and fuel cladding temperatures meet the thermal requirements of ISG-11 [7].

### A.3.1 Description of Thermal Design Criteria

The MP197HB TC is designed to passively reject decay heat under Normal Conditions of Transport (NCT) and Hypothetical Accident Conditions (HAC) while maintaining packaging temperatures and pressures within specified limits. Objectives of the thermal analyses performed for this evaluation include:

a) Determination of maximum component temperatures with respect to cask materials limits to ensure components perform their intended safety functions,

b) Determination of temperature distributions to support the calculation of thermal stresses,

c) Determination of the TC cavity gas temperature to support containment pressure calculations, and

d) Determination of the maximum fuel cladding temperature.

Chapter A.1 presents the principal design bases for the MP197HB TC.

Several thermal design criteria are established for the MP197HB TC to ensure that the package meets all its functional and safety requirements. These are:

- Maximum fuel cladding temperature limits of 752°F (400°C) for NCT and 1,058°F (570°C) for HAC are considered for the fuel assemblies with an inert cover gas as concluded in ISG-11 [7].
- Containment of radioactive material and gases is a major design requirement. Seal temperatures must be maintained within specified limits to satisfy the leak tight containment requirement. A maximum temperature limit of 400°F (204°C) is considered for the Fluorocarbon seals (Viton O-rings) in the containment vessel ([18] and [19]) for NCT and HAC.
- To maintain the stability of the neutron shield resin, a maximum allowable temperature of 320°F (160°C) is considered for the neutron shield [17] for NCT.
- Based on [25], the onset of polypropylene thermal degradation associated with weight loss starts at 230°C to 250°C (446°F to 482°F). Although the breakdown of the polymer leading to volatile products begins above 300°C (572°F), no significant weight loss occurs below 350°C (662°F). A temperature limit of 445°F (229°C) is considered conservatively for polypropylene to prevent thermal degradation of resin in trunnion plugs.
- To prevent melting of the gamma shield (lead) under NCT, an allowable maximum temperature of 621°F (327.5°C – melting point of lead) is considered for the gamma shield [5].
- A temperature limit of 320°F (160°C) is considered for wood to prevent excessive reduction in structural properties at elevated temperatures [20].

- In accordance with 10 CFR 71.43(g) [6] the maximum temperature of the accessible packaging surfaces in the shade is limited to 185°F (85°C).

The NCT ambient temperature range is –20°F to 100°F (-29°C to 38°C) per 10 CFR 71.71(b) [6]. In general, all the thermal criteria are associated with maximum temperature limits and not minimum temperatures. All materials can be subjected to the minimum environment temperature of -40°F (-40°C) without adverse effects as required by 10 CFR 71.71 (c)(2) [6].

Thermal performance of MP197HB TC is evaluated based on finite element analyses using ANSYS computer code [27].

The following thermal design criteria are established for 69BTH and 37PTH DSCs to satisfy the functional and safety requirements.

- Maximum fuel cladding temperature limits of 752°F (400°C) for NCT and 1,058°F (570°C) for HAC are considered for the fuel assemblies with an inert cover gas as concluded in ISG-11 [7].
- Based on ISG-11 [7], the fuel cladding temperature is limited to 400°C (752°F) for short term operation such as vacuum drying.
- The maximum DSC cavity internal design pressures are summarized below:

| Operating condition | 69BTH DSC | 37PTH DSC |
|---|---|---|
| Normal Conditions of Transport (NCT) (3% rods ruptured) | 15 psig | 15 psig |
| Hypothetical Accident Conditions (HAC) (100% rods ruptured) | 140 psig | 140 psig |

The thermal performance of 69BTH and 37PTH DSCs is evaluated based on finite element analyses using ANSYS computer code [27].

### A.3.1.1 Design Features

#### A.3.1.1.1 MP197HB TC

The MP197HB transport cask includes optional features such as an aluminum internal sleeve to accommodate DSC types with outer diameters smaller than 69.75" and an aluminum shell with external circular fins. The external circular fins are optional for heat loads greater than 26 kW to add more margin in the fuel cladding temperature. The TC design features for different DSC types considered for transportation in MP197HB TC are listed in the table below.

MP197HB TC Design Features

| DSC type | DSC OD (in.) | TC Sleeve | TC External Fins | Max. DSC Heat Load for Transport (kW) |
|---|---|---|---|---|
| 69BTH | 69.75 | No | No | 26.0 |
| | | | Yes (optional) (3) | 29.2 |
| | | | Yes (optional) (3) | 32.0 |
| 61BTH Type 1 (1) | 67.25 | Yes | No | 22.0 |
| 61BTH Type 2 (1) | 67.25 | Yes | No | 24.0 |
| 61BT | 67.25 | Yes | No | 18.3 |
| 37PTH | 69.75 | No | No | 22.0 |
| 32PTH/32PTH Type 1 | 69.75 | No | No | 26.0 |
| 32PTH1 Type 1 | 69.75 | No | No | 26.0 |
| 32PTH1 Type 2 | 69.75 | No | No | 24.0 |
| 32PT | 67.19 | Yes | No | 24.0 |
| 24PTH-S or -L (w/ Al inserts)(1) | 67.19 | Yes | No | 26.0 |
| 24PTH-S or –L (w/o Al inserts)(1) | 67.19 | Yes | No | 26.0 |
| 24PTH-S-LC (1) | 67.19 | Yes | No | 24.0 (2) |
| 24PT4 | 67.19 | Yes | No | 24.0 |

Notes:
(1) 61BTHF and 24PTHF *DSCs* have the same dimensions and use the same MP197HB features as DSC types 61BTH and 24PTH, respectively.
(2) The 24PTH-S-LC DSC is allowed for 24 kW heat load. The analyis assumes a heat load of 26 kW for conservatism.
(3) The external fins are optional to enhance heat transfer and provide larger margin for the cladding temperature.

The MP197HB TC consists of multiple shells which conduct the decay heat to the cask outer surface. The other thermal design feature of the cask is the conduction path created by the aluminum boxes that contain the neutron shielding material as described in Chapter A.5. The neutron shielding material is provided by a resin compound cast into long slender aluminum boxes placed around the gamma shield shell and enclosed within a steel shell (shield shell). The aluminum boxes are designed to fit tightly against the steel shell surfaces, thus improving the heat transfer across the neutron shield.

The external circular fins can be used optinally for the transport of DSCs with heat load exceeding 26 kW.

Heat dissipates from the packaging outer surfaces via natural convection and radiation. The outer surface of the shield shell is painted white to enhance the thermal radiation exchange with ambient.

The design of the steel-encased wood impact limiters is described in Chapter A.1, Section A.1.2. These components are included in the thermal analysis because of their contribution as a thermal insulator. The impact limiters provide protection to the lid and bottom regions from the external heat input due to fire during the HAC thermal event.

A personnel barrier prevents access to the outer surfaces of the cask body. The barrier, which consists of a stainless steel mesh attached to stainless steel tubing, encloses the

cask body between the impact limiters, and have an open area fraction of approximately 80%.

The gaps considered in the thermal model of MP197HB TC are described in Section A.3.3.1.1.

#### A.3.1.1.2 69BTH DSC

The 69BTH DSC design is similar to the 61BTH DSC design documented in Appendix T, associated with Amendment 10 to Part 72 CoC 1004 for the Standardized NUHOMS® System [3], with the maximum decay heat load per canister of 32.0 kW for off-site transportation. The 69BTH DSC consists of a shell assembly, which provides confinement and shielding, and an internal basket assembly which locates and supports the fuel assemblies.

The basket structure consists of 9 and 6 compartment fuel cell subassemblies held in place by basket rails in combination with a holddown ring. The compartment subassemblies are held together by welded stainless plates wrapped around the fuel compartments, which also retain the aluminum and/or neutron absorbing plates sandwiched between the fuel compartments. The aluminum and neutron absorbing plates provide the necessary criticality control and heat conduction paths from the fuel cells to the perimeter of subassemblies. The aluminum plates retained between the subassemblies provide the heat conduction paths from the subassemblies to the perimeter of the basket. The space between the fuel compartments assembly and the DSC shell is bridged by solid aluminum transition rails.

No convection heat transfer is considered within the basket for conservatism. Radiation heat transfer is considered implicitly between the fuel rods and the fuel compartment in calculation of transverse effective fuel conductivity. No other radiation heat transfer is considered within the 69BTH DSC models.

The decay heat from the canister is carried to the inner shell of the MP197HB cask via conduction, convection, and radiation. Convection heat transfer in the annulus between the DSC outer shell and the cask inner shell is not considered in the thermal evaluation for conservatism.

#### A.3.1.1.3 37PTH DSC

The 37PTH DSC design is similar to the 32PT DSC design documented in [1], Appendix M with a maximum decay heat load per canister of 22.0 kW for off-site transportation. The 37PTH DSC consists of a shell assembly, which provides confinement and shielding, and an internal basket assembly which locates and supports the fuel assemblies.

The basket is an assembly of welded stainless steel plates that make up a grid for 37 fuel compartments. Each fuel compartment accommodates aluminum and/or neutron absorbing plates that provide the necessary criticality control and heat conduction paths from the fuel assemblies to the basket grid. The space between the fuel compartments grid assembly and the perimeter of the DSC shell is bridged by solid aluminum transition rails.

There are two 37PTH canister types: A short canister type designated as the 37PTH-S and a medium canister type designated as the 37PTH-M. Use of spacers may be required to accommodate short fuel assemblies.

No convection heat transfer is considered within the basket for conservatism. Radiation heat transfer is considered implicitly between the fuel rods and the fuel compartment in calculation of transverse effective fuel conductivity. No other radiation heat transfer is considered within the 37PTH DSC models.

The decay heat from the canister is carried to the inner shell of the MP197HB cask via conduction, convection, and radiation. Convection heat transfer in the annulus between the DSC outer shell and the cask inner shell is not considered in the thermal evaluation for conservatism.

#### A.3.1.1.4 Other DSC Types

The design features of DSC types 61BT, 32PT, and 24PTH are described in [1], Appendices K, M, and P, respectively. The design features of 24PT4 DSC are described in [2], Appendix A. The design features of DSC types 61BTH and 32PTH1 are described in Appendices T and U, respectively, associated with Amendment 10 to Part 72 CoC 1004 for the Standardized NUHOMS® System [3]. The design features of 32PTH and 32PTH Type 1 DSCs are described in [4].

### A.3.1.2 Content's Decay Heat

The thermal analysis for MP197HB TC loaded with existing DSCs currently qualified for storage along with 69BTH and 37PTH DSCs is based on a range of maximum total heat load of 18.3 kW to 32 kW per DSC.

The maximum decay heat loads of 26.0, 29.2, and 32.0 kW are considered for transport of 69BTH DSC in combination with various design features of MP197HB TC listed in Section A.3.1.1.1.

The maximum decay heat loads for transport of DSC types 61BTH Type 1, 61BT, 32PT, and 24PT4 are equal to the maximum heat loads for storage conditions i.e., 22.0 kW, 18.3 kW, 24.0 kW, and 24.0 kW, respectively as shown in Section A.3.1.1.1 based on [3], [1], and [2].

The maximum decay heat load for transport of DSC types 32PTH, 32PTH Type 1, 32PTH1 Type 1, 24PTH-S, and 24PTH-L are considered equal to 26.0 kW.

The maximum decay heat load for 24PTH-S-LC is 24 kW [1]. Therefore, the results of 24PTH-S or -L (without aluminum inserts) DSC shell temperatures with 26 kW heat load is bounding for use with the 24PTH-S-LC DSC with 24 kW heat load.

The maximum decay heat load for transport of DSC types 61BTH Type 2 and 32PTH1 Type 2 are considered equal to 24.0 kW in order to maintain the maximum DSC shell temperature below the values reported for normal transfer conditions in Appendix T.4 and Appendix U.4 of the SAR associated with Amendment 10 to Part 72 CoC 1004 for the Standardized NUHOMS® System [3].

The maximum decay heat load for 37PTH DSC is equal to 22.0 kW for transport operations.

61BTHF and 24PTHF DSCs contain failed fuel and have lower heat loads than 61BTH and 24PTH DSCs, respectively. Nevertheless, it is considered in the thermal analysis that the heat loads for 61BTHF and 24PTHF DSCs are the same as those for 61BTH and 24PTH DSCs, respectively.

The MP197HB TC is designed to transport a payload of up to 56.0 tons of dry irradiated and/or contaminated non-fuel bearing solid materials in secondary containers. The decay heat load of the radioactive material is limited to 5 kW, which is well below the heat loads specified for the cask loaded with DSCs.

The permitted heat load zoning configurations (HLZC) for all DSCs are listed in Chapter A.1, Appendix 1.4.1 through Appendix 1.4.9. These design basis HLZCs are symmetrical and show maximum allowable heat load per FA and per DSC, which result in bounding maximum fuel cladding and DSC component temperatures. Possible asymmetry in HLZC (within specified FA and DSC limits) means reduction of heat load in a particular FA resulting in reduction of local and maximum temperatures of fuel cladding and DSC components.
A peaking factor is considered along the active fuel length for calculation of the decay heat profile of the fuel assemblies as described in Section A.3.3.1.4 and Section A.3.3.1.6 for 69BTH and 37PTH DSCs, respectively.

A description of the detailed analyses of MP197HB TC, 69BTH and 37PTH DSCs for NCT and HAC is provided in Section A.3.3 and Section A.3.4, respectively. These analyses demonstrate that the maximum temperatures and pressures for other DSC types under transport conditions of 10 CFR 71 are bounded by the evaluations provided in [1], [2], [3], and [4] under storage/transfer conditions of 10 CFR 72.

Summaries of the maximum temperatures and pressures are provided in Section A.3.1.3 and Section A.3.1.4, respectively. The thermal evaluation concludes that for the maximum heat loads listed in Section A.3.1.1.1 all design criteria listed in Section A.3.1 are satisfied.

### A.3.1.3 Summary Tables of Temperatures

The maximum and minimum MP197HB TC and DSC component temperatures for NCT are summarized in Table A.3–11. The component temperatures remain within the allowable range for NCT.

The maximum MP197HB TC and DSC component temperatures for cold conditions at -20°F and -40°F ambient without insolance are presented in Table A.3–12 and Table A.3–13. These temperatures are used for the structural evaluation of 69BTH and 37PTH DSCs.

The maximum accessible surface temperatures under shade are 121°F and 163°F for impact limiter shell and personnel barrier as calculated in Section A.3.3.1.2.

The maximum transient temperatures of the MP197HB TC and DSC components and the time at which they occur are summarized in Table A.3–19 for HAC. The resins and

wood are assumed to be decomposed or charred after fire accident. Therefore, the maximum temperatures for these components are irrelevant for HAC. The maximum fuel cladding, gamma shield and seal temperatures remain below the allowable limits and ensure the integrity of the fuel cladding and the containment boundary for HAC.

### A.3.1.4 Summary Tables of Maximum Pressures

The maximum internal pressures inside MP197HB TC cavity are calculated in Section A.3.3.3 for NCT and Section A.3.4.3 for HAC. The maximum internal pressures of the MP197HB TC cavity are summarized in Table A.3–20. The maximum pressures inside canister cavities of 69BTH and 37PTH DSCs are listed in Table A.3–22. The maximum internal pressures for all DSCs proposed for transport in MP197HB TC are summarized in Table A.3–23. These pressures remain below the design pressures for NCT and HAC *considered for the structural evaluation.*

## A.3.2 Material Properties and Component Specifications

### A.3.2.1 Material Properties

The following tables provide the thermal properties of materials used in the analysis of the MP197HB TC with DSCs. *Each table is valid for all the models unless it is specifically noted in the title of the table.*

1. Bounding PWR Fuel Assembly for 37PTH *DSC*

Calculation of the effective properties for homogenized PWR fuel assemblies in a 37PTH DSC are discussed in Section A.3.6.5.1. The bounding effective properties for PWR fuel assemblies in 37PTH DSC are listed below.

**Homogenized PWR Fuel Assemblies in Four Corner Fuel Compartments in 37PTH DSC**

| Temp (°F) | Transverse Conductivity (Btu/hr-in-°F) | Temp (°F) | Axial Conductivity (Btu/hr-in-°F) | Temp (°F) | Specific Heat (Btu/lbm-°F) | Density ($lbm/in^3$) |
|---|---|---|---|---|---|---|
| 178 | 0.0168 | 200 | 0.0456 | 80 | 0.05924 | |
| 267 | 0.0195 | 300 | 0.0481 | 260 | 0.06538 | |
| 357 | 0.0230 | 400 | 0.0506 | 692 | 0.07255 | |
| 448 | 0.0273 | 500 | 0.0527 | 1502 | 0.07779 | 0.1114 |
| 541 | 0.0323 | 600 | 0.0548 | | | |
| 635 | 0.0380 | 800 | 0.0594 | | | |
| 730 | 0.0444 | | | | | |
| 826 | 0.0513 | | | | | |

**Homogenized PWR Fuel Assemblies in Other Fuel Compartments in 37PTH DSC**

| Temp (°F) | Transverse Conductivity (Btu/hr-in-°F) | Temp (°F) | Axial Conductivity (Btu/hr-in-°F) | Bounding effective specific heat and density are the same as those for corner fuel assemblies. |
|---|---|---|---|---|
| 138 | 0.0174 | 200 | 0.0454 | |
| 233 | 0.0199 | 300 | 0.0478 | |
| 328 | 0.0238 | 400 | 0.0503 | |
| 423 | 0.0285 | 500 | 0.0524 | |
| 519 | 0.0340 | 600 | 0.0545 | |
| 616 | 0.0403 | 800 | 0.0591 | |
| 714 | 0.0473 | | | |
| 812 | 0.0552 | | | |

Note:
(1) Only 95% of the axial effective conductivity calculated in [1, Appendix M, Section M.4.8] for 32PT DSC is considered in the 37PTH DSC model for conservatism.

2. Bounding BWR Fuel Assembly for 69BTH *DSC*

Calculation of the effective properties for homogenized BWR fuel assemblies in 69BTH DSC are discussed in Section A.3.6.5.2. The bounding effective properties for BWR fuel assemblies in 69BTH DSC are listed below.

**Homogenized BWR Fuel Assemblies in 69BTH DSC**

| Temperature (°F) | k, Transverse (Btu/hr-in-°F) | k, Axial (Btu/hr-in-°F) | ρ ($lb_m/in^3$) | $C_p$ (Btu/$lb_m$-°F) |
|---|---|---|---|---|
| 200 | 0.0157 | 0.0402 | 0.103 | 0.0575 |
| 300 | 0.0181 | | | |
| 400 | 0.0211 | | | |
| 500 | 0.0246 | | | |
| 600 | 0.0285 | | | |
| 700 | 0.0328 | | | |
| 800 | 0.0375 | | | |

3. SA-240, Type 304 Stainless Steel [10]

| Temperature (°F) | k (Btu/hr-in-°F) | ρ ($lbm/in^3$) | $C_p$ (Btu/$lb_m$-°F) |
|---|---|---|---|
| 70 | 0.717 | 0.284 | 0.116 |
| 100 | 0.725 | | 0.117 |
| 200 | 0.775 | | 0.122 |
| 300 | 0.817 | | 0.125 |
| 400 | 0.867 | | 0.129 |
| 500 | 0.908 | | 0.131 |
| 600 | 0.942 | | 0.133 |
| 700 | 0.983 | | 0.135 |
| 800 | 1.025 | | 0.136 |
| 900 | 1.058 | | 0.137 |
| 1000 | 1.092 | | 0.138 |

4. SA-240 Type 316 [2, Section 4.2.c]

| Temperature (°F) | k (Btu/hr-in-°F) | ρ ($lbm/in^3$) | $C_p$ (Btu/$lb_m$-°F) |
|---|---|---|---|
| 70 | 0.642 | 0.285 | 0.117 |
| 100 | 0.658 | | 0.118 |
| 200 | 0.700 | | 0.121 |
| 300 | 0.750 | | 0.126 |
| 400 | 0.792 | | 0.126 |
| 500 | 0.833 | | 0.130 |
| 600 | 0.875 | | 0.132 |
| 700 | 0.917 | | 0.134 |
| 800 | 0.958 | | 0.135 |
| 900 | 1.000 | | 0.137 |
| 1000 | 1.033 | | 0.137 |

5. SA-182-F6NM [10]

| Temperature (°F) | k (Btu/hr-in-°F) | ρ (lbm/in$^3$) | $C_p$ (Btu/lb$_m$-°F) |
|---|---|---|---|
| 70 | 1.183 | 0.284 | 0.105 |
| 100 | 1.183 | | 0.107 |
| 200 | 1.192 | | 0.112 |
| 300 | 1.200 | | 0.117 |
| 400 | 1.208 | | 0.122 |
| 500 | 1.208 | | 0.128 |
| 600 | 1.217 | | 0.135 |
| 700 | 1.217 | | 0.142 |
| 800 | 1.225 | | 0.150 |
| 900 | 1.225 | | 0.157 |
| 1000 | 1.225 | | 0.166 |

6. SA-516-70 or A36 [10]

| Temperature (°F) | k (Btu/hr-in-°F) | ρ (lbm/in$^3$) | $C_p$ (Btu/lb$_m$-°F) |
|---|---|---|---|
| 70 | 2.275 | 0.284 | 0.105 |
| 100 | 2.300 | | 0.108 |
| 200 | 2.317 | | 0.116 |
| 300 | 2.275 | | 0.122 |
| 400 | 2.208 | | 0.127 |
| 500 | 2.142 | | 0.131 |
| 600 | 2.075 | | 0.136 |
| 700 | 2.008 | | 0.142 |
| 800 | 1.933 | | 0.148 |
| 900 | 1.858 | | 0.156 |
| 1000 | 1.758 | | 0.163 |

7. SA-203, Gr. E or SA-350-LF3 [10]

| Temperature (°F) | k (Btu/hr-in-°F) | ρ (lbm/in$^3$) | $C_p$ (Btu/lb$_m$-°F) |
|---|---|---|---|
| 70 | 1.975 | 0.284 | 0.105 |
| 100 | 1.967 | | 0.107 |
| 200 | 1.958 | | 0.113 |
| 300 | 1.950 | | 0.119 |
| 400 | 1.925 | | 0.124 |
| 500 | 1.892 | | 0.130 |
| 600 | 1.850 | | 0.135 |
| 700 | 1.800 | | 0.140 |
| 800 | 1.750 | | 0.147 |
| 900 | 1.692 | | 0.154 |
| 1000 | 1.642 | | 0.163 |

8. Aluminum, Type 1100 [10]

| Temperature (°F) | k (Btu/hr-in-°F) | ρ ($lb_m/in^3$) | $C_p$ (Btu/$lb_m$-°F) |
|---|---|---|---|
| 70 | 11.092 | 0.098 | 0.214 |
| 100 | 10.983[1] | | 0.216 |
| 150 | 10.833 | | 0.219 |
| 200 | 10.708 | | 0.222 |
| 250 | 10.608 | | 0.224 |
| 300 | 10.517 | | 0.227 |
| 350 | 10.442 | | 0.229 |
| 400 | 10.375 | | 0.232 |

Note: [1] *The input files of the ANSYS models for the baskets contain a thermal conductivity of 11.150 Btu/hr-in-°F (133.8 Btu/hr-ft-°F) instead of 10.983 Btu/hr-in-°F. Since this value is used only at 100°F and since* the basket temperature is over 150°F for all analyzed cases, this value does not affect the results in this SAR.

9. Aluminum, Type 6063 [10]

| Temperature (°F) | k (Btu/hr-in-°F) | ρ ($lb_m/in^3$) | $C_p$ (Btu/$lb_m$-°F) |
|---|---|---|---|
| 70 | 10.067 | 0.098 | 0.213 |
| 100 | 10.025 | | 0.215 |
| 150 | 9.975 | | 0.218 |
| 200 | 9.917 | | 0.221 |
| 250 | 9.875 | | 0.223 |
| 300 | 9.842 | | 0.226 |
| 350 | 9.833 | | 0.228 |
| 400 | 9.800 | | 0.230 |

10. Aluminum, Type 6061 [10]

| Temperature (°F) | k (Btu/hr-in-°F) | ρ ($lb_m/in^3$) | $C_p$ (Btu/$lb_m$-°F) |
|---|---|---|---|
| 70 | 8.008 | 0.098 | 0.213 |
| 100 | 8.075 | | 0.215 |
| 150 | 8.167 | | 0.218 |
| 200 | 8.250 | | 0.221 |
| 250 | 8.317 | | 0.223 |
| 300 | 8.383 | | 0.226 |
| 350 | 8.442 | | 0.228 |
| 400 | 8.492 | | 0.230 |

11. Gamma Shield, ASTM B29 Lead [24]

| Temperature (°F) | k (Btu/hr-in-°F) | ρ ($lb_m/in^3$) | $C_p$ (Btu/$lb_m$-°F) |
|---|---|---|---|
| -100 | 1.767 | 0.413 | 0.030 |
| -10 | 1.733 | 0.411 | 0.030 |
| 80 | 1.700 | 0.409 | 0.031 |
| 260 | 1.637 | 0.406 | 0.032 |
| 440 | 1.579 | 0.402 | 0.033 |
| 620 | 1.512 | 0.398 | 0.034 |

12. Neutron Shield Resin (Vyal B) [17]

| Temperature (°F) | k (Btu/hr-in-°F) | ρ ($lb_m/in^3$) | $C_p$ (Btu/$lb_m$-°F) |
|---|---|---|---|
| 104 | 0.039 | 0.06 | 0.256 |
| 140 | | | 0.260 |
| 176 | | | 0.282 |
| 212 | | | 0.301 |
| 284 | | | 0.358 |
| 320 | | | 0.380 |

13. Trunnion Plug Resin (Polypropylene) [5]

| Temperature (°F) | k (Btu/hr-in-°F) | ρ ($lb_m/in^3$) | $C_p$ (Btu/$lb_m$-°F) |
|---|---|---|---|
| All temperatures | 0.0067 | 0.032 | 0.46 |

14. Wood [20]

| Minimum conductivity, $k_{min}$ = 0.0019 Btu/hr-in-°F for NCT and cool-down period, see MP197 SAR, Section 3.2, Item 8 | | |
|---|---|---|
| Maximum conductivity, $k_{max}$ = 0.0378 Btu/hr-in-°F during fire period, see MP197 SAR, Section 3.2, Item 8 | | |
| **Temperature (°F)** | **ρ ($lb_m/in^3$) (1)** | **$C_p$ (Btu/$lb_m$-°F)** |
| 100 | 0.007 | 0.312 |
| 200 | 0.006 | 0.363 |
| 300 | 0.005 | 0.414 |
| 400 | 0.005 | 0.466 |
| 500 | 0.004 | 0.517 |
| 600 | 0.004 | 0.568 |

Note: (1) The wood density is calculated based on thermal diffusivity using $\alpha = \frac{k}{\rho c_P}$ with

$\alpha$ = *0.00025 $in^2/s$ (0.9 $in^2/hr$) based on Wood Handbook [20],*
k = conductivity =0.0019 (Btu/hr-in-°F),
ρ = density ($lbm/in^3$), and
$c_P$ = specific heat (Btu/lbm-°F).

15. Helium [21]

| Temperature (K) | k (W/m-K) | Temperature (°F) | k (Btu/hr-in-°F) |
|---|---|---|---|
| 300 | 0.1499 | 80 | 0.0072 |
| 400 | 0.1795 | 260 | 0.0086 |
| 500 | 0.2115 | 440 | 0.0102 |
| 600 | 0.2466 | 620 | 0.0119 |
| 800 | 0.3073 | 980 | 0.0148 |
| 1000 | 0.3622 | 1340 | 0.0174 |
| 1050 | 0.3757 | 1430 | 0.0181 |

The above data are calculated base on the following polynomial function from [21]

$k = \sum C_i T_i$ for conductivity in(W/m-K) and T in (K)

| For 300 < T < 500 K | | for 500< T < 1050 K | |
|---|---|---|---|
| C0 | -7.761491E-03 | C0 | -9.0656E-02 |
| C1 | 8.66192033E-04 | C1 | 9.37593087E-04 |
| C2 | -1.5559338E-06 | C2 | -9.13347535E-07 |
| C3 | 1.40150565E-09 | C3 | 5.55037072E-10 |
| C4 | 0.0E+00 | C4 | -1.26457196E-13 |

No density or specific heat is considered for helium for conservatism.

16. Air [21]

| Temperature (K) | k (W/m-K) | Temperature (°F) | k (Btu/hr-in-°F) |
|---|---|---|---|
| 250 | 0.02228 | -10 | 0.0011 |
| 300 | 0.02607 | 80 | 0.0013 |
| 400 | 0.03304 | 260 | 0.0016 |
| 500 | 0.03948 | 440 | 0.0019 |
| 600 | 0.04557 | 620 | 0.0022 |
| 800 | 0.05698 | 980 | 0.0027 |
| 1000 | 0.06721 | 1340 | 0.0032 |

The above data are calculated base on the following polynomial function from [21]

$k = \sum C_i T_i$ for conductivity in(W/m-K) and T in (K)

| For 250 < T < 1050 K | |
|---|---|
| C0 | -2.2765010E-03 |
| C1 | 1.2598485E-04 |
| C2 | -1.4815235E-07 |
| C3 | 1.7355064E-10 |
| C4 | -1.0666570E-13 |
| C5 | 2.4766304E-17 |

No density or specific heat is considered for air in the thermal models for conservatism. Specific heat, viscosity, density and Prandtl number of air are used to calculate heat transfer coefficients described in Section A.3.3.1.1 based on the following data from [21].

$c_p = \sum A_i T_i$ for specific heat in (kJ/kg-K) and T in (K)

| For 250 < T < 1050 K | |
|---|---|
| A0 | 0.103409E+1 |
| A1 | -0.2848870E-3 |
| A2 | 0.7816818E-6 |
| A3 | -0.4970786E-9 |
| A4 | 0.1077024E-12 |

$\mu = \sum B_i T_i$ for viscosity (N-/m$^2$)×10$^6$ and T in (K)

| For 250 < T < 600 K | | For 600 < T < 1050 K | |
|---|---|---|---|
| B0 | -9.8601E-1 | B0 | 4.8856745 |
| B1 | 9.080125E-2 | B1 | 5.43232E-2 |
| B2 | -1.17635575E-4 | B2 | -2.4261775E-5 |
| B3 | 1.2349703E-7 | B3 | 7.9306E-9 |
| B4 | -5.7971299E-11 | B4 | -1.10398E-12 |

$\rho = P / RT$ for density (kg/m$^3$) with P=101.3 kPa; R = 0.287040 kJ/kg-K; T = air temp in (K)

$Pr = c_p \mu / k$ Prandtl number

## 17. Effective Conductivity for Paired Aluminum and Boral in 69BTH DSC

(See Section A.3.3.1.5 for calculation of effective properties)

| Conductivity of Boral Core Material | | |
|---|---|---|
| Temp | $k_c$ [1] | $k_{c\_90\%}$ |
| (°F) | (Btu/hr-in-°F) | (Btu/hr-in-°F) |
| 100 | 4.136 | 3.723 |
| 500 | 3.698 | 3.328 |

| $t_{total}$ = 0.25" total thickness for paired Al/Poison<br>$t_{model}$ = 0.21" total thickness for paired Al/Poison as modeled<br>$t_{core}$ = 0.16" Boral core thickness<br>$t_{Al}$ = 0.09" Aluminum thickness | | | | $t_{total}$ = 0.375" total thickness for paired Al/Poison<br>$t_{model}$ = 0.375" total thickness for paired Al/Poison as modeled<br>$t_{core}$ = 0.16" Boral core thickness<br>$t_{Al}$ = 0.215" Aluminum thickness | | | |
|---|---|---|---|---|---|---|---|
| Temp | $k_{Al}$ [10] | $k_{core}$ [3] | $k_{eff,across}$ | Temp | $k_{Al}$ [10] | $k_{core}$ [3] | $k_{eff,across}$ |
| (°F) | (Btu/hr-in-°F) | (Btu/hr-in-°F) | (Btu/hr-in-°F) | (°F) | (Btu/hr-in-°F) | (Btu/hr-in-°F) | (Btu/hr-in-°F) |
| 70 | 11.092 | 3.752 | 4.137 | 70 | 11.092 | 3.752 | 6.046 |
| 100 | 10.983 [4] | 3.723 | 4.104 [4] | 100 | 10.983 [4] | 3.723 | 5.995 [4] |
| 200 | 10.708 | 3.624 | 3.996 | 200 | 10.708 | 3.624 | 5.839 |
| 300 | 10.517 | 3.525 | 3.893 | 300 | 10.517 | 3.525 | 5.697 |
| 400 | 10.375 | 3.427 | 3.793 | 400 | 10.375 | 3.427 | 5.563 |
| 650 | 10.042 [2] | 3.180 | 3.543 | 650 | 10.042 [2] | 3.180 | 5.229 |
| | | | | | | | |
| Temp | $k_{Al}$ [10] | $k_{core}$ [3] | $k_{eff,along}$ | Temp | $k_{Al}$ [10] | $k_{core}$ [3] | $k_{eff,along}$ |
| (°F) | (Btu/hr-in-°F) | (Btu/hr-in-°F) | (Btu/hr-in-°F) | (°F) | (Btu/hr-in-°F) | (Btu/hr-in-°F) | (Btu/hr-in-°F) |
| 70 | 11.092 | 3.752 | 7.612 | 70 | 11.092 | 3.752 | 7.960 |
| 100 | 10.983 [4] | 3.723 | 7.543 [4] | 100 | 10.983 [4] | 3.723 | 7.885 [4] |
| 200 | 10.708 | 3.624 | 7.350 | 200 | 10.708 | 3.624 | 7.686 |
| 300 | 10.517 | 3.525 | 7.193 | 300 | 10.517 | 3.525 | 7.534 |
| 400 | 10.375 | 3.427 | 7.057 | 400 | 10.375 | 3.427 | 7.410 |
| 650 | 10.042 [2] | 3.180 | 6.727 | 650 | 10.042 [2] | 3.180 | 7.114 |

Notes:

[1] Taken from data in [26]

[2] Extrapolated from data in [10]

[3] Inter- and extrapolated from data of 90% Boral core conductivity

[4] A conductivity value of 11.150 Btu/hr-in-°F is used instead of 10.983 Btu/hr-in-°F for $k_{Al}$ at 100°F. This increases the effective conductivity by approximately 1% for paired aluminum and Boral plates in the ANSYS model. Since the calculated basket temperature is over 100°F for all analyzed cases, use of this higher value does not affect the results in this SAR.

## 18. Effective Conductivity for Paired Aluminum and MMC in 69BTH DSC

(See Section A.3.3.1.5 for calculation of effective properties)

| $t_{total}$ = 0.25" total thickness for paired Al/Poison<br>$t_{model}$ = 0.21" total thickness for paired Al/Poison as modeled<br>$t_{core}$ = 0.175" MMC thickness<br>$t_{Al}$ = 0.075" Aluminum thickness | | | | $t_{total}$ = 0.375" total thickness for paired Al/Poison<br>$t_{model}$ = 0.375" total thickness for paired Al/Poison as modeled<br>$t_{core}$ = 0.175" MMC thickness<br>$t_{Al}$ = 0.200" Aluminum thickness | | | |
|---|---|---|---|---|---|---|---|
| Temp | $k_{Al}$ [10] | $k_{MMC}$ [1] | $k_{eff,across}$ | Temp | $k_{Al}$ [10] | $k_{MMC}$ [1] | $k_{eff,across}$ |
| (°F) | (Btu/hr-in-°F) | (Btu/hr-in-°F) | (Btu/hr-in-°F) | (°F) | (Btu/hr-in-°F) | (Btu/hr-in-°F) | (Btu/hr-in-°F) |
| 70 | 11.092 | 5.78 | 5.673 | 70 | 11.092 | 5.78 | 7.766 |
| 100 | 10.983 | 5.78 | 5.663 | 100 | 10.983 | 5.78 | 7.737 |
| 200 | 10.708 | 5.78 | 5.636 | 200 | 10.708 | 5.78 | 7.664 |
| 300 | 10.517 | 5.78 | 5.617 | 300 | 10.517 | 5.78 | 7.611 |
| 400 | 10.375 | 5.78 | 5.602 | 400 | 10.375 | 5.78 | 7.571 |
| 650 | 10.042 [2] | 5.78 | 5.567 | 650 | 10.042 [2] | 5.78 | 7.474 |
| | | | | | | | |
| Temp | $k_{Al}$ [10] | $k_{MMC}$ [1] | $k_{eff,along}$ | Temp | $k_{Al}$ [10] | $k_{MMC}$ [1] | $k_{eff,along}$ |
| (°F) | (Btu/hr-in-°F) | (Btu/hr-in-°F) | (Btu/hr-in-°F) | (°F) | (Btu/hr-in-°F) | (Btu/hr-in-°F) | (Btu/hr-in-°F) |
| 70 | 11.092 | 5.78 | 8.781 | 70 | 11.092 | 5.78 | 8.615 |
| 100 | 10.983 | 5.78 | 8.743 | 100 | 10.983 | 5.78 | 8.557 |
| 200 | 10.708 | 5.78 | 8.644 | 200 | 10.708 | 5.78 | 8.410 |
| 300 | 10.517 | 5.78 | 8.576 | 300 | 10.517 | 5.78 | 8.308 |
| 400 | 10.375 | 5.78 | 8.525 | 400 | 10.375 | 5.78 | 8.233 |
| 650 | 10.042 [2] | 5.78 | 8.406 | 650 | 10.042 [2] | 5.78 | 8.055 |

Notes:
[1] The lowest conductivity is taken from data in [3]
[2] Extrapolated from data in [10]

## 19. Effective Conductivity for Paired Aluminum and Borated Aluminum in 69BTH DSC

(See Section A.3.3.1.5 for calculation of effective properties)

| $t_{total}$ = 0.25" total thickness for paired Al/Poison<br>$t_{model}$ = 0.21" total thickness for paired Al/Poison as modeled<br>$t_{core}$ = 0.175" Borated Aluminum thickness<br>$t_{Al}$ = 0.075" Aluminum thickness | | | | $t_{total}$ = 0.375" total thickness for paired Al/Poison<br>$t_{model}$ = 0.375" total thickness for paired Al/Poison as modeled<br>$t_{core}$ = 0.175" Borated Aluminum thickness<br>$t_{Al}$ = 0.200" Aluminum thickness | | | |
|---|---|---|---|---|---|---|---|
| Temp | $k_{Al}$ [10] | $k_{BAl}$ [1] | $k_{eff,across}$ | Temp | $k_{Al}$ [10] | $k_{BAl}$ [1] | $k_{eff,across}$ |
| (°F) | (Btu/hr-in-°F) | (Btu/hr-in-°F) | (Btu/hr-in-°F) | (°F) | (Btu/hr-in-°F) | (Btu/hr-in-°F) | (Btu/hr-in-°F) |
| 70 | 11.092 | 7.39 | 6.896 | 70 | 11.092 | 7.39 | 8.988 |
| 100 | 10.983 [3] | 7.50 | 6.962 [3] | 100 | 10.983 [3] | 7.50 | 9.027 [3] |
| 200 | 10.708 | 7.88 | 7.185 | 200 | 10.708 | 7.88 | 9.169 |
| 300 | 10.517 | 8.18 | 7.365 | 300 | 10.517 | 8.18 | 9.282 |
| 400 | 10.375 | 8.48 | 7.537 | 400 | 10.375 | 8.48 | 9.396 |
| 650 | 10.042 [2] | 9.15 | 7.895 | 650 | 10.042 [2] | 9.15 | 9.604 |
| | | | | | | | |
| Temp | $k_{Al}$ [10] | $k_{BAl}$ [1] | $k_{eff,along}$ | Temp | $k_{Al}$ [10] | $k_{BAl}$ [1] | $k_{eff,along}$ |
| (°F) | (Btu/hr-in-°F) | (Btu/hr-in-°F) | (Btu/hr-in-°F) | (°F) | (Btu/hr-in-°F) | (Btu/hr-in-°F) | (Btu/hr-in-°F) |
| 70 | 11.092 | 7.39 | 10.118 | 70 | 11.092 | 7.39 | 9.363 |
| 100 | 10.983 [3] | 7.50 | 10.173 [3] | 100 | 10.983 [3] | 7.50 | 9.358 [3] |
| 200 | 10.708 | 7.88 | 10.387 | 200 | 10.708 | 7.88 | 9.386 |
| 300 | 10.517 | 8.18 | 10.576 | 300 | 10.517 | 8.18 | 9.428 |
| 400 | 10.375 | 8.48 | 10.773 | 400 | 10.375 | 8.48 | 9.491 |
| 650 | 10.042 [2] | 9.15 | 11.210 | 650 | 10.042 [2] | 9.15 | 9.625 |

Notes:

[1] Inter- and extrapolated from data in [3]

[2] Extrapolated from data in [10]

[3] A conductivity value of 11.150 Btu/hr-in-°F is used instead of 10.983 Btu/hr-in-°F for $k_{Al}$ at 100°F. This increases the effective conductivity by approximately 1% for paired aluminum and Boral plates in the ANSYS model. Since the calculated basket temperature is over 100°F for all analyzed cases, use of this higher value does not affect the results in this SAR.

## 20. Effective Conductivity for Dummy Aluminum Assemblies *in 69BTH DSC*

(See Section A.3.3.1.5 for calculation of effective properties)

| | | |
|---|---|---|
| $a_{dummy}$ = | 5.875 | in |
| $t_{gap}$ = | 0.0625 | in |
| $w_{comp}$ = | 6 | in |

| Temp | $k_{Al6061}$ [10] |
|---|---|
| (°F) | (Btu/hr-in-°F) |
| 70 | 8.008 |
| 100 | 8.075 |
| 200 | 8.250 |
| 300 | 8.383 |
| 400 | 8.492 |
| 650 | 8.492 (1) |

| Temp | $k_{He}$ (2) | Temp | $k_{He}$ |
|---|---|---|---|
| (°F) | (Btu/hr-in-°F) | (°F) | (Btu/hr-in-°F) |
| -10 | 0.0064 | 70 | 0.0071 |
| 80 | 0.0072 | 100 | 0.0074 |
| 260 | 0.0086 | 200 | 0.0081 |
| 440 | 0.0102 | 300 | 0.0090 |
| 620 | 0.0119 | 400 | 0.0098 |
| 980 | 0.0148 | 650 | 0.0121 |
| 1340 | 0.0174 | | |

| Temp | $R_{th\_He1}$ | $R_{th\_Al6061}$ | $R_{th\_He2}$ | $R_{th,tr,dummy}$ | $k_{eff,tr,dummy}$ | $k_{eff,ax,dummy}$ |
|---|---|---|---|---|---|---|
| (°F) | (Btu/hr-in-°F) | (Btu/hr-in-°F) | (Btu/hr-in-°F) | (Btu/hr-in-°F) | (Btu/hr-in-°F) | (Btu/hr-in-°F) |
| 70 | 1.4648 | 0.1249 | 13218.8 | 3.0546 | 0.327 | 7.678 |
| 100 | 1.4162 | 0.1238 | 12779.5 | 2.9562 | 0.338 | 7.742 |
| 200 | 1.2807 | 0.1212 | 11557.4 | 2.6827 | 0.373 | 7.910 |
| 300 | 1.1632 | 0.1193 | 10496.3 | 2.4456 | 0.409 | 8.037 |
| 400 | 1.0581 | 0.1178 | 9548.5 | 2.2340 | 0.448 | 8.142 |
| 650 | 0.8579 | 0.1178 | 7741.9 | 1.8336 | 0.545 | 8.142 |

Notes:

(1) Al6061 conductivity increases at higher temperatures. Increasing of the Al6061 conductivity is conservatively ignored for calculation of effective conductivity of aluminum dummy assembly.

(2) See Section A.3.2.1, material # 15 for helium properties.

## 21. Effective Conductivity for Boral Plates in 37PTH DSC

(See Section A.3.3.1.7 for calculation of effective properties)

| Conductivity of Boral Core Material | | |
|---|---|---|
| Temp | $k_c$ [1] | $k_{c\_90\%}$ |
| (°F) | (Btu/hr-in-°F) | (Btu/hr-in-°F) |
| 100 | 4.136 | 3.723 |
| 500 | 3.698 | 3.328 |

$t_{total}$ = 0.075" total thickness for Boral plate
$t_{model}$ = 0.075" total thickness for Boral plate as modeled
$t_{core}$ = 0.06" Boral core thickness
$t_{Al}$ = 0.015" Aluminum clad thickness

| Temp | $k_{Al}$ [10] | $k_{core}$ | $k_{eff,across}$ |
|---|---|---|---|
| (°F) | (Btu/hr-in-°F) | (Btu/hr-in-°F) | (Btu/hr-in-°F) |
| 100 | 10.983 | 3.723 | 4.290 |
| 500 | 10.242 [2] | 3.328 | 3.848 |

| Temp | $k_{Al}$ [10] | $k_{core}$ | $k_{eff,along}$ |
|---|---|---|---|
| (°F) | (Btu/hr-in-°F) | (Btu/hr-in-°F) | (Btu/hr-in-°F) |
| 100 | 10.983 | 3.723 | 5.175 |
| 500 | 10.242 [2] | 3.328 | 4.711 |

Notes:
[1] Taken from data in [26]
[2] Extrapolated from data in [10]

## 22. Effective Heat Transfer Coefficients for External Fins @ 100°F Ambient

(See Section A.3.3.1.3 for calculation of effective properties)

| | | |
|---|---|---|
| fin_h = | 3.0 | fin height (in) |
| fin_p = | 1.0 | fin pitch (in) |
| fin_t = | 0.156 | fin thickness (in) |
| fin_n = | 3 | No. of fins in model |
| $D_o$ = | 98.25 | cask diameter (in) |
| $D_f$ = | 104.25 | fin diameter (in) |
| $D_f/D_o$ = | 1.061 | |
| A_eff = | 77.2 | area of un-finned surface ($in^2$) |

From Rohsenow Handbook [21]

| $D_f/D_o$ | c | b |
|---|---|---|
| 1.36 | 0.62 | 0.29 |
| 1.14 | 0.59 | 0.27 |
| Extrapolated for this calculation based on above data | | |
| 1.061 | 0.579 | 0.263 |

| $T_s$ (°F) | $T_{amb}$ (°F) | $Q_{react}$ (Btu/hr) | $A_{eff}$ ($in^2$) | $h_{eff}$ (Btu/hr-$in^2$-°F) |
|---|---|---|---|---|
| 120 | 100 | 31.295 | 77.2 | 0.0203 |
| 140 | 100 | 71.639 | 77.2 | 0.0232 |
| 160 | 100 | 116.59 | 77.2 | 0.0252 |
| 180 | 100 | 165.15 | 77.2 | 0.0268 |
| 200 | 100 | 216.89 | 77.2 | 0.0281 |
| 220 | 100 | 271.55 | 77.2 | 0.0293 |
| 240 | 100 | 329.01 | 77.2 | 0.0305 |
| 260 | 100 | 388.75 | 77.2 | 0.0315 |
| 280 | 100 | 452.15 | 77.2 | 0.0326 |
| 300 | 100 | 518.00 | 77.2 | 0.0336 |
| 320 | 100 | 586.59 | 77.2 | 0.0346 |
| 340 | 100 | 658.05 | 77.2 | 0.0355 |

23. Effective Heat Transfer Coefficients for External Fins @ -20°F Ambient
(See Section A.3.3.1.3 for calculation of effective properties)

| $T_s$ (°F) | $T_{amb}$ (°F) | $Q_{react}$ (Btu/hr) | $A_{eff}$ ($in^2$) | $h_{eff}$ (Btu/hr-$in^2$-°F) |
|---|---|---|---|---|
| 0 | -20 | 26.511 | 77.2 | 0.0172 |
| 20 | -20 | 61.325 | 77.2 | 0.0199 |
| 40 | -20 | 99.88 | 77.2 | 0.0216 |
| 60 | -20 | 141.15 | 77.2 | 0.0229 |
| 80 | -20 | 184.56 | 77.2 | 0.0239 |
| 100 | -20 | 229.46 | 77.2 | 0.0248 |
| 120 | -20 | 278.04 | 77.2 | 0.0257 |
| 140 | -20 | 329.65 | 77.2 | 0.0267 |
| 160 | -20 | 382.98 | 77.2 | 0.0276 |
| 180 | -20 | 437.79 | 77.2 | 0.0284 |
| 200 | -20 | 494.84 | 77.2 | 0.0291 |
| 220 | -20 | 553.94 | 77.2 | 0.0299 |

24. Effective Heat Transfer Coefficients for External Fins @ -40°F Ambient
(See Section A.3.3.1.3 for calculation of effective properties)

| $T_s$ (°F) | $T_{amb}$ (°F) | $Q_{react}$ (Btu/hr) | $A_{eff}$ ($in^2$) | $h_{eff}$ (Btu/hr-$in^2$-°F) |
|---|---|---|---|---|
| -20 | -40 | 26.044 | 77.2 | 0.0169 |
| 0 | -40 | 60.344 | 77.2 | 0.0196 |
| 20 | -40 | 98.33 | 77.2 | 0.0212 |
| 40 | -40 | 139.00 | 77.2 | 0.0225 |
| 60 | -40 | 181.83 | 77.2 | 0.0236 |
| 80 | -40 | 226.42 | 77.2 | 0.0245 |
| 100 | -40 | 272.53 | 77.2 | 0.0252 |
| 120 | -40 | 321.95 | 77.2 | 0.0261 |
| 140 | -40 | 374.39 | 77.2 | 0.0270 |
| 160 | -40 | 427.93 | 77.2 | 0.0277 |
| 180 | -40 | 483.57 | 77.2 | 0.0285 |
| 200 | -40 | 541.13 | 77.2 | 0.0292 |

## 25. Radial Effective Conductivity for Helium in DSC Shell/TC Inner Shell Gap

(See Section A.3.3.1.3 for calculation of effective properties

| | | |
|---|---|---|
| $D_{o,DSC}$ = | 69.75 | DSC OD (in) |
| $D_{i,TC}$ = | 70.50 | Cask ID (in) |
| L = | 10 | Model height (in) |

| $T_{DSC}$ (°F) | $T_{TC}$ (°F) | $q_{react}$ (Btu/hr) | $T_{avg}$ (°F) | $k_{\_eff}$ (Btu/hr-in-°F) |
|---|---|---|---|---|
| 110 | -20 | 506 | 45 | 0.0080 |
| 153 | 30 | 506 | 92 | 0.0084 |
| 195 | 80 | 506 | 138 | 0.0090 |
| 237 | 130 | 506 | 183 | 0.0097 |
| 279 | 180 | 506 | 230 | 0.0104 |
| 296 | 200 | 506 | 248 | 0.0108 |
| 339 | 250 | 506 | 294 | 0.0116 |
| 382 | 300 | 506 | 341 | 0.0126 |
| 426 | 350 | 506 | 388 | 0.0136 |
| 470 | 400 | 506 | 435 | 0.0148 |
| 515 | 450 | 506 | 482 | 0.0160 |
| 560 | 500 | 506 | 530 | 0.0173 |
| 606 | 550 | 506 | 578 | 0.0187 |
| 652 | 600 | 506 | 626 | 0.0202 |
| 698 | 650 | 506 | 674 | 0.0217 |
| 745 | 700 | 506 | 722 | 0.0233 |
| 791 | 750 | 506 | 771 | 0.0251 |

## 26. Radial Effective Conductivity for Helium in DSC Shell/TC Internal Sleeve Gap

(See Section A.3.3.1.3 for calculation of effective properties)

| | | |
|---|---|---|
| $D_{o,DSC}$ = | 67.19 | DSC OD (in) |
| $D_{i,Sleeve}$ = | 68.00 | Cask ID (in) |
| L = | 10 | Model height (in) |

| $T_{DSC}$ (°F) | $T_{Sleeve}$ (°F) | $q_{react}$ (Btu/hr) | $T_{avg}$ (°F) | $k_{\_eff}$ (Btu/hr-in-°F) | $k_{\_eff}$ in Model [1] (Btu/hr-in-°F) |
|---|---|---|---|---|---|
| 297 | 200 | 487 | 249 | 0.0115 | 0.0102 |
| 339 | 250 | 487 | 295 | 0.0125 | 0.0111 |
| 382 | 300 | 487 | 341 | 0.0136 | 0.0121 |
| 425 | 350 | 487 | 388 | 0.0148 | 0.0132 |
| 469 | 400 | 487 | 435 | 0.0161 | 0.0144 |
| 514 | 450 | 487 | 482 | 0.0175 | 0.0156 |
| 559 | 500 | 487 | 529 | 0.0191 | 0.0170 |
| 604 | 550 | 487 | 577 | 0.0207 | 0.0185 |
| 650 | 600 | 487 | 625 | 0.0225 | 0.0201 |
| 696 | 650 | 487 | 673 | 0.0244 | 0.0217 |
| 742 | 700 | 487 | 721 | 0.0263 | 0.0235 |
| 789 | 750 | 487 | 770 | 0.0285 | 0.0254 |

Note:
[1] For conservatism, approximately 90% of the calculated effective conductivity values are considered in the model.

## 27. Axial Effective Conductivities for Bottom Shield Plug and Top Inner Cover Plate

(See Section A.3.3.1.3 for calculation of effective properties)

**Top inner cover plate for all DSC types except 24PT4**

Plate thickness = 0.75 in
Gap thickness = 0.0625 in
Two axial gaps

| Temp (°F) | k_SS304 (Btu/hr-in-°F) | Temp (K) | k_air (W/m-K) | k_air (Btu/hr-in-°F) | k_eff (Btu/hr-in-°F) |
|---|---|---|---|---|---|
| 70 | 0.717 | 294.4 | 0.0257 | 0.0012 | 0.0086 |
| 100 | 0.725 | 311.1 | 0.0269 | 0.0013 | 0.0090 |
| 200 | 0.775 | 366.7 | 0.0308 | 0.0015 | 0.0103 |
| 300 | 0.817 | 422.2 | 0.0345 | 0.0017 | 0.0115 |
| 400 | 0.867 | 477.8 | 0.0381 | 0.0018 | 0.0127 |
| 500 | 0.908 | 533.3 | 0.0415 | 0.0020 | 0.0138 |
| 600 | 0.942 | 588.9 | 0.0449 | 0.0022 | 0.0149 |
| 700 | 0.983 | 644.4 | 0.0482 | 0.0023 | 0.0160 |
| 800 | 1.025 | 700.0 | 0.0514 | 0.0025 | 0.0171 |
| 900 | 1.058 | 755.6 | 0.0545 | 0.0026 | 0.0181 |
| 1,000 | 1.092 | 811.1 | 0.0576 | 0.0028 | 0.0191 |

**Bottom shield plug for all DSC types except 24PT4**

Plate thickness = 3 in
Gap thickness = 0.0625 in
Two axial gaps

| Temp (°F) | k_A36 (Btu/hr-in-°F) | Temp (K) | k_air (W/m-K) | k_air (Btu/hr-in-°F) | k_eff (Btu/hr-in-°F) |
|---|---|---|---|---|---|
| 70 | 2.275 | 294.4 | 0.0257 | 0.0012 | 0.030 |
| 100 | 2.300 | 311.1 | 0.0269 | 0.0013 | 0.032 |
| 200 | 2.317 | 366.7 | 0.0308 | 0.0015 | 0.037 |
| 300 | 2.275 | 422.2 | 0.0345 | 0.0017 | 0.041 |
| 400 | 2.208 | 477.8 | 0.0381 | 0.0018 | 0.045 |
| 500 | 2.142 | 533.3 | 0.0415 | 0.0020 | 0.049 |
| 600 | 2.075 | 588.9 | 0.0449 | 0.0022 | 0.053 |
| 700 | 2.008 | 644.4 | 0.0482 | 0.0023 | 0.056 |
| 800 | 1.933 | 700.0 | 0.0514 | 0.0025 | 0.060 |
| 900 | 1.858 | 755.6 | 0.0545 | 0.0026 | 0.063 |
| 1,000 | 1.758 | 811.1 | 0.0576 | 0.0028 | 0.067 |

## 28. Axial Effective Conductivities for Cover Plates of 24PT4 DSC

(See Section A.3.3.1.3 for calculation of effective properties)

**Top outer cover plate for 24PT4 DSC**

Plate thickness = 1.25 in
Gap thickness = 0.0625 in
One axial gap

| Temp (°F) | k_SS316 (Btu/hr-in-°F) | Temp (K) | k_air (W/m-K) | k_air (Btu/hr-in-°F) | k_eff (Btu/hr-in-°F) |
|---|---|---|---|---|---|
| 70 | 0.642 | 294.4 | 0.0257 | 0.0012 | 0.025 |
| 100 | 0.658 | 311.1 | 0.0269 | 0.0013 | 0.026 |
| 200 | 0.700 | 366.7 | 0.0308 | 0.0015 | 0.030 |
| 300 | 0.750 | 422.2 | 0.0345 | 0.0017 | 0.033 |
| 400 | 0.792 | 477.8 | 0.0381 | 0.0018 | 0.037 |
| 500 | 0.833 | 533.3 | 0.0415 | 0.0020 | 0.040 |
| 600 | 0.875 | 588.9 | 0.0449 | 0.0022 | 0.043 |
| 700 | 0.917 | 644.4 | 0.0482 | 0.0023 | 0.046 |
| 800 | 0.958 | 700.0 | 0.0514 | 0.0025 | 0.049 |

**Bottom inner cover plate for 24PT4 DSC**

Plate thickness = 2 in
Gap thickness = 0.0625 in [1]
One axial gap

| Temp (°F) | k_SS316 (Btu/hr-in-°F) | Temp (K) | k_air (W/m-K) | k_air (Btu/hr-in-°F) | k_eff (Btu/hr-in-°F) |
|---|---|---|---|---|---|
| 70 | 0.642 | 294.4 | 0.0257 | 0.0012 | 0.038 |
| 100 | 0.658 | 311.1 | 0.0269 | 0.0013 | 0.040 |
| 200 | 0.700 | 366.7 | 0.0308 | 0.0015 | 0.046 |
| 300 | 0.750 | 422.2 | 0.0345 | 0.0017 | 0.051 |
| 400 | 0.792 | 477.8 | 0.0381 | 0.0018 | 0.056 |
| 500 | 0.833 | 533.3 | 0.0415 | 0.0020 | 0.061 |
| 600 | 0.875 | 588.9 | 0.0449 | 0.0022 | 0.066 |
| 700 | 0.917 | 644.4 | 0.0482 | 0.0023 | 0.071 |
| 800 | 0.958 | 700.0 | 0.0514 | 0.0025 | 0.075 |

Note: [1] The axial gap between the bottom inner cover plate and the bottom shield plug is integrated in the axial effective conductivity for bottom shield plug as well. Considering this additional gap for the bottom inner cover maximizes the DSC shell temperature in the radial direction and is therefore conservative for steady state analysis.

## 29. Axial Effective Conductivities for Lead Shield Plugs of 24PT4 DSC

(See Section A.3.3.1.3 for calculation of effective properties)

**Top shield plug for 24PT4 DSC**

Plate thickness = 3.38 in
Gap thickness = 0.025 in
Two axial gaps

| Temp (°F) | k_lead (Btu/hr-in-°F) | Temp (K) | k_air (W/m-K) | k_air (Btu/hr-in-°F) | k_eff (Btu/hr-in-°F) |
|---|---|---|---|---|---|
| -100 | 1.767 | 200 | 0.0182 | 0.0009 | 0.0582 |
| -10 | 1.733 | 250 | 0.0223 | 0.0011 | 0.0706 |
| 80 | 1.700 | 300 | 0.0261 | 0.0013 | 0.0820 |
| 260 | 1.637 | 400 | 0.0330 | 0.0016 | 0.1024 |
| 440 | 1.579 | 500 | 0.0395 | 0.0019 | 0.1206 |
| 620 | 1.512 | 600 | 0.0456 | 0.0022 | 0.1371 |

**Bottom shield plug for 24PT4 DSC**

Plate thickness = 2.88 in
Gap thickness = 0.025 in
Two axial gaps

| Temp (°F) | k_lead (Btu/hr-in-°F) | Temp (K) | k_air (W/m-K) | k_air (Btu/hr-in-°F) | k_eff (Btu/hr-in-°F) |
|---|---|---|---|---|---|
| -100 | 1.767 | 200 | 0.0182 | 0.0009 | 0.0500 |
| -10 | 1.733 | 250 | 0.0223 | 0.0011 | 0.0607 |
| 80 | 1.700 | 300 | 0.0261 | 0.0013 | 0.0706 |
| 260 | 1.637 | 400 | 0.0330 | 0.0016 | 0.0883 |
| 440 | 1.579 | 500 | 0.0395 | 0.0019 | 0.1042 |
| 620 | 1.512 | 600 | 0.0456 | 0.0022 | 0.1187 |

## 30. Effective Conductivities for TC Slide Rail

(See Section A.3.3.1.3 for calculation of effective properties)

Slide rail thickness = 0.12 in
Gap thickness = 0.01 in

| Temp (°F) | k_SS304 (Btu/hr-in-°F) | Temp (K) | k_He (W/m-K) | k_He (Btu/hr-in-°F) | k_eff (Btu/hr-in-°F) |
|---|---|---|---|---|---|
| 70 | 0.717 | 294.4 | 0.1482 | 0.0071 | 0.076 |
| 100 | 0.725 | 311.1 | 0.1533 | 0.0074 | 0.079 |
| 200 | 0.775 | 366.7 | 0.1697 | 0.0082 | 0.087 |
| 300 | 0.817 | 422.2 | 0.1861 | 0.0090 | 0.095 |
| 400 | 0.867 | 477.8 | 0.2038 | 0.0098 | 0.104 |
| 500 | 0.908 | 533.3 | 0.2236 | 0.0108 | 0.113 |
| 600 | 0.942 | 588.9 | 0.2429 | 0.0117 | 0.122 |
| 700 | 0.983 | 644.4 | 0.2610 | 0.0126 | 0.131 |
| 800 | 1.025 | 700.0 | 0.2781 | 0.0134 | 0.139 |
| 900 | 1.058 | 755.6 | 0.2945 | 0.0142 | 0.147 |
| 1,000 | 1.092 | 811.1 | 0.3104 | 0.0149 | 0.154 |

31. Effective Conductivity of Internal Sleeve
(See Section A.3.3.1.3 for calculation of effective properties)

| Temperature | $k_{Al}$ [1] | $k_{He}$ [2] | $k_{eff,axl,1}$ | $k_{eff,axl}$ | $k_{eff,rad}$ |
|---|---|---|---|---|---|
| (°F) | (Btu/hr-in-°F) | (Btu/hr-in-°F) | (Btu/hr-in-°F) | (Btu/hr-in-°F) | (Btu/hr-in-°F) |
| 70 | 8.008 | 0.0071 | 1.894 | 1.808 | 7.646 |
| 100 | 8.075 | 0.0074 | 1.947 | 1.859 | 7.710 |
| 150 | 8.167 | 0.0077 | 2.030 | 1.938 | 7.798 |
| 200 | 8.250 | 0.0081 | 2.111 | 2.016 | 7.878 |
| 250 | 8.317 | 0.0085 | 2.190 | 2.091 | 7.941 |
| 300 | 8.383 | 0.0090 | 2.276 | 2.173 | 8.005 |
| 350 | 8.442 | 0.0094 | 2.362 | 2.255 | 8.061 |
| 400 | 8.492 | 0.0098 | 2.445 | 2.335 | 8.109 |

Notes:
[1] See Section A.3.2.1 material # 10 for the lowest aluminum properties.
[2] Interpolated / extrapolated between data in Section A.3.2.1 material # 15 for helium.

Thermal radiation at the external surfaces of the packaging is considered for thermal analysis. The outer surface of the cask shield shell is painted white. Reference [22] gives an emissivity between 0.92 and 0.96 and a solar absorptivity between 0.09 and 0.23 for white paints. To account for dust and dirt and to bound the problem, the thermal analysis uses a solar absorptivity of 0.3 and an emissivity of 0.9 for the white painted surfaces.

The outer surfaces of the impact limiter shells are uncoated stainless steel. An emissivity of 0.587 is considered for these surfaces based on [15]. Solar absorptance values of 0.39 and 0.47 are given in [34] for rolled and machined stainless steel plates. For conservatism, it is assumed that the solar absorptivity of stainless steel is equal to emissivity.

The emissivity of rolled stainless steel plates is 0.578 as considered in [15]. The emissivity for rolled steel sheets is 0.657 as reported in [5], Table 10-17. The transport cask inner shell is stainless steel clad. The emissivity value of 0.587 is considered for both the DSC shell (stainless steel) and the transport cask inner shell (stainless steel clad) in the calculation of thermal radiation exchange between these shells.

The emissivity of anodized aluminum is between 0.84 and 0.72 for temperatures between 296K and 484K (between 73°F and 411°F) and its solar absorptivity is between 0.12 and 0.16 ([21], Table A.7.2). An emissivity of 0.70 and a solar absorptivity of 0.16 are considered for the finned aluminum shell of MP197HB cask in this analysis.

After a fire, the cask outer surfaces will be partially covered in soot. Based on [22], emissivity and solar absorptivity of soot are 0.95. The HAC thermal analysis conservatively assumes an absorptivity of 1.0 and an emissivity of 0.9 for the post fire, cool-down period.

Various ASME code years are called for various DSCs in the MP197HB TC. Except for 24PT4, the other DSC types are covered by ASME code from 1998 to 2006 as shown in the following table.

**Applicable Code Years for Each Canister Design**

| Canister Design | Applicable Storage License | ASME B&PV Code Year |
|---|---|---|
| NUHOMS® 32PTH | 1030 | 1998 w/ 2000 Addenda |
| NUHOMS® 32PTH1 | 1004 | 1998 w/ 2000 Addenda |
| NUHOMS® 37PTH | *Note (1)* | 2004 w/2006 Addenda |
| NUHOMS® 69BTH | *Note (1)* | 2004 w/2006 Addenda |
| NUHOMS® 24PT4 | 1029 | 1992 thru1994 Addenda |
| NUHOMS® 24PTH | 1004 | 1998 w/ 2000 Addenda |
| NUHOMS® 32PT | 1004 | 1998 w/ 2000 Addenda |
| NUHOMS® 61BT | 1004 | 1998 w/ 1999 Addenda |
| NUHOMS® 61BTH | 1004 | 1998 w/ 2000 Addenda |
| NUHOMS® 61BTH *with failed fuel (61BTHF)* | *Note (1)* | 2004 w/2006 Addenda |
| NUHOMS® 24PTH *with failed fuel (24PTHF)* | *Note (1)* | 2004 w/2006 Addenda |

*Note (1): These DSCs are currently not a part of CoC 1004 but will be added at a later date via amendment.*

The shell and cover plates of all DSC types except for 24PT4 consist of stainless steel SA-240, type 304 (SS304). There are no changes in thermal conductivity of SS304 in ASME 1998 to 2006 in temperature range from 70 to 700°F. This range properly covers the DSC shell temperature for all DSC types in this calculation.

The shield plugs of all DSC types except for 24PT4 consist of carbon steel A36. The changes in the A36 conductivity between ASME code years 1998 to 2006 are limited to ±0.9%. This small change has no significant effect on the thermal evaluation.

The thermal properties for 24PT4 DSC are taken from UFSAR for standardized advanced NUHOMS® system [2]. These properties are based on ASME code 1992 through 1994 addenda and used in this calculation without any changes.

### A.3.2.2 Component Specifications

The components for which thermal technical specification are necessary are the MP197HB containment seals and poison plates used in DSC basket.

#### A.3.2.2.1 MP197HB TC

The seals used in the packaging are the Fluorocarbon seals (Viton O-rings). The seals will have a minimum and maximum temperature rating of -40°F and 400°F, respectively.

#### A.3.2.2.2 69BTH DSC

The 69BTH DSC design allows the use of different neutron absorber materials based on the heat load zoning configuration (HLZC). Boral, Metal Matrix Composite (MMC), or Borated Aluminum can be used as poison materials for HLZC # 1, # 2 and # 3 in 69BTH basket. For 69BTH basket with HLZC # 4, only borated aluminum can be used as poison material. The HLZCs for 69BTH are described in Section A.3.3.1.4

#### A.3.2.2.3 37PTH DSC

The 37PTH DSC design allows the use of different neutron absorber materials. Boral plates paired with Al1100 plates or single plates of metal matrix composite (MMC) or

borated aluminum can be used as poison materials in 37PTH basket with 22 kW heat load.

The following table summarizes the poison material configuration allowed for 69BTH and 37PTH basket designs:

**Heat Load Zoning Configurations for 69BTH and 37PTH DSCs in MP197HB**

| | DSC type | HLZC | Poison Material | Max. Heat Load (kW) |
|---|---|---|---|---|
| 1 | 69BTH | 1 or 2 | Boral / MMC / Borated Aluminum | 26.0 |
| 2 | 69BTH | 3 | Boral / MMC / Borated Aluminum | 29.2 |
| 3 | 69BTH | 4 | Borated Aluminum | 32.0 |
| 4 | 37PTH | --- | Boral Paired Al / Single MMC/Borated Al | 22 |

The neutron absorber materials in 69BTH and 37PTH baskets are subjected to the following minimum thermal conductivity, which are used in the canister thermal analyses.

**Minimum Conductivity of Poison Material**

| Boral Core Matrix | | | |
|---|---|---|---|
| Temperature (°F) | Conductivity (W/cm-K) [26] | Conductivity (Btu/hr-in-°F) | 90% Conductivity[1] (Btu/hr-in-°F) |
| 100 | 0.859 | 4.136 | 3.723 |
| 500 | 0.768 | 3.698 | 3.328 |
| Metal Matrix Composite (MMC) | | | |
| Temperature (°F) | Conductivity (Btu/min-in-°F), | Conductivity (Btu/hr-in-°F) | |
| | | | |
| All temperatures | 0.0964 [3] | 5.78 | |
| Borated Aluminum | | | |
| Temperature (°F) | Conductivity (Btu/min-in-°F) [3] | Conductivity (Btu/hr-in-°F) | |
| 68 | 0.123 | 7.38 | |
| 212 | 0.132 | 7.92 | |
| 392 | 0.141 | 8.46 | |
| 482 | 0.145 | 8.70 | |

Note: [1] The conductivity of Boral core is reduced by 10% and used in thermal analysis

## A.3.3 Thermal Evaluation under Normal Conditions of Transport

The NCT ambient conditions are used for the determination of the maximum fuel cladding temperature, the maximum MP197HB TC and DSC temperatures, the containment pressure, and the thermal stresses. These steady state environmental conditions correspond to maximum daily averaged ambient temperature of 100°F and to 10 CFR 71.71(c)(1) [6] insolation averaged over a 24 hour period.

Ambient conditions for NCT are taken from 10 CFR 71 [6] and applied to the boundaries of the cask model. These conditions are listed in the following table.

**Normal Conditions of Transport**

| Case # | Ambient temperature (°F) | Insolance | Purpose |
|---|---|---|---|
| 1 | 100 | Yes | Maximum Component Temperatures |
| 2 | -20 | No | Cold conditions for Structural Analysis |
| 3 | -40 | No | Maximum Thermal Stress |
| 4 | 100 | No | Maximum Accessible Surface Temperature |

Except for DSC types 69BTH and 37PTH, all other DSC types considered for transport in MP197HB TC are analyzed for storage/transfer conditions under 10 CFR 72 [8]. The safety analysis reports (SAR) for these DSC types under storage/transfer conditions are presented in [1], [2], [3], and [4].

### A.3.3.1 Thermal Models

The MP197HB TC loaded with a DSC is analyzed based on finite element models developed using the ANSYS computer code [27]. ANSYS is a comprehensive thermal, structural and fluid flow analysis package. ANSYS is capable of solving steady state and transient thermal analysis problems in one, two, or three dimensions. Heat transfer via a combination of conduction, radiation, and convection can be modeled by ANSYS.

Three finite element models are developed for analyses of the MP197HB TC loaded with DSC.

a) A half-symmetric, three-dimensional finite element model of the MP197HB TC is developed using ANSYS [27], version 8.1. The model contains the cask shells, cask bottom plate, cask lid, impact limiters, DSC shell, and DSC end plates without the basket. The DSC dimensions correspond to nominal DSC dimensions listed in Table A.3–1 for variations of the MP197HB model. SOLID70 elements are used to model the components including the gaseous gaps. Impact limiter gussets, cask slide rails, and trunnion plug plates are modeled using SHELL57 elements. Surface elements SURF152 are used for applying the insolation boundary conditions.

b) A half-symmetric, three-dimensional finite element model of the 69BTH basket and DSC is developed using ANSYS [27], version 8.1. The model contains the DSC shell, the DSC cover plates, shield plugs, aluminum rails, basket plates, and homogenized fuel assemblies. Only SOLID70 elements are used in the 69BTH DSC/basket model.

c) A three-dimensional finite element model of the 37PTH DSC/basket model is developed using ANSYS [27], version 8.1. The model contains the DSC shell, the DSC cover plates, shield plugs, aluminum rails, basket plates, and homogenized fuel assemblies. Only SOLID70 elements are used in the 37PTH DSC/basket model.

The DSC shell temperatures for NCT are retrieved from the MP197HB transport cask model and transferred to the DSC/basket models to evaluate the maximum fuel cladding and basket component temperatures. The models are run with steady state conditions for NCT evaluations.

The nominal dimensions with the following gaps are used to develop the finite element models.

A.3.3.1.1 MP197HB TC Model

The following assumptions are considered in the MP197HB TC model:

- DSC types without spacer are centered axially in the transport cask. For DSC types with the spacer, a 0.5" gap is considered between the DSC outer top cover plate and the cask lid. These assumptions reduce the axial heat transfer and maximize the DSC shell temperatures, which in turn result in higher fuel cladding temperatures.
- Heat load is simulated by heat flux distributed uniformly over the basket length on the radial inner surface of the DSC shell.
- Since the transfer operation occurs in horizontal position, the lower halves of the cask cylindrical surfaces are not exposed to insolance. No solar heat flux is considered over these surfaces. To remove any uncertainty about the solar impact on the vertical surfaces, the entire surface areas of vertical surfaces are considered for application of the solar heat flux.
- For the cask with optinal external fins, insolance is applied only over the radial surfaces of the shield shell and fins. Insolance over the vertical surfaces of the fins is ignored. This approach is justified since the shadow of the exposed fins covers most of the other fins and the cask outer surface.
- No convection is considered within the cask cavity.
- No convection is considered between the cask ends and the thermal shields.
- No heat transfer is considered within the bearing block.
- No heat transfer is considered through spacers used at the bottom of TC for short DSC types.
- Heat dissipations from lateral surfaces of the skid straps, inner radial surface of impact limiter recess, thermal shield outer rings, and neutron shield end caps are conservatively neglected.
- No thermal radiation to ambient is considered for the cask surfaces in contact with the transport skid saddles.

- Radiation heat exchange is considered between the DSC and the cask inner shell/internal sleeve by calculating effective conductivities for helium in this region.

The following gaps are considered in the MP197HB TC model:

a) 0.0625" axial gap between thermal shield and impact limiter shell,
b) 0.0625" axial gap between thermal shield standoffs and the cask top or bottom end surfaces,
c) 0.10" diametrical gap between cask lid and cask inner shell,
d) 0.01" axial gap between cask lid and cask flange,
e) 0.01" axial gap between ram closure plate and cask bottom plate,
f) 0.01" radial gaps between neutron shield boxes and surrounding shells,
g) 0.025" radial gap between gamma shield and cask outer shell,
h) 0.01" radial gaps between the cask inner shell and aluminum sleeve,
i) 0.01" radial gap between the finned aluminum shell and the cask shield shell,
j) 0.0625" axial gaps between the DSC bottom shield plug and bottom cover plates,
k) 0.0625" axial gaps between the DSC top inner cover and the adjacent top shield plug and top outer cover plate,
l) 0.025" axial gaps between the lead shield plugs and encapsulating plates for 24PT4 DSC,
m) 0.01" gaps between trunnion replacement plugs and the trunnion attachment blocks.

The 0.0625" gaps between thermal shield, impact limiter shell, and cask top or bottom end surfaces are based on the main SAR, Section 3.4.1.1 assumptions and account for the 0.06" thick weld overlay conservatively.

The 0.01" gap between cask lid/ cask flange and ram closure plate/cask bottom plate account for thermal resistance between bolted components. The 0.01" radial gaps between the neutron shield boxes and the surrounding shells is also based on main SAR, Section 3.4.1.1 assumptions.

The gap of 0.025" assumed between gamma shield and cask outer shell is justified in Section A.3.6.7.1.

The radial gap of 0.01" assumed between the finned aluminum shell and the cask shield shell is justified in Section A.3.6.7.2.

The 0.0625" and 0.025" axial gaps between DSC end plates maximize the radial heat transfer through DSC shell toward the cask to bound the maximum component temperatures conservatively.

The width of TC slide rail is 3". For conservatism, a gap of 0.01" with a contact width of 0.12" is considered between the TC slide rails and the DSC shell at 168° and 192° orientations. The 0° orientation is located at the top of the horizontal TC as shown in Chapter A.1, the drawings in Appendix A.1.4.10.

The finned shell is divided into three axial sections with one inch distance between adjacent sections. No finned shell is considered over the trunnion plugs in the model. Since the finned shell is designed as a continuous shell which covers the trunnion plugs, the model which has fewer fins is conservative for thermal analysis of transport cask under NCT.

The nominal dimensions considered for DSCs in MP197HB model are listed in Table A.3–1. For each basket type, the shortest cavity length is considered for the analysis to bound the maximum decay heat flux.

To provide thermal input for structural evaluation, a heat load of 23.2 kW (along with 22.0 kW) is considered for the 37PTH DSC. Since the heat load of 23.3 kW is higher than the design heat load of 22.0 kW, this assumption is conservative for the structural evaluation of the 37PTH DSC.

Decay heat load is applied as a uniform heat flux over the inner surface of the DSC shell covering the basket length. The decay heat flux applied in the TC model is calculated as follows.

$$q'' = \frac{Q}{\pi D_i L_b}$$

q" = decay heat flux (Btu/hr-in$^2$)
Q = decay heat load (Btu/hr) (to convert from kW multiply by 3412.3)
$D_i$ = DSC inner diameter (in)
$L_b$ = Basket length (in)

The applied decay heat values in the model are listed below.

**DSC Decay Heat Flux**

| DSC Type | Heat Load (kW) | (Btu/hr) | $D_i$ (in) | $L_b$ (in) | Decay heat flux (Btu/hr-in$^2$) |
|---|---|---|---|---|---|
| 69BTH | 26.0 | 88,720 | 68.75 | 164 | 2.505 |
| | 29.2 | 99,639 | | | 2.813 |
| | 32.0 | 109,194 | | | 3.083 |
| 61BTH Type 1 [1] | 22.0 | 75,071 | 66.25 | 164 | 2.199 |
| 61BTH Type 2 [1] | 24.0 | 81,895 | 66.25 | 164 | 2.399 |
| 61BT | 18.3 | 62,445 | 66.25 | 164 | 1.829 |
| 37PTH | 22.0 | 75,071 | 68.75 | 162 | 2.146 |
| 32PTH / 32PTH Type 1 | 26.0 | 88,720 | 68.75 | 162 | 2.536 |
| 32PTH1 Type 1 | 26.0 | 88,720 | 68.75 | 162 | 2.536 |
| 32PTH1 Type 2 | 24.0 | 81,895 | 68.75 | 162 | 2.341 |
| 32PT | 24.0 | 81,895 | 66.19 | 166.10 | 2.371 |
| 24PTH (all types)[1] [2] | 26.0 | 88,720 | 66.19 | 168.60 | 2.531 |
| 24PT4 | 24.0 | 81,895 | 66.19 | 179.13 | 2.199 |

Notes:
[1] DSC types 61BTHF and 24PTHF has the same dimensions and heat loads as DSC types 61BTH and 24PTH, respectively.
[2] The allowable heat load for 24PTH-S-LC DSC is 24 kW. A heat load of 26 kW is assumed conservatively in the analysis for 24PTH-S-LC.

Radiation and conduction between the DSC and the TC inner shell / internal sleeve is considered by calculating effective conductivities for helium gaps between the components listed above. Calculation of the helium effective conductivity within this gap is described in Section A.3.3.1.3.

Insolance is applied as a heat flux over the TC outer surfaces using average insolence values from 10 CFR 71 [6]. The insolance values are averaged over 24 hours and multiplied by the surface absorptivity factor to calculate the solar heat flux. The solar heat flux values used in the MP197HB TC model are summarized below.

**Solar Heat Flux**

| Surface Material | Shape | Insolance over 12 hrs[6] (gcal/cm$^2$) | Solar Absorptivity | Total solar heat flux averaged over 24 hrs (Btu/hr-in$^2$) |
|---|---|---|---|---|
| Stainless Steel | Curved | 400 | 0.587 [(1)] | 0.2505 |
| | Flat vertical | 200 | 0.587 [(1)] | 0.1252 |
| White Paint (shield shell) | Curved | 400 | 0.30 | 0.1280 |
| Anodized Aluminum | Curved | 400 | 0.16 | 0.0683 |
| Plain aluminum | Flat vertical | 200 | 0.10 | 0.0213 |

Note: [(1)] Solar absorptivity of stainless steel is taken equal to its emissivity. See Section A.3.2.1 for justification.

The cask external fins are not considered explicitly in the TC model. Instead, an effective heat transfer coefficient is applied over the outer surface of the un-finned aluminum shell to simulate the heat dissipation from this area. The methodology to calculate the effective heat transfer coefficient for external fins is described in Section A.3.3.1.3.

Convection and radiation heat transfer from the un-finned cask surfaces are combined together as total heat transfer coefficients. The total heat transfer coefficients are calculated using free convection correlations from Rohsenow Handbook [21] and are incorporated in the model using ANSYS macros. The ANSYS macros used in this calculation are listed in Appendix A.3.6.1.

The total heat transfer coefficient, $h_t$, is used to combine the convection and radiation heat transfer together.

$$h_t = h_r + h_c$$

Where,

$h_r$ = radiation heat transfer coefficient (Btu/hr-in$^2$-°F)

$h_c$ = free convection heat transfer coefficient (Btu/hr-in$^2$-°F)

The radiation heat transfer coefficient, $h_r$, is given by the equation:

$$h_r = \varepsilon F_{w\infty} \left[ \frac{\sigma(T_w^4 - T_{amb}^4)}{T_w - T_{amb}} \right] \quad \text{Btu/hr-in}^2\text{-°F}$$

Where,

$\varepsilon$ = surface emissivity
$F_{12}$ = view factor from surface 1 to ambient = 1
$\sigma$ = $0.1714 \times 10^{-8}$ Btu/hr-ft$^2$-°R$^4$
$T_w$ = surface temperature (°R)
$T_{amb}$ = ambient temperature (°R)

Surface emissivity values are discussed in Section A.3.2.1.

The natural convection coefficients are calculated using handbook correlations [21] and are incorporated in the model using ANSYS macros. These correlations are described below.

**For horizontal cylinders:**

$$Ra = Gr\ \mathrm{Pr} \quad ; \quad Gr = \frac{g\,\beta\,(T_w - T_\infty)\,D^3}{\nu^2}$$

$$Nu_l = \frac{2f}{\ln(1 + 2f / Nu^T)} \text{ with}$$

$$Nu^T = 0.772\,\overline{C}_l\,Ra^{1/4} \quad ; f = 1 - \frac{0.13}{(Nu^T)^{0.16}};\ \overline{C}_l = 0.515 \text{ for gases [21]}$$

$$Nu_t = \overline{C}_t\,Ra^{1/3}$$

$\overline{C}_t = 0.103$ for air with Pr ≈ 0.71 [21]

$$Nu = \left[(Nu_l)^m + (Nu_t)^m\right]^{1/m} \qquad with \quad m = 10 \quad for \quad 10^{-10} < Ra < 10^7$$

$$h_c = \frac{Nu\,k}{D}$$

The above correlations are incorporated in ANSYS model via macro "HTOT_HCL.mac" listed in Section A.3.6.1.

**For vertical flat surfaces:**

$$Ra = Gr\ \mathrm{Pr} \quad ; \quad Gr = \frac{g\,\beta\,(T_w - T_\infty)\,L^3}{\nu^2}$$

$$Nu_l = \frac{2.0}{\ln(1 + 2.0 / Nu^T)} \text{ with}$$

$$Nu^T = \overline{C}_l\,Ra^{1/4}\ ;\ \overline{C}_l = 0.515 \text{ for gases [21]}$$

$$Nu_t = C_t^V\,f\,Ra^{1/3} / \left(1 + 1.4 \times 10^9\ \mathrm{Pr}/Ra\right) \quad \text{with}$$

$$C_t^V = \frac{0.13\,\mathrm{Pr}^{0.22}}{(1 + 0.61\,\mathrm{Pr}^{0.81})^{0.42}} \qquad f = 1.0 + 0.078\left(\frac{T_w}{T_\infty} - 1\right)$$

$$Nu = \left[(Nu_l)^m + (Nu_t)^m\right]^{1/m} \qquad with \quad m = 6 \quad for \quad 1 < Ra < 10^{12}$$

$$h_c = \frac{Nu\, k}{L}$$

The above correlations are incorporated in ANSYS model via macro "HTOT_VPL.mac" listed in Section A.3.6.1.

**For horizontal flat surfaces facing downwards:**

The following correlations are used only for the outer surface of the bearing block at the lower half of the TC.

$$Ra = Gr\ \mathrm{Pr} \quad ; \quad Gr = \frac{g\,\beta(T_w - T_\infty)(L^*)^3}{\nu^2}$$

$$Nu_l = \frac{2.5}{\ln(1 + 2.5/Nu^T)} \qquad \text{with}$$

$$Nu^T = \frac{0.527}{\left(1 + (1.9/\mathrm{Pr})^{9/10}\right)^{2/9}}\ Ra^{1/5}$$

$$Nu = Nu_l \qquad for \quad 10^3 < Ra < 10^{10}$$

$$h_c = \frac{Nu\, k}{L^*}$$

The above correlations are incorporated in ANSYS model via macro "HTOT_HPD.mac" listed in Section A.3.6.1.

The following parameters are used in the above correlations.

g = gravitational constant = 9.81 ($m/s^2$)
β = expansion coefficient = 1/T (1/K)
T = absolute temperature (K)
ν = kinematic viscosity ($m^2/s$)
L = height of the vertical surface (in)

D = diameter of the horizontal cylinder (in)

$$L^* = \frac{A}{p} = \frac{heated\ area}{heated\ perimeter} = 1.2''$$ (shortest surface of bearing block)

k = air conductivity (W/m-K)

During transportation, the DSC shell rests on four slide rails in the TC. These rails are Nitronic 60 stainless steel plates welded to the inner shell of the TC. The thickness of the slide rail is 0.12" when no internal sleeve is used. The slide rail at the 180° orientation is 0.06" thick and is not in contact with the DSC shell. The same configuration is considered for the small diameter DSC and the internal sleeve.

The angle between the lower rail and the vertical plane is 12 degree. Considering this configuration as shown in Figure A.3–1, the distance between the centerline of the DSC and the centerline of the cask is calculated as follows.

$$R_2^2 = R_1^2 + x^2 - 2R_1 x\,Cos(\alpha)$$

With,

$R_1 = D_{i,\,TC}/2 - t_{rail}$
$R_2 = D_{o,\,DSC}/2$
$\alpha = 12°$
x = Distance between the DSC and TC centerlines
$D_{i,\,TC}$ = Inner diameter of TC or internal sleeve
$D_{o,\,DSC}$ = DSC outer diameter
$t_{rail}$ = cask slide rail thickness = 0.12″

The calculated values for x are listed in the following table. In the ANSYS model, the DSC is shifted down by the amount of x in the Cartesian y-direction within the TC cavity.

**Distance between DSC and TC Centerlines**

| DSC Type | $D_{i,TC}$ (in) | $D_{o,DSC}$ (in) | $R_1$ (in) | $R_2$ (in) | α (degree) | x (in) |
|---|---|---|---|---|---|---|
| 69BTH<br>37PTH<br>32PTH<br>32PTH1 | 70.5 | 69.75 | 35.130 | 34.875 | 12 | 0.261 |
| 61BT<br>61BTH<br>61BTHF | 68 | 67.25 | 33.880 | 33.625 | 12 | 0.261 |
| 32PT<br>24PTH<br>24PTHF<br>24PT4 | 68 | 67.19 | 33.880 | 33.595 | 12 | 0.291 |

To simplify the model, the lower cask slide rails at 168° and 192° orientations are modeled using shell elements with the conductivity of Nitronic 60 and a helium gap of 0.01″. The effects of the other cask slide rails are conservatively omitted. The slide rail width is 3″. For conservatism, a contact width of 0.12″ is considered between the lower rails and the DSC shell.

The axial gaps considered between DSC cover plates and shield plugs are integrated into bottom shield plug and top inner cover plates. The axial gaps considered for the lead shield plugs of 24PT4 are also integrated into the shield plug material. The axial effective conductivities are calculated for these components in Section A.3.3.1.3. The conductivity in radial direction remained unchanged and equal to the conductivity of the corresponding material.

To reduce the complexity of the model, effective conductivities are calculated for the internal sleeve in axial and radial directions. The methodology to calculate the effective conductivity of the internal sleeve is described in Section A.3.3.1.3. These effective

conductivities are conservative since the number and the assumed gaps between the internal sleeve pieces are larger than those considered for the proposed internal sleeve.

The material properties used in the MP197HB model are listed in Section A.3.2.1.

The seal o-rings are not explicitly considered in the models. The maximum seal temperatures are retrieved from the models by selecting the nodes at the locations of the corresponding seal o-rings.

The geometry of the TC model and the gaps are shown in Figure A.3–2 through Figure A.3–5. Mesh sensitivity of the MP197HB model is discussed in Appendix A.3.6.2.1.

Typical boundary conditions for TC model under NCT are shown in Figure A.3–6 through Figure A.3–8.

#### A.3.3.1.2 Calculation of Maximum Accessible Surface Temperature

A personnel barrier installed on the transport skid between the two impact limiters of MP197HB TC limits the accessible packaging surfaces to the impact limiter and barrier outer surfaces. The personnel barrier has an open area of at least 80%. Radiation heat transfer between the cask and the barrier will be minimal due to the small radiation view factor between the cask and the barrier. Due to large distance between the barrier and cask outer surface, the free convection heat transfer around TC remains undisturbed. The transport configuration is shown in the drawings in Chapter A.1, Appendix A.1.4.10.

The TC model described in Section A.3.3.1.1 is run without insolance to determine the accessible surface temperature of the impact limiters in the shade. A heat load of 32 kW and boundary conditions at 100°F and no insolance are considered in the cask model to bound the maximum accessible surface temperature under shade.

The maximum accessible surface temperature of impact limiters under these conditions is 121°F. The maximum temperature of the cask outer surface is 302°F and belongs to a part of shield shell uncovered by the external fins in the model. The maximum temperature of the personnel barrier is calculated based on the maximum temperature of the cask outer surface using the following methodology.

The personnel barrier is exposed to thermal radiation from the cask shield shell / finned shell and dissipates heat via thermal radiation and natural convection to ambient. Since the personnel barrier is far apart from the cask shield shell, it is not exposed to the hot air streams from the cask. *This assumption is justified in Section A.3.3.1.2.1.*

The heat balance for the personnel barrier is shown schematically in Figure A.3–9. The following conservative assumptions are considered to simplify the heat balance.

- Convection heat dissipation from the barrier is omitted completely.
- Radiation heat dissipation to ambient from barrier surfaces facing the cask is omitted.
- The maximum cask outer surface temperature is considered for the cask entire outer surface facing the barrier.
- An emissivity of 0.9 is considered for the cask outer surface. Based on discussion in Section A.3.2.1, the emissivities for shield shell and finned shell are

0.9 and 0.7, respectively. The assumed emissivity of 0.9 maximizes the radiation heat from the cask toward the personnel barrier conservatively.

The simplified heat balance for the personnel barrier is as follows.

$$q_{in,rad} = q_{out,rad}$$

$$q_{in,rad} = \frac{\sigma\left(T_{shell}^{\ 4} - T_{PB}^{\ 4}\right)}{\frac{1-\varepsilon_{shell}}{\varepsilon_{shell} A_{shell}} + \frac{1}{F_{PB-shell} A_{PB}} + \frac{1-\varepsilon_{PB}}{\varepsilon_{PB} A_{PB}}}$$

$q_{out,rad} = q_{1,rad,amb} + q_{2,rad,amb}$, $q_{1,rad,amb} = 0$ (conservatively, omitted in this analysis)

$$q_{2,rad,amb} = \frac{\sigma\left(T_{PB}^{\ 4} - T_{\infty}^{\ 4}\right)}{\frac{1-\varepsilon_{PB}}{\varepsilon_{PB} A_{PB}} + \frac{1}{F_{PB-\infty} A_{PB}}}$$

$\sigma$ = Stefan-Boltzmann constant = 0.119E-10 (Btu/hr-in$^2$-°R$^4$)
$T_{shell}$ = maximum cask shield shell temperature (°R)
$T_{PB}$ = maximum personnel barrier temperature (°R)
$T_{\infty}$ = ambient temperature = 100 °F = 560 °R
$\varepsilon_{shell}$ = emissivity of TC outer surface = 0.9
$\varepsilon_{PB}$ = emissivity of personnel barrier SS304 = 0.587 (see discussion in Section A.3.2.1)
$F_{PB\text{-}shell}$ = view factor from personnel barrier to cask shield shell
$F_{PB\text{-}\infty}$ = view factor from personnel barrier (not facing cask) to ambient = 1.0
$A_{PB}$ = surface area of personnel barrier (in$^2$)
$A_{shell}$ = surface area of cask shield shell (in$^2$)

The dimensions of the cask shield shell ($D_{shell}$) and personnel barrier ($l_{PB}$) are 97.75" and 52.38", respectively as shown in the drawings in Chapter A.1, Appendix A.1.4.10.

$$\frac{A_{shell}}{A_{PB}} = \frac{\pi D_{shell}/2}{l_{PB}} = \frac{\pi \times 97.75/2}{52.38} = 2.931$$

The view factor of a long strip element to a parallel cylinder is given in [21], Chapter7, Appendix B, Page 7.80 as follows. The dimensions are defined in Figure A.3–9.

$$F_{d1-2} = \frac{Y}{X^2 + Y^2}$$

With
Y = y/r, X = x/r
y = 58" (See the drawings in Appendix A.1.4.10)
r = 97.75/2 = 48.875" (See the drawings in Appendix A.1.4.10)

Integration of the above incremental view factor over the length of the strip barrier gives the view factor of the strip to the cask.

$$F_{1-2} = \frac{1}{l_{PB}} \int_0^{l_{PB}} \left( \frac{Y}{X^2 + Y^2} \right) dx$$

Considering $L=l_{PB}/r$ and $dX=dx/r$, gives the view factor of the personnel barrier to the cask.

$$F_{1-2} = \frac{1}{L} \int_0^{L} \left( \frac{Y}{X^2 + Y^2} \right) dX = \frac{1}{L} \left( \tan^{-1} \frac{L}{Y} \right) = \frac{r}{l_{PB}} \tan^{-1} \left( \frac{l_{PB}}{y} \right) = 0.685$$

Since the personnel barrier has an open area of 80%, a factor of 0.2 should be considered to calculate the view factor of the personnel barrier mesh to the cask.

$$F_{PB-shell} = F_{1-2} \times 0.2 = 0.137$$

The substitution of the above values in the heat balance of the personnel barrier gives the maximum temperature of the personnel barrier as 152°F.

An additional analysis is performed considering insolation for TC model with 32 kW heat load, 100°F ambient, and no external fins. Under these conditions, the maximum cask shield shell temperature is 335°F. Using the same methodology as described above gives a maximum personnel barrier temperature of 163°F.

*A.3.3.1.2.1 Personnel Barrier and Hot Stream from Cask*

*The assumption that the personnel barrier is not exposed to hot air stream from the cask shield shell can be justified by calculation of the thermal boundary layer thickness around the lower half of the cask. This calculation demonstrates that the thermal boundary layer thickness is smaller than the shortest distance between the personnel barrier and the cask and therefore the personnel barrier remains out of the hot air stream from the cask.*

*The large diameter of the cask and the relative large temperature difference between the cask outer surface and ambient temperature suggest that the free convection over the cylinder is a turbulent flow.*

*The theoretical and experimental studies of the free convection and its related thermal boundary layer thickness are widely available and well documented ([43], [45], [46], and [47]). These correlations can be used to determine the free convection thermal boundary layer thickness over the horizontal MP197HB cask. These studies show that the thickness of the free convection thermal boundary layer is inversely proportional to a power of the local Nusselt number for laminar or turbulent flows.*

$$\frac{\delta}{x} = \frac{C f(Pr)}{Nu_x^{\,m}} \qquad (1)$$

*$\delta$ = local thermal boundary layer thickness*
*x = local position*
*f(Pr) = a function of Prandtl number*
*$Nu_x$ = local Nusselt number*
*m and c = constant values*

*For instance, the theoretical calculation in reference [46] determines the following equation for a free convection laminar flow over flat vertical plates.*

$$\frac{\delta}{x} = \frac{2}{Nu_x}$$

*This equation means that c = 2, f(Pr) =1, and m = 1 in equation (1).*

*The correlations to determine the free convection thermal boundary layer thickness and local Nusselt number over a vertical flat plate in turbulent flow are documented in references [44] and [45]. These correlations are shown below.*

$$\frac{\delta_x}{x} = 0.565\, Gr_x^{-0.1}\, Pr^{-8/15} \left(1 + 0.494\, Pr^{2/3}\right)^{0.1} \qquad [44] \qquad (2)$$

$$Gr_x = \frac{g\beta\Delta T\, x^3}{\upsilon^2}$$

$$Nu_x = 0.0295 \left[\frac{Pr^7}{\left(1 + 0.494\, Pr^{2/3}\right)^6}\right]^{1/15} Gr_x^{2/5} \qquad [45]$$

$$Nu_L = 0.834\, Nu_x \qquad [45] \qquad (3)$$

*An examination of the above equations shows that the thermal boundary layer thickness is reversely proportional to the* $Nu_x^{0.25}$ *for turbulent free convection over a vertical flat plate.*

*Considering the relationship between the thermal boundary layer thickness and the local Nusselt number, the boundary layer thickness over a horizontal cylinder in free convection turbulent flow can be determined using the correlations over a vertical flat plate and the inverse ratio of the local Nusselt numbers. Since the correlations for the average Nusselt numbers of free convection for vertical flat plates and horizontal cylinders are known better than the local Nusselt numbers, the ratio of the local Nusselt numbers are extended to include the average Nusselt numbers and avoid elimination of any functions related to Prandtl number.*

$$\frac{\delta_{D0}}{\delta_x} = \frac{\delta_L}{\delta_x} \cdot \frac{\delta_D}{\delta_L} \cdot \frac{\delta_{D0}}{\delta_D}$$

$$\frac{\delta_{D0}}{\delta_x} = \left(\frac{Nu_x}{Nu_L}\right)^p \left(\frac{Nu_L}{Nu_D}\right)^q \left(\frac{Nu_D}{Nu_{D0}}\right)^r \qquad (4)$$

*$\delta_{D0}$ = thermal boundary layer thickness at midsection of a horizontal cylinder ($\alpha$ = 0)*
*$\delta_x$ = thermal boundary layer thickness at height of x for a vertical flat plate*
*$Nu_x$ = local Nusselt number for a vertical flat plate at height x*
*$Nu_L$ = average Nusselt number for a vertical flat plate at height L*
*$Nu_{D0}$ = local Nusselt number at midsection of a horizontal cylinder ($\alpha$ = 0)*
*$Nu_D$ = average Nusselt number for a horizontal cylinder with outer diameter of D*
*p, q, and r = constant parameters*

*Based on the discussion for the thermal boundary layer thickness over a vertical flat plate above, the constant parameter p in equation (4) is 0.25.*

*An extensive study on free convection over large diameter, horizontal cylinders conducted in reference [48] shows that the onset of turbulent transition occurs at a point passing the midsection of the cylinder by five degree even for large Rayleigh numbers so that the free convection over the lower half of the cylinder remains laminar.*

*Since the personnel barrier designed for MP197HB cask is extended only to the midsection of the cask, the correlations for free convection laminar flow over horizontal cylinders can be used to determine the thermal boundary layer thickness at this location.*

*The free convection local Nusselt number over a horizontal cylinder in laminar flow in air is given in reference [47] as follows.*

$$Nu_{D\alpha} = 0.604\, Gr_D^{1/4}\, \phi(\alpha) \qquad [47]$$

$$Gr_D = \frac{g\beta \Delta T\, D^3}{\upsilon^2}$$

| $\alpha$ | -90° | -60° | -30° | 0° | 30° | 60° | 75° | 90° |
|---|---|---|---|---|---|---|---|---|
| $\phi(\alpha)$ | 0.76 | 0.75 | 0.72 | 0.66 | 0.58 | 0.46 | 0.36 | 0 |
| | Bottom half | | | Top half | | | | |

*The local Nusselt number at the midsection of the cylinder at $\alpha$ = 0 is:*

$$Nu_{D0} = 0.604\, Gr_D^{1/4} \times 0.66$$

*Based on the above correlation, the average Nusselt number over the horizontal cylinder is:*

$$Nu_D = \frac{1}{180}\int_{-90}^{90} Nu_{D\alpha}\, d\alpha = 0.604\, Gr_D^{1/4} \times \frac{1}{180}\int_{-90}^{90} \phi(\alpha)\, d\alpha$$

*The integration of $\phi(\alpha)$ over the range of -90° to 90° performed using the data in the above table gives:*

$$Nu_D = 0.604\, Gr_D^{1/4} \times 0.6025$$

*Comparison of the correlations for $Nu_{D0}$ and $Nu_D$ gives:*

$$Nu_D = \frac{0.6025}{0.66} Nu_{D0} = 0.913\, Nu_{D0} \qquad (5)$$

*Since the equation (5) is based on free convection laminar flow, the constant parameter r in equation (4) is equal to 1.*

*The ratio of the average Nusselt numbers for vertical flat plate and horizontal cylinder can be determined using the corresponding correlations shown in Section A.3.3.1.1.*

*The thickness of the boundary layer at the midsection of the cask can be determined by substitution of the correlations for the local and average Nusselt numbers into equation (4). The height (L) of the vertical flat plate can be set equal to the outer diameter of the cask (D) for this evaluation. Average of the cask outer surface and ambient temperatures are considered in calculation of the Nusselt numbers.*

*As seen above, the correlations for the local and average Nusselt numbers depend on the Grashof and Prandtl numbers, which in turn depend on the cask outer surface temperature. A sensitivity analysis is performed to cover the effects of a wide range of cask temperatures from 200°F to 500°F on the thickness of free convection thermal boundary layer at the midsection of the cask. This sensitivity analysis starts with variation of Grashof and Prandtl numbers as summarized in the following table.*

***Variation of Grashof, Prandtl, and Rayleigh Numbers***

$T_\infty$ =100°F
For L=D

| $T_{cask}$ | $T_{cask}$ | $T_\infty$ | $T_{avg}$ | $\beta$ | $\nu$ | Gr | Pr | Ra |
|---|---|---|---|---|---|---|---|---|
| (F) | (K) | (K) | (K) | (1/K) | ($m^2$/s) | (---) | (---) | (---) |
| 200 | 367 | 311 | 339 | 2.95E-03 | 2.235E-05 | 4.931E+10 | 0.71 | 3.490E+10 |
| 300 | 422 | 311 | 367 | 2.73E-03 | 2.849E-05 | 5.609E+10 | 0.70 | 3.948E+10 |
| 400 | 478 | 311 | 394 | 2.54E-03 | 3.516E-05 | 5.135E+10 | 0.70 | 3.602E+10 |
| 500 | 533 | 311 | 422 | 2.37E-03 | 4.232E-05 | 4.415E+10 | 0.70 | 3.091E+10 |

*The values in the above table are calculated based on air properties shown in Section A.3.2.1, Item 16, at the average air temperature. As seen in the above table, the Grashof number varies between 5.6E10 and 4.4E10, the Prandtl number varies between 0.70 and 0.71, and the Rayleigh number varies between 3.1E10 and 4.0E10 for the cask outer surface temperatures between 200°F and 500°F. Since the variation of Prandtl is relative small, an average Prandtl number of 0.70 is considered in the sensitivity analysis to calculate the average Nusselt numbers for a vertical flat plate ($Nu_L$) and a horizontal cylinder ($Nu_D$). To bound the variation of the Rayleigh number conservatively, the average Nusselt numbers $Nu_L$ and $Nu_D$ are evaluated for a wider range between 1E10 and 1E11.*

*As shown in Section A.3.3.1.1, the correlation for $Nu_L$ depends on $C_t^v$ and f factors, which in turn depend on Prandtl number and surface temperature, respectively. $C_t^v$ is a weak function of Prandtl number. The variation of the f factor is determined for a cask outer surface temperature from 200°F to 500°F. The variations of these values are summarized in the following table.*

***Variation of $C_t^v$ and f in Calculation of $Nu_L$***

$T_\infty$ =100°F

| Pr | $C_t^v$ | $T_{cask}$ | f |
|---|---|---|---|
| (---) | (---) | (°F) | (---) |
| 0.70 | 0.103 | 200 | 1.014 |
| 0.71 | 0.103 | 300 | 1.028 |
| Average | 0.103 | 400 | 1.042 |
| | | 500 | 1.056 |
| | | Average | 1.035 |

*The average values of $C_t^v$ and f from the above table are considered in calculation of $Nu_L$. The variation of the average Nusselt numbers $Nu_L$ and $Nu_D$ and their ratios summarized in the table below.*

***Variation of $Nu_L/Nu_D$***

*Vertical Flat Plate*
*Pr = 0.70*

| Ra | $Nu^T$ | $Nu_l$ | $C_t^v$ | f | $Nu_t$ | $Nu_L$ |
|---|---|---|---|---|---|---|
| (---) | (---) | (---) | (---) | (---) | (---) | |
| 1.00E+10 | 162.86 | 163.9 | 0.103 | 1.035 | 208.5 | 216.0 |
| 2.00E+10 | 193.67 | 194.7 | 0.103 | 1.035 | 275.0 | 280.5 |
| 5.00E+10 | 243.53 | 244.5 | 0.103 | 1.035 | 384.0 | 388.1 |
| 8.00E+10 | 273.89 | 274.9 | 0.103 | 1.035 | 452.4 | 456.1 |
| 1.00E+11 | 289.61 | 290.6 | 0.103 | 1.035 | 488.5 | 492.0 |

*Horizontal Cylinder*
*Pr = 0.70*

| Ra | $Nu^T$ | F | $Nu_l$ | $\overline{C}_t$ | $Nu_t$ | $Nu_D$ | $Nu_L/Nu_D$ |
|---|---|---|---|---|---|---|---|
| (---) | (---) | (---) | (---) | (---) | (---) | (---) | (---) |
| 1.00E+10 | 125.73 | 0.940 | 126.7 | 0.103 | 221.9 | 222.0 | 0.973 |
| 2.00E+10 | 149.51 | 0.942 | 150.5 | 0.103 | 279.6 | 279.6 | 1.003 |
| 5.00E+10 | 188.00 | 0.944 | 188.9 | 0.103 | 379.5 | 379.5 | 1.023 |
| 8.00E+10 | 211.44 | 0.945 | 212.4 | 0.103 | 443.8 | 443.8 | 1.028 |
| 1.00E+11 | 223.58 | 0.945 | 224.5 | 0.103 | 478.1 | 478.1 | 1.029 |
| | | | | | | Average | 1.011 |

*As shown in the above table, the ratio of $Nu_L$ to $Nu_D$ varies between 0.973 and 1.029 for the range of considered Rayleigh numbers. An average value of 1.011 is considered for this ratio to use in equation (4). Since this ratio is close to one, the constant parameter q in equation (4) does not have any significant effect and can be omitted.*

*Substitution of the local and average Nusselt number ratios from equation (3), equation (5), and the table of $Nu_L/Nu_D$ variations into equation (4) gives:*

$$\delta_{D0} = (1/0.834)^{0.25} \times 1.011 \times 0.913\ \delta_x$$

*Using $\delta_x$ from equation (2) in the above equation determines the range of boundary layer thickness at the midsection of the cask as summarized in the following table.*

***Thickness of the Thermal Boundary Layer***

*$T_\infty$ = 100°F*
*L = D = 97.75"*

| $T_{cask}$ | $T_{cask}$ | $T_\infty$ | $T_{avg}$ | Gr | Pr | $\delta_x/L$ | $\delta_x$ | $\delta_{D0}$ |
|---|---|---|---|---|---|---|---|---|
| (°F) | (K) | (K) | (K) | (---) | (---) | (---) | (in) | (in) |
| 200 | 367 | 311 | 339 | 4.931E+10 | 0.71 | 0.060 | 5.9 | **5.7** |
| 300 | 422 | 311 | 367 | 5.609E+10 | 0.70 | 0.059 | 5.8 | **5.6** |
| 400 | 478 | 311 | 394 | 5.135E+10 | 0.70 | 0.060 | 5.9 | **5.7** |
| 500 | 533 | 311 | 422 | 4.415E+10 | 0.70 | 0.061 | 6.0 | **5.7** |

*As seen in the above table, the variation of the thermal boundary layer thickness is small and its maximum value at the midsection of the cask is 5.7" for a uniform cask surface temperature of 500°F. Based on data shown in Section A.3.3.1.2, the shortest distance between the outer surface of the cask and the personnel barrier is over 9".*

*Shortest distance = distance to cask centerline – cask OD/2 = 58 – 97.75 / 2 = 9.125"*

*The conservatively evaluated boundary layer thickness of 5.7" is much smaller than shortest distance between the outer surface of the cask and the personnel barrier. Therefore, the personnel barrier remains out of the hot air streams flowing around the cask outer surface.*

A.3.3.1.3 Effective Thermal Properties in MP197HB TC Model

***1) Effective Heat Transfer Coefficient for External Fins***

To reduce the complexity of the TC model, an effective heat transfer coefficient is calculated for the external fins based on the geometry shown in the drawings in Chapter A.1, Appendix A.1.4.10. Circular external fins are welded to an aluminum shell which will be installed over the outer surface of the TC shield shell to enhance heat dissipation for heat loads over 26 kW. An effective heat transfer coefficient is calculated for the external fins which includes the convection and radiation heat transfer to ambient. The following dimensions are considered for the fins.

- Fin height = 3.0"
- Fin thickness = 0.156"
- Fin pitch = 1.0"

A sub-model of the TC outer surface is developed for this purpose using ANSYS [27].

This sub-model considers a 30 degree segment of the aluminum shell with three circular external fins. Figure A.3–10 shows the sub-model of the finned shell.

Convection boundary conditions are applied over the outer surfaces of the fins in the model using surface load (SF) commands in ANSYS [27]. SHELL57 elements are overlaid on the external surfaces of the fins to create radiation super-element. The radiation shell elements are shown in Figure A.3–10. Thermal radiation from the outer surfaces is modeled using /AUX12 processor. Ambient temperatures of 100°F, -20°F, and -40°F are considered for convection and radiation.

An emissivity of 0.70 is considered for the anodized aluminum for exposed finned surfaces as shown in Section A.3.2.1.

Fixed temperature boundary conditions are applied over the inner surface of the aluminum shell. The amount of heat dissipation is retrieved from the model using reaction solution command (PRRSOL) in ANSYS [27]. The effective heat transfer coefficient is calculated as follows.

$$h_{eff} = \frac{Q_{react}}{A_{eff}(T_s - T_{amb})}$$

$h_{eff}$ = effective heat transfer coefficient over finned surface (Btu/hr-in$^2$)
$Q_{react}$ = heat input entering the cask shield shell (reaction solution) retrieved from model (Btu/hr)
$T_s$ = shield shell inner surface temperature (fixed temperature boundary conditions) (°F)
$T_{amb}$ = ambient temperature (°F) = 100°F, -20°F, and -40°F
$A_{eff}$ = outer surface area of the un-finned shield shell (in$^2$).

Since the $h_{eff}$ will be applied over the un-finned surface of the aluminum shell, $A_{eff}$ is the area of the un-finned surface.

$A_{eff} = \pi D_o (3 \times fin\ pitch)(30/360)$ = π × 98.25 × 3 × 1.0 × (30/360) = 77.2 in$^2$

Convection heat transfer coefficients are calculated using correlations from Rohsenow Handbook [21], page 4.39 and 4.40, equations 4.68 to 4.70b. The correlations used for convection coefficients are:

$$Nu = \frac{h\,S}{k}; \qquad \zeta = \frac{D_o}{D_f}; \qquad Ra = \frac{g\beta(T_w - T_{amb})S^3}{\nu\alpha}\frac{S}{D_f}; \quad \Pr = \frac{\nu}{\alpha}$$

$D_o$ = outer diameter of un-finned surface = 98.25"
$D_f$ = outer diameter of circular fins = (98.25 + 2×3.0) = 104.25"
S = fin pitch = 1.0"
g = gravitational constant =9.81 (m/s$^2$)
β = expansion coefficient = 1/T (1/K)
T = absolute temperature (K)
ν = kinematic viscosity (m$^2$/s)
α = thermal diffusivity (m$^2$/s)
k = air conductivity (W/m-K)

On fin tips:

$Nu = c\ Ra^b$ for $2 \le Ra \le 10^4$ with c and b defined in Section A.3.2.1 material #. 22.

On fin lateral surfaces together with the supporting shell:

$$Nu = C_0\, Ra_0^{\,p}\left\{1 - \exp\left[-\left(\frac{C_1}{Ra_0}\right)^{C_2}\right]\right\}^{C_3} \qquad \text{for } 1.0 \le \frac{D_f}{D_o} \le 1.67$$

where $C_0 = -0.15 + 0.3\zeta + 0.32\zeta^{16}$ $C_1 = -180 + 480\zeta - 1.4\,\zeta^{-8}$

$C_2 = 0.04 + 0.9\zeta$ $C_3 = 1.3\ (1 - \zeta) + 0.0017\ \zeta^{-12}$

$p = 0.25 + C_2\ C_3$ $Ra_0 = Ra/\zeta$

Properties are evaluated at wall temperature as required in [21]. Air properties used for these correlations are listed in Section A.3.2.1, material # 16.

The results for the effective heat transfer coefficient are summarized in Section A.3.2.1 material # 22, 23, and 24 for ambient temperatures of 100°F, -20°F, and -40°F, respectively.

***2) Effective Conductivity for Helium Gap between DSC and TC/Sleeve***

Effective conductivities are calculated for helium between the DSC and the TC inner shell / internal sleeve to account for conduction and radiation between these components. Based on discussion in Section A.3.2.1, a conservative emissivity of 0.587 is considered for the DSC shell and TC inner shell.

The inner surface of the internal sleeve is anodized. Based on discussion in Section A.3.2.1, a conservative emissivity of 0.7 is considered for the anodized/painted surface of the internal sleeve.

The effective conductivity of helium within the gap between the DSC shell and TC inner shell is calculated based on a detailed sub-model of this region. This sub-model considers a 10" high, 30 degree segment of the shells. Conductivity of helium is considered for the gap between the shells. Radiation between surfaces is modeled using /AUX12 processor. Figure A.3–11 shows the sub-model of the DSC shell and the TC inner shell.

In the DSC/TC sub-model, a heat flux of 2.813 Btu/hr-in$^2$ equivalent to 29.2 kW (see Section A.3.3.1.1) is applied on the radial surface of the innermost shell (DSC shell) and fixed temperature boundary conditions are applied over the radial surface of the outermost shell (TC inner shell).

The nodes of the gap between the DSC shell and TC inner shell build up the radiation super element (MATRIX50). To avoid convergence problems, the heat flux or fixed temperature boundary conditions are not applied directly on the nodes of the radiation super element. Instead the heat flux is applied on the innermost nodes of the DSC shell and the fixed temperatures are applied on the outermost nodes of the TC shell.

The effective conductivity is calculated as follows.

$$k_{eff} = \frac{(q_{react} \times 360/30)\ \ln(D_{i,TC}/D_{o,DSC})}{2\pi \times 10 \times (T_{DSC} - T_{TC})}$$

Where,

$q_{react}$ = reaction solution retrieved from the model (Btu/hr)

$D_{i,TC}$ = inner diameter of TC inner shell = 70.5"

$D_{o,DSC}$ = outer diameter of DSC for 69BTH, 37PTH, 32PTH, and 32PTH1 = 69.75"

$T_{TC}$ = temperature of the TC inner shell innermost nodes (°F)

$T_{DSC}$ = average temperature of DSC shell (°F)

The conductivity of SA-240, type 304 is considered for the TC inner shell in this sub-model. Since the TC inner shell material is SA-203 and has higher conductivity than SA-240, type 304, this approach is conservative.

Due to high conductivity of the metallic shells, the temperature gradient across the shells is very small (< 1°F). Therefore the actual temperature gradient across the gap is slightly lower than the temperature gradient between the shells ($T_{DSC} - T_{TC}$) considered in the above equation. This results in a slightly underestimated effective conductivity across the gap, which is conservative for the purpose of this calculation.

The average temperature of the DSC shell is retrieved from the model using "ETABLE" commands in ANSYS [27]. The fixed temperature boundary condition applied on the outermost node of TC shell is considered as TC temperature.

The $q_{react}$ depends on the applied heat flux. Since the effect of $q_{react}$ is accounted for in the equation for $k_{eff}$, the calculated $k_{eff}$ values can be used for other heat loads considered in this analysis.

The effective conductivity values for the helium within the gap between the DSC shell and the TC inner shell are summarized in Section A.3.2.1, material # 25.

The calculated effective conductivity in Section A.3.2.1, material # 25 is applied only in radial direction for the gap between the DSC shell and the TC inner shell. The conductivity in axial direction is set equal to helium conductivity for conservatism.

As shown in Section A.3.3.1.1, the gap size between the 61BTH or 61BT DSC shell and the internal sleeve is equal to the gap size between the large diameter DSC shells (69BTH, 37PTH, 32PTH, and 32PTH1) and the TC inner shell. Since the assumed emissivity of 0.587 for TC inner shell is lower than the emissivity of anodized aluminum, the above effective conductivity calculated for the gap between the large diameter DSC and TC inner shell can be used conservatively for the gap between the DSC and the internal sleeve for DSC types 61BTH and 61BT.

For small diameter DSC types, 32PT, 24PTH, and 24PT4, an effective conductivity is calculated for the gap between the DSC shell and TC internal sleeve using the same methodology described above with the following data.

$D_{i,sleeve}$ = inner diameter of TC internal sleeve = 68.0"
$D_{o,DSC}$ = outer diameter of small diameter DSC types = 67.19"
$\varepsilon_{DSC}$ = 0.587 (emissivity of steel or stainless steel, see Section A.3.2.1)
$\varepsilon_{sleeve}$ = 0.7 (emissivity of anodized aluminum, see Section A.3.2.1)

The effective conductivity values for the helium within the gap between the small DSC shell and the TC internal sleeve are listed in Section A.3.2.1, material # 26.

This analysis uses the effective conductivity values from Section A.3.2.1, material # 26 for the gaps between the DSC shell and TC internal sleeve for 32PT, 24PTH, and 24PT4 DSC types only in radial direction. The conductivity in axial direction is set equal to helium conductivity for conservatism.

### *3) Effective Conductivity for DSC Top and Bottom Cover Plates*

Axial air gaps of 0.0625" are considered between the carbon steel/stainless steel shield plugs and cover plates for all DSC types. These gaps account for contact resistance and fabrication imperfections between these components and adjacent plates. In addition, axial gaps of 0.025" are considered on both sides of lead shield plugs for 24PT4 DSC.

For simplification of the model, the axial air gaps of 0.0625" are integrated into DSC bottom shield plug and DSC top inner cover plate for all DSC types except for 24PT4.

Single axial air gaps of 0.0625" are integrated into DSC bottom inner cover plate and DSC top outer cover plate for 24PT4 DSC. The axial gaps of 0.025" are also integrated into the lead shield plugs of 24PT4 DSC.

An effective conductivity in the axial direction is calculated for these components. The conductivities of these components remain unchanged in the radial direction.

The gaps and the plates build up serial thermal resistances in the axial direction. The effective conductivity through these serial pieces is:

$$k_{eff} = \frac{t_{plate} + n \cdot t_{gap}}{\frac{t_{plate}}{k_{plate}} + \frac{n \cdot t_{gap}}{k_{air}}}$$

Where,

$k_{eff}$ = effective conductivity in axial direction (Btu/hr-in-°F)

$t_{plate}$ = thickness of targeted plate
(bottom shield plug and top inner cover plate for all DSC types except 24PT4)
(bottom inner cover plate, top outer cover plate, and lead shield plugs for 24PT4 DSC)

$t_{gap}$ = 0.0625" between steel shield plugs and stainless steel plates
0.025" between lead shield plugs and stainless steel plates

$k_{plate}$ = conductivity of A36 steel for bottom shield plug (all DSC except 24PT4)
conductivity of SS304 steel for top cover plate (all DSC except 24PT4)
conductivity of SS316 steel for top outer cover and bottom inner cover plates for 24PT4
conductivity of lead for lead shield plugs of 24PT4 DSC (Btu/hr-in-°F)

$k_{air}$ = conductivity of air (Btu/hr-in-°F)

n = number of gaps
= 2 for gaps between shield plugs and cover plates for all DSC types except 24PT4
=1 for gap between top shield plug and outer cover plate for 24PT4
=1 for gap between bottom shield plug and outer cover plate for 24PT4
=2 for gaps between lead shield plugs and encapsulating stainless steel plates for 24PT4

The conductivity values are taken from Section A.3.2.1.

Based on data in Table A.3–1, the smallest DSC shield plug thickness is 3" and the smallest DSC top cover plate thickness is 0.75". These values are considered to

calculate the axial effective conductivities conservatively for all DSC types except for 24PT4. The thicknesses of cover plates for 24PT4 are as follows.

24PT4 DSC top outer cover plate =1.25"
24PT4 DSC bottom inner cover plate =2.0"
24PT4 DSC top lead shield plug = 3.38"
24PT4 DSC bottom lead shield plug = 2.88"

The axial effective conductivities for bottom shield plug and top inner cover plates of all DSC types except 24PT4 are listed in Section A.3.2.1, material # 27.

The axial effective conductivities calculated for top/bottom inner cover plates and lead shield plugs of 24PT4 DSC are listed in Section A.3.2.1, material # 28 and 29, respectively.

### *4) Effective Conductivity for TC Slide Rails*

A helium gap of 0.01" is considered between the slide rail and DSC shell to account for the contact resistance. For simplification of the model, this gap is integrated into the slide rail model and an effective conductivity is calculated for this component. The calculated effective conductivity for the slide rail is applied conservatively in all directions.

The gap and the slide rail built up serial thermal resistances along the rail height. The effective conductivity through these serial pieces is:

$$k_{eff} = \frac{t_{rail} + t_{gap}}{\frac{t_{rail}}{k_{rail}} + \frac{t_{gap}}{k_{He}}}$$

Where,
$k_{eff}$ = effective conductivity (Btu/hr-in-°F)
$t_{rail}$ = thickness of TC slide rail = 0.12"
$t_{gap}$ = thickness of gap = 0.01"
$k_{rail}$ = conductivity of TC slide rails (Nitronic 60)
$k_{He}$ = conductivity of helium (Btu/hr-in-°F)

The conductivity values are taken from Section A.3.2.1. The effective conductivities for the TC slide rail are listed in Section A.3.2.1, material # 30.

### *5) Effective Conductivity for Internal Sleeve*

The designed shape of the aluminum internal sleeve is shown in the drawings in Chapter A.1, Appendix A.1.4.10. As seen in this drawing, there is virtually no gap between the segments of the internal sleeve. A different shape is considered for the internal sleeve in the TC model. The assumed shape includes 120 individual aluminum pieces with 39 radial gaps and three axial gaps. The thicknesses of the radial and axial gaps are respectively 0.25" and 0.188" as shown in Figure A.3–12. In addition, the material properties of the inner shell elements in contact with the cask slide rails are changed to those of helium to avoid any direct conduction between these two

components. Since the considered shape of the internal sleeve in the TC model includes more gaps, it is conservative to use it for thermal analysis of the transport cask under NCT.

To reduce the complexity of the TC model, an effective conductivity is calculated for the assumed shape of the internal sleeve shown in Figure A.3–12. The following dimensions are considered for the internal sleeve in the thermal model.

| | |
|---|---|
| Sleeve ID = | 68 in. |
| Sleeve OD = | 70.5 in. |
| Total length = | 196 in. |
| No. of pieces in axial direction = | 4 in. |
| No. of segments in radial direction = | 40 in. |
| Axial gap = | 0.188 in. |
| Radial gap = | 0.25 in. |

**Axial Effective Conductivity**

Along one segment of the sleeve, there are four sections of aluminum pieces with 0.1875" gaps between them in the axial direction (see Figure A.3–12, at bottom). The thermal resistance through these serial pieces is:

$$R_{axl,1} = 4\,R_{Al} + 3\,R_{gap}$$

$$R_{axl,1} = \frac{L_t}{k_{eff}.A}; \qquad R_{Al} = \frac{L_{Al}}{k_{Al}.A}; \quad R_{gap} = \frac{L_{gap}}{k_{He}.A}$$

$L_t$ = 196"
$L_{gap}$ = 0.1875"
$L_{Al}$ = (196 – 3×0.1875) / 4 = 48.86"
$k_{eff}$ = effective conductivity of one axial segment (Btu/hr-in-°F)
$k_{Al}$ = conductivity of aluminum (Btu/hr-in-°F)
$k_{He}$ = conductivity of helium (Btu/hr-in-°F)
A = surface area of one segment ($in^2$)

Rearranging the above equations gives:

$$k_{eff,axl,1} = \frac{L_t}{\left(\frac{4\,L_{Al}}{k_{Al}} + \frac{3\,L_{gap}}{k_{He}}\right)}$$

The axial segments are parallel to each other. Due to low conductivity of helium in comparison to aluminum, helium conductivity can be conservatively ignored. The total axial effective conductivity is then proportional to the ratio of the surface area for the aluminum segments in cross section to the total cross-sectional area of the internal sleeve, which is equivalent to the ratio of aluminum segment angle to the nominal angle (see Figure A.3–12).

$$k_{eff,axl} = k_{eff,axl,1} \times \frac{\theta_{Al}}{\theta_{nom}}$$

with $\theta_{nom} = \frac{360}{40} = 9^\circ$

$$\theta_{Al} = \theta_{nom} - \frac{gap_{rad}}{D_{o,sleeve}/2} \times \frac{180}{\pi} = 8.6^\circ$$

$gap_{rad}$ = radial gap =0.25"
$D_{o,sleeve}$ = 70.5"

**Radial Effective Conductivity**

Forty aluminum segments in the radial direction build up parallel resistances perpendicular to the direction of heat flow from the center to the periphery. Again, the total radial effective conductivity can be set proportional to the ratio of the angle for one aluminum segment ($\theta_{Al}$) to the nominal angle of each segment ($\theta_{nom}$).

$$k_{eff,rad} = k_{Al} \times \frac{\theta_{Al}}{\theta_{nom}}$$

The effective conductivity values calculated for the sleeve are summarized in Section A.3.2.1, material # 31.

A.3.3.1.4 69BTH DSC Model

The following assumptions and conservatism are considered for the 69BTH DSC model:

The fuel assemblies contained in the DSC basket are intact fuel assemblies. Since the damaged fuel assemblies are loaded in the outermost fuel compartment cells, they do not affect the maximum temperatures or the maximum temperature gradients in this evaluation. *A sensitivity analysis is conducted to bound the effects of the damaged fuel assemblies on the thermal performance of the MP197HB cask considering the worst case condition, in which the high burnup damaged fuel assemblies becomes rubble. This sensitivity analysis is discussed in Section A.3.6.9.*

No convection is considered within the canister cavity.

Only helium conduction is considered from the basket upper surface to the canister top shield plug.

Radiation is considered only implicitly between the fuel rods and the fuel compartment walls in the calculation of effective fuel conductivity. No other radiation heat exchange is considered within the basket model.

Active fuel length for BWR fuel assemblies is 144" [11] and starts about 7.5" from the bottom of the basket [11]. The total length of the basket assembly is 176.5".

The following gaps are considered in the DSC canister/basket model at thermal equilibrium:

a) 0.30" diametrical hot gap between the basket outer surface and the canister inner surface. This gap is justified in Section A.3.6.7.3.

b) 0.125" axial gap between the bottom of the basket and the DSC bottom inner cover plate

c) 0.01" gap between any two adjacent plates or components in the cross section of the basket.

d) 0.125" gap in axial direction between the aluminum rail pieces.

e) 0.01" gap between the sections of the paired aluminum and poison plates in axial direction.

f) 0.1" gap between the two small aluminum rails at the basket corners.

g) 0.1" gap between the two pieces of large aluminum rails at 0° -180° and 90° - 270° orientations.

h) 0.0625" gap between DSC shield plugs and DSC cover plates for calculation of effective conductivities in axial direction.

No gap is considered between the paired poison and aluminum plates. The 0.01" gaps considered on either side of the paired plates account for the thermal resistance between the multiple plates. This assumption is justified in Section A.3.6.7.4.

The gaps considered between the aluminum rail segments are larger than the nominal cold gaps and are therefore conservative. The axial gaps considered between the aluminum rail pieces in the axial direction are larger than the tolerances considered for the rails and are therefore conservative.

The benchmarking of finite element models against test data in [35] shows that the 0.01" gaps considered between adjacent plates or components in the cross section of the basket account conservatively for the tolerances and contact resistances.

*In the fabrication, the diametrical gap between the basket and canister shell assigned as gap "a" above is controlled by dimensional inspections of the diameters of the basket and canister shell.*

*The structure of the 69BTH basket is similar to the 61BT and 61BTH baskets approved in accordance with 10 CFR 72 regulations. The uniform gap of 0.01" assigned as gap "c" above considered in the thermal model between any two adjacent components in the cross section of the 69BTH basket has the same size as the corresponding gaps considered in the 61BT and 61BTH baskets. In practical terms, fabrication of the 69BTH basket requires very tightly compressed assembly in order to fit the basket into the shell. Interfaces are formed as components and parts are assembled. The fit between mating components, for example between fuel compartment tubes and adjacent sheets, cannot practically be measured. Fabrication methods provide for the tightest practical assembly of these parts.*

*The gaps between adjacent components are related only to the flatness and roughness tolerances of the plates. The micro gaps related to these tolerances are non-uniform and provide interference contact at some areas and gaps on the other areas as shown schematically in the figure in Section A.3.6.7.2. For the purpose of thermal evaluation, surfaces of intermittent contact between adjacent components are conservatively*

*modeled as a uniform gap of 0.01". As shown in SAR Section A.3.6.7.4, the assumed gap size of 0.01" is approximately two times larger than the contact resistances between the adjacent components. It should be noted that for conservatism no contact pressure was considered between the components. This assumption implies that no friction exists between the components within the basket, which adds to the conservatism considered in the size of this uniform gap. In reality, there is sufficient friction that 61BT baskets have been lifted during fabrication using only the friction on the perimeter of the four-compartment subassemblies.*

*The 0.01" axial gaps between the sections of the paired aluminum and poison sheets assigned as gap "e" above are shown in SAR Figure A.3-17. The 0.1" gaps between the rail segments assigned as gaps "f" and "g" above are shown in SAR Figure A.3-15. These gaps are not located in the primary heat flow paths. A sensitivity analysis is performed to determine the effect of these gaps on the thermal performance. The results of this sensitivity analysis show that doubling the size of these gaps increases the maximum temperatures by less than 1 °F. Therefore, the effects of these gaps on the thermal performance are insignificant.*

The thickness of paired aluminum and poison plates within the wrapped compartment blocks of 69BTH basket is 0.25". This thickness is reduced to 0.21" to accommodate for the size of the gaps and maintain the outer basket diameter contained within the DSC inner diameter. An effective conductivity is calculated for these plates in Section A.3.3.1.5 to maintain the conductivity of plates within the basket. All other dimensions are based on nominal dimensions for 69BTH basket.

Paired aluminum and poison plates are considered as one homogenized material in the 69BTH basket model. The effective conductivities for paired aluminum poison plates are calculated in Section A.3.3.1.5.

To reduce the complexity of the 69BTH basket model, the contact resistances between the DSC shield plugs and DSC cover plates are integrated into the bottom shield plug and top inner cover plate. Axial effective conductivities are calculated for top and bottom shield plugs of DSC in Section A.3.3.1.3 and listed in Section A.3.2.1. The conductivities of these components remain unchanged in the radial direction.

Decay heat load is applied as heat generation boundary conditions over the elements representing homogenized fuel assemblies. The base heat generation rate is multiplied by peaking factors along the axial fuel length to represent the axial decay heat profile. A correction factor is used to avoid degradation of decay heat load due to imperfections in application of peaking factors. The heat generation rates used in this analysis is calculated as follows.

$$\dot{q}''' = \left( \frac{q}{a^2 L_a} \times PF \right) \times CF$$

where,
q = Decay heat load per assembly defined for each loading zone
a = Width of the homogenized fuel assembly = 6.0"
$L_a$ =Active fuel length = 144"
PF = Peaking Factor
CF = correction factor = 1.00697 for 69BTH

The base heat generation rates used in 69BTH basket model are listed in the following table.

**Base Heat Generation Rates for 69BTH**

| Heat Load in the Model (KW) | $\dot{q}'''$ value without PF (Btu/hr-in$^3$) | Heat Load in the Model (KW) | $\dot{q}'''$ value without PF (Btu/hr-in$^3$) |
|---|---|---|---|
| 0.10 | 0.0663 | 0.50 | 0.3314 |
| 0.25 | 0.1657 | 0.55 | 0.3646 |
| 0.30 | 0.1988 | 0.60 | 0.3977 |
| 0.40 | 0.2651 | 0.70 | 0.4640 |
| 0.45 | 0.2983 | | |

The active fuel length for fuel assembly LaCrosse is only 85", which is significantly shorter than the other fuel assemblies considered for transport in the 69BTH DSC. The heat load of this fuel assembly fuel should be lower than the longer fuel assemblies to maintain the same temperature distribution in 69BTH DSC.

Since conduction and effective conductivities are the only heat transfer paths considered in the 69BTH DSC, the temperatures are directly proportional to the fuel assembly heat load and reversely proportional to the active fuel length and effective fuel conductivity. Therefore, the following equations determine the reduction in heat load for fuel assembly LaCrosse to maintain the 69BTH temperatures at the same level as those determined for the bounding fuel assembly.

$$\left( \frac{q}{L_a \, k_{eff}} \right)_{LaCrosse} = \left( \frac{q}{L_a \, k_{eff}} \right)_{BoundingFA}$$

$$q_{LaCrosse} = q_{boundingFA} \frac{L_{a,LaCrosse}}{L_{a,BoundingFA}} \cdot \frac{k_{eff,LaCrosse}}{k_{eff,boundingFA}}$$

With,
$k_{eff}$ = effective fuel assembly conductivity (Btu/hr-in-°F)
q = Decay heat load per assembly defined for each loading zone (Btu/hr)
$L_a$ =Active fuel length (in)
= 144 " for bounding fuel assembly
= 85" for LaCrosse fuel assembly

Based on calculations described in Section A.3.6.5.2, the transverse and axial effective conductivities of fuel assembly LaCrosse are at least 19.9% higher than those for the bounding fuel assembly. Substitution of these values in the above equation gives the reduction of the heat load for fuel assembly LaCrosse.

$$q_{LaCrosse} = q_{boundingFA} \frac{85}{144} \times 1.199 = 0.708\, q_{bundingFA}$$

The heat load for LaCrosse fuel assembly should be reduced to 70% of the heat load for bounding fuel assembly to maintain the 69BTH DSC temperatures at the same level calculated for the bounding fuel assembly.

**Axial Heat Flux Profile**

In-core data from an operating BWR facility forms the basis for the evaluation. The data provides the burnup and moderator density for 25 axial locations along the length of a fuel assembly. Five fuel assemblies at different locations in the reactor core are utilized to generate a burnup (peaking factor) distribution for the assembly. The resulting axial heat flux profile is shown in Figure T.4-37 associated with Amendment 10 to Part 72 CoC 1004 for the Standardized NUHOMS® System [3].

The heat flux profile shown in Figure T.4-37 [3] is used in the thermal model of the Transnuclear, Inc. TN-68 dry transport/storage cask [36], which can accommodate BWR spent fuel with a maximum bundle average burnup of 45,000 MWd/MTU. The maximum bundle-average burnup allowed in 69BTH DSCs is 70,000 MWd/MTU, which is considerably higher than 45,000 MWd/MTU for TN-68. Reference [12] shows that at a higher burnup, the heat flux shape tends to flatten with a reduction in the maximum axial peaking factor in the middle region, and the flux shape becomes more pronounced in the fuel end regions. The reduction of the maximum axial peaking factor in a more flattened heat flux shape will result in lower fuel cladding temperatures. Therefore, the application of a heat flux shape for a lower burnup spent fuel (45,000 MWd/MTU) on a higher burnup spent fuel (70,000 MWd/MTD) is conservative.

Axial decay heat profile for BWR fuel assemblies is the same as the one described in Appendix T, Section T.4.6.4 associated with Amendment 10 to Part 72 CoC 1004 for the Standardized NUHOMS® System [3]. The peaking factors from Appendix T, Section T.4.6.4 [3] are converted to match the regions defined for the fuel assemblies in 69BTH DSC/basket model. These peaking factors are listed in Table A.3–2 and are shown in the following figure.

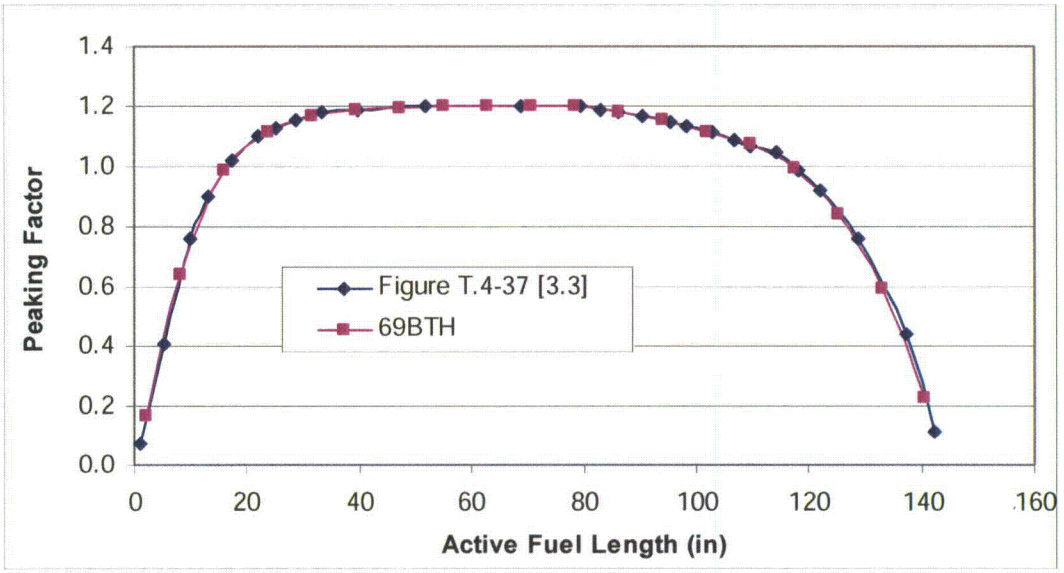


**Peaking Factor Curve for BWR Fuels**

As seen in Table A.3–2, the normalized area under peaking factor curve is smaller than 1.0. To avoid any degradation of decay heat load, a correction factor of 1.00697 calculated as follows is used when applying the peaking factors.

$$\textit{Nomalized Area under Curve} = \frac{\text{Area under Axial Heat Profile}}{\text{Active Fuel Length}} = 0.99308$$

Active fuel length = 144"

$$\textit{Correction Factor} = \frac{1}{\textit{Normalized Area under Curve}} = 1.00697$$

The heat generating rates for the elements representing the active fuel are calculated based on the HLZCs for each basket type. The HLZCs and their restrictions for 69BTH basket are shown in the following figures.

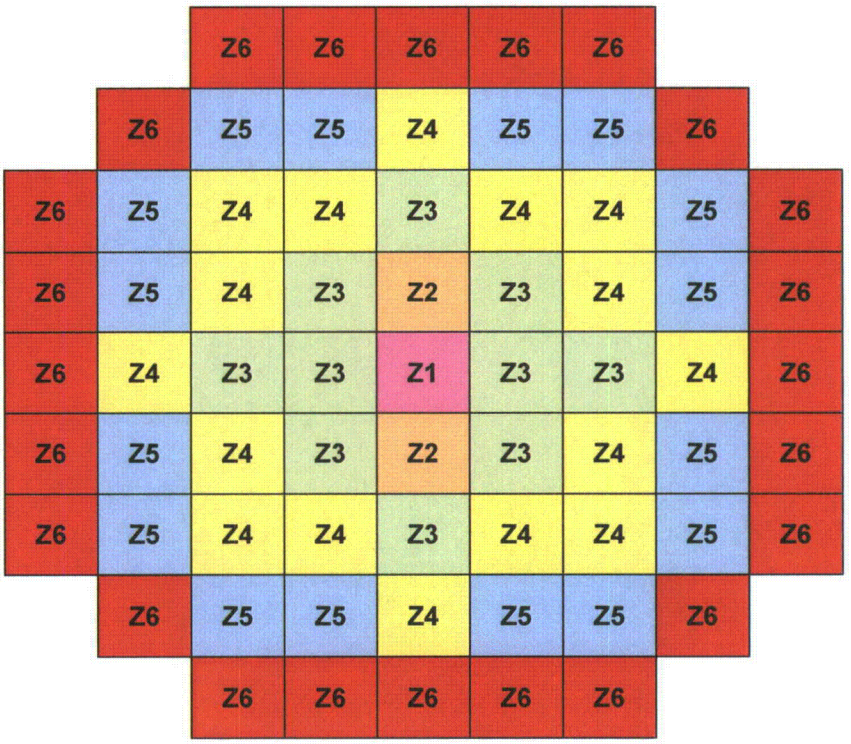


| | Zone 1 | Zone 2 | Zone 3 | Zone 4 | Zone 5 | Zone 6 |
|---|---|---|---|---|---|---|
| Max. Decay Heat (kW/FA) [3] | 0.10 | 0.27 | 0.30 | 0.40 | 0.55 | 0.45 |
| No. of Fuel Assemblies [1] | 1 | 2 | 10 | 16 | 16 | 24 |
| Max. Decay Heat per Zone (kW) [3] | 0.10 | 0.54 | 3.0 | 6.4 | 8.8 | 10.8 |
| Max. Decay Heat per DSC (kW) | 26.0 [2] [3] | | | | | |

Notes: [1] Total number of fuel assemblies is 69 for HLZC # 1.
[2] Adjust payload to maintain the total DSC heat load within the specified limit.
[3] Reduce the maximum decay heat to 70% of the listed values for LaCrosse Fuel assembly. The total decay heat for LaCrosse fuel assembly is 18.2 kW per DSC for HLZC No. 1.

**Heat Load Zoning Configuration No. 1 for 69BTH Basket**

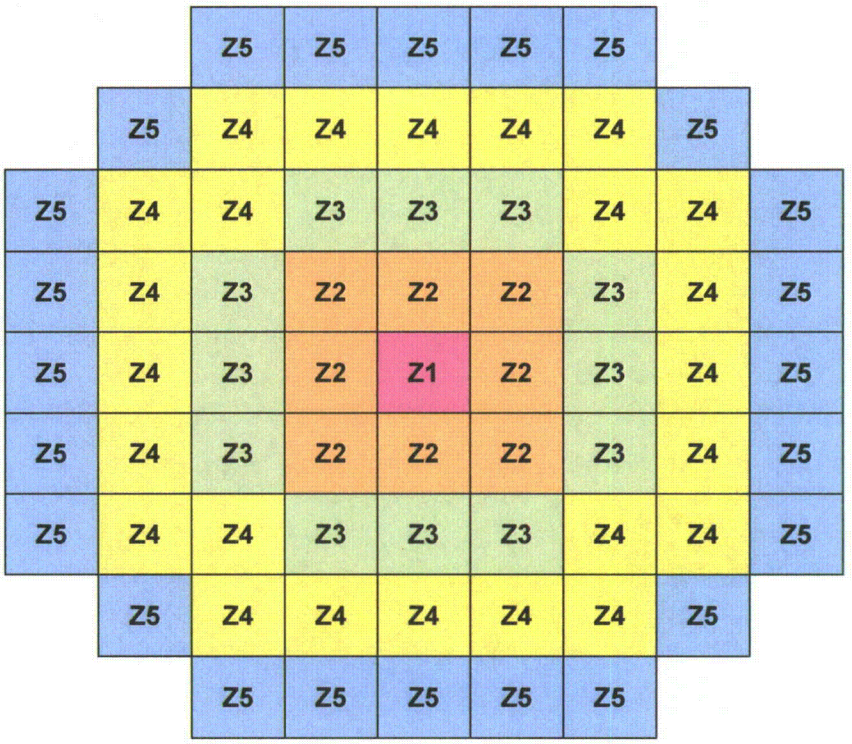


| | Zone 1 | Zone 2 | Zone 3 | Zone 4 | Zone 5 |
|---|---|---|---|---|---|
| Max. Decay Heat (kW/FA) [4] | 0.25 | 0.0 [1] | 0.40 | 0.60 | 0.50 |
| No. of Fuel Assemblies [2] | 1 | 0 | 12 | 24 | 24 |
| Max. Decay Heat per Zone (kW) [4] | 0.25 | 0 | 4.8 | 14.4 | 12.0 |
| Max. Decay Heat per DSC (kW) | 26.0 [3] [4] | | | | |

Notes: [1] Aluminum dummy assemblies replace the fuel assemblies in zone 2
[2] Total number of fuel assemblies is 61 for HLZC # 2
[3] Adjust payload to maintain the total DSC heat load within the specified limit
[4] Reduce the maximum decay heat to 70% of the listed values for LaCrosse Fuel assembly. The total decay heat for LaCrosse fuel assembly is 18.2 kW per DSC for HLZC No. 2.

**Heat Load Zoning Configuration No. 2 for 69BTH Basket**

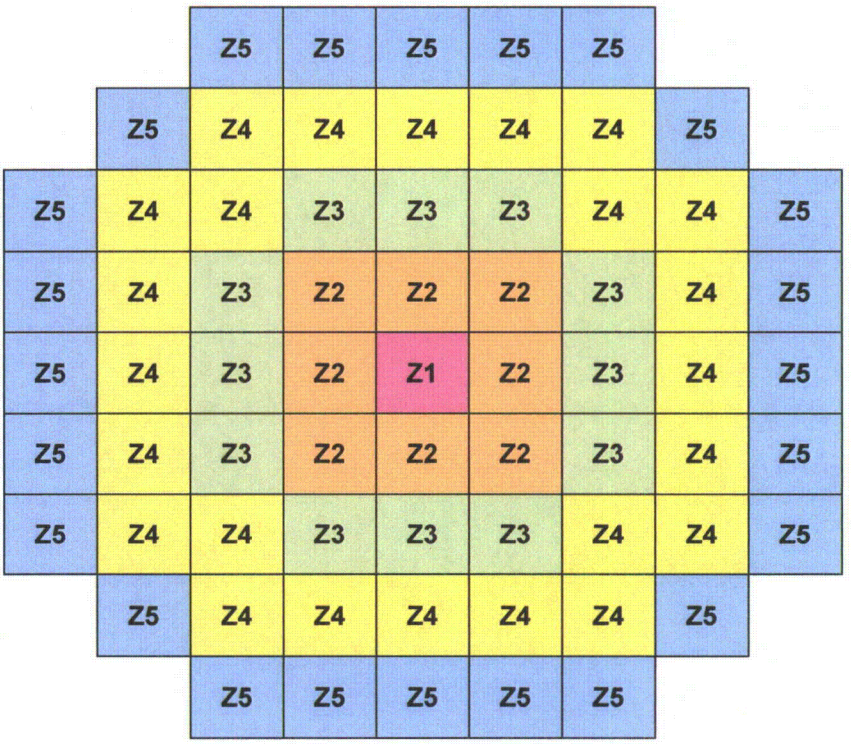


| | Zone 1 | Zone 2 | Zone 3 | Zone 4 | Zone 5 |
|---|---|---|---|---|---|
| Max. Decay Heat (kW/FA) [4] | 0.25 | 0.0 [1] | 0.40 | 0.60 | 0.50 |
| No. of Fuel Assemblies [2] | 1 | 0 | 12 | 24 | 24 |
| Max. Decay Heat per Zone (kW) [4] | 0.25 | 0 | 4.8 | 14.4 | 12.0 |
| Max. Decay Heat per DSC (kW) | 29.2 [3] [4] | | | | |

Notes: [1] Aluminum dummy assemblies replace the fuel assemblies in zone 2.
[2] Total number of fuel assemblies is 61 for HLZC # 3.
[3] Adjust payload to maintain the total DSC heat load within the specified limit.
[4] Reduce the maximum decay heat to 70% of the listed values for LaCrosse Fuel assembly. The total decay heat for LaCrosse fuel assembly is 20.4 kW per DSC for HLZC No. 3.

**Heat Load Zoning Configuration No. 3 for 69BTH Basket**

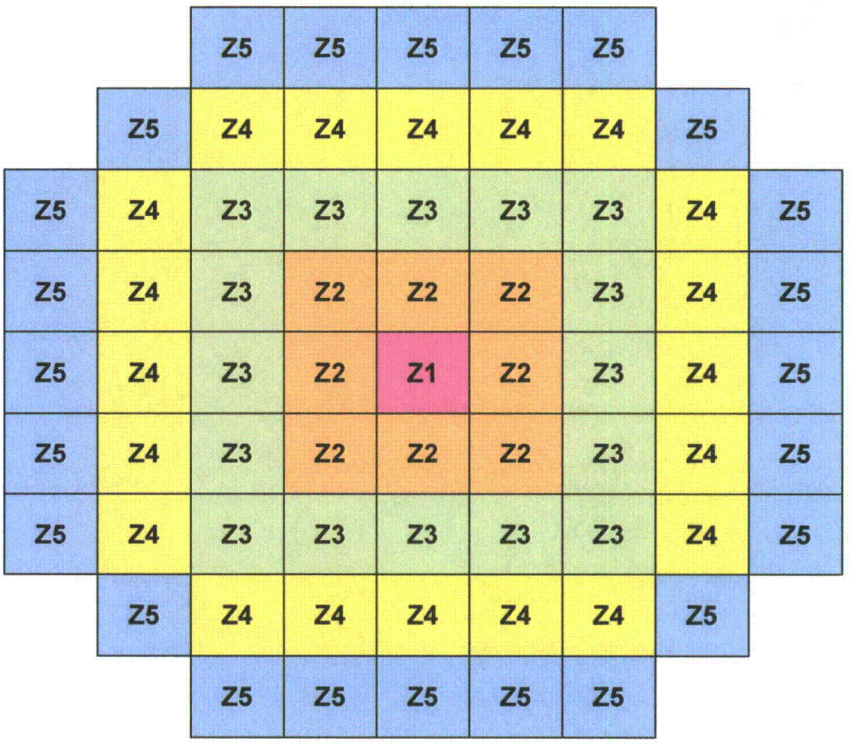


| | Zone 1 | Zone 2 | Zone 3 | Zone 4 | Zone 5 |
|---|---|---|---|---|---|
| Max. Decay Heat (kW/FA) [4] | 0.0 [1] | 0.45 | 0.0 [2] | 0.70 | 0.60 |
| No. of Fuel Assemblies [3] | 0 | 8 | 0 | 20 | 24 |
| Max. Decay Heat per Zone (kW) [4] | 0 | 3.6 | 0 | 14.0 | 14.4 |
| Max. Decay Heat per DSC (kW) | 32.0 [4] | | | | |

Notes: [1] The fuel compartment in zone 1 remains empty
[2] Aluminum dummy assemblies replace the fuel assemblies in zone 3
[3] Total number of fuel assemblies is 52.
[4] Reduce the maximum decay heat to 70% of the listed values for LaCrosse Fuel assembly. The total decay heat for LaCrosse fuel assembly is 22.4 kW per DSC.
[5] Borated Aluminum is the only poison material allowed for HLZC #4.

**Heat Load Zoning Configuration No. 4 for 69BTH Basket**

The DSC shell temperatures for NCT at 100°F, -20°F and -40°F are retrieved from the MP197HB transport cask model described in Section A.3.3.1.1 and transferred to the basket models.

The material properties used in the 69BTH DSC/basket model are listed in Section A.3.2.1

The effective thermal conductivities for paired aluminum/poison plates and for dummy aluminum assemblies are calculated in Section A.3.3.1.5.

The geometry of the DSC model and the gaps are shown in Figure A.3–13 through Figure A.3–17. Mesh sensitivity of the model is discussed in Appendix A.3.6.2.2.

Typical boundary conditions for the DSC basket model are shown in Figure A.3–18.

### A.3.3.1.5 Effective Thermal Properties in 69BTH DSC Basket

***1) Effective Conductivity for Paired Aluminum and Poison Plates in 69BTH DSC***

Paired aluminum and poison plates are considered as one homogenized material in the 69BTH basket model. The possible combinations for paired aluminum and poison plates are summarized in the following table.

**Combinations for Paired Al/Poison Plates in 69BTH Basket**

| | | Paired Plated within Compartment Blocks | Paired Plated between Compartment Blocks |
|---|---|---|---|
| Al/Boral | Total Thickness | 0.25" | 0.375" |
| | Boral Plate Thickness | 0.25" | 0.25" |
| | Boral Core Thickness | 0.16" | 0.16" |
| | Al Plate Thickness | 0 | 0.125" |
| Al/Borated Al or Al/MMC | Total Thickness | 0.25" | 0.375" |
| | Poison Plate Thickness | 0.175" | 0.175" |
| | Al Plate Thickness | 0.075" | 0.200" |

The paired plates built up parallel thermal resistances along their length and serial thermal resistances across their thickness. The gaps considered between the paired plates and their adjacent basket plates at the cross section account for the contact resistance between the plates.

The effective conductivities of the paired plates are calculated as follows:

$$k_{eff,along} = \frac{k_{poison} \times t_{poison} + k_{Al} \times t_{Al}}{t_{model}}$$ along the length (parallel resistances)

$$k_{eff,across} = \frac{t_{model}}{\frac{t_{poison}}{k_{poison}} + \frac{t_{Al}}{k_{Al}}}$$ across the thickness (serial resistances)

where,

$k_{poison}$ = conductivity of poison plate or conductivity of core material for Boral (Btu/hr-in-°F)
$t_{poison}$ = thickness of poison plate or thickness of core material for Boral (in)

$k_{Al}$ = conductivity of Al 1100 (Btu/hr-in-°F)
$t_{Al}$ = thickness of aluminum plate or aluminum clad for Boral (in)
$t_{model}$ = thickness paired Al/Poison plates in the model (in)

For conservatism, the conductivity of Boral core is reduced by 10% for calculation of effective conductivities.

The calculated effective conductivity values for paired aluminum and poison plates are listed in Section A.3.2.1 material # 17 to 19.

Borated aluminum plates can be used for all HLZCs in 69BTH basket. Boral or MMC plates paired with aluminum 1100 plates can be used for HLZC # 1, # 2, and # 3 but shall not be used for HLZC # 4 with 32 kW heat load.

A comparison between material # 17 and 18 in Section A.3.2.1 shows that the effective conductivities for paired aluminum and MMC plates are higher than those for paired aluminum and Boral plates for the entire temperature range. Therefore, the effective conductivities of paired aluminum and Boral plates are considered to bound the maximum component temperatures for HLZC # 1, # 2, and # 3.

The effective conductivities for paired aluminum and borated aluminum plates are used only for HLZC # 4.

***2) Effective Conductivity for Dummy Aluminum Assemblies***

Aluminum dummy assemblies replace the fuel assemblies in assigned compartments defined in the 69BTH basket for HLZC # 2 through # 4 as shown in Section A.3.3.1.4.

The dummy assemblies are considered as aluminum blocks with a cross section of 5.875" × 5.875" and a length equal to BWR fuel assemblies. A uniform gap of 0.0625" is considered around the cross section of the dummy assembly within the fuel compartment.

The effective conductivity in transverse direction is a combination of serial and parallel thermal resistances shown in the following Figure A.3–19. The transverse effective conductivity for dummy assembly is calculated as follows.

$$k_{eff,tr,dummy} = \frac{1}{R_{eff,tr,dummy}}$$

with

$$R_{eff,tr,dummy} = 2R_{th,He1} + \frac{1}{\left(\frac{2}{R_{th,He2}} + \frac{1}{R_{th,Al}}\right)}$$

where

$$R_{th,He1} = \frac{t_{gap}}{k_{He}\, w_{comp}}; \qquad R_{th,He2} = \frac{a_{dummy}}{k_{He}\, t_{gap}}; \qquad R_{th,Al} = \frac{a_{dummy}}{k_{Al6061}\, a_{dummy}} = \frac{1}{k_{Al6061}}$$

$a_{dummy}$ = width of dummy assembly = 5.875"
$w_{comp}$ = inner width of fuel compartment = 6.0"

$t_{gap}$ = thickness of gap between dummy assembly and fuel compartment =0.0625"
$k_{Al6061}$ = conductivity of Al 6061 (Btu/hr-in-°F)
$k_{He}$ = conductivity of Helium (Btu/hr-in-°F)

The conductivity of helium is conservatively ignored in the axial direction. The axial transverse effective conductivity for dummy assemblies is calculated as follows.

$$k_{eff,ax,dummy} = \frac{a_{dummy}^{2}}{w_{comp}^{2}} k_{Al6061}$$

The calculated effective conductivities for dummy assembly are listed in Section A.3.2.1 material # 20.

***3) Effective Thermal Properties of 69BTH DSC Basket***

The DSC basket effective density, thermal conductivity and specific heat are calculated for use in the transient analyses of the MP197HB under HAC.

**Dimensions of the Homogenized 69BTH DSC Basket**

| DSC Type | 69BTH |
|---|---|
| Basket OD (in) | 68.75 |
| Basket length (in) | 164 |
| Top grid assembly OD (in) | 68.75 |
| Top grid assembly length (in) | 14.4 |

The basket effective density $\rho_{eff\ basket}$, and specific heat $c_{p\ eff\ basket}$ are calculated as volumetric and weight average, respectively using the following equations.

$$\rho_{eff\ basket} = \frac{\sum W_i}{V_{basket}} = \frac{W_{steel} + W_{Al} + W_{poison} + W_{fuel}}{L_{basket} \cdot \pi \cdot D_{basket}^{2} / 4}$$

$$c_{p\,eff\ basket} = \frac{\sum W_i \cdot c_{pi}}{\sum W_i} = \frac{W_{steel} \cdot c_{p\,steel} + W_{Al} \cdot c_{p\,Al} + W_{poison} \cdot c_{p\,poison} + W_{fuel} \cdot c_{pfuel}}{W_{steel} + W_{Al} + W_{poison} + W_{fuel}}$$

Where: $W_i$ = weight of basket components
$V_{model}$ = total volume of basket in FE model
$L_{basket}$ = basket length = 164 in.
$D_{basket}$ = basket OD = 68.75 in.

$c_{p\,i}$ = specific heat of basket materials.

The specific heat and density values used in the above equations are listed in Section A.3.2.1. The following assumptions are used in the calculation of the basket effective density and specific heat calculation:

- Specific heat of SA 240, type 304 and Al 6061 are considered for stainless steel and aluminum components, respectively.
- For poison material $c_p$ values are conservatively assumed equal to those for 6061 aluminum.

- For aluminum at T > 400°F $c_p$ value is conservatively assumed equal to its value at 400°F.
- Conservatively, Helium is not included in density and specific heat calculation.

The same approach as described above for the basket is used to calculate the effective density $\rho_{eff\ top\ grid}$, for top grid assembly (hold-down ring) of 69BTH DSC.

$$\rho_{eff\ topgrid} = \frac{\sum W_i}{V_{topgrid}} = \frac{W_{steel}}{L_{topgrid} \cdot \pi \cdot D_{topgrid}^{\ 2} / 4}$$

Where: $W_{steel}$ = weight of steel in top grid assembly
$V_{topgrid}$ = total volume of top grid assembly in FE model
$L_{topgrid}$ = top grid assembly length in FE model = 14.4"
$D_{topgrid}$ = top grid assembly OD in FE model = 68.75"

Since no density and specific heat are considered for the helium, the specific heat of the top grid assembly is equal to the specific heat of steel.

The calculation of the effective density and effective specific heat for the 69BTH basket are summarized in Table A.3–3 and Table A.3–4, respectively.

To calculate the effective thermal conductivities, the 69BTH basket with Boral poison plates is chosen. A 26" long slice of 69BTH basket is created by selecting the nodes and elements of the basket from the finite element model described in Section A.3.3.1.4. The length of the slice model is twice the length of the aluminum plates and the axial gaps between them. The slice model is shown in Figure A.3–20.

To calculate the axial effective conductivity of the baskets, constant temperature boundary conditions are applied at the top and bottom of the slice models. No heat generation is considered for the fuel elements in these cases. The axial effective conductivity is calculated using the following equation.

$$k_{basket,axl} = \frac{Q_{axl} \times L}{A_{slice} \times \Delta T} \times 0.95$$

Where:
$Q_{axl}$ = Amount of heat leaving the upper face of the slice model – reaction solution of the uppermost nodes (Btu/hr)
L = Length of the model = 26" for 69BTH
$A_{slice}$ = Surface area of the upper (or bottom) face of the basket slice model = 1856 $in^2$ for 69BTH ($=\pi/8 \times D_{basket}^{\ 2}$)
$\Delta T = (T_2 - T_1)$ =Temperature difference between upper and lower faces of the model (°F)
$T_2$ = Constant temperature applied on the upper face of the model (°F)
$T_1$ = Constant temperature applied on the lower face of the model (°F)

Only 95% of the estimated axial effective conductivity is considered for conservatism.

Typical applied boundary conditions are shown in Figure A.3–21.

In determining the temperature dependent axial effective conductivities an average temperature equal to $(T_1 + T_2)/2$, is used for the basket temperature. The axial effective conductivities for 69BTH basket are listed in Table A.3–5.

The axial effective conductivity for the top grid assembly of 69BTH basket is calculated considering only the 14.4" high plates. The effects of the extension, base plate, and short plates are conservatively ignored. The assumed geometry of the top grid assembly is shown in Figure A.3–22. The following equation is used to calculate the axial effective conductivity for the top grid assembly.

$$k_{topgrid,axl} = k_{SS304} \frac{A_{plates}}{A_{model}}$$

Where: $k_{SS304}$ = conductivity of stainless steel, see Section A.3.2.1 (Btu/hr-in-°F)
$A_{plates}$ = Surface area of the 14.4" high plates, see Figure A.3–22 ($in^2$)
$A_{model}$ = Surface area of the homogenized top grid assembly model
= $\pi/4 \times D_{basket}^2 = 3712\ in^2$

The axial effective conductivities for the top grid assembly are listed in Table A.3–5.

The basket slice models are also used to calculate the transverse effective conductivity of the basket. For this purpose, constant temperature boundary conditions are applied on the outermost nodes of the slice model and heat generating conditions are applied over the fuel elements.

The heat generation rates for the slice model of 69BTH basket are calculated based on the HLZC # 1 shown in Section A.3.3.1.4 with a total heat load of 26 kW and a peaking factor of 1.2 for BWR assemblies.

The following equation is given in [23] for long solid cylinders with uniformly distributed heat sources.

$$T = T_o + \frac{\dot{q}\, r_o^2}{4k}\left[1 - \left(\frac{r}{r_o}\right)^2\right]$$

With $T_o$ = Temperature at the outer surface of the cylinder (°F)
T = Maximum temperature of cylinder (°F)
$\dot{q}$ = Heat generation rate (Btu/hr-$in^3$)
$r_o$ = Outer radius = $D_{basket}/2$ = 34.375" for 69BTH basket
r = Inner radius = 0 for slice model
k = Conductivity (Btu/hr-in-°F)

The above equation is rearranged to calculate the transverse effective conductivity of the basket as follows. Only 95% of the estimated radial effective conductivity is considered for conservatism.

$$\dot{q} = \frac{Q_{rad}}{V}$$

$$k_{basket,rad} = \frac{Q_{rad} \cdot r_0^2}{4 \cdot V \cdot \Delta T} \times 0.95 = \frac{0.95\, Q_{rad}}{2\pi \cdot L \cdot \Delta T} \text{ for 69BTH}$$

With $Q_{rad}$ = Amount of heat leaving the periphery of the slice model – Reaction solution of the outermost nodes (Btu/hr)

L = Length of the slice model = 26″ for 69BTH
V = Volume of the slice model = $(\pi r_0^2 L)/2$ for 69BTH
$\Delta T = (T_{max} - T_o)$ = Difference between maximum and the outer surface temperatures
in (°F)

Since the surface area of the fuel assemblies at the basket cross section is much larger than the other components, assuming a uniform heat generation is a reasonable approximation to calculate the radial effective conductivity.

Typical applied boundary conditions are shown in Figure A.3–21.

In determining the temperature dependent transverse effective conductivities an average temperature equal to $(T_{max} + T_o)/2$, is used for the basket temperature.

The transverse (radial) effective conductivities of the 69BTH basket are listed in Table A.3–6.

The effect of stainless steel in the top grid assembly is ignored conservatively in the radial direction. The effective conductivity of the top grid assembly is set equal to helium conductivity in the radial direction.

A.3.3.1.6 37PTH DSC Model

The following assumptions and conservatism are considered for the 37PTH DSC model:

The fuel assemblies contained in the 37PTH basket are intact fuel assemblies. Since the damaged fuel assemblies are loaded in the outermost fuel compartment cells, they do not affect the maximum temperatures or the maximum temperature gradients in this evaluation.

No convection is considered within the DSC cavity.

Radiation is considered only implicitly between the fuel rods and the fuel compartment walls in the calculation of effective fuel conductivity. No other radiation heat exchange is considered within the basket model.

The modeled active fuel length for PWR fuel assemblies is 144″ with the length of the bottom fitting about 4″ based on WE 14x14 PWR fuel assembly [37]. The total length of the basket assembly is 162″.

The following gaps are considered in the 37PTH basket/DSC model at thermal equilibrium:

a) 0.45″ diametrical hot gap between the basket outer surface and the canister inner surface. This assumed gap is larger than the nominal cold gap and is therefore conservative.

b) 0.45" diametrical hot gap between the shield plugs and the canister shell inner surface.
The maximum diametrical cold gaps between the top and bottom shield plugs and the canister shell inner surface are 0.18" and 0.25", respectively. The assumed hot gap is therefore conservative.

c) 0.01" gap between the basket rails and compartment plates.

d) 0.0075" gap between any two adjacent plates or components within the cross section of fuel compartments.

e) 0.125" gap in axial direction between the aluminum rail pieces. This gap is larger than the axial tolerances considered for rail aluminum pieces and therefore conservative.

f) Two pieces of MMC plates with 0.0075" contact gap as shown in Figure A.3–26 are conservatively assumed to model single MMC plate in the model.

g) 0.01" gap between any two adjacent plates between shield plugs and canister cover plates.

h) 0.1" axial gap between the canister inner bottom plate and bottom basket assembly.

It has been shown in [1], Appendix M, Section M.4.4.1.1, that the 0.01" and 0.0075" gaps considered in the basket cross section account adequately for tolerances and contact resistances in a similar basket design.

Fourteen single aluminum plates with 0.125" nominal thickness are considered in the fuel compartments. The thickness of single aluminum plate is modeled as 0.1325". To account for this thickness change, an effective conductivity is estimated by a conservative reduction factor of 0.926 (=0.125"/0.135") to maintain the conductivity of aluminum plates within the basket. All other dimensions are based on nominal dimensions for the 37PTH basket/DSC model.

A total thickness of 0.075" is considered for Boral plates with a maximum core thickness of 0.06". It is considered that the single MMC or borated aluminum plates have a thickness of 0.125".

The nominal widths of fuel compartments are 9" for four corner compartments and 8.725" for all other compartments. The corresponding nominal compartment opening sizes are 8.875" for fuel assemblies in the corner compartments and 8.6" for the other fuel assemblies. The widths of all compartments are reduced to 8.6" in 37PTH DSC model to accommodate for the size of the gaps and maintain the outer basket diameter contained within the canister inner diameter. Due to reduced size of the compartments, the compartment opening widths are 8.46" for all the fuel assemblies in the 37PTH DSC model.

Due to the reduced compartment opening in 37PTH DSC model, the related heat generation rates are increased by 10.0% ($=8.875^2 / 8.46^2$) for corner fuel assemblies and 3.3% ($=8.6^2 / 8.46^2$) for all other fuel assemblies. The transverse effective fuel

conductivity is calculated using the following equation from Appendix T, Section T.4.8.1.4 associated with Amendment 10 to Part 72 CoC 1004 for the Standardized NUHOMS® System [3].

$$k_{eff} = \frac{q''' a^2}{(T_c - T_o)}(0.29468)$$

With

$k_{eff}$ = transverse effective fuel conductivity (Btu/hr-in-°F)

$q'''$ = volumetric heat generation rate (Btu/hr-in$^3$)

$$q''' = \frac{Q}{4a^2 L_a}$$

Q = decay heat load (Btu/hr)

a= half of the compartment width (in.)

$L_a$ = Active fuel length (in.)

$T_c$ = maximum temperature of fuel assembly (°F)

$T_o$ = compartment wall temperature (°F)

Since the increase of the heat generation rate and the decrease of the compartment opening size cancel each other out in the above equation, the transverse effective fuel conductivity calculated for compartment openings of 8.875" and 8.6" can be used in the 37PTH DSC model with compartment openings of 8.46" without affecting the maximum fuel cladding temperature.

Except for the four corner compartments, 32PT and 37PTH baskets have similar fuel compartment material and configuration. Since the opening size of these compartments in the 37PTH DSC (8.6") is smaller than the compartment opening size of the 32PT DSC (8.7"), the bounding (lowest) effective properties for homogenized PWR fuel assemblies in 32PT basket taken from [1], Appendix M, Section M.4.2 can be used conservatively for the 37PTH DSC model for all fuel assemblies except the ones located in the four corner compartments. The bounding fuel assembly is WE 14x14 PWR fuel assembly.

Only 95% of the axial effective fuel conductivity calculated for 32PT DSC in [1], Appendix M, Section M.4.2 is considered for use in the 37PTH DSC model for conservatism. This value is utilized in 37PTH DSC model for all fuel assemblies except the ones located in the four corner compartments.

Based on [1], Drawing NUH24PTH-1003 SAR, sheet 2 of 7, Rev. 1, the compartment opening size for 24PTH DSC is 8.9" and the material of the compartments for 24PTH DSC is stainless steel SA 240, type 304. Since the compartment opening size for the four corner compartments in the 37PTH DSC (8.875") is smaller than the compartment opening size of the 24PTH DSC (8.9") and the emissivity of anodized aluminum used in the four corner compartments of 37PTH is higher than the emissivity of stainless steel, the bounding (lowest) effective fuel properties calculated for 24PTH DSC in [1], Appendix P, Section P.4.2 can be used conservatively for the fuel assemblies located in the four corner compartments in the 37PTH DSC model. The bounding effective fuel

conductivity used for the four corner fuel assemblies in the 37PTH DSC model belongs to WE 14x14 PWR fuel assembly taken from [1], Appendix P, Section P.4.2.

Decay heat load is applied as heat generation boundary conditions over the elements representing homogenized fuel assemblies. The base heat generation rate is multiplied by peaking factors along the axial fuel length to represent the axial decay heat profile. A correction factor is used to avoid degradation of decay heat load due to imperfections in application of peaking factors. The heat generation rates used in this analysis is calculated as follows.

$$\dot{q}''' = \left( \frac{q}{a^2 L_a} \times PF \right) \times CF$$

where,
q = Decay heat load per assembly defined for each loading zone
a = Width of the homogenized fuel assembly in model = 8.46"
$L_a$ =Active fuel length = 144"
PF = Peaking Factor
CF = correction factor = 1.002 for 37PTH

The base heat generation rates used in the 37PTH basket model are listed in the following table.

**Base Heat Generation Rates for 37PTH**

| Heat Load in the Model (KW) | $\dot{q}'''$ value without PF (Btu/hr-in$^3$) |
|---|---|
| 0.40 | 0.1327 |
| 0.60 | 0.1991 |
| 0.70 | 0.2322 |

### Axial Heat Flux Profile

The normalized axial burnup profile for typical PWR fuels with burnup higher than 30 GWd/MTU is taken from DOE/RW0472 [12]. The peaking factors from [12] are converted to match the regions defined for the fuel assembly in the 37PTH finite element model.

The maximum bundle-average burnup allowed in 37PTH DSCs is 65,000 MWD/MTU, which is considerably higher than 30,000 MWD/MTU referenced in the report. Research [12] shows that at a higher burnup, the heat flux shape tends to flatten with a reduction in the maximum axial peaking factor in the middle region, and the flux shape becomes more pronounced in the fuel end regions. The reduction of maximum axial peaking factor in a more flattened heat flux shape will result in lower fuel cladding temperatures. Therefore, the application of heat flux shape for a lower burnup spent fuel (30,000 MWD/MTU) on a higher burnup spent fuel (65,000 MWD/MTD) is conservative. These peaking factors are listed in Table A.3–7 and are shown in the following figure.

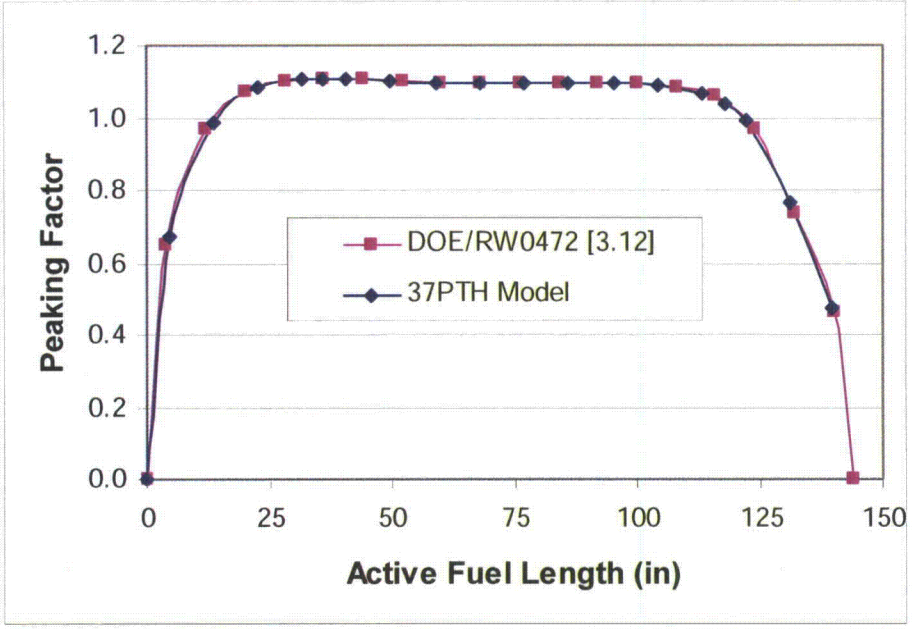


**Peaking Factor Curve for PWR Fuels**

As seen in Table A.3–7, the normalized area under the peaking factor curve is smaller than 1.0. To avoid any degradation of decay heat load, a correction factor of 1.002 calculated as follows is used when applying the peaking factors.

$$Nomalized\ Area\ under\ Curve = \frac{\text{Area under Axial Heat Profile}}{\text{Active Fuel Length}} = 0.998$$

Active fuel length = 144"

$$Correction\ Factor = \frac{1}{Normalized\ Area\ under\ Curve} = 1.002$$

The heat generating rates for the elements representing the active fuel are calculated based on the HLZC for 37PTH DSC. The HLZC and its restrictions for 37PTH basket are shown in the following figure.

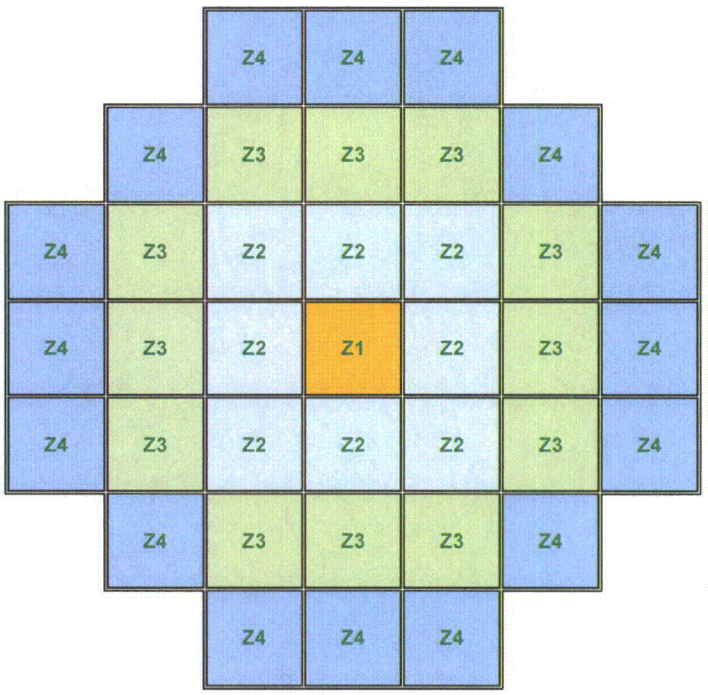


| | Zone 1 | Zone 2 | Zone 3 | Zone 4 |
|---|---|---|---|---|
| Max. Decay Heat (kW/FA) | 0.40 | 0.40 | 0.60 | 0.70 |
| No. of Fuel Assemblies | 1 | 8 | 12 | 16 |
| Max. Decay Heat per Zone (kW) | 0.4 | 3.2 | 7.2 | 11.2 |
| Max. Decay Heat per DSC (kW) | 22.0 | | | |

**Heat Load Zoning Configuration for 37PTH Basket**

The DSC shell temperatures for NCT at 100°F, -20°F and -40°F are retrieved from the MP197HB transport cask model described in Section A.3.3.1.1 and transferred to the basket models.

The material properties used in the 37PTH basket/DSC model are listed in Section A.3.2.1.

Section A.3.2.2.3 shows that the conductivity of MMC plate is lower than those of borated aluminum plate. Therefore, the conductivity of MMC plate is considered for single poison plates in the 37PTH basket model to bound the maximum component temperatures.

The effective thermal conductivities for Boral plates are calculated in Section A.3.3.1.7.

The geometry of the DSC model and the gaps are shown in Figure A.3–23 through Figure A.3–27.

Mesh sensitivity of the model is discussed in Appendix A.3.6.2.3.

Typical boundary conditions for DSC basket model are shown in Figure A.3–28.

A.3.3.1.7 Effective Thermal Properties of 37PTH DSC Basket

***1) Effective Conductivity for Boral Plates in 37PTH DSC***

Boral plates are considered as one homogenized material in the 37PTH basket model. The total thickness of the Boral plate is 0.075" with a core thickness of 0.06" in the 37PTH basket.

The Boral core and its aluminum claddings built up parallel thermal resistances along their length and serial thermal resistances across their thickness. The effective conductivities of the Boral plate are calculated using equations for $k_{eff,along}$ and $k_{eff,across}$ described in Section A.3.3.1.4 with the following parameters.

$k_{poison}$ = conductivity of core material for Boral (Btu/hr-in-°F)
$t_{poison}$ = thickness of core material for Boral = 0.06 in
$k_{Al}$ = conductivity of Al 1100 (Btu/hr-in-°F)
$t_{Al}$ = thickness of aluminum clad for Boral = 0.015 in
$t_{model}$ = thickness of Boral plates in the model =0.075 in

For conservatism, the conductivity of Boral core is reduced by 10% for calculation of effective conductivities.

The calculated effective conductivity values for Boral plates in 37PTH basket model are listed in Section A.3.2.1 material # 21.

A.3.3.2 Heat and Cold

Table A.3–8 and Table A.3–9 present the maximum temperatures for TC components and DSC Shells.

The DSC types 61BTH, 61BT, 32PTH, 32PTH1, 32PT, 24PTH, and 24PT4 are evaluated previously for normal transfer conditions under 10 CFR 72 requirements. The DSC shell temperature profiles of these DSCs in MP197HB model are compared with the corresponding profiles from 10 CFR 72 SARs in Section A.3.6.3. It is shown that the fuel cladding and the basket component temperatures in 10 CFR 72 SARs represent the bounding values for these DSCs under transport conditions.

Therefore, no additional analysis is performed for the DSCs previously evaluated under 10 CFR 72 conditions. The maximum fuel cladding and the basket component temperatures for these DSCs are taken from 10 CR 72 SARs and reported as the bounding values for transport conditions.

The maximum temperatures for DSC contents for all DSCs to be transported in MP197HB TC for NCT are listed in Table A.3–10.

The heat load of the secondary containers is limited to 5 kW and is bounded by the DSC heat loads of 18.3 kW to 32 kW. The maximum component temperatures of the MP197HB TC loaded with a secondary container are therefore bounded by those evaluated for TC loaded with DSCs. The content of the secondary containers are irradiated and/or contaminated non-fuel bearing solid materials, which have temperature limits significantly higher than the fuel cladding. Due to the lower heat load of secondary container, the maximum temperature of thecontent will be less than the basket and fuel

cladding temperatures loaded in the DSCs. Therefore, no additional analysis is required for the secondary containers.

As calculated in Section A.3.3.1.2, the maximum accessible surface temperatures for impact limiter and personnel barrier are 121°F and *163*°F, respectively. These temperatures are well below the limit of 185°F defined in Section A.3.1.

The thermal analysis of NCT demonstrates that the MP197HB TC with up to 32 kW heat load meets all applicable requirements. The highest maximum temperatures are summarized in Table A.3–11.

The maximum temperatures calculated using conservative assumptions are well below specified limits. The seal O-rings are not explicitly considered in the models. The maximum seal temperatures are retrieved from the models by selecting the nodes at the locations of the corresponding seal O-rings. The maximum seal temperature (382°F, 194°C) for NCT is below the long-term limit of 400°F (204°C) specified for continued seal function.

The maximum neutron shield temperature is 290°F (143°C) for NCT, which is below the long term limit of 320°F (160°C). No degradation of the neutron shielding is expected.

The maximum temperature of gamma shield is 397°F (203°C) for NCT, which is well below the melting point of lead (621°F, 327°C).

The predicted maximum fuel cladding temperature *of 674*°F *(357*°C) *for the maximum heat load of 32kW* is well within the allowable fuel temperature limit of 752°F (400°C) for NCT.

The temperature distributions for NCT with 100°F ambient and insolation are shown in Figure A.3–29 to Figure A.3–34.

Under the minimum ambient temperature of -40°F (-40°C), the resulting packaging component temperatures will approach -40°F if no credit is taken for the decay heat load. Since the package materials, including containment structures and the seals, continue to function at this temperature, the minimum temperature condition has no adverse effect on the performance of the MP197HB TC.

The maximum component temperatures for ambient temperatures of -40°F and -20°F with maximum decay heat and no insulation are calculated for 69BTH DSC and 37PTH DSC to use for structural evaluations. These temperatures are listed in Table A.3–12 and Table A.3–13.

The average temperatures of helium gas in TC cavity, and the average temperatures of fuel assemblies and helium within 37PTH and 69BTH DSC cavities for NCT are listed in Table A.3–14. These temperatures are used to evaluate the maximum internal pressures within TC and DSC cavities.

Thermal stresses for the MP197HB TC loaded with DSC are discussed in Chapter A.2. The maximum normal operating pressure for the MP197HB TC is discussed in Section A.3.3.3. The performance of the MP197HB TC loaded with DSCs for HAC is discussed in Section A.3.4.

### A.3.3.3 Maximum Normal Operating Pressure

#### A.3.3.3.1 MP197HB TC Operating Pressure

The following assumptions are considered to determine the maximum pressures within the MP197HB TC cavity during NCT when the TC is loaded with DSCs.

- All dimensions used in calculation of the maximum pressures are nominal.
- Length of the DSCs and the spacer in the axial direction are selected to minimize TC cavity volume and increase pressure.
- Length of the sleeve is conservatively assumed equal to the length of the TC cavity.
- The spacer is considered as a solid cylinder in this calculation.
- 98% of the TC cavity free volume is conservatively used in calculating the maximum pressures.
- The initial temperature of helium backfill in the cask cavity is assumed to be 70°F.
- The maximum initial pressure of the helium backfill in the cask cavity is 3.5 (2.5 $\pm$ 1) psig.
- For HAC, the highest average temperature of helium in the cask cavity in the transient run is considered for calculation of the maximum pressure.

The average helium temperatures in the cask cavity are retrieved from the MP197HB model described in Section A.3.3.1.1. The data used in calculating the pressures in the MP197HB TC cavity during NCT and HAC are listed below.

**Data used in Calculation of Maximum Pressures in TC Cavity**

| DSC Type | Heat Load kW | $OD_{DSC}$ in | $L_{DSC}$ in | $T_{avg, he,NCT}$ °F | $T_{avg, he,HAC}$ °F | $ID_{Shell}$ in | $L_{TC}$ in |
|---|---|---|---|---|---|---|---|
| 69BTH | 32 | 69.75 | 196.04 | 339 | 387 | 70.5 | 199.25 |
| 37PTH | 22 | 69.75 | 189.25 | 269 | N/A | | |
| 32PTH | 26 | 69.75 [4] | 185.75 [4] | 301 | | | |
| 32PTH, Type 1 | 26 | 69.75 [4] | 193.00 [4] | | | | |
| 32PTH1, Type 1 | 26 | 69.75 [3] | 198.50 [3] | | | | |
| 32PTH1, Type 2 | 24 | 69.75 [3] | 198.50 [3] | 288 | | | |
| **DSC Type** | | $OD_{DSC}$ | $L_{DSC}$ | $T_{avg, he,NCT}$ | $T_{avg, he,HAC}$ | $ID_{Sleeve}$ | |
| 61BTH, Type 1 [1] | 22 | 67.25 [3] | 196.04 [3] | 301 | N/A | 68 | |
| 61BTH, Type 2 [1] | 24 | 67.25 [3] | 196.04 [3] | 316 | | | |
| 61BT | 18 | 67.25 [1] | 196.04 [1] | 273 | | | |
| 32PT | 24 | 67.19 [1] | 192.55 [1] | 281 | | | |
| 24PTH, (all types) [1] | 26 | 67.19 [1] | 186.67 [1] | 297 | 333 | | |
| 24PT4 | 24 | 67.19 [2] | 196.30 [2] | 313 | N/A | | |

Note:
[1] DSCs 61BTHF and 24PTHF have the same dimensions and use the same MP197HB features as DSCs 61BTH and 24PTH, respectively. The thermal expansion of 61BTHF and 24PTHF DSCs is bounded by values for 61BTH and 24PTH DSCs and is not analyzed separately.

Where,

$OD_{DSC}$ = Outer Diameter of the DSC, *in*

$L_{DSC}$ = Length of the DSC, *in*

$T_{avg,he,NCT}$ = Average Temperature of helium for NCT

$T_{avg,he,HAC}$ = Average Temperature of helium for HAC

$ID_{Shell}$ = Inner diameter of TC inner shell, in

$ID_{Sleeve}$ = Inner diameter of sleeve, in

$L_{TC}$ = MP197HB Cavity Length, in

The spacer data used in calculating the pressures in the MP197HB TC cavity during NCT and HAC are listed below.

**Spacer Data used in Calculating Maximum Pressures**

| DSC Type | $L_{Spacer}$ (in) | $OD_{Spacer}$ (in) |
|---|---|---|
| 69BTH | 2.2 | 69.75 |
| 61BT/61BTH Type 1 and 2 | 2.2 | 67.25 |
| 37PTH | 9 | 69.75 |
| 32PTH | 12.5 | 69.75 |
| 32PTH Type 1 | 5.25 | 69.75 |
| 32PTH1 Type 1 and Type 2 | N/A [1] | N/A [1] |
| 32PT | 5.7 | 67.25 |
| 24PTH (all types) | 11.7 | 67.25 |
| 24PT4 | 2.2 | 67.25 |

Note: [1] 32PTH1-L is used in calculating the cask cavity pressures.

where,

$L_{Spacer}$ = Length of the spacer, *in*

$OD_{Spacer}$ = Outer Diameter of the Spacer Disc, *in*

The free volume of the MP197HB cask cavity is determined based on the dimensions presented in the above tables. The free volume of the MP197HB cask cavity is calculated as:

$$V_{free,cc} = \frac{\pi}{4} * \left[ (ID_{Cask}^2 * L_{TC}) - (OD_{DSC}^2 * L_{DSC} + OD_{Spacer}^2 * L_{Spacer}) \right]$$

where,

$ID_{Cask}$ = $ID_{Shell}$, Inner diameter of the cask inner shell for DSCs without sleeve, in

= $ID_{Sleeve}$, Inner diameter of the cask sleeve for DSCs with sleeve, in

The number of moles of helium in the cask cavity is calculated using the ideal gas law and is as follows:

$$n_{he,Initial} = \frac{P_{initial} * (6894.8 Pa/psi) * V_{free,cc} * (1.6387 * 10^{-5} m^3/in^3)}{R * T_{avg,He} (5/9 K/^oR)}$$

The maximum pressure in the cask cavity for NCT is calculated as:

$$P_{NCT} = \frac{\left(1.4504 * 10^{-4} \frac{psia}{Pa}\right) * (n_{he,initial}) * R * T_{avg,he,NCT} * (5/9 K/^oR)}{0.98 * V_{free,cc} * (1.6387 * 10^{-5} m^3/in^3)}$$

where,

$T_{avg,He}$ = Initial Average Temperature of helium
$R$ = Universal gas constant, $8.314 J/(mol - K)$
$n_{he,initial}$ = number of moles of helium in MP197HB cask cavity, $g - moles$
$P_{initial}$ = Initial pressure in the MP197HB cask cavity, *psia*
$P_{NCT}$ = Pressure in the MP197HB cask cavity during NCT, *psia*
$V_{free,cc}$ = Free volume of MP197HB cask cavity, $in^3$

The maximum pressures in the cask cavity calculated for loaded MP197HB TC are presented in Table A.3–20. The case of the 69BTH DSC in MP197HB TC with 32 kW heat load is bounding for the maximum TC cavity pressure for all DSCs. The maximum pressure in the cask cavity of the MP197HB TC for NCT is 12.7 psig.

Due to low heat load of the secondary containers and expected low amount of fission gas release, the internal pressure of the cask loaded with the DSCs is bounding for the cask loaded with the secondary containers.

#### A.3.3.3.2 69BTH DSC Operating Pressure

The maximum internal pressure for the 69BTH DSC within MP197HB TC for NCT is determined based on the maximum allowable heat load for each HLZC discussed in Section A.3.3.1.4 and maximum burnup of 70 GWD/MTU. The limiting fuel assembly type considered in this evaluation is the FANP 9x9-2 assembly.

The calculations account for the canister free volume, the quantities of canister backfill gas, fuel rod fill gas, and fission products and the average canister cavity gas temperature. The internal canister pressures are then calculated using ideal gas law.

$$P_{can} = \frac{n_{total} R T_{avg,can}}{V_{free,can}}$$

Where:
$n_{total}$ = Total number of moles of gases within canister cavity (lb-moles),
R = Universal gas constant (10.73 psia-$ft^3$/lb-moles-°R),
$T_{avg,can}$ = DSC cavity average temperature (°R),

$V_{free,can}$ = DSC free volume ($ft^3$), and
$P_{can}$ = DSC internal pressure (psia).

The following assumptions and conservatisms are considered in calculating the maximum internal pressures within the 69BTH DSC:

- The DSC internal pressure is calculated below for the most limiting normal, and accident cases for the 69BTH DSC. For these cases, 3% and 100% of the fuel rods are assumed to rupture, 100% of the fuel rod helium fill gas and 30% of the fission gases are assumed to be released into the DSC cavity [9]. The methodology for DSC internal pressure calculations is in accordance with the methodology used for the 61BTH DSC associated with Amendment 10 to Part 72 CoC 1004 for the Standardized NUHOMS® System [3].

- The amount of fission gasses produced by the "generic" BWR fuel assembly (FA) is obtained from the 61BTH methodology ([3], Appendix T, Section T.4.6.6.4).

- The DSC cavity average helium temperatures calculated in 69BTH DSC in Sections A.3.3.1.4 and A.3.4 for limiting FANP 9x9-2 fuel assembly, are assumed to bound average helium temperatures for the rest of 69BTH fuel assemblies (FA).

- Similar to the 61BTH DSC, the 69BTH DSC is assumed to be backfilled with helium to a pressure of 3.5 (2.5 ± 1.0) psig after vacuum drying [3].

- An average temperature of 212°F equal to water boiling temperature is considered for the DSC shell during backfill operation.

- The initial temperature of fuel rod plenum fill gas is assumed to be at room temperature (70°F or 530°R). This is a reasonable assumption since the process takes place in a controlled environment.

- The highest burnup of 70 GWD/MTU proposed for the 69BTH DSC is assumed for the pressure calculation. Maximum burnup creates a bounding case for the amount of fission gases produced in the fuel rod during reactor operation.

- The highest weight and volume of fuel assembly was conservatively used because it displaces the most of free DSC cavity volume.

- The bounding (maximum) plenum volume among all fuel assemblies $V_{pl}$=2.136 $in^3$ (For SVEA FAs) is conservatively used in this calculation.

- The bounding (maximum) initial rod pressure ($p_{initial}$) of 160 psia (For SVEA FAs) is used.

- Only 98% of the DSC free cavity volume is used for pressure calculation.

### *1) Free DSC Cavity Volume*

The volume of helium in the DSC cavity is calculated based on 69BTH weight calculations provided in Chapter A.2. The 69BTH DSC cavity free volume is calculated as DSC cavity volume minus basket, dummy assemblies (DA) and fuel assemblies' volume. The free volume for helium in the DSC is calculated as,

$V_{He\_DSC} = V_{He\_DSC\_w/o\_FA} - V_{FAs} - V_{DAs}$

Where,

$V_{He\_DSC}$ = Free helium volume in DSC

$V_{He\_DSC\_w/o\_FA}$ = Helium volume outside fuel compartments in DSC cavity

$V_{FAs}$ = Helium volume within compartment containing fuel assemblies

$V_{DAs}$ = Helium volume within compartment containing dummy assemblies

The 69BTH DSC free helium volume and DSC cavity volumes used for pressure calculations are summarized in Table A.3–21 and Table A.3–22, respectively.

### *2) Average Helium Temperature*

The average helium temperature in the DSC cavity is calculated based on DSC thermal analysis presented in Section A.3.3.1.4 and weight data provided in Chapter A.2 as volumetric average:

$$T_{He\_DSC} = (V_{He\_in\_FA\_act\_fuel} \cdot T_{He\_in\_FA\_act\_fuel} + V_{He\_in\_DA\_act\_fuel} \cdot T_{He\_in\_DA\_act\_fuel} + V_{He\_DSC\_out\_FA/DA\_act\_fuel} \cdot T_{He\_DSC\_out\_FA/DA\_act\_fuel}) / V_{He\_DSC.}$$

where,

$T_{He\_DSC}$ = Temperature of helium in DSC

$V_{He\_in\_FA\_act\_fuel}$ = Volume of helium in FAs along active fuel

$T_{He\_in\_FA\_act\_fuel}$ = Temperature of FAs along active fuel

$V_{He\_in\_DA\_act\_fuel}$ = Volume of helium outside DAs along active fuel

$T_{He\_in\_DA\_act\_fuel}$ = Temperature of DAs along active fuel

$V_{He\_DSC\_out\_FA/DA\_act\_fuel}$ = Rest of helium volume in DSC outside FAs and DAs along active fuel

$T_{He\_DSC\_out\_FA/DA\_act\_fuel}$ = Temperature of helium in cavity outside FAs and DAs along active fuel

Calculation of the average temperature of helium in 69BTH and 37PTH DSCs cavity for NCT and HAC is summarized in Table A.3–21.

### *3) Quantity of Helium Fill Gas in DSC*

The 69BTH DSC free volume is assumed to be filled with 3.5 psig (18.2 psia) of helium. The average temperature of helium during backfill is evaluated based on linear extrapolation of helium average temperatures versus DSC shell temperatures for cold and hot NCT. A DSC shell temperature equal to water boiling temperature of 212°F is assumed during backfill operation. The average helium temperatures for 69BTH DSC in MP197HB at ambient temperature of -40°F and 100°F are calculated using the method

described above. The evaluation of average helium backfill temperature for 69BTH and 37PTH DSCs is shown in the following table.

**Evaluation of Helium Backfill Temperature**

| | 69BTH | DSC | | 37PTH | DSC | |
|---|---|---|---|---|---|---|
| Operation | Transport $T_{amb}$=100°F | Transport $T_{amb}$=-40°F | He backfill | Transport $T_{amb}$=100°F | Transport $T_{amb}$=-40°F | He backfill |
| $T_{DSC\ shell\ av}$, °F | 420 | 288 | 212 | 357 | 259 | 212 |
| $T_{he\ av}$, °F | 538 | 448 | **396** | 500 | 413 | **371** |
| $T_{he\ av}$, °R | - | - | **856** | - | - | **831** |

These average helium temperatures are used to estimate the number of moles of helium backfill in the DSC in accordance with the methodology of [1], Appendix P, Section P.4.6.5.4 for 24PTH DSC.

Using the ideal gas law,

$PV = nRT,$

$n = PV / RT,$

$R = 8.314 J/(mol \cdot K).$

The quantity of helium in the DSC for the 69BTH DSC for HLZC #1 is:

$$n_{he,std} = \frac{(18.2\ psia)(6894.8\ Pa/psi)(258413\ in^3)(1.6387 \cdot 10^{-5}\ m^3/in^3)}{(8.314\ J/(mol \cdot K))(856°R)(5/9\ K/°R)},$$

$$n_{he,std} = 134.39\ g-moles.$$

The initial 69BTH DSC helium fill gas quantities are listed in Table A.3–22.

### *4) Quantity of Fill Gas in Fuel Rod*

The volume of the helium fill gas in a fuel rod for the limiting (by number of fuel rods) SVEA fuel assemblies, at cold, unirradiated conditions is assumed to be 2.136 $in^3$ (maximum among all 69BTH fuels). There are at most 100 fuel rods in an SVEA fuel assembly with a maximum fill pressure of 145.3 psig (160 psia).

The fill gas is assumed to be at room temperature (70°F or 530°R). Per the ideal gas law, the quantity of fuel rod fill gas in 69 assemblies is:

$$n_{he} = \frac{(160\ psia)(6894.8\ Pa/psi)(69 \cdot 100 \cdot 2.136\ in^3)(1.6387 \cdot 10^{-5}\ m^3/in^3)}{(8.314\ J/(mol \cdot K))(530°R)(5/9\ K/°R)},$$

$$n_{he} = 108.91\ g-moles.$$

Based on 10 CFR 71 [6], the maximum fraction of the fuel pins that are assumed to rupture and release their charge gas for normal and accident conditions is 3% and 100%, respectively. Table A.3–22 summarizes the amount of helium fill gas released for the 69BTH DSC for NCT and HAC.

***5) Quantity of Gases released as a Result of Irradiation***

For the 69BTH DSC, the quantity of gases released as a result of irradiation for the "generic" BWR fuel assembly is 20.2 g-moles as shown in Appendix T, Section T.4.6.6.4 associated with Amendment 10 to Part 72 CoC 1004 for the Standardized NUHOMS® System [3]. The total gas moles (per fuel assembly) are then multiplied by the 30% release fraction to obtain the number of moles contributing to 69BTH DSC cavity gas pressure.

The amount of gas released from one assembly because of irradiation is adjusted to burnup of 70,000 MWD/MTU as follows.

$n_{ig\ 1\ FA}$ = *20.2 g-moles*70,000/62,000 * 0.3 = 6.84 g-moles*

Table A.3–22 presents the amount of gas released into the DSC cavity by fuel assemblies $n_{ig}$ for normal and accident conditions assuming a 30% gas release from the fuel pellets [9] and a 3% and 100% rod rupture percentage, respectively.

***6) Maximum Normal Operating Pressure Calculation***

Calculation of the maximum pressure in the 69BTH DSC HLZC #1 for normal conditions of transport is shown below. In accordance with [9], 3% of the fuel rods are assumed to be ruptured. The total amount of gas in the DSC cavity is therefore:

$$n_{DSC-NCT} = n_{he\ initial} + n_{he\ fuel\ rod\ release} + n_{ig},$$

$$n_{DSC-NCT} = 134.39 + 3.27 + 14.16 = 151.82 \quad g-moles$$

Ruptured pins will vent plenum gas until it comes into equilibrium with the DSC pressure; therefore, the plenum volume within the ruptured pins can be included in the total DSC internal volume. For a 3% pin rupture the additional volume is therefore:

$$V_{pin\ plenum} = 100\ pins/assy \cdot 2.136\ in^3/pin \cdot 69\ assy/basket \cdot 0.03 = 442.15\ \ in^3.$$

The maximum normal operating pressure (MNOP) for this configuration is then,

$$P_{DSC-NCT} = \frac{\left(1.4504 \cdot 10^{-4}\ \frac{psia}{Pa}\right)(151.82\ g-moles)(8.314\ J/(mol \cdot K))(984\ ^\circ R)(5/9\ K/^\circ R)}{(258413\ in^3 + 442.15\ in^3)(1.6387 \cdot 10^{-5}\ m^3/in^3)},$$

$$P_{DSC-NCT} = 23.59\ psia\ (8.89\ psig)$$

The maximum pressures are summarized in Table A.3–22. As seen from Table A.3–22, the maximum internal pressures in the 69BTH DSC *calculated based on thermal conditions are lower than the design pressures considered for the structural evaluation.*

A.3.3.3.3 37PTH DSC Operating Pressure

The maximum internal pressure for the 37PTH DSC within the MP197HB TC for NCT is determined based on the maximum allowable heat load of 22 kW discussed in Section A.3.3.1.6 and maximum burnup of 65 GWD/MTU. Although BW 15x15 fuel assembly is not allowed for transport in the 37PTH DSC, it is considered as the limiting fuel assembly type in this evaluation for conservatism.

Calculation of Maximum Normal Operating Pressure inside the 37PTH DSC follows the same methodology as described for 69BTH DSC in Section A.3.3.3.2.

The following assumptions and conservatisms are considered in calculating the maximum internal pressures within the 37PTH DSC:

a) The DSC internal pressure is calculated for the most limiting normal, and accident cases. For these cases, 3% and 100% of the fuel rods are assumed to rupture, 100% of the fuel rod helium fill gas and 30% of the fission gases are assumed to be released into the DSC cavity [9]. The methodology for DSC internal pressure calculations is in accordance with the methodology used for the 32PTH1 associated with Amendment 10 to Part 72 CoC 1004 for the Standardized NUHOMS® System [3].

b) The following fuel assemblies are considered bounding for internal DSC pressure analyses performed for 32PTH1, 32PTH, 24PTH, and 24PT4 DSCs:
WE 15x15 - for 32PTH DSC [4],
BW 15x15 - for 24PTH DSC [1],
CE 16x16 – for 24PT4 DSC [2].
Since BW15x15 is bounding by amount of irradiation gases [30], it is selected for this analysis.

c) The 37PTH DSC is assumed to be backfilled with helium to a pressure of 2.5 ± 1.0 psig after vacuum drying similar to the 32PTH1 DSC [3].

d) The fuel rod plenum fill temperature is assumed to be room temperature (70°F or 530°R). This is a reasonable assumption since the process takes place in a controlled environment.

e) The BW 15x15 fuel assembly used in the pressure calculation is assumed to be burned to 65 GWD/MTU, which is the highest burnup proposed for the 37PTH DSC configuration. Assuming maximum burnup creates a bounding case for the amount of fission gases produced in the fuel rod during reactor operation.

f) The average helium temperatures used in this calculation for 37PTH DSC configuration are obtained from the thermal analysis of 37PTH DSC short length configuration. The medium length 37PTH DSC results are bounded by the short length 37PTH DSC results, and hence, it is conservative to use the short cavity results.

g) Data of bounding BW15x15 fuels assembly with control components (CC) is conservatively used for calculating internal pressure for 37PTH DSC.

h) The short length 37PTH DSC design with lowest free volume and fill gas amount is conservatively used in this calculation.

i) Only 98% of DSC free cavity volume is used for pressure calculation.

***1) Free DSC Cavity Volume***

Free DSC Cavity volume for the 37PTH DSC is calculated using the same methodology used for the 69BTH in Section A.3.3.3.2.

The 37PTH DSC free helium volume and conservative DSC cavity volumes used for pressure calculations are summarized in Table A.3–21 and Table A.3–22, respectively.

***2) Average Helium Temperature***

Average Helium Temperature for the 37PTH DSC is calculated using the same methodology used for 69BTH in Section A.3.3.3.2.

The 37PTH DSC average helium temperature used for pressure calculations are calculated and summarized in Table A.3–21 and Table A.3–22, respectively.

***3) Quantity of Helium Fill Gas in DSC***

Helium Fill Gas in DSC for the 37PTH DSC is calculated using the same methodology used for 69BTH in Section A.3.3.3.2.

The initial 37PTH DSC helium fill gas quantities are listed in Table A.3–22.

***4) Quantity of Fill Gas in Fuel Rod and Gases released as a Result of Irradiation***

The total free gas in fuel rod, which includes fuel rod fill gas and gases released because of irradiation for bounding BW15x15 FA is provided in Table 7-14 of [30] for maximum burnup of 55000 MWD/MTU and extrapolated linearly for 65000 MWD/MTU as shown in the following table.

**Amount of Gas released from Fuel Rods (BW15x15 FA)**

| **Burnup**, MWD/MTU | **Total Free Gas at STP,** ($cm^3$) |
|---|---|
| 55,000 | 1400 |
| 65,000 | 1665 [(1)] |

Note:
[(1)] Extrapolated value.

For 37PTH DSC, the amount of fill gas in fuel rods and fission gases released as results of irradiation are combined and the total is shown in Table A.3–22.

**5) Quantity of Gas in Control Components**

The 37PTH DSC PWR fuel assembly may include control components (CCs). The evaluation of gas quantities for CCs is based on the BW15x15 CCs documented in [1] Appendix J, Section J.4. For the controlling BW 15x15 assembly, up to 37 CCs may be present. These CCs are assumed to have an initial helium fill of 14.7 psia, and if 100% of the boron is consumed, and 30% released into the DSC, a total of 82.94 g-moles of gas could be released to the DSC assuming 100% cladding rupture (based on 53.8 g-mol for 24 BPRA in the 24P DSC, from [1] Appendix J, Section J.4).

The percentage of CCs rods ruptured during normal and accident conditions is assumed to be 3% and 100%, respectively, similar to the assumptions for the fuel rod rupturing. The maximum amount of gas released to the DSC cavity from the CCs $n_{cc}$ for normal and accident conditions is given in Table A.3–22.

**6) Maximum Normal Operating Pressure Calculation**

Calculation of the maximum pressure in 37PTH DSC follows the same methodology as used for 69BTH DSC in Section A.3.3.3.2.

The maximum pressures for 37PTH DSC are summarized in Table A.3–22. As seen from Table A.3-22, the maximum internal pressures in 37PTH DSC *calculated based on thermal conditions are lower than the design pressures considered for the structural evaluation.*

A.3.3.3.4 Internal Pressure for DSCs analyzed for Storage/Transfer

The maximum internal pressures for 61BTH, 61BT, 32PTH, 32PTH1, 32PT, 24PTH, and 24PT4 DSCs for storage and transfer conditions under 10 CFR 72 requirements are determined in [1], [2],[3], and [4].

Based on discussions in Section A.3.3.2 the maximum fuel cladding and basket component temperatures for 61BTH, 61BT, 32PTH, 32PTH1, 32PT, 24PTH, and 24PT4 DSC in MP197HB TC for transport conditions (10 CFR 71) are bounded by temperatures for storage and transfer conditions (10 CFR 72) and no DSC thermal analysis is required. It is also applicable to the average gas temperatures in DSC cavity. Therefore, the internal pressure in a DSC for NCT with 3% ruptured fuel rods can be evaluated interpolating between the internal pressures calculated for normal storage/transfer conditions with 1% ruptured fuel rods and off-normal storage/transfer conditions with 10% ruptured fuel rods. Higher average helium temperatures for accident storage and transfer conditions compared to normal temperatures provide additional conservatism in the internal pressure calculation for NCT.

Since 100% percent of ruptured fuel rods is assumed for both transfer accident conditions and transport HAC and maximum DSC shell temperatures for transfer accident conditions bound those for transport HAC as noted in Section A.3.4 (which results in lower average DSC helium temperature), the internal pressures calculated for storage licensed DSCs for transfer accident conditions bound the internal pressures for transport in MP197HB TC during HAC.

As seen from Table A.3-23, the maximum internal pressures in storage licensed DSCs *calculated based on thermal conditions are lower than the design pressures considered for the structural evaluation.*

A.3.3.3.5 Operating Pressures for 61BTHF and 24PTHF DSCs

As shown in Chapter 4, Table 4-28 of [4] for 32PTH DSC, a loading configuration with 50% intact and 50% damaged fuel assemblies results in negligible increase (~0.1 psi) in maximum internal pressure for bounding accident conditions.

The number of failed and damaged fuel assemblies for 61BTHF and 24PTHF DSCs is 16 and 12, respectively. Therefore, the maximum pressures calculated for 61BTH DSC and 24PTH DSC reported in Table A.3–23 can be used for 61BTHF and 24PTHF DSCs. As seen from Table A.3–23, the maximum internal pressures in storage licensed DSCs *calculated based on thermal conditions are lower than the design pressures considered for the structural evaluation.*

### A.3.3.4 Thermal Evaluation for Loading/Unloading Operations

Vacuum drying is considered as a normal condition for wet loading operations. The fuel transfer operations for wet loading occur when the MP197HB and the loaded DSC are in the spent fuel pool. The fuel is always submerged in free-flowing pool water permitting heat dissipation. After completion of fuel loading, the TC and DSC are removed from the pool and the DSC is drained, dried, sealed and backfilled with helium. These operations occur when the annulus between the TC and DSC remains filled with water.

The water in the annulus is replenished with fresh water to prevent boiling and maintain the water level if excessive evaporation occurs. Presence of water within the annulus maintains the maximum DSC shell temperature below the boiling temperature of water in open atmosphere (212°F).

Water in the DSC cavity is forced out of the cavity (blowdown operation) before the start of vacuum drying. Helium is used as the medium to remove water and subsequent vacuum drying occurs with a helium environment in the DSC cavity. The vacuum drying operation does not reduce the pressure sufficiently to reduce the thermal conductivity of the helium in the canister cavity ([3], Appendix T, Section T.4 based on [5], [32], and [33]).

With helium being present during vacuum drying operations, the maximum temperatures including the maximum fuel cladding temperature are bounded by those calculated for transport operation if the DSC shell temperature under NCT is higher than the DSC shell temperature of 212°F maintained during vacuum drying. As shown in Table A.3–8 and Table A.3–9 for all DSCs in MP197HB TC, all DSC shell minimum temperatures are higher than 212°F. Therefore, no additional thermal evaluation is needed.

Presence of helium during blowdown and vacuum drying operations eliminates the thermal cycling of fuel cladding during helium backfilling of the DSCs subsequent to vacuum drying. Therefore, the thermal cycling limit of 65°C (117°F) for short term operations set by ISG-11 [7] is satisfied for vacuum drying operation in MP197HB.

The bounding unloading operation considered is the reflood of the DSCs with water. For unloading operations, the DSC is filled with the spent fuel pool water through its siphon port. During this filling operation, the DSC vent port is maintained open with effluents routed to the plant's off-gas monitoring system.

The maximum fuel cladding temperature during reflooding event is significantly less than the vacuum drying condition owing to the presence of water/steam in the canister cavity. Based on the above rational, the maximum cladding temperature during unloading operation is bounded by the maximum fuel cladding temperature for vacuum drying operation.

Initially, the pool water is added to the canister cavity containing hot fuel and basket components, some of the water will flash to steam causing internal cavity pressure to rise. This steam pressure is released through the vent port. The procedures specify that the flow rate of the reflood water be controlled such that the internal pressure in the canister cavity does not exceed *the maximum pressure specified for reflooding*

*operations as noted in Chapter A.7, Appendices A.7.7.1 through A.7.7.9.* This is assured by monitoring the maximum internal pressure in the canister cavity during the reflood event. The reflood for the DSC is considered as a Service Level D event and the design pressures of the DSCs are well above *15 psig for the 32PTH DSC and 20 psig for the other DSCs (see Chapter A.7, Appendices A.7.7.1 through A.7.7.9).* Therefore, there is sufficient margin in the DSC internal pressure during the reflooding event to assure that the canister will not be over pressurized.

The effects of the thermal loads on the fuel cladding during reflooding operations are evaluated in Appendix T, Section T.4.7.3 and Appendix U, Section U.4.7.3 for BWR and PWR fuel assemblies respectively, associated with Amendment 10 to Part 72 CoC 1004 for the Standardized NUHOMS® System [3]. Since the same fuel assemblies are handled in the DSCs contained in MP197HB, these evaluations remain valid for this calculation.

## A.3.4 Thermal Evaluation under Hypothetical Accident Conditions

The thermal performance of the MP197HB TC loaded with DSCs with heat load up to 32 kW is evaluated in this section under the HAC described in 10 CFR 71.73 [6]. This evaluation is performed primarily to demonstrate the containment integrity of the MP197HB TC for HAC. This is assured as long as the O-rings seals in the cask lid and cask bottom plate remain below 400°F (204°C) and the cask cavity pressure is less than the design pressure as specified in Section A.3.1.

The finite element model of the MP197HB TC developed in Section A.3.3.1.1 is modified in this evaluation to determine the maximum component temperatures for HAC. For the transient runs considering HAC conditions, the basket and hold-down ring (if applicable) are homogenized. SOLID70 elements are used to model the homogenized basket and hold-down ring. The elements for other components are the same as those described in Section A.3.3.1.1.

Ambient conditions for HAC are based on 10 CFR 71 [6] requirements and are applied on the boundaries of the cask model. These conditions are listed below.

**Hypothetical Accident Conditions for MP197HB**

| Period | Ambient temperature (°F) | Insolance | Duration (hr) |
|---|---|---|---|
| Initial Conditions | 100 | Yes | N/A |
| Fire | 1475 | No | 0.5 |
| Wood Smoldering | 100 | Yes | 0.5 |
| Cool-Down | 100 | Yes | N/A |

The assumptions and conservatism considered in evaluation for HAC are described in Sections A.3.4.1 and A.3.4.2.

### A.3.4.1 Initial Conditions

The initial temperatures for the MP197HB TC transient model before the fire accident are determined using the same boundary conditions for NCT (100°F ambient with insolation) described in Section A.3.3.1.1 except that the decay heat load is applied as a uniform heat generation rate over the homogenized basket for the transient runs.

$$q''' = \frac{Q}{(\pi/4)\, D_i^{\,2}\, L_b}$$

$q'''$ = decay heat generation rate (Btu/hr-in$^3$)
$Q$ = decay heat load (Btu/hr) (to convert from kW multiply by 3412.3)
$D_i$ = DSC inner diameter (in)
$L_b$ = Basket length (in)

The decay heat generation rates used in the transient model are listed below.

**Decay Heat Generation Rate**

| DSC Type | Heat Load (kW) | Heat Load (Btu/hr) | $D_i$ (in) | $L_b$ (in) | Decay heat Generation Rate (Btu/hr-in$^3$) |
|---|---|---|---|---|---|
| 69BTH | 26.0 | 88,720 | 68.75 | 164 | 0.1457 |
| | 32.0 | 109,194 | 68.75 | 164 | 0.1794 |
| 24PTH | 26.0 | 88,720 | 66.19 | 168.60 | 0.1529 |

All the assumptions and conservatism described in Section A.3.3.1.1 for the MP197HB model are valid for determination of initial conditions.

### A.3.4.2 Fire Test Conditions

No fire test is performed. Instead, the fire conditions are simulated using the finite element model of the MP197HB TC.

Based on the requirements in 10 CFR 71, part 73 [6], a fire temperature of 1475 °F, fire emissivity of 0.9 and a period of 30 minutes are considered for the fire conditions. A bounding forced convection coefficient of 4.5 Btu/hr-ft$^2$-°F is considered during burning period based on data from reference [13]. Surface emissivity of 0.8 is considered for the packaging surfaces exposed to fire based on 10 CFR 71, part 73 [6].

The total heat transfer coefficient during fire is determined using the following equations.

$$h_{t,fire} = h_{r,fire} + h_{c,fire}$$

Where,

$h_{r,fire}$ = fire radiation heat transfer coefficient (Btu/hr-in$^2$-°F)

$h_{c,fire}$ = forced convection heat transfer coefficient during fire = 4.5 Btu/hr-in$^2$-°F

The radiation heat transfer coefficient, $h_{r,fire}$, is given by the equation:

$$h_{r,fire} = \varepsilon_w F_{wf} \left[ \frac{\sigma(\varepsilon_f T_f^4 - T_w^4)}{T_f - T_w} \right] \quad \text{Btu/hr-in}^2\text{-°F}$$

where,

$\varepsilon_w$ = TC outer surface emissivity = 0.8 [6]

$\varepsilon_f$ = fire emissivity = 0.9 [6]

$F_{wf}$ = view factor from TC surface to fire = 1.0

$\sigma$ = 0.1714 $\times 10^{-8}$ Btu/hr-ft$^2$-°R$^4$

$T_w$ = surface temperature (°R)

$T_f$ = fire temperature = 1475°F = 1,935°R

The sensitivity study that documents the effects of fire emissivity of 1.0 on the thermal performance of the MP197HB TC is documented in Appendix A.3.6.8.

The following gaps are reduced from 0.0625" under NCT to 0.01" under HAC to maximize the heat input from the fire toward the cask after free drop:

a) 0.01" axial gap between thermal shield and impact limiter case
b) 0.01" axial gap between thermal shields and cask top or bottom end surface

The following modifications are considered for the MP197HB TC model to maximize the heat input from the fire toward the cask during fire period and bound the maximum temperatures during the cool-down period.

a) The thermal properties of the gaps considered for initial conditions are changed to the properties for one of the adjacent components. The thermal properties of these gaps are restored after the fire during cool-down period. These gaps are listed in Table A.3–15.

b) Based on the cask slide rail thickness and orientation shown in Figure A.3–1, the gap between the lowest point of the DSC shell and the cask inner shell is maximized when the DSC centerlines are shifted by x" calculated in Section A.3.3.1.1. For the HAC analysis, the DSC centerlines are considered to be shifted by the same amount as described in Section A.3.3.1.1 to maximize the initial and the cool-down temperatures for TC and DSC components.

c) As noted in Section A.3.3.1.1, axial and radial gaps are considered for internal sleeve. These gaps are removed during the fire period by changing the material properties of internal sleeve to those of aluminum 6061. The assumed gaps within the internal sleeve are restored for the cool-down period by changing its material properties to the effective values calculated in Section A.3.4.2.1.

d) The cask slide rails are assumed to be in contact with DSC shell during the fire period. The properties of the cask slide rail are changed to helium or a dummy material with a conductivity of 1×10-8 Btu/hr-in-°F for cool-down period.

e) It is assumed that the cask is equipped with external fins for 32 kW head load and the external fins maintain their shape during the fire and completely melt away after the fire. The finned shell and the gap between the finned shell and the shield shell outer surface remain in place after the fire. Due to these assumptions, the maximum component temperatures for the cask with the external fins bound those for the cask without the external fins for 32 kW heat load under the HAC.

f) The neutron shield resin and the trunnion plug resin assumed to remain intact during the fire period and disintegrate completely after the fire. Air with conduction only properties replaces these resins during the cool-down period.

g) Based on structural evaluation in Chapter A.2, the aluminum blocks of thermal shield will be crushed due to end drop accident. This crush causes also local deformation of impact limiter at the location of the aluminum blocks, which creates a relative large gap between the thermal shield and the impact limiter plates at these locations. The magnitude of deformation is larger at the lateral segments and smaller at the central segment of the impact limiter. A uniform height of 0.25" is considered for aluminum blocks after the drop accident. This value is smaller than the average block heights shown in Chapter A.2. This assumption bounds conservatively the heights of the aluminum blocks to maximize the heat input from the fire toward the seals, particularly for the port seals and ram closure plate seal located beneath the central segment of the impact limiter.

h) No heat dissipation is considered for the impact limiter outer surfaces to evaluate the maximum canister shell temperatures under steady state cool-down conditions.

In order to maximize the heat input from the fire toward the TC, the impact limiters of the MP197HB TC model are modified to reflect deformation due to drop accidents. The crush depths of impact limiters are determined in Chapter A.2 based on end, side, corner, and slap down accident drops. The minimum distances between the TC and the surface of the damaged impact limiters are recalculated based on the crush depths given in Chapter A.2 and depicted in Figure A.3–35 and Figure A.3–36. For conservatism, the maximum crush depth experienced by the impact limiter in a given direction is assumed to occur everywhere on the impact limiter.

Comparison between Figure A.3–35 and Figure A.3–36 shows that the maximum deformation is caused by the side and corner drop accidents. The shortest distances between the TC and the surface of the damaged impact limiter are 9.25″ and 8″ in the radial and axial directions, respectively.

To bound the shortest distances conservatively in the model, the shortest distances between the TC and the surface of the damaged impact limiter are reduced to 8.25″ and 7″ in the radial and axial directions, respectively. To implement this, the cask the impact limiters outer diameter is reduced from 126″ to 101″ and the length of the impact limiter is reduced from 58″ to 34.5″. The shortest distances between the TC and the surface of the damaged impact limiters in the model are calculated as follows.

Shortest distance for radial direction: $(OD_{IL,crush} - OD_{TO}) / 2 = (101 - 84.5) / 2 = 8.25''$

Impact limiter height after drop ($H_{IL,crush}$) = 34.5″

Length of Impact limiter above the cask bottom plate / lid ($h_{1,IL}$) = 27.5″ (see Figure A.3–35 for end drop)

Shortest distance for axial direction: $(H_{IL,crush} - h_{1,IL}) = (34.5 - 27.5) = 7.0''$

Since the shortest distances between the cask and the deformed impact limiters are considered uniformly in all directions, the thermal model bounds conservatively the deformations determined in Section A.2. The geometry of the TC model with deformed impact limiters is shown in Figure A.3–37.

Although the impact limiters are locally deformed during the drop accident, they remain attached to the cask. Since the welds of the impact limiter shell do not break, the wood within the impact limiter shell cannot access air and would char but not burn during the hypothetical fire accident. Hence, the steel encased wood impact limiters still protect the bottom plate and the lid of the cask from direct exposure to fire.

Although unlikely, the worst-case damage due to a hypothetical puncture condition based on 10 CFR 71.73 [6] may result in tearing off the outer steel skin of the impact limiter, crushing the wood out of the damaged area, and exposing the partially contained wood to the hypothetical fire conditions.

A study of fire performance of wood at elevated temperatures and heat fluxes [14] shows that the surface temperature for the rapid spontaneous ignition of wood is between 330 °C and 600 °C (626 °F and 1,112 °F). Based on standard fire test (ASTM E119, 1988) reported in [14], if a thick piece of wood is exposed to fire temperatures

between 815 °C and 1,038 °C (1,500 °F and 1,900 °F), the outermost layer of wood is charred. At a depth of 13mm (~0.5") from the active char zone, the wood is only 105 °C (220 °F). This behavior is due to the low conductivity of wood and fire retardant characteristics of char.

It is also shown that the char forming rate under high temperature fire conditions is between 37 mm/hr for soft woods and 55 mm/hr for hard woods. Redwood has a char rate of 46 mm/hr [14].

Based on the shortest distance considered between the TC and impact limiter in the axial direction, the thickness of Redwood at the central segment of the impact limiter is approximately 6" (152 mm) in the model. Assuming the redwood is compressed after drop accident, a char rate of 55 mm/hr can be considered for the wood in the central segment of the impact limiter. The time interval for the charring until the active char zone reaches 13 mm above the inner surface of the center cover plate can be calculated as follows.

$$\text{(Redwood thickness -13) / char rate} = \frac{(152-13)}{55} = 2.5 \text{ hr}$$

After this moment, the temperature of active char would be gradually imposed at the impact limiter inner surface. It takes another 14 minutes until the last 13 mm of Redwood is charred as shown below.

$$\text{(Thickness of last portion of hot Redwood) / char rate} = \frac{13}{55} = 0.24 \text{ hr} = 14.2 \text{ min}$$

During the last 14 minutes the inner surface of the impact limiter is exposed to the high temperature of the active char.

The impact of charring wood on the cask is maximized if the inner surface of the impact limiter is exposed to active char immediately after fire for 14 minutes.

To bound the problem and remain conservative, it is considered in the finite element model that the inner surface of the impact limiter inner cover is exposed to the char wood temperature for 30 minutes immediately after the end of fire. A char wood temperature of 900°F is considered for these conditions, which is approximately the average of the maximum and minimum char wood temperatures given in [14].

No heat dissipation is considered for the open surface of the torn segment after this period, assuming conservatively that this surface is entirely covered with a thin layer of low conductivity wood char.

For the MP197HB TC containing a BWR DSC, the heat load is closer to the rear impact limiter. The ram closure plate and the test O-rings are located within a radius of 18.5" from the TC centerline in the cask bottom plate. Considering the location of the seal O-rings and the impact limiter segments, the worst case condition occurs for MP197HB TC containing a BWR DSC when the center segment of the rear impact limiter (from centerline to OD 40") is punctured.

For the MP197HB TC containing a PWR DSC, the heat load is closer to the front impact limiter due to the use of cask spacers at the bottom of the cask. The cask lid O-ring and

the vent and test O-rings are located outside the radius of 32.25". Therefore, the worst case condition occurs for the MP197HB TC containing a PWR DSC when a lateral segment of the front impact limiter (from ID 40" OD 126") is punctured.

Based on thermal analysis presented in Section A.3.3.1.1 and results shown in Table A.3–8 and Table A.3–9 for NCT, the maximum seal temperatures of MP197HB TC are bounded by

69BTH DSC with 32 kW heat load in TC with external fins,
69BTH DSC with 26 kW heat load in TC without internal sleeve, and
24PTH DSC with 26 kW heat load in TC with an internal sleeve and without external fins.

To determine the peak seal temperatures for HAC, a series of transient runs with the above bounding maximum heat loads are performed. The transient runs are listed in the following table.

**List of Transient Runs**

| Case No. | DSC Type | Fuel Type | Heat Load (kW) | External Fins | Internal Sleeve |
|---|---|---|---|---|---|
| 1 | 69BTH | BWR | 32 | Yes | No |
| 2 | 69BTH | BWR | 26 | No | No |
| 3 | 24PTH | PWR | 26 | No | Yes |

As noted previously, the basket and hold-down ring are homogenized for the transient runs considering HAC conditions. The properties for homogenized baskets and hold-down ring are calculated in Section A.3.3.1.5 for 69BTH DSC and in [1], Appendix P, Section P.4 for 24PTH DSC.

Transient runs are performed for 20 hours after the fire. The results of the transient runs discussed in Section A.3.4.3 show that the maximum temperatures of cask components are declining so that the maximum cask component temperatures at 20 hours after the fire accident bound the maximum temperatures for the steady state conditions.

Due to large thermal mass of the basket, the maximum basket component temperatures will be achieved under steady state conditions after the fire accident. The results of transient runs discussed in Section A.3.4.3 verify this conclusion. Steady state runs are performed for all DSC types in this calculation.

The DSC shell temperature profiles from steady state runs are used to determine the maximum basket component temperatures including the maximum fuel cladding temperature during HAC.

The steady state runs performed in this calculation are listed below.

**List of Steady State Runs for Cool-Down Period**

| Case No. | DSC Type | Heat Load (kW) | External Fins | Internal Sleeve |
|---|---|---|---|---|
| 1 | 69BTH | 32.0 | Yes, Melted | No |
| 2 | 69BTH | 29.2 | Yes, Melted | No |
| 3 | 69BTH | 26.0 | No | No |
| 4 | 24PTH | 26.0 | No | Yes |
| 5 | 61BTH Type 1 | 22.0 | No | Yes |
| 6 | 61BTH Type 2 | 24.0 | No | Yes |
| 7 | 61BT | 18.3 | No | Yes |
| 8 | 37PTH | 22.0 | No | No |
| 9 | 32PTH / 32PTH Type 1 | 26.0 | No | No |
| 10 | 32PTH1 Type 1 | 26.0 | No | No |
| 11 | 32PTH1 Type 2 | 24.0 | No | No |
| 12 | 32PT | 24.0 | No | Yes |
| 13 | 24PT4 | 24.0 | No | Yes |

For the post fire conditions, it is assumed that all external surfaces are covered with soot. The solar absorptivity of soot is 0.95 [22]. To bound the problem, the thermal analysis uses a solar absorptivity of 1.0 and an emissivity of 0.9 for the packaging outer surfaces during the cool-down period.

Insolance during the post fire, cool-down conditions is applied as a heat flux over the TC outer surfaces using average insolence values from 10 CFR 71 [6]. The insolance values are averaged over 24 hours and multiplied by the surface absorptivity factor to calculate the solar heat flux. The solar heat flux values used in MP197HB TC model for cool-down conditions are summarized below.

**Solar Heat Flux for Cool-Down Period**

| Surface Material | Shape | Insolance over 12 hrs [6] ($gcal/cm^2$) | Solar Absorptivity | Total solar heat flux averaged over 24 hrs ($Btu/hr\text{-}in^2$) |
|---|---|---|---|---|
| All materials | Curved | 400 | 1.0 | 0.4267 |
| | Flat vertical | 200 | 1.0 | 0.2133 |

For cool-down conditions, convection and radiation heat transfer from the TC outer surfaces are combined together as total heat transfer coefficients using the same methodology described in Section A.3.3.1.1 with an emissivity of 0.9 representing the soot covered external surfaces.

The finite element models described in Section A.3.3.1.1 are used for the steady state runs considering cool-down conditions. These models are modified to consider the deformed shape of the impact limiters. In addition, the material properties of neutron shield resin and trunnion plug resin are changed to air (conduction only) to conservatively bound the conductivity of charred or decomposed resins after fire.

The following modifications are considered for the steady state runs to maximize the DSC shell temperatures conservatively.

a) Homogenized baskets are not considered in the steady state runs for the cool-down period. Instead decay heat fluxes are applied on the inner surface of the DSC shells using the same methodology and values described in Section A.3.3.1.1 for NCT.

b) Adiabatic boundary conditions are imposed on the impact limiter outer surfaces for steady state runs under cool-down conditions.

The other boundary conditions and the surface properties for steady state runs are the same as those considered for cool-down period in transient runs.

The material properties used in the MP197HB model are listed in Section A.3.2.1.

The geometry of the TC model with deformed impact limiters is shown in Figure A.3–37.

Typical boundary conditions for HAC are shown in Figure A.3–38 and Figure A.3–39.

For the 69BTH and 37PTH DSCs, the DSC shell temperature profiles retrieved form the post fire steady state runs are applied to the DSC/basket finite element models to determine the maximum fuel cladding and basket component temperatures during HAC. For all other DSC types, comparison between the maximum DSC shell temperatures for HAC and accident transfer conditions is used to bound the maximum fuel cladding and basket component temperatures.

The finite element models of 69BTH DSC and 37PTH DSC described in Section A.3.3.1.4 and Section A.3.3.1.6, respectively are used for HAC thermal analysis calculation without any modifications. The methodology and the heat generation boundary conditions for these models are the same as those described in Section A.3.3.1.4 and Section A.3.3.1.6. The DSC shell temperatures for post fire, cool-down conditions are retrieved from the MP197HB transport cask models and transferred to the DSC/basket models. All other boundary conditions for 69BTH DSC and 37PTH DSC models remain the same as those described in Section A.3.3.1.4 and Section A.3.3.1.6 without any modification.

### A.3.4.2.1 Effective Properties in the MP197HB TC HAC Model

The effective properties for 69BTH basket, 69BTH top grid assembly are calculated in Section A.3.3.1.5 and are used in HAC analysis.

The effective properties for 24PTH basket are based on data for 24PTH-S or –L without inserts from [1], Appendix P, Section P.4.2, Item 13 and are used in HAC analysis.

**Effective Density for the Cask Internal Sleeve**

The effective conductivities for the cask internal sleeve were calculated in Section A.3.3.1.3. Since no density and no specific heat is considered for helium, the specific heat for the internal sleeve is equal to specific heat of aluminum.

$m_{He} = \rho_{He} \times V_{gaps} = 0$
$c_{P,He} = 0$

$$C_{p,eff} = \frac{m_{Al} \cdot C_{P,Al} + m_{He} \cdot C_{P,He}}{m_{Al} + m_{He}} = C_{p,Al}$$

The effective density of the cask internal sleeve is calculated as follow.

$Vol_1$ = Volume of one piece as shown in Figure A.3–12.

$$= \frac{\pi}{4}\left(D_o^{\,2} - D_i^{\,2}\right) \cdot \frac{\theta_{Al}}{360} \cdot L_{Al} = 317.4 \text{ in}^3$$

$D_o$ = OD of internal sleeve = 70.5" (Section A.3.3.1.5)
$D_i$ = ID of internal sleeve =68" (Section A.3.3.1.5)
$\theta_{Al}$ = angel of one internal sleeve piece = 8.6° (Section A.3.3.1.5)
$L_{Al}$ = length of one internal sleeve piece = 48.86" (Section A.3.3.1.5)

$V_{Sleeve}$ =Volume of internal sleeve = No. of pieces × $Vol_1$ = 4 × 40 × 317.4 = 50,784 in$^3$

$V_{Total}$ = Volume occupied by internal sleeve = $\frac{\pi}{4}\left(D_o^{\,2} - D_i^{\,2}\right) \cdot L_{Sleeve}$ = 53,301 in$^3$

$L_{Sleeve}$ = 196" (Section A.3.3.1.5)

$$\rho_{eff,Sleeve} = \rho_{Al} \cdot \frac{V_{Sleeve}}{V_{Total}} = 0.098 \times \frac{50{,}784}{53{,}301} = 0.098 \times 0.95 = 0.093 \text{ lbm/in}^3$$

**Effective Heat Transfer Coefficient for Cask External Fins**

Since the cask external fins are not considered explicitly in the TC model, an effective total heat transfer coefficient is calculated for finned shell based on the area ratio of the finned surface to the un-finned base.

$$\text{Fin factor} = \frac{A_{finned}}{A_{base}} = 7.193$$

$$A_{finned} = \frac{\pi}{4}\left[(98.25 + 2\times 3)^2 - (98.25)^2\right] \times 2 + \pi(1 - 0.156) \times 98.25 + \pi(0.156)(98.25 + 2\times 3)$$

$A_{finned}$ = 2220.1 in$^2$

$A_{base} = \pi(98.25)(1)$ = 308.7 in$^2$

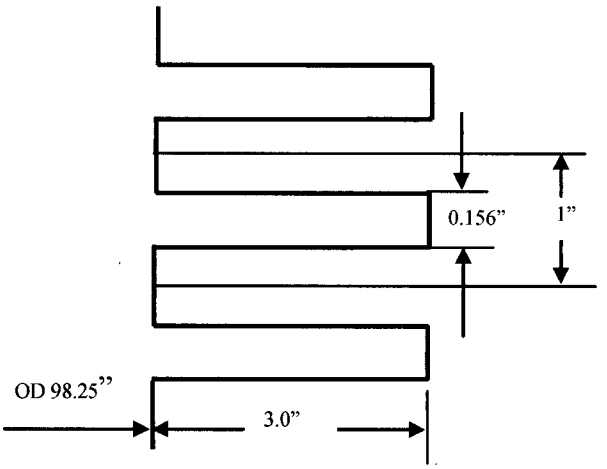


As noted, the finned shell in the thermal model is shorter and has fewer fins than the designed finned shell. To be conservative for the fire simulation, the effective total heat transfer coefficient for the finned shell is applied on the entire radial outer surface of the TC located between the two impact limiters.

It is assumed that the fins melt away after the fire but the shell and the gap between the finned shell and the shield shell remains in place. Therefore, the convection coefficient

over the cask outer surface is determined using the correlations for horizontal cylinder described in Section A.3.3.1.1.

### A.3.4.3 Maximum Temperatures and Pressure

The maximum component temperatures for transient runs are listed in Table A.3–16.

The seal o-rings are not explicitly considered in the models. The maximum seal temperatures are retrieved from the models by selecting the nodes at the locations of the corresponding seal o-rings.

The time temperature histories for the TC components, DSC shell, and homogenized basket are shown in Figure A.3–40 through Figure A.3–42. As seen in time temperature histories, the basket temperature increases steadily during cool-down period. It indicates that the maximum basket component temperatures will be reached for steady state conditions after fire. This behavior was expected due to large thermal mass of the basket and the relative large gap between the DSC shell and the cask inner shell.

The maximum DSC shell temperatures for steady state runs are listed in Table A.3–17.

The DSC types 61BTH, 61BT, 32PTH, 32PTH1, 32PT, 24PTH, and 24PT4 are evaluated previously for accident transfer conditions under 10 CFR 72 requirements. The DSC shell temperature profiles of these DSCs in MP197HB model are compared with the corresponding profiles from 10 CFR 72 SARs in Appendix A.3.6.3. Based on discussions in Appendix A.3.6.3, the fuel cladding and the basket component temperatures for accident transfer conditions under 10 CFR 72 represent the bounding values for these DSCs for HAC under 10 CFR 72 requirements.

Therefore, no additional analysis is performed for the DSCs previously evaluated under 10 CFR 72 conditions. The maximum fuel cladding and the basket component temperatures for these DSCs are taken from 10 CFR 72 SARs and reported as the bounding values for HAC.

The maximum temperatures for DSC contents for all DSCs to be transported in MP197HB TC for HAC are listed in Table A.3–18.

The maximum TC and DSC component temperatures for HAC are summarized in Table A.3–19. Table A.3–19 shows that the maximum temperatures of the MP197HB components calculated for HAC are lower than the allowable limits.

The maximum seal temperature for fluorocarbon seals is 386°F at drain port for 32 kW heat load in 69BTH DSC when TC is equipped with external fins. This temperature is below the long-term limit of 400°F specified for continued seal function.

The maximum temperature of gamma shield (lead) is 552°F, which is well below the lead melting point of 621°F.

The maximum fuel cladding temperature is between 668°F and 693°F for 69BTH DSC with 26 kW to 32 kW heat loads. For 37PTH DSC, the bounding maximum fuel cladding temperature is 671°F with 22 kW heat load. These temperatures are well below the limit of 1,058°F (570°C) established in [7].

The maximum fuel cladding temperature for the DSC types evaluated at higher heat loads for transfer conditions under 10 CFR 72 remain below the allowable limit of 1,058°F (570°C).

The resins and wood are assumed to be decomposed or charred after fire accident. Therefore, the maximum temperatures for these components are irrelevant for HAC.

Typical temperature distributions for the MP197HB TC under HAC are shown in Figure A.3–43 and Figure A.3–44.

Typical temperature distributions for the 69BTH and 37PTH DSC under HAC are shown in Figure A.3–45 through Figure A.3–48.

The maximum pressures in the cask and canister cavities for HAC are calculated using the same methodology described in Section A.3.3.3.

### *1) MP197HB TC Cask Cavity HAC Pressure*

The maximum cask cavity pressure in the MP197HB TC for HAC is calculated using the same methodology and assumptions as described for NCT in Section A.3.3.3. The nomenclature used is defined in Section A.3.3.3.

The maximum pressure in the cask cavity for HAC is calculated as:

$$P_{HAC} = \frac{\left(1.4504*10^{-4}\,\frac{psia}{Pa}\right)*(n_{he,initial})*R*T_{avg,he,HAC}*(5/9K/^{o}R)}{0.98*V_{free,cc}*(1.6387*10^{-5}m^{3}/in^{3})}$$

As seen from Table A.3–20 for NCT the case of 69BTH DSC in MP197HB with 32 heat load is bounding for the maximum TC cavity pressure for all DSCs. Therefore, the 69BTH DSC in MP197HB provides bounding cavity pressure for HAC as well. Based on $T_{avg,he,HAC}$ of 387°F for 69BTH DSC with 32 kW heat load shown in Table A.3–14 and the methodology presented in Section A.3.3.3, the maximum pressure in the cask cavity of MP197HB TC for HAC is calculated as 14.4 psig.

### *2) Internal Pressure for 69BTH and 37PTH DSCs under HAC*

The maximum pressures in the 69BTH and 37PTH DSCs for HAC are calculated using the same methodology described in Section A.3.3.3. Per 10 CFR 71 [6], the percentage of fuel rods ruptured for accident cases is 100%. The total quantity of moles released to 69BTH DSC cavity is, therefore,

$$n_{DSC-HAC} = n_{he\ initial} + n_{he\ fuel\ rod\ release,HAC} + n_{ig,HAC}$$

$$n_{DSC-HAC} = 134.39 + 108.91 + 472.09 = 715.39\,g-moles$$

The maximum accident operating pressure for this configuration is then,

$$P_{DSC-HAC} = \frac{\left(1.4504 \cdot 10^{-4} \frac{psia}{Pa}\right)(715.39\,g-moles)(8.314\,J/(mol \cdot K))(992°R)(5/9\,K/°R)}{(258415\,in^3 + 14738.40\,in^3)(1.6387 \cdot 10^{-5}\,m^3/in^3)},$$

$$P_{DSC-HAC} = 106.17\,psia\ (91.47\,psig).$$

The maximum internal pressures inside 37PTH and 69BTH DSCs are summarized in Table A.3–22. The maximum internal pressures are 102.64 psig and 95.54 psig for the 37PTH DSC and 69BTH DSC under HAC, respectively. These maximum *calculated* internal DSC pressures are below the design *pressure of 140 psig specified in Section A.3.1 for HAC structural evaluations of the* 69BTH and 37PTH DSCs.

Based on discussions in Section A.3.3.3.4, the maximum internal pressures for DSCs analyzed for accident storage/transfer conditions under 10 CFR 72 requirements remain bounding for transport conditions under HAC. The evaluated DSC internal pressures for DSCs to be transported within MP197HB TC are summarized in Table A.3–23. As seen in Table A.3–23, the maximum *calculated* internal pressures under HAC remains below the corresponding design *pressures considered for the structural evaluations for HAC* for all DSC types.

### A.3.4.4 Maximum Thermal Stresses

Thermal stresses for the MP197HB TC loaded with DSCs are discussed in Chapter A.2.

### A.3.4.5 Accident Conditions for Fissile Material Packages for Air Transport

The MP197HB TC is not designed for air transportation. Therefore, the accident conditions for air transport are irrelevant.

## A.3.5 References


1. Updated Final Safety Analysis Report for the Standardized NUHOMS® Horizontal Modular Storage System for Irradiated Nuclear Fuel, NUH-003, Rev. 11.
2. Updated Final Safety Analysis Report for the Standardized Advanced NUHOMS® Horizontal Modular Storage System for Irradiated Nuclear Fuel, ANUH-01.0150, Rev. 3.
3. *Same as Reference 1.*
4. Final Safety Analysis Report for NUHOMS® HD Horizontal Modular Storage System for Irradiated Nuclear Fuel, Rev. 2.
5. Perry, Chilton, Chemical Engineers' Handbook, 5th Edition, 1973.
6. U.S. Code of Federal Regulations, Part 71, Title 10, "Packaging and Transportation of Radioactive Material."
7. U.S. NRC, Spent Fuel Project Office, Interim Staff Guidance, ISG-11, Rev 3, Cladding Considerations for the Transportation and Storage of Spent Fuel.
8. U.S. Code of Federal Regulations, Part 72, Title 10, Licensing Requirements for the Independent Storage of Spent Nuclear Fuel and High-Level Radioactive Waste.
9. U.S. Nuclear Regulatory Commission, Standard Review Plan for Transportation Packages for Spent Nuclear Fuel, Final Report, NUREG-1617, January 2000.
10. ASME Boiler and Pressure Vessel Code, Section II, Part D, Material Properties, 2004.
11. Moore, R. S., Notz, K. J., Physical Characteristics of GE BWR Fuel Assemblies, Oak Ridge National Laboratory, Report No. ORNL/TM-10902, June 1989.
12. Report, Topical Report on Actinide-Only Burnup Credit for PWR Spent Nuclear Fuel Packages, Office of Civilian Radioactive Waste Management, DOE/RW-0472, Revision 2, September 1998.
13. Gregory, et al., Thermal Measurements in a Series of Long Pool Fires, SANDIA Report, SAND 85-0196, TTC-0659, 1987.
14. Mitchell S. Sweet, Fire Performance of Wood: Test Methods and Fire Retardant Treatments, Fire Safety of Wood Products, USDA Forest Service, http://www.fpl.fs.fed.us/documnts/pdf1993/sweet93a.pdf
15. Bucholz, J. A., Scoping Design Analysis for Optimized Shipping Casks Containing 1-, 2-, 3-, 5-, 7-, or 10-Year old PWR Spent Fuel, Oak Ridge National Laboratory, January, 1983, ORNL/CSD/TM-149.
16. NOT USED

17. Test Report, Properties to be Considered for Safety for Resin Vyal B, Transnuclear International, Report No. DI/RI-A-1-5-02, Rev. 1, 2006.

18. Parker O-ring Handbook 5700, Y2000 Edition, 1999.

19. Parker O-ring Division, Material Report Number KJ0835, 1989.

20. U.S. Department of Agriculture, Forest Service, Wood Handbook: Wood as an Engineering Material, March 1999.

21. Rohsenow, Hartnett, Cho, Handbook of Heat Transfer, 3rd Edition, 1998.

22. Siegel, Howell, Thermal Radiation Heat Transfer, 4th Edition, 2002.

23. Kreith, Frank, Principles of Heat Transfer, 3rd Edition, 1973.

24. Rohsenow, Hartnett, Handbook of Heat Transfer Fundamentals, 2nd Edition, 1985.

25. Kumar, Madras, Thermal Degradation Kinetics of Isotatic and Atactic Polypropylene, Journal of Applied Polymer Science, Vol. 90, 2206-2213, 2003.

26. AAR Brooks & Perkins, Advanced Structural Division, "Boral® The Neutron Absorber," Product Performance Report 624.

27. ANSYS computer code and On-Line User's Manuals, Version 8.1 and 10.0.

28. NOT USED

29. NOT USED

30. Plannel, et al., "Topical Report, Extended Fuel Burnup Demonstration Program. Transport Considerations for Transnuclear Casks," Project 1014, DOE/ET 34014-11, TN-E-4226.Transnuclear Inc., 1983.

31. Nylund, O., Hjarne, L., "The SVEA BWR Fuel, Eight Years of Further development," ABB atom AB, Fuel Division, Vaesteras, Sweden.

32. Roth, A., "Vacuum Technology," 2nd Edition, 1982.

33. Lide, David, R., "CRC Handbook of Chemistry and Physics," 83rd edition, 2002-2003, CRC Press.

34. Henninger, J. H., "Solar Absorptance and Thermal Emittance of Some Common Spacecraft Thermal-Control Coatings," NASA Scientific and Technical Information Branch, NASA Reference Publication 1121, 1984.

35. Calculation, "TN-24P Benchmarking Analysis Using ANSYS," Transnuclear, Inc., Calculation No. NUH32PT.0408, Revision 0, provided to USNRC in TN Letter NUH03-03-04, Dated January 24, 2003, "Response to Request for Additional Information (RAI) and Submittal of Revision 4 of Application for Amendment No. 5 to the NUHOMS® Certificate of Compliance No. 1004 (TAC NO. L23343), Docket No. 72-1004."

36. Updated Final Safety Analysis Report for TN-68 Dry Storage Cask, Revision 4. Certificate of Compliance No. 1027, Amendment 1.

37. U.S. Department of Energy, "Characteristics of Spent Nuclear Fuel, High- Level Waste, and Other Radioactive Wastes Which May Require Long-Term Isolation, Appendix 2A," U.S Department of Energy, Office of Civilian Radioactive Waste Management, DOE/RW-0184, Volume 3 of 6, December, 1987.

38. M. M. Yovanovich, J. R. Culham, P. Teertstra, "Calculating Interface Resistance," Electronics Cooling, Vol. 3, No. 2, May 1997.

39. Amiss, J. M., et al., "Machinery's Handbook," 24th Edition, Industrial Press, 1992 - Fig. 5, pg 672.

40. Aluminum Association, Inc., "Aluminum Standards and Data," 10th Edition, 1990 - Table 2.1, pg 33.

41. ASME Boiler and Pressure Vessel Code, Section II, Part A, "Ferrous Material Specification," 1998 and 2000 addenda - Table 2.

42. Gordon England Company, "Microhardness Test," http://www.gordonengland.co.uk/hardness/microhardness.htm

*43. Eckert, "Introduction to the Transfer of Heat and Mass," 1st Edition, 1950.*

*44. Eckert and Jackson, "Analysis of Turbulent Free-Convection Boundary Layer on Flat Plate," NASA Technical Reports, Report Number NACA-TN-2207, 1950.*

*45. Kays, Crawford, and Weigand, "Convective Heat and Mass Transfer," 4th Edition, 2005.*

*46. Holman, "Heat Transfer," 8th Edition, 1997.*

*47. Kreith, "Principles of Heat Transfer," 3rd Edition, 1973.*

*48. Misumi, Suzuki, and Kitamura, "Fluid Flow and Heat Transfer of Natural Convection around Large Horizontal Cylinders: Experiments with Air," Heat Transfer --Asian Research, 32 (4), 2003.*

*49. T. Eric Skidmore, "Performance Evaluation of O-Ring Seals in Model 9975 Packaging Assemblies (U)," Savannah River Technology Center, WSRC-TR-98-00439, December 1998.*

*50. Oak Ridge National Laboratory, "Effect of Fuel Failure on Criticality Safety and Radiation Dose for Spent Fuel Casks," by K.R. Elam, J.C. Wagner and C.V. Parks, NUREG/CR-6835 (ORNL/TM-2002/255), September 2003.*

*51. H. J. Rack, G. A. Knorovsky, "An Assessment of Stress-Strain Data Suitable for Finite-Element Elastic-Plastic Analysis of Shipping Containers," Sandia Laboratories, NUREG/CR-0481, SAND77-1872 R-7, 1978.*

## A.3.6 Appendices

***Proprietary information on pages A.3-97 to A.3-102 withheld pursuant to 10 CFR 2.390***

### A.3.6.2 Mesh Sensitivity

#### A.3.6.2.1 MP197HB TC Model Mesh Sensitivity

A slice of the MP197HB TC model containing 69BTH DSC shell is recreated for mesh sensitivity analysis. The length of the TC slice model is 24" and includes the DSC shell and cask shells. The mesh density of this model is the same as the mesh density of the geometry model used in Section A.3.3.1.1 from z=30.5" to z=60.34" except that the element size is decreased from 3.73" to 3.0" in the axial direction. The slice model contains 26,744 elements and 29,574 nodes.

For the purpose of mesh sensitivity analysis, the mesh density of the slice model is increased to more than five folds of its original value so that the number of elements and nodes are increased to 147,376 and 154,564, respectively.

Ambient temperature of 100°F with insolation and a decay heat of 26 kW are considered as boundary conditions for both TC slice models with coarse and fine meshes. The boundary conditions are applied using the same methodology as described in Section A.3.3.1.1.

The differences between the maximum temperature for coarse and fine mesh models are less than 1°F. It concludes that the TC model described in Section A.3.3.1.1 is mesh insensitive and the results are adequately accurate for evaluation.

#### A.3.6.2.2 Mesh Sensitivity for the 69BTH DSC Model

The mesh sensitivity analysis for the 69BTH DSC described in Section A.3.3.1.4 is performed based on a slice model of 69BTH DSC with Boral poison plates. The slice model is 26" long and is recreated by selecting the nodes and elements of the 69BTH DSC model from z=50.8" to z=76.8". The length of the slice model is twice the length of the aluminum plates and the axial gaps between them. This model contains 124,968 elements and 137,423 nodes.

A fine mesh model for the same slice is recreated. The number of elements and nodes in the fine meshed model are almost tripled to 391,644 and 414,874, respectively.

A fixed temperature of 400°F on the outer surface of the DSC shell and a decay heat of 26 kW with HLZC # 1 is selected as boundary conditions for the mesh sensitivity analysis of 69BTH DSC. A peaking factor of 1.2 is considered to apply the heat generation rate on the homogenized fuel assemblies. The heat generation boundary conditions are applied using the same methodology as described in Section A.3.3.1.4.

The differences between the maximum temperature for coarse and fine mesh models are approximately 1.0°F. It concludes that the 69BTH DSC model described in Section A.3.3.1.4 is mesh insensitive and the results reported are adequately accurate for evaluation.

### A.3.6.2.3 Mesh Sensitivity for the 37PTH DSC Model

The 37PTH DSC model described in Section A.3.3.1.6 containing paired Boral and aluminum plates is selected for mesh sensitivity analysis. The homogenized fuel assemblies in this model are modeled using a 10x10 mesh at the cross section with the largest mesh size of 0.95"×0.95". This model contains 385,933 elements and 409,836 nodes.

A fine mesh model is created for the 37PTH DSC in which the mesh density of the fuel assembly is increased to 12x12 with the largest mesh size of 0.76" ×0.76". The number of elements and nodes in the fine mesh model are increased to 508,605 and 536,592, respectively.

The DSC shell temperature profile retrieved from MP197HB transport cask model for NCT at ambient temperature of 100°F with insolation and a decay heat of 22 kW are selected as boundary conditions for the sensitivity analysis of 37PTH DSC. The boundary conditions are applied using the same methodology as described in Section A.3.3.1.6. The differences between the maximum temperature for coarse and fine mesh models are less than 1.5°F. It concludes that the 37PTH DSC model described in Section A.3.3.1.6 is mesh insensitive and the results reported are adequately accurate for evaluation.

### A.3.6.3 Justification for Bounding Temperature Profiles

DSC types 61BTH Type 1 and 2, 61BT, 32PTH, 32PTH Type 1, 32PTH1 Type 1 and 2, 32PT, 24PTH, and 24PT4 are evaluated in [1], [2], [3], and [4] for storage/transfer conditions under 10 CFR 72 requirements. For these DSCs, the DSC shell temperature profile is retrieved from the transfer cask model and applied as boundary conditions to the DSC/basket model. The DSC shell temperatures and the heat generation rates within the homogenized fuel assemblies are the only boundary conditions used for each DSC/basket model. The same approach is used in this evaluation to determine the maximum fuel cladding and basket component temperatures for transportation in MP197HB TC. In this approach for each DSC type, a lower DSC shell temperature at the hottest cross section of the basket model, where the peaking factors are at their highest level, results in lower fuel cladding and basket component temperature provided that the heat load remain unchanged. In the case of a lower heat load, the fuel cladding and basket component temperature decease, even when the DSC shell temperature remain unchanged.

The maximum DSC shell temperature for normal transfer conditions under 10 CFR 72 (without air circulation) occurs generally in the mid section of the DSC where the fuel assembly has its highest peaking factor while the maximum DSC shell temperature for NCT under 10 CFR 71 occurs toward the ends of the DSC shell where it is covered by impact limiters. To illustrate this fact, the DSC shell temperature profiles for 61BTH DSC and 24PTH DSC under NCT and normal transfer conditions at 100°F ambient are compared in Figure A.3–51 and Figure A.3–52.

Based on peaking factor profiles discussed in Sections A.3.3.1.4 and A.3.3.1.6, the maximum peaking factor region is located between ~36.1" and ~84.9" for BWR and

between ~28.0" to ~100.0" for PWR fuel assemblies. These locations are measured from the bottom of active fuel length. The active fuel length starts approximately 7.5" and 4.0" measured from the bottom of the fuel assembly for BWR and PWR fuel assemblies, respectively.

To quantify the differences between the DSC shell temperatures under NCT and normal transfer conditions, the maximum DSC shell temperature for each DSC type under NCT is retrieved at the above locations from the MP197HB TC model and shown in Table A.3–8 and Table A.3–9. These temperatures give the maximum DSC shell temperature in the region of highest peaking factors, where the maximum fuel cladding temperatures are expected

The maximum DSC shell temperatures for NCT under 10 CFR 71 requirements are compared to the corresponding data for transfer conditions under 10 CFR 72 requirements in Table A.3–24.

As shown in Table A.3–24, the maximum DSC shell temperature for NCT at the mid section, where the highest peaking factors are located, is 7 to 17°F lower than the absolute maximum DSC shell temperature for the NCT. Both of these values are lower than the maximum DSC shell temperature for normal transfer conditions.

Since the DSC shell temperatures for NCT at the ends and at mid section are lower than those for the normal transfer conditions, the DSC shell temperature profile for normal transfer conditions gives the bounding values for the basket and fuel cladding temperatures.

For DSC types, 61BTH Type 2, 32PTH, 32PTH Type 1, 32PTH Type 1 and 2, 24PTH-S, and 24PTH-L the maximum heat loads for transport conditions are lower than the maximum heat loads for transfer conditions. Therefore for these DSC types, even lower basket and fuel cladding temperatures are expected for NCT.

Based on this discussion, the thermal analysis results for DSCs in 10 CFR 72 SARs ([1], [2], [3] and [4]) under normal transfer conditions are applicable for NCT and represent the bounding fuel cladding and basket component temperatures.

Based on the comparison shown in the lower half of Table A.3–24, the maximum DSC shell temperatures for HAC under 10 CFR 71 requirements are also lower than the corresponding ones for accident transfer conditions under 10 CFR 72 requirements. The same arguments as above are therefore valid for HAC of transport as well. Therefore, the thermal analysis results for DSCs in 10 CFR 72 SARs ([1], [2], [3] and [4]) under accident transfer conditions are bounding for HAC and no further thermal analyses are required for these DSC types.

*To provide additional assurance that the above arguments are valid and the fuel cladding and the basket component temperatures in 10 CFR Part 72 SARs represent the bounding values for transport conditions, the DSC type 24PTH-S (without Al inserts) is selected for evaluation under NCT.*

*Among the DSC types previously evaluated for storage applications and proposed for transport in MP197HB, DSC type 24PTH-S (without Al inserts) has the smallest margin*

*(19°F) for the maximum fuel cladding temperature under storage conditions and has the second highest heat load for transportation conditions (26 kW) after the 69BTH DSC.*

*Consistent with the approach described in Section A.3.3.1.4, the DSC shell temperature profile for 24PTH DSC is retrieved from the cask model and applied as boundary conditions to the detailed model of the 24PTH-S DSC/basket. The DSC/basket model of 24PTH-S is identical to the model previously used for storage conditions in 10 CFR 72 UFSAR [1], Appendix P. A uniform heat load zone configuration with the maximum heat load of 26 kW is applied in the DSC model. The results of this case are compared with the results used in the SAR to demonstrate the conservative nature of the approach.*

*Comparisons of the maximum DSC component temperatures are listed in the following table.*

***Comparison of the Maximum Temperatures for 24PTH-S DSC***

| ***DSC Type*** | ***24PTH-S (w/o Al inserts)*** | | |
|---|---|---|---|
| *HLZC* | *Uniform (1.3 kW/FA)* | *Uniform (1.08 kW/FA)* | |
| *Operating Condition* | *Normal Transfer 31.2 kW UFSAR [1], Tables P.4-10, -14 and -16* | *NCT 26 kW* | *Additional Thermal Margin* |
| | $T_{Transfer}$ (°F) | $T_{NCT}$ (°F) | ($T_{Transfer}$ – $T_{NCT}$) (°F) |
| *Fuel Cladding* | *733* | *664* | *+69* |
| *Fuel Compartment* | *682* | *616* | *+66* |
| *Al/Poison* | *681* | *615* | *+66* |
| *DSC Shell* | *475* | *463* | *+12* |

*As seen in the above table, the maximum fuel cladding and basket component temperatures for the DSC type 24PTH-S (without Al inserts) under NCT are more than 60°F lower than the bounding values listed in the UFSAR [1]. This large difference demonstrates that the comparison of the DSC shell temperatures as discussed above is a conservative approach to bound the maximum fuel cladding and basket component temperatures for transport conditions.*

### A.3.6.4 Acceptance Criteria for Coating Damages for MP197HB TC

During handling and operation of MP197HB transport cask (TC), the painted surfaces of the shield shell for the un-finned cask or the anodized/painted surfaces of the finned aluminum shell for the finned cask can be scratched, peeled off, or physically damaged. The emissivity and solar absorptivity of the painted and anodized surfaces are considered as inputs for the thermal evaluation. Physical damages on the coating

change the emissivity and absorptivity values of the surface, which affect the thermal performance of the cask.

This section determines acceptance criteria for the surface area of the damaged coating below which the effects on the thermal performance of the cask are insignificant.

The following assumptions and conservatism are considered in this section in addition to those described in Section A.3.3.1.1 for thermal evaluation of MP197HB TC with damaged surfaces.

- When the paint on the shield shell is damaged, the steel surface of the shield shell is exposed to ambient. In this case, emissivity and absorptivity of steel are considered for the area of damaged paint.
- An emissivity of 0.657 is reported in [5], Table 10-17 for rolled steel sheets. For conservatism, and emissivity of 0.587 is considered for steel in this section.
- When the coated surface (anodized or painted) on the external fins is damaged, the aluminum surface of these components is exposed to ambient. In this case, emissivity and absorptivity of plain, polished aluminum are considered for the damaged area.
- For polished, plain aluminum, an emissivity between 0.102 and 0.113, and a solar absorptivity between 0.09 and 0.10 are reported in [21], Table A.7.2. To bound the problem, emissivity and solar absorptivity of 0.1 are considered for the scratched surfaces of the external fins. All other material properties used in this analysis are presented in Section A.3.2.1.

Physical damages such as surface scratches or paint peel-offs expose the material beneath the coating to ambient and change the emissivity and absorptivity of the damaged area. To provide practical criteria for the coating damages, a temperature rise of approximately 1°F is considered for the maximum DSC shell temperature. Based on the thermal analysis presented in Section A.3.3, the increase in the maximum fuel cladding temperature is less than 1°F if the temperature rise of the maximum DSC shell temperature is limited to 1°F.

Considering the large margins to the temperature limits reported in Section A.3.3 for TC/DSC component and fuel cladding temperatures, this amount of rise for the maximum DSC shell and fuel cladding temperatures has insignificant effect on the thermal and structural performance of MP197HB and the DSCs loaded in it.

The finite element models of the MP197HB TC described in Section A.3.3.1.1 containing 69BTH DSC are used in this evaluation for cases when no internal sleeve is used. The un-finned MP197HB TC model is used with the maximum heat load of 26 kW and the MP19HB TC model with external fins is used with the maximum heat load of 32 kW. These models represent the maximum heat loads when no inner sleeve is used in MP197HB TC

The finite element model of the MP197HB TC described in Section A.3.3.1.1 with 24PTH DSC is used for the case that an internal sleeve is used to load a small diameter DSC. This model with the maximum heat load of 26 kW represents the maximum heat load when an internal sleeve is used in MP197HB TC.

As noted in Section A.3.3.1.1, the external finned shell considered for the thermal model of MP197HB has a different length than the designed shell. Since this calculation is a comparative analysis for damaged and undamaged coatings, the conclusion remains valid, although the assumed and designed external fin shells have different lengths.

Normal conditions of transport (NCT) at 100°F ambient with insolation are described in Section A.3.3.1.1 considered for the analyses. The analyses are performed using ANSYS, version 8.1 [27].

Two cases can be considered to develop acceptance criteria for coating damages:

1. Removal of a large portion of coating concentrated in one location
2. Multiple scratches and small peel-off spots scattered around the shield shell or finned shell

These two cases are discussed in the following sections.

**Large Areal Damage – Case 1**

The location and the size of a large damaged coating area affect the temperature profile on the cask surface. To bound the problem, it is considered that the large damaged coating area is located at the mid-length of the cask where the fuel assembly has its highest peaking factor. Based on discussions in Section A.3.6.3, the maximum peaking factor region is located between ~43.6" and ~92.4" for BWR fuel assemblies and between ~32" and ~104" for PWR fuel assemblies. The distances are measured in both cases from the bottom of the fuel assemblies. The maximum peaking factor region covers the z coordinates from z=31.3" to z=80.1" in the MP197HB TC model with 69BTH DSC and coordinates from z=30.65" to z=102.65" in the MP197HB TC model with 24PTH DSC considered in this analysis.

It is considered that the area of the damaged anodized coating is 250 $in^2$ for the anodized surface of the internal sleeve, 500 $in^2$ for the painted shield shell, and 2,000 $in^2$ for the coated surface of the external fins. The damaged coating area is located at the top of the cask in the middle of the maximum peaking factor region to maximize its effect on the DSC shell and fuel cladding temperatures.

The location of the damaged anodized coating on the internal sleeve is from z=58.75" to z=74.55" in the MP197HB TC model with 24PTH DSC which is 28.1" from each ends of the maximum peaking factor region. This length is selected so that the arc length of the curved surface is approximately equal to the length of the damaged area. The surface area of the damaged internal sleeve coat in this model is:

$$A_c = \frac{\theta_c}{360} \times \pi \times ID_{sleeve} \times L_c = 250 \text{ in}^2$$

$A_c$ = Surface area of damaged internal sleeve anodized coat ($in^2$)

$\frac{\theta_c}{360} \times \pi \times ID_{sleeve}$ = arc length of the curved surface (in.)

$\theta_c$ = angle of damaged internal sleeve anodized coat $\approx$ 26.6°

$ID_{sleeve}$ = inner diameter of internal sleeve= 68"

$L_c$ = length of damaged internal sleeve anodized coat = 74.55 – 58.75 = 15.8"

Since the model is half-symmetric, only half of the above damaged area (approximately 125 $in^2$) is considered in the model. This area covers approximately 13.3° of the inner surface of the sleeve. The nodes located in the annulus between the internal sleeve and the DSC shell are adjusted in the cask model, to represent this area.

The emissivity of anodized coating was considered for the internal sleeve in the model of the MP197HB TC with 24PTH DSC described in Section A.3.3.1.1. Since the emissivity of painted coat is higher than the emissivity of anodized coat as shown in Section A.3.2.1, the model with anodized coated internal sleeve represents the bounding case. The emissivity of the damaged anodized area is changed to emissivity of polished aluminum (0.1) as discussed previously. This change affects the effective conductivity calculated for the gap between the internal sleeve and 24PTH DSC shell.

To calculate the effect of damaged anodized coating on the effective conductivity for the gap between the internal sleeve and DSC shell, the TC sub-model discussed in Section A.3.3.1.3 and shown in Figure A.3–11 is rerun with surface emissivity of 0.1 for internal sleeve. No other changes are considered for this sub-model. The results for the effective conductivity are summarized in the following table. These effective conductivities are used in the MP197HB TC model with 24PTH DSC for the area of the damaged anodized coating of internal sleeve.

All other material properties and boundary conditions are identical to those used in Section A.3.3.1.1 and remain unchanged in this calculation.

**Radial Effective Conductivity for Helium in Gap between DSC Shell and Internal Sleeve with Damaged Anodized Coating**

Between DSC Shell and Cask Internal Sleeve
(Mat # 39 in the ANSYS model)

| | | |
|---|---|---|
| $D_{o,DSC}$ = | 67.19 | DSC OD (in) |
| $D_{i,Sleeve}$ = | 68.00 | Cask ID (in) |
| L = | 10 | Model height (in) |

| $T_{DSC}$ (°F) | $T_{Sleeve}$ (°F) | $q_{react}$ (Btu/hr) | $T_{avg}$ (°F) | $k_{\_eff}$ (Btu/hr-in-°F) |
|---|---|---|---|---|
| 321 | 200 | 487 | 261 | 0.0092 |
| 365 | 250 | 487 | 307 | 0.0097 |
| 408 | 300 | 487 | 354 | 0.0103 |
| 453 | 350 | 487 | 401 | 0.0109 |
| 497 | 400 | 487 | 449 | 0.0115 |
| 542 | 450 | 487 | 496 | 0.0121 |
| 587 | 500 | 487 | 543 | 0.0128 |
| 632 | 550 | 487 | 591 | 0.0135 |
| 678 | 600 | 487 | 639 | 0.0142 |
| 725 | 650 | 487 | 687 | 0.0149 |
| 771 | 700 | 487 | 736 | 0.0157 |
| 818 | 750 | 488 | 784 | 0.0164 |

The location of the damaged paint on shield shell is from z=44.5" to z=66.9" in the un-finned cask model, which is 13.2" from each ends of the maximum peaking factor region in the MP197HB TC with 69BTH DSC. This length is selected so that the arc length of the curved surface is approximately equal to the length of the damaged area. The surface area of damaged paint in this model is:

$$A_P = \frac{\theta_P}{360} \times \pi \times OD_{shield} \times L_p = 500 \text{ in}^2$$

$A_P$ = Surface area of damaged paint ($in^2$)

$\frac{\theta_P}{360} \times \pi \times OD_{shield}$ = arc length of the curved surface (in.)

$\theta_P$ = angle of damaged paint area $\approx$ 26.16°

$OD_{shield}$ = shield shell outer diameter = 97.75"

$L_P$ = length of damaged paint area = 66.9 – 44.5 = 22.4"

Since the model is half-symmetric, only half of the above damaged area (approximately 250 $in^2$) is considered in the model. This area covers approximately 13.1° of the shield shell outer surface. The nodes located on the shield shell in the un-finned cask model for MP197HB TC with 69BTH DSC, are adjusted to represent this area.

The emissivity and solar absorptivity of the damaged paint area are changed to emissivity and solar absorptivity of steel (0.587 in this analysis), which affects the solar heat flux and the total heat transfer coefficient calculated for the shield shell in the model.

Based on Section A.3.3.1.1, the solar heat flux over curved, steel surfaces is 0.2505 Btu/hr-in$^2$. This solar heat flux is used in the un-finned cask model for the damaged paint areas of the shield shell.

The macro "HTOT_HCL.mac" described in Section A.3.3.1.1 is used to calculate the total heat transfer coefficient for the shield shell. The same macro is used in this calculation with a surface emissivity value of 0.587 for the damaged paint areas of the shield shell.

The boundary conditions on the other surfaces are identical to those described in Section A.3.3.1.1 and remain unchanged in this calculation.

The external fins are not explicitly considered in the finned TC model as described in Section A.3.3.1.1. Instead, an effective heat transfer coefficient is applied over the outer surface of the un-finned aluminum shell to simulate the heat dissipation from this area. Due to this methodology, an effective surface area is calculated as follows to represent the damaged anodized coating of 2000 in$^2$.

$$A_{eff,A} = A_A \times \frac{A_{footprint}}{A_{finned}}$$

$A_{eff,A}$ = effective surface area of damaged anodized coating (in$^2$)
$A_A$ = surface area of damaged anodized coating = 2000 in$^2$
$A_{footprint}$ = surface area of the footprint for finned shell for one fin (in$^2$)
$A_{finned}$ = total surface area of the fins and finned shell for one fin (in$^2$)

$$A_{footprint} = \pi \times OD_{shell} \times P_{fin} = 308.7 \text{ in}^2$$

$$A_{finned} = \pi \times OD_{shell} \times (P_{fin} - t_{fin}) + 2 \times \frac{\pi}{4}\left(OD_{fin}^{\ 2} - OD_{shell}^{\ 2}\right) + \pi \times OD_{fin} \times t_{fin} = 2{,}220.1 \text{ in}^2$$

$OD_{shell}$ = finned aluminum shell outer diameter = 98.25"
$P_{fin}$ = Fin pitch =1"
$t_{fin}$ = fin thickness = 0.156"
$OD_{fin}$ = fin outer diameter =104.25"

The effective surface area for the damaged anodized coating ($A_{eff,A}$) is 278 in$^2$. For conservatism, an effective surface area of 295 in$^2$ is considered in the model.

The location of the damaged coating for external fins is from z=47.1" to z=64.3" in the finned cask model, which is 15.8" from each ends of the maximum peaking factor region. This length is selected so that the arc length of the curved surface is approximately equal to the length of the damaged area. The effective surface area of damaged external fins coating in this model is:

$$A_{eff,A} = \frac{\theta_A}{360} \times \pi \times OD_{shell} \times L_A = 295 \text{ in}^2$$

$\theta_A$ = angle of damaged external fins coating area = 20.0°

$\frac{\theta_A}{360} \times \pi \times OD_{shell}$ = arc length of the curved surface (in)

$OD_{shell}$ = external aluminum shell outer diameter = 98.25"
$L_A$ = length of damaged external fins coating area = 64.3 – 47.1 = 17.2"

Since the model is half-symmetric, only half of the effective damaged area (approximately 147 $in^2$) is considered in the model. This area covers approximately 10.0° of the shield shell outer surface. The nodes located on the finned shell in the finned cask model, are adjusted to represent this area.

The emissivity and solar absorptivity of anodized coating were considered for the external fins in the original model of the finned cask. Since the emissivity of painted coat is higher than the emissivity of anodized coat as shown in Section A.3.2.1, the model with anodized coated external fins represents the bounding case. The emissivity and solar absorptivity of the damaged anodized area are changed to 0.1 which is the emissivity and solar absorptivity of polished aluminum in this analysis. This change affects solar heat flux and the effective heat transfer coefficient for the external fins with damaged anodized coating.

Based on the methodology described in Section A.3.3.1.1, the insolance value for a curved surface (400 $gcal/cm^2$) is averaged over 24 hours and multiplied by the surface absorptivity of polished aluminum to calculate the solar heat flux over fin areas with damaged anodized coating. The resultant solar heat flux is 0.0427 $Btu/hr\text{-}in^2$. This solar heat flux is used in the finned cask model for the effective surface area of the damaged anodized coating.

To calculate the effect of damaged anodized coating on the effective heat transfer coefficient for the external fins, the TC sub-model discussed in Section A.3.3.1.3 and shown in Figure A.3–10 is rerun with surface emissivity of 0.1. No other changes are considered for this sub-model. The results for the effective heat transfer coefficients are summarized in the following table. The effective heat transfer coefficients listed in the following table are used in the finned cask model for the effective surface area of the damaged anodized coating.

All other material properties and boundary conditions are identical to those in the used in Section A.3.3.1.1 and remain unchanged in this calculation.

**Effective Heat Transfer Coefficients for External Fins @ 100°F Ambient**

| | | |
|---|---|---|
| fin_h = | 3.0 | fin height (in) |
| fin_p = | 1.0 | fin pitch (in) |
| fin_t = | 0.156 | fin thickness (in) |
| fin_n = | 3 | No. of fins in model |
| $D_o$ = | 98.25 | cask diameter (in) |
| $D_f$ = | 104.25 | fin diameter (in) |
| $D_f/D_o$ = | 1.061 | |
| A_eff = | 77.2 | area of un-finned surface ($in^2$) |

From Rohsenow Handbook [21]

| $D_f/D_o$ | c | b |
|---|---|---|
| 1.36 | 0.62 | 0.29 |
| 1.14 | 0.59 | 0.27 |
| Extrapolated for this calculation based on above data | | |
| 1.061 | 0.579 | 0.263 |

| $T_s$ (°F) | $T_{amb}$ (°F) | $Q_{react}$ (Btu/hr) | $A_{eff}$ ($in^2$) | $h_{eff}$ (Btu/hr-$in^2$-°F) |
|---|---|---|---|---|
| 120 | 100 | 22.760 | 77.2 | 0.0147 |
| 140 | 100 | 53.748 | 77.2 | 0.0174 |
| 160 | 100 | 88.42 | 77.2 | 0.0191 |
| 180 | 100 | 125.73 | 77.2 | 0.0204 |
| 200 | 100 | 165.16 | 77.2 | 0.0214 |
| 220 | 100 | 206.40 | 77.2 | 0.0223 |
| 240 | 100 | 248.94 | 77.2 | 0.0230 |
| 260 | 100 | 293.54 | 77.2 | 0.0238 |
| 280 | 100 | 339.55 | 77.2 | 0.0244 |
| 300 | 100 | 386.94 | 77.2 | 0.0251 |
| 320 | 100 | 435.62 | 77.2 | 0.0257 |
| 340 | 100 | 485.80 | 77.2 | 0.0262 |

## Scattered Multiple Scratches and Small Peel-off Spots – Case 2

If the accumulated surface area of the multiple coating damages is smaller than the concentrated large damaged area considered in Case 1, the effects of the multiple damages are bounded by Case 1. Therefore, this calculation focuses on Case 1 for determination of the acceptance criteria for damaged coatings.

The maximum component temperatures for TC with damaged coatings under hot NCT with ambient temperature of 100°F and insolation are listed in the following table.

**Maximum Temperatures of TC/DSC Shell with Damaged and Undamaged Coatings**

| TC type<br>DSC type / Heat load<br>Conditions | TC with External Fins and No Internal Sleeve<br>69BTH DSC / 32 kW<br>NCT @ 100°F with Insolation | | | TC with No Fins/ No Internal Sleeve<br>69BTH DSC / 26 kW<br>NCT @ 100°F with Insolation | | | TC with Internal Sleeve and No Fins<br>24PTH DSC / 26 kW<br>NCT @ 100°F with Insolation | | |
|---|---|---|---|---|---|---|---|---|---|
| Damaged Coat on External Fins 2000 $in^2$ | Yes | No | --- | N/A | N/A | --- | N/A | N/A | --- |
| Damaged Paint over Shield Shell 500 $in^2$ | N/A | N/A | --- | Yes | No | --- | No | No | --- |
| Damaged Coat on Internal Sleeve 250 $in^2$ | N/A | N/A | --- | N/A | N/A | --- | Yes | No | --- |
| Component | $T_{max}$ (°F) | $T_{max}$ (°F) | $\Delta T$ (°F) | $T_{max}$ (°F) | $T_{max}$ (°F) | $\Delta T$ (°F) | $T_{max}$ (°F) | $T_{max}$ (°F) | $\Delta T$ (°F) |
| DSC shell | 484.0 | 483.8 | 0.2 | 451.6 | 451.1 | 0.5 | 464.0 | 464.0 | 0.0 |
| Cask internal sleeve | N/A | N/A | N/A | N/A | N/A | N/A | 346.7 | 346.7 | 0.0 |
| Cask inner shell | 367.4 | 367.3 | 0.1 | 350.9 | 350.7 | 0.2 | 343.0 | 343.0 | 0.0 |
| Gamma shield | 365.7 | 365.6 | 0.1 | 349.6 | 349.4 | 0.2 | 335.0 | 335.0 | 0.0 |
| Outer shell | 351.9 | 351.8 | 0.1 | 337.5 | 337.2 | 0.3 | 294.9 | 294.9 | 0.0 |
| Shield shell | 305.1 | 305.0 | 0.1 | 299.1 | 299.0 | 0.1 | 464.0 | 464.0 | 0.0 |
| Finned Shell | 229.4 | 229.4 | 0.0 | N/A | N/A | N/A | N/A | N/A | N/A |
| Cask lid | 266.9 | 266.9 | 0.0 | 265.4 | 265.3 | 0.1 | 336.0 | 336.0 | 0.0 |
| Cask bottom plate | 353.3 | 353.2 | 0.1 | 338.6 | 338.4 | 0.2 | 281.9 | 281.9 | 0.0 |
| Cask lid seal | 268.1 | 268.1 | 0.0 | 266.4 | 266.4 | 0.0 | 335.6 | 335.6 | 0.0 |
| Ram plate seal | 351.8 | 351.7 | 0.1 | 337.3 | 337.1 | 0.2 | 280.4 | 280.4 | 0.0 |
| Drain port seal @ bottom | 351.4 | 351.3 | 0.1 | 337.1 | 336.9 | 0.2 | 281.2 | 281.2 | 0.0 |
| Test seal @ bottom | 349.4 | 349.3 | 0.1 | 335.5 | 335.2 | 0.3 | 278.9 | 278.9 | 0.0 |
| Vent & test seal @ top | 266.7 | 266.6 | 0.1 | 265.2 | 265.1 | 0.1 | 335.9 | 335.9 | 0.0 |
| Wood in Impact limiter | 302.5 | 302.5 | 0.0 | 291.5 | 291.3 | 0.2 | 289.1 | 289.1 | 0.0 |

Note: (1) This value is the maximum DSC shell temperature in the region where the fuel assemblies have the maximum peaking factor.

As seen, the maximum DSC shell temperatures increase by 0.2°F for coating damages on external fins, 0.5°F for coating damages on shield shell, and 0.0°F for coating damages on inner sleeve. As noted previously, the rise in the maximum fuel cladding temperatures are lower than the above values and are therefore limited to less than 1°F.

A rise of less than 1°F for the maximum fuel cladding temperature is insignificant for the thermal performance of MP197HB.

Since the temperature rises are limited to 1°F, the effects of the coating damages on the thermal and structural performance of MP197HB are insignificant, if the accumulated coating damages are limited to:

- 2,000 $in^2$ for coating on external fins,
- 500 $in^2$ for paint on shield shell, and
- 250 $in^2$ for coating on internal sleeve.

### A.3.6.5 Effective Thermal Properties of the Fuel Assemblies

This section presents the methodology and determines the bounding effective thermal conductivity, specific heat and density for the fuel assemblies to be transported within

the MP197HB TC for use in the analysis of the thermal performance. The types of fuel assemblies to be transported in MP197HB TC are listed in Chapter A.1, Section A.1.4.

### A.3.6.5.1 Effective Thermal Properties for PWR Fuel Assemblies

The PWR fuel assemblies proposed for transportation in the MP197HB TC are listed in Chapter A.1, Section A.1.4. All of these PWR fuel assemblies are studied in [1] through [4]. There are minor deviations between the dimensions of the fuel assemblies listed in Chapter A.1, Section A.1.4 and those studied in [1] through [4], which have no effect on the bounding effective PWR fuel properties.

For PWR FAs, the effective fuel properties of FA WE14x14 are the bounding minimum values for all PWR FAs based on the SARS ([1] to [4]).

For the same FAs in the identical fuel compartment material and configuration, effective fuel properties for the large nominal opening sizes are lower than those for small nominal opening sizes.

For the 37PTH DSC, there are two kinds of nominal opening sizes for fuel compartments: 8.875" for four corner fuel compartments and 8.6" for the other fuel compartments. In addition, two of the compartment walls are covered with anodized aluminum/poison plates. Since the emissivity of the anodized plates is higher than the emissivity of stainless steel and the compartment opening size is smaller than 9" for the corner compartments, the effective fuel properties calculated in [1], Appendix P, Section P.4.2 based on 9.0" nominal opening size with WE14x14 FA for 24PTH DSC represent the bounding values for the fuel assemblies in the corner compartments in the 37PTH DSC.

The configuration of the other fuel compartments in the 37PTH DSC are identical to those in the 32PT DSC described in [1], Appendix M. Since the compartment opening in the 37PTH DSC (8.6") is smaller than the compartment opening in the 32PT DSC (8.7") and the compartment configurations are identical, the effective fuel properties calculated in [1], Appendix M, Section M.4.2 based on 8.7" nominal opening size with WE14x14 FA for the 32PT DSC represent the bounding values for the fuel assemblies in the compartments other than the four corner ones in the 37PTH DSC.

Based on the above discussion, no further analysis is required for PWR fuel assemblies for the 37PTH DSC model. The bounding effective properties for PWR fuel assemblies to use in the MP197HB thermal analysis are listed in Section A.3.2.1 material # 1

### A.3.6.5.2 Effective Thermal Properties for BWR Fuel Assemblies

The BWR fuel assemblies proposed for transportation in the MP197HB TC are listed in Chapter A.1, Section A.1.4. Most of the proposed BWR fuel assemblies are studied in [3], Appendix T. The characteristics of the BWR fuel assemblies listed in Chapter A.1, Section A.1.4 are identical to those studied in [3], Appendix T.

Based on the study in [3], Appendix T, Section T.4.8, fuel assembly FANP 9x9-2 has the bounding transverse effective conductivity and fuel assembly Siemens QFA has the bounding axial effective conductivity, bounding effective density, and bounding effective specific heat.

BWR fuel assemblies listed in Chapter A.1, Section A.1.4 for transportation in the MP197HB TC, but not studied in [3], Appendix T, Section T.4.8 are:

- FANP 9x9, TN ID 9x9-81,
- LaCrosse, TN ID 10x10-100, and
- SVEA fuel assemblies.

The effective properties for these fuel assemblies are evaluated in this section to determine the bounding effective properties to use in the MP197HB TC and 69BTH DSC thermal analysis. The effective properties in [3], Appendix T, Section T.4.8 are calculated for stainless steel fuel compartments with a nominal opening size of 6". The same compartment material and size are considered in evaluation of the effective properties.

Effective properties for the above three BWR FAs are calculated using the methodologies and material properties approved in UFSAR for NUHOMS® system ([1], Appendices M and P) and associated with Amendment 10 to Part 72 CoC 1004 for the Standardized NUHOMS® System [3]. For the LaCrosse fuel assembly, a stainless steel cladding emissivity of 0.70 is considered in this evaluation. Perry in [5], Table 10-17, gives an emissivity between 0.62 and 0.82 for steel/stainless steel sheets heated or covered with shiny oxide layer. The assumed emissivity for the stainless steel cladding of the LaCrosse fuel assembly remain with this range and is therefore acceptable.

**Effective Properties for Fuel Assembly FANP 9x9**

The characteristics of fuel assembly FANP 9x9 (TN ID 9x9-81) shown in Chapter A.1, Section A.1.4 are identical to those for fuel assembly FANP 9x9-2 (TN ID 9x9-79/2) except for the number of fuel rods. The number of fuel rods for fuel assembly FANP 9x9 varies between 72 and 81 while fuel assembly FANP 9x9-2 has 79 fuel rods.

Due to the steel/stainless steel sheets steel/stainless steel sheets increased number of fuel rods in FANP 9x9 in comparison to FANP 9x9-2, the effective axial conductivity, density, and specific heat for FANP 9x9 is higher than those for FANP 9x9-2 and does not represent the bounding minimum values.

The two-dimensional finite element model used to determine the transverse effective conductivity of the fuel assembly FANP 9x9 is shown in the following figure. A correction factor of 1.0262 is used to increase the heat generation rate in the 2D model. This correction factor compensates the imperfection of the pellet cross section area in the model.

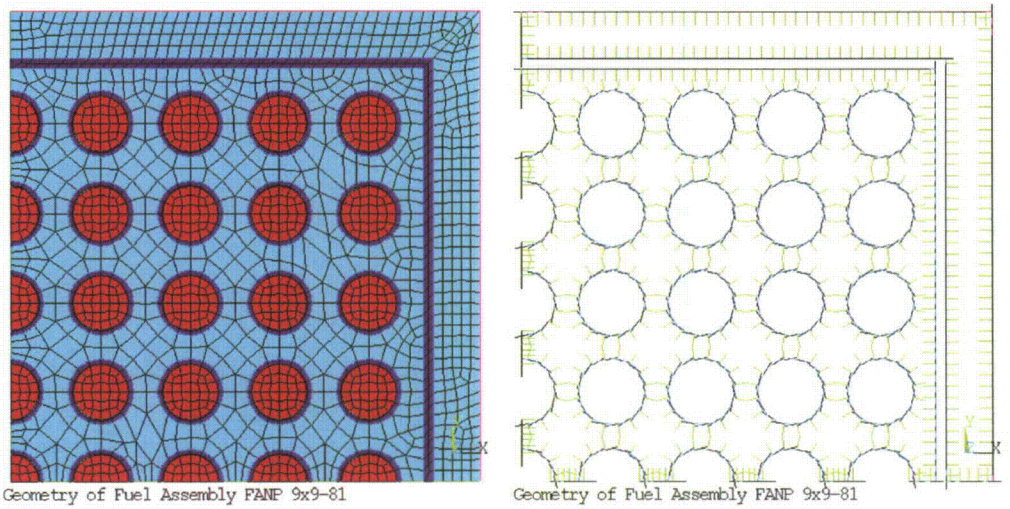


**Quarter Symmetric FE Model for Fuel Assembly FANP 9x9**

### Effective Properties for Fuel Assembly LaCrosse

Fuel assembly LaCrosse consists of stainless steel cladding as indicated in Section A.1.4. This evaluation assumes a fuel cladding temperature limit of 752 °F (400 °C) for stainless steel cladding, which is identical to the limit for the Zircaloy cladding.

The two-dimensional finite element model used to determine the transverse effective conductivity of the fuel assembly LaCrosse is shown in the following figure. A correction factor of 1.0262 is used to increase the heat generation rate in the 2D model. This correction factor compensates the imperfection of the pellet cross section area in the model.

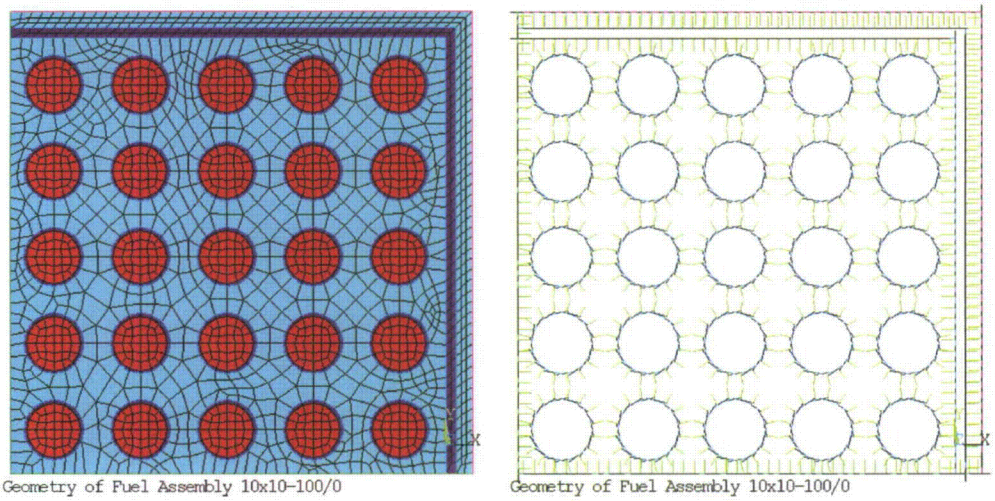


**Quarter Symmetric FE Model for Fuel Assembly LaCrosse**

### Effective Properties for SVEA Fuel Assemblies

SVEA fuel assemblies are described in detail in [31]. Based on [31], the SVEA fuel assemblies provide larger heat transfer areas and lower heat fluxes in comparison to conventional BWR fuel assemblies with similar fuel rod arrays. In addition, the SVEA fuel assemblies consist of sub-channels which arrange the fuel rods closer to the periphery of the assembly. These factors result in higher transverse effective conductivity for these fuel types.

The sub-channels in SVEA fuel assemblies provide also more Zircaloy in comparison to conventional BWR fuel assemblies with similar fuel rod arrays. Therefore, the axial effective conductivity, effective density, and effective specific heat of the SVEA fuel assemblies are higher than those for comparable conventional BWR fuel assemblies.

To verify that the effective properties of SVEA fuel assemblies are bounded by comparable conventional BWR fuel assemblies, the effective properties of fuel assembly SVEA-92 (TN ID ABB-10-2) with four 5x5 sub-bundles are evaluated in this section.

The two-dimensional finite element model of the fuel assembly SVEA-92 used to determine the transverse effective conductivity is shown in the following figure. A correction factor of 1.0262 is used to increase the heat generation rate in the 2D model. This correction factor compensates the imperfection of the pellet cross section area in the model.

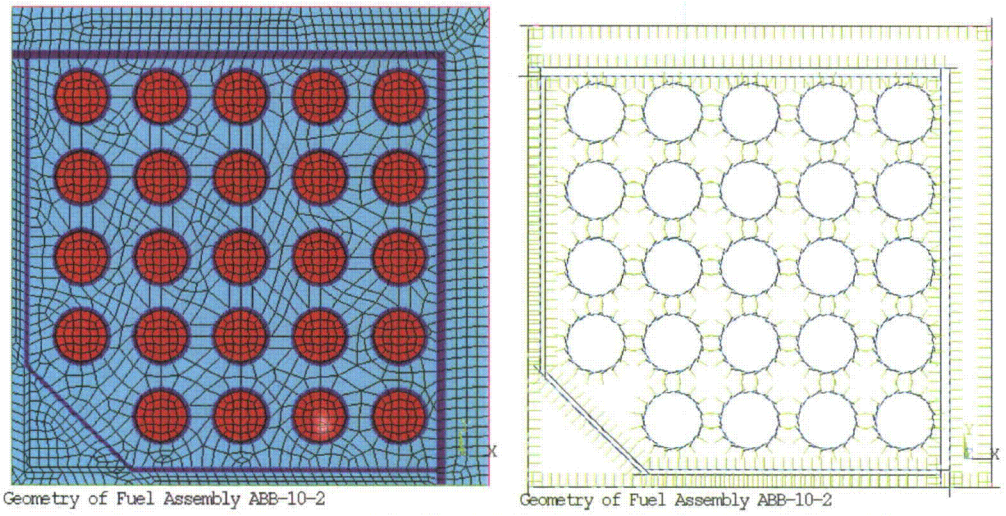


**Quarter Symmetric FE Model for Fuel Assembly SVEA-92**

### Transverse Effective Conductivity

The results of the two-dimensional models for fuel assemblies FANP 9x9, LaCrosse, and SVEA-92 are summarized in the following table.

**Fuel Assembly Transverse Effective Conductivity**

| **FANP 9x9 (9x9-81)** | | | |
|---|---|---|---|
| Fuel Compartment Wall Temperature (°F) | Maximum Fuel Temperature (°F) | Average Fuel Temperature (°F) | Transverse Conductivity $K_{eff, FANP9x9}$ (Btu/hr-in-°F) |
| 200 | 228 | 214 | 0.0156 |
| 300 | 324 | 312 | 0.0184 |
| 400 | 420 | 410 | 0.0217 |
| 500 | 517 | 509 | 0.0255 |
| 600 | 615 | 607 | 0.0299 |
| 700 | 713 | 706 | 0.0348 |
| 800 | 811 | 805 | 0.0402 |
| **LaCrosse (10x10-100/0)** | | | |
| Fuel Compartment Wall Temperature (°F) | Maximum Fuel Temperature (°F) | Average Fuel Temperature (°F) | Transverse Conductivity $K_{eff, LaCrosse}$ (Btu/hr-in-°F) |
| 200 | 240 | 220 | 0.0194 |
| 300 | 334 | 317 | 0.0228 |
| 400 | 429 | 415 | 0.0267 |
| 500 | 525 | 512 | 0.0313 |
| 600 | 621 | 611 | 0.0365 |
| 700 | 719 | 709 | 0.0421 |
| 800 | 816 | 808 | 0.0483 |
| **SVEA-92 (ABB-10-2)** | | | |
| Fuel Compartment Wall Temperature (°F) | Maximum Fuel Temperature (°F) | Average Fuel Temperature (°F) | Transverse Conductivity $K_{eff, SVEA-92}$ (Btu/hr-in-°F) |
| 100 | 122 | 111 | 0.0199 |
| 200 | 220 | 210 | 0.0226 |
| 300 | 317 | 309 | 0.0255 |
| 400 | 415 | 408 | 0.0289 |
| 500 | 513 | 507 | 0.0327 |
| 600 | 612 | 606 | 0.0370 |

As seen, transverse effective conductivities for FANP 9x9 FA present the lowest conductivity values. The transverse effective conductivities for fuel assembly FANP 9x9 are compared to the bounding values from [3], Appendix T, Section T.4.8 and listed in the following table.

**Transverse $K_{eff}$ for FANP 9x9 and Bounding Values**

| Average Fuel Temperature ($^{o}$F) | Transverse Conductivity $K_{eff, FANP9x9}$ (Btu/hr-in-$^{o}$F) | Transverse Conductivity $K_{eff, bounding}$ [1] (Btu/hr-in-$^{o}$F) | $\frac{K_{eff,FANP9x9} - K_{eff,bounding}}{K_{eff,bounding}}$ (---) |
|---|---|---|---|
| 214 | 0.0156 | 0.0160 | -2.5% |
| 312 | 0.0184 | 0.0185 | -0.1% |
| 410 | 0.0217 | 0.0215 | 1.0% |
| 509 | 0.0255 | 0.0249 | 2.3% |
| 607 | 0.0299 | 0.0288 | 3.9% |
| 706 | 0.0348 | 0.0331 | 5.1% |
| 805 | 0.0402 | 0.0378 | 6.6% |

Note: [1] Bounding values from [3], Appendix T, Section T.4.8

As seen, the transverse effective fuel conductivities from [3], Appendix T, Section T.4.8 remain the bounding values except for low operating temperatures below ~315°F (~157°C). For all practical purposes, the operating temperature of fuel assemblies within the 69BTH DSC is above 315°F. Therefore, the values from [3], Appendix T, Section T.4.8 remains the bounding values to be used in the thermal analysis.

### Axial Effective Conductivity

The axial effective conductivities calculated for fuel assemblies FANP 9x9, LaCrosse, and SVEA-92 are compared to the bounding values from [3], Appendix T, Section T.4.8 in the following table.

**Fuel Assembly Axial Effective Conductivity**

| | FANP 9x9 (9x9-81) | LaCrosse (10x10-100/0) | SVEA-92 (ABB-10-2) | |
|---|---|---|---|---|
| No of fuel rods | 81 | 100 | 96 | |
| OD fuel rod (in) | 0.424 | 0.395 | 0.378 | |
| Clad thickness (in) | 0.03 | 0.0210 | 0.0243 | |
| Sub-channel Area (in$^2$) [1] | N/A | N/A | 0.59 | |
| Cladding area (in$^2$) | 3.01 | 2.47 | 3.18 | |
| Compartment area (in$^2$) | 36.0 | 36.0 | 36.0 | |
| Temp (°F) | $K_{eff,axial}$ (Btu/hr-in-°F) | $K_{eff,axial}$ (Btu/hr-in-°F) | $K_{eff,axial}$ (Btu/hr-in-°F) | Bounding Value [2] $K_{eff,axial}$ (Btu/hr-in-°F) |
| 70 | 0.0503 | 0.0491 | 0.0532 | 0.0402 |
| 100 | | 0.0497 | | |
| 200 | | 0.0531 | | |
| 300 | | 0.0560 | | |
| 700 | | 0.0674 | | |
| 1000 | | 0.0748 | | |

Notes:
[1] The area of sub-channel is determined using the FE model of SVEA-92.
[2] Bounding values are from [3], Appendix T, Section T.4.8

As seen, the axial effective fuel conductivity from [3], Appendix T, Section T.4.8 remains the bounding value to be used in the thermal analysis.

**Effective Density and Specific Heat**

The effective density ($\rho_{eff}$) and specific heat ($c_{P,\ eff}$) calculated for fuel assemblies FANP 9x9, LaCrosse, and SVEA-92 are compared to the bounding values from [3], Appendix T, Section T.4.8 in the following table.

**Fuel Assembly Effective Density and Specific Heat**

| | FANP 9x9 (9x9-81) | LaCrosse (10x10-100/0) | SVEA-92 (ABB-10-2) | |
|---|---|---|---|---|
| No of fuel rods | 96 (1) | 81 | 96 | |
| OD fuel rod (in) | 0.395 | 0.424 | 0.378 | |
| Clad thickness (in) | 0.0210 | 0.03 | 0.0243 | |
| No of water tubes | 4 (1) | 0 | 0.59 | |
| Pellet OD (in) | 0.3465 | 0.3565 | 0.3224 | |
| Fuel length (in) | 85 | 150 | 150.59 | Bounding Values (2) |
| Cladding area ($in^2$) | 2.47 | 3.01 | 3.18 | |
| $UO_2$ area ($in^2$) | 9.05 | 8.09 | 7.84 | |
| Compartment area ($in^2$) | 36.0 | 36.0 | 36.0 | |
| Cladding volume ($in^3$) | 210 | 451 | 479 | |
| $UO_2$ volume ($in^3$) | 769 | 1213 | 1180 | |
| Compartment volume ($in^3$) | 3060 | 5400 | 5421 | |
| $Density_{eff}$ ($lbm/in^3$) | 0.119 | 0.109 | 0.107 | 0.103 |
| $c_{P,\ eff}$ (Btu/lbm-°F) | 0.0658 | 0.0578 | 0.0579 | 0.0575 |

Notes:
(1) Fuel assembly FANP 9x9 can optionally contain up to four water rods. To determine the lowest possible density and specific heat, four water rods are considered for fuel assembly FA FANP 9x9.
(2) Bounding values are from [3], Appendix T, Section T.4.8

As seen, the effective density and specific heat from [3], Appendix T, Section T.4.8 remain the bounding values to be used in the thermal analysis.

The effective conductivities along with specific heat and density used for BWR fuel assemblies are summarized in Section A.3.2.1 material # 2.

### A.3.6.6 Thermal Analysis of 24PTHF and 61BTHF DSCs in the MP197HB TC

The 24PTHF and 61BTHF DSCs are proposed for transportation of damaged and failed fuel assemblies in the MP197HB. The failed fuel assemblies are to be encapsulated in individual failed fuel cans (FFCs) that are designed to fit into the 61BTHF and 24PTHF basket fuel compartments. The 24PTHF and 61BTHF DSCs have the same basket configurations as those for 24PTH and 61BTH DSCs except for additional FFCs to store failed fuel assemblies.

Damaged FAs are assemblies containing missing or partial fuel rods or fuel rods with known or suspected cladding defects greater than hairline cracks or pinhole leaks. Damaged FA may be stored in the certain basket locations and does not require a separate FFC.

Failed FA is defined as any fuel assembly damage exceeding above damaged FA such as ruptured fuel rod, severed fuel rod, loose fuel pellets or fuel assemblies that cannot be handled by normal means. Failed FAs may contain breached rods, grossly breached rods, and other defects such as missing or partial rods. Failed FA can not be handled by normal means and requires a separate FFC to store.

The 24PTHF DSC can accommodate up to a maximum of 12 damaged fuel assemblies or up to eight failed FAs placed in the outermost fuel compartments as shown in Figure A.3–49. It is assumed in this evaluation that the 24PTHF DSC is loaded with four damaged FAs and eight failed FAs to bound the maximum temperatures.

The 61BTHF DSC can accommodate up to a maximum of 16 damaged fuel assemblies or up to four failed FAs placed in corner 2x2 fuel compartment assemblies as shown in Figure A.3–50. It is assumed in this evaluation that 61BTHF DSC is loaded with 12 damaged FAs and four failed FAs to bound the maximum temperatures.

The following assignments are used in the section for 24PTHF and 61BTHF DSCs.

| | **With Al inserts/ Aluminum Rails** | **Without Al inserts /Aluminum Rails** |
|---|---|---|
| 24PTH | Type 1 | Type 2 |
| 61BTH | Type 2 | Type 1 |

A.3.6.6.1 Effective Thermal Conductivity of Damaged Fuel

For PWR FAs, damaged WEO 17x17 PWR FA with minimum conductivity pitch size provides the minimum effective transverse conductivity for a damaged FA in the 32PTH DSC as discussed in [4], Section 4.14.3. For BWR FAs, damaged GE-2 BWR FA with a pitch of 0.607" provides the minimum and bounding effective transverse conductivity for a damaged FA in 61BT DSC as discussed in [1], Appendix K, Section K.4.8.1.

As listed in [4], Section 4.14.3 and [1], Appendix K, Section K.4.8.1, the damaged FA thermal conductivities in transverse direction are about 69% to 71% of the intact PWR FA thermal conductivity and about 82% to 85% of the intact BWR FA thermal conductivity. To bound the reduction in transverse thermal conductivity of damaged FAs in 24PTHF and 61BTHF DSCs, the effective transverse conductivities for intact FAs in 24PTH DSC and 61BTH DSC are reduced by 65% and 80% to use for the damaged PWR and BWR FAs, respectively.

Reconfiguration of fuel rods as a consequence of damaged grids doesn't have any impact on axial thermal conductivity of the damaged fuel. To bound the reduction in axial thermal conductivity due to the cladding defects, the axial effective conductivities for the intact FAs in 24PTH DSC and 61BTH DSC are reduced by 90% for the damaged PWR and BWR FAs.

The following tables summarize the bounding fuel thermal properties for 24PTHF and 61BTHFdamaged/intact FAs.

**Bounding Damaged Fuel Thermal Conductivities for 24PTHF FAs**

| Keff_rad | | | Keff_axl | | |
|---|---|---|---|---|---|
| Temp | Intact Fuel [1] | Damaged Fuel [2] | Temp | Intact Fuel [1] | Damaged Fuel [3] |
| °F | Btu/min-in-°F | Btu/min-in-°F | °F | Btu/min-in-°F | Btu/min-in-°F |
| 178 | 2.798E-04 | 1.819E-04 | 200 | 7.596E-04 | 6.836E-04 |
| 267 | 3.257E-04 | 2.117E-04 | 300 | 8.014E-04 | 7.213E-04 |
| 357 | 3.829E-04 | 2.489E-04 | 400 | 8.432E-04 | 7.589E-04 |
| 448 | 4.547E-04 | 2.956E-04 | 500 | 8.781E-04 | 7.903E-04 |
| 541 | 5.389E-04 | 3.503E-04 | 600 | 9.129E-04 | 8.216E-04 |
| 635 | 6.326E-04 | 4.112E-04 | 800 | 9.896E-04 | 8.906E-04 |
| 730 | 7.398E-04 | 4.809E-04 | | | |
| 826 | 8.558E-04 | 5.563E-04 | | | |

Notes:
[1] Bounding thermal conductivities for 24PTH intact FA listed in [1] Appendix P, Section P.4.2.1.
[2] Based on 65% of bounding intact fuel thermal conductivities for transverse direction.
[3] Based on 90% of bounding intact fuel thermal conductivities for axial direction.

**Bounding Damaged Fuel Thermal Conductivities for 61BTHF FAs**

| | $K_{eff\_rad}$ | | $K_{eff\_axl}$ | |
|---|---|---|---|---|
| Temp | Intact Fuel [1] | Damaged Fuel [2] | Intact Fuel [1] | Damaged Fuel [3] |
| °F | Btu/min-in-°F | Btu/min-in-°F | Btu/min-in-°F | Btu/min-in-°F |
| 200 | 2.618E-04 | 2.094E-04 | 6.720E-04 | 6.048E-04 |
| 300 | 3.021E-04 | 2.417E-04 | | |
| 400 | 3.520E-04 | 2.816E-04 | | |
| 500 | 4.104E-04 | 3.283E-04 | | |
| 600 | 4.756E-04 | 3.805E-04 | | |
| 700 | 5.468E-04 | 4.374E-04 | | |
| 800 | 6.250E-04 | 5.000E-04 | | |

Notes:
[1] Bounding thermal conductivities for 61BTH intact FA listed in [3] Appendix T, Section T.4.2.1.
[2] Based on 80% of bounding intact fuel thermal conductivities for transverse direction.
[3] Based on 90% of bounding intact fuel thermal conductivities for axial direction.

The FFC is required to encapsulate failed FA before loading it into the fuel compartment. To bound effective thermal conductivity of the FFC containing failed FAs, helium thermal conductivity is conservatively assumed for the space within a compartment loaded with a FFC.

### A.3.6.6.2 Heat Generation Rates

The base heat generation rates are calculated assuming uniform heat loads for fuel assemblies loaded in 24PTHF and 61BTHF DSCs. The nominal fuel cell openings are 8.9 $in^2$ for 24PTHF DSC and 6.0 $in^2$ for 61BTHF DSC.

The conditions of failed FAs are unknown under NCT. The worse case condition occurs when the heat load from a failed FA is concentrated in the region where the intact FAs have the maximum peaking factor. Based on the decay heat profiles discussed in Sections A.3.3.1.4 and A.3.3.1.6, the maximum peaking factor region is located

between 36.1" to 84.9" for BWR FAs and between 28.0" to 100.0" for PWR FA. These locations are measured from the bottom of the active fuel length. This gives minimum heat load lengths of 48.8" (=84.9"-36.1") and 72.0" (=100.0"-28.0") for failed BWR and PWR FAs in 61BTHF and 24PTHF DSCs, respectively.

An unlikely hypothetical accident case is postulated in which the defected cladding of damaged FAs might break entirely in consequence of a drop accident and fuel pellets could be released in the compartment space. The concentration of the decay heat for the fuel rubble is maximized when all the rubble are compressed to a minimum length at one end of the fuel compartment.

The minimum length of the fuel rubble is calculated using equation (3) in [1] Appendix K, Section K.4.8.1.2. The shortest fuel rubble heights of 54" for a PWR FA and 50" for a BWR FA are calculated based on minimum fuel assembly volumes for WE14x14 and Siemens QFA 9x9 in this evaluation.

The following assumptions are considered for calculation of heat generation rates for failed FAs under NCT and HAC:

a) Active fuel length of 72" with uniform peaking factor of 1.11 for failed FA in 24PTHF under NCT. The heat load is concentrated in the region of the maximum peaking factors for intact fuel assemblies.

b) Minimum rubble length of 54" with peaking factor of 1.0 for failed and damaged FAs in 24PTHF under HAC. Fuel rubbles are collected at the top end of the fuel compartment (hot end).

c) Active fuel length of 48.8" with uniform peaking factor of 1.20 for failed FA in 61BTHF under NCT. The heat load is concentrated in the region of the maximum peaking factors for intact fuel assemblies

d) Minimum rubble length of 50" with peaking factor of 1.0 for failed and damaged FAs in 61BTHF under HAC. Fuel rubbles are collected at the bottom end of the fuel compartment (hot end).

The following equations calculate the base heat generation rates for the maximum allowable heat loads of 26 kW and 24 KW defined in Section A.3.1 for 24PTHF and 61BTHF DSCs in MP197HB TC under NCT and HAC, respectively:

**For 1.083 kW/FA (26 kW / 24 FA) heat load in 24PTHF Intact/Damaged FAs under NCT**

$$\dddot{q} = \frac{1.11 \cdot (1.083)\,kW \cdot 3412.3 \frac{Btu/hr}{kW} \cdot \frac{1\,hr}{60\,\min}}{(8.9\,in)^2 \cdot 140.6\,in} = 6.14e-3 \frac{Btu}{\min \cdot in^3},$$

**For 1.083 kW/FA (26 kW / 24 FA) heat load in 24PTHF Failed FAs under NCT**

$$\ddot{q} = \frac{1.11 \cdot (1.083)\,kW \cdot 3412.3 \frac{Btu/hr}{kW} \cdot \frac{1\,hr}{60\,\min}}{(8.9\,in)^2 \cdot 72\,in} = 1.20e-2 \frac{Btu}{\min \cdot in^3},$$

Note the above heat generation rate calculated for 72" for failed FAs is applied over 73.37" (from z-coordinates 48.18" to 120.55") in the model which is conservative.

**For 1.083 kW/FA (26 kW / 24 FA) heat load in 24PTHF Intact under HAC**

$$\ddot{q} = \frac{1.11 \cdot (1.083)\,kW \cdot 3412.3 \frac{Btu/hr}{kW} \cdot \frac{1\,hr}{60\,\min}}{(8.9\,in)^2 \cdot 140.6\,in} = 6.14e-3 \frac{Btu}{\min \cdot in^3},$$

**For 1.083 kW/FA (26 kW / 24 FA) heat load in 24PTHF Failed/Damaged FAs under HAC**

$$\ddot{q} = \frac{1.00 \cdot (1.083)\,kW \cdot 3412.3 \frac{Btu/hr}{kW} \cdot \frac{1\,hr}{60\,\min}}{(8.9\,in)^2 \cdot 54\,in} = 1.44e-2 \frac{Btu}{\min \cdot in^3},$$

Note the above heat generation rate calculated for 54" for failed/damaged FAs is applied over 55.93" (from z-coordinates 120.55" to 176.48") in the model which is conservative.

**For 0.393 kW/FA (24 kW/61 FA) heat load in 61BTHF Intact/Damaged FAs under NCT**

$$\ddot{q} = \frac{1.00 \cdot (0.393\,kW) \cdot 3412.3 \frac{Btu/hr}{kW} \cdot \frac{1\,hr}{60\,\min}}{(6.0\,in)^2 \cdot 144.0\,in} \cdot = 4.31e-3 \frac{Btu}{\min \cdot in^3},$$

**For 0.393 kW/FA (24 kW/61 FA) heat load in 61BTHF Failed FAs under NCT**

$$\ddot{q} = \frac{1.20 \cdot (0.393\,kW) \cdot 3412.3 \frac{Btu/hr}{kW} \cdot \frac{1\,hr}{60\,\min}}{(6.0\,in)^2 \cdot 48.8\,in} = 1.53e-2 \frac{Btu}{\min \cdot in^3},$$

**For 0.393 kW/FA (24 kW/61 FA) heat load in 61BTHF Intact FAs under HAC**

$$\ddot{q} = \frac{1.00 \cdot (0.393\,kW) \cdot 3412.3 \frac{Btu/hr}{kW} \cdot \frac{1\,hr}{60\,\min}}{(6.0\,in)^2 \cdot 144.0\,in} \cdot = 4.31e-3 \frac{Btu}{\min \cdot in^3},$$

**For 0.393 kW/FA (24 kW/61 FA) heat load in 61BTHF Failed/Damaged FAs under HAC**

$$\ddot{q} = \frac{1.00 \cdot (0.393\,kW) \cdot 3412.3 \frac{Btu/hr}{kW} \cdot \frac{1\,hr}{60\,\min}}{(6.0\,in)^2 \cdot 50.0\,in} = 1.24e-2 \frac{Btu}{\min \cdot in^3}.$$

Note the above heat generation rate calculated for 50" for failed/damaged FAs is applied over 50.89" (from z-coordinates 7.9" to 58.79") in the model which is conservative.

A.3.6.6.3 Calculation of Thermal Performance of the 24PTHF and 61BTHF DSC with Damaged/Failed Fuel

The maximum fuel cladding and basket component temperatures for the 24PTHF DSC are determined using the finite element models for the 24PTH-S DSC (w/o Al insert) described in [1] and the 61BTH Type 1 DSC (w/o Al R90 rail) in [3] without any geometrical modifications in this evaluation.

The DSC shell temperatures for hot normal and accident hypothetical accident conditions of transport are taken from the MP197HB TC models described in Section A.3.3.1.1 and Section A.3.4 and transferred to the above DSC/basket models.

A.3.6.6.4 Maximum Temperature of Failed Fuel Canister Wall

The maximum temperature of failed fuel canister wall is calculated using conduction through helium as follows.

$$T_{FFC} - T_{comp} = \frac{q'' \cdot d_{gap}}{K_{He}}$$

$T_{FFC}$ = maximum temperature of failed fuel canister wall (°F)
$T_{comp}$ = maximum temperature of fuel compartment containing failed fuel canister (°F) (retrieved from FE model)
$d_{gap}$ = gap size between the fuel compartments and failed fuel canister
= 0.05" for 24PTHF DSC and 0.08" for 61BTHF DSC.
$k_{He}$ = helium conductivity at $T_{comp}$ (Btu/min-in-°F)

The heat flux from failed fuel canister is calculated as follows

$$q'' = \frac{q}{4w \cdot h} \cdot PF$$

q = heat load of failed fuel (Btu/min-in$^2$)
w = fuel compartment opening width (in)
h = assumed height of failed fuel (in)
PF = peaking factor

### A.3.6.6.5 Evaluation of 61BTHF and 24PTHF DSCs for NCT and HAC

The maximum fuel cladding and basket component temperatures for 24PTHF Type 2 and 61BTHF Type 1 DSCs are collected in the following tables.

For NCT conditions, the maximum fuel cladding temperature is 674°F for the 24PTHF DSC with a maximum heat load of 26 kW and 711°F for the 61BTHF DSC with a maximum heat load of 24 kW.

For HAC conditions, the maximum fuel cladding temperature is 705°F for the 24PTHF DSC with a maximum heat load of 26 kW and 719°F for the 61BTHF DSC with a maximum heat load of 24 kW.

The maximum fuel cladding and basket temperatures for the 24PTHF Type 1 DSC with aluminum inserts and the 61BTHF Type 2 DSC with aluminum rails are bounded by the 24PTHF Type 2 DSC without aluminum insets and the 61BTHF Type 1 DSC without aluminum rails.

As seen in the following table, the maximum fuel cladding temperatures calculated for NCT and HAC conditions are well below the allowable limits for 24PTHF/61BTHF DSCs. All design criteria specified in Section A.3.1 are herein satisfied.

**61BTHF and 24PTHF Maximum Temperatures for NCT and HAC**

| Transport Condition | Heat Load (kW) | $T_{max, Fuel}$ (°F) | $T_{max, Comp}$ (°F) | $T_{max, Al/Poison}$ (°F) | $T_{max, Rail}$ (°F) | Fuel Cladding Limit (°F) |
|---|---|---|---|---|---|---|
| 24PTHF Type 1@ NCT (w/ Al inserts) (1) | 26.0 | <674 | <628 | <627 | <485 | |
| 24PTHF Type 2 @ NCT (w/o Al inserts) | 26.0 | 674 | 628 | 627 | 485 | 752 [7] |
| 24PTHF Type 2 @ NCT (w/o Al inserts) (1) | 24.0 | <674 | <628 | <627 | <485 | |
| 24PTHF Type 1@ HAC (w/ Al inserts) (1) | 26.0 | <705 | <658 | <657 | <521 | |
| 24PTHF Type 2@ HAC (w/o Al inserts) | 26.0 | 705 | 658 | 657 | 521 | 1,058 [7] |
| 24PTHF Type 2@ HAC (w/o Al inserts) (1) | 24.0 | <705 | <658 | <657 | <521 | |
| 61BHF Type 1 @ NCT (w/o Al R90 Rail) | 22.0 | <711 (3) (4) | <688 (3) (4) | <687 (3) (4) | <575 (3) (4) | 752 [7] |
| 61BTHF Type 2 @ NCT (w/ Al R90 Rail) (2) | 24.0 | <711 | <688 (5) | <687 (5) | <575 (5) | |
| 61BHF Type 1 @ HAC (w/o Al R90 Rail) | 22.0 | <719 (3) | <696 (3) | <696 (3) | <605 (3) | 1,058 [7] |
| 61BTHF Type 2 @ HAC (w/ Al R90 Rail) (2) | 24.0 | <719 | <696 | <696 | <605 | |

Notes:
(1) Bounded by 24PTHF Type 2 (w/o Al insert) DSC with 26 kW heat load under transport conditions.
(2) Bounded by 61BTHF Type 1 (w/o Al R90 rail) DSC with 24 kW heat load under transport conditions.
(3) This temperature is calculated for 24 kW heat load instead of 22 kW heat load for conservatism.
(4) The small difference between this temperature and the one estimated in Table A.3–10 is due to the conservatism in note (3).

(5) Effect of aluminum inserts are omitted in calculation of this temperature for conservatism. The slight difference between this temperature and the one evaluated in Table A.3–10 has insignificant effect on thermal/structural performance.

**The maximum temperatures for Failed Fuel Canisters**

| Transport Condition | Normal Condition of Transport (NCT) | | Accident Condition of Transport (HAC) | |
|---|---|---|---|---|
| DSC Type | 24PTHF | 61BTHF | 24PTHF | 61BTHF |
| Heat Load | 26 kW | 24 kW | 26 kW | 24 kW |
| Component | $T_{max}$ (°F) | $T_{max}$ (°F) | $T_{max}$ (°F) | $T_{max}$ (°F) |
| Failed Fuel Compartment | 601 | 606 | 645 | 645 |
| Failed Fuel Canister | 608 | 615 | 653 | 652 |

### A.3.6.7 Justification of Hot Gaps

The following hot gaps assumed in the MP197HB TC, 69BTH DSC, and 37PTH DSC models are justified in this section.

a) The radial gap of 0.025" assumed between the gamma shield and the cask outer shell in MP197HB TC model.

b) The radial gap of 0.01" assumed between the finned aluminum shell and the cask shield shell in MP197HB TC model.

c) The diametrical hot gap of 0.30" between the basket outer surface and the DSC shell inner surface in 69BTH DSC model.

d) The 0.01" gaps considered on either side of the paired poison and aluminum plates in 69BTH DSC/basket model.

#### A.3.6.7.1 Gap between Gamma Shield and Cask Outer Shell

A radial air gap of 0.025" is assumed between the gamma shield (lead) and the TC outer shell within the finite element model of MP197HB described in Section A.3.3.1.1. This air gap is due to the differential thermal expansion of the cask body and the gamma shield.

The following assumptions are made for the verification of the gap:

- The cask body nominal dimensions *are taken* at 70°F.
- During the lead pour the cask body and lead *temperatures* are *held above the melting point of lead* at 620°F.
- *Because of the controlled cooling process used after lead pour is completed, the lead solidifies from the bottom upward and thus is always covered with molten lead. Any void volume or gap due to contraction of the solidifying lead is filled with molten lead which then solidifies.*
- The inner diameter of the gamma shell (lead) is equal to the outer diameter of the inner cask shell at thermal equilibrium.

The average coefficients of thermal expansion for SA-203, Gr. E and lead are listed in the following table.

**Thermal Expansion Coefficients**

| Temperature (°F) | SA203, Gr. E α (in/in-°F) [10] |
|---|---|
| 70 | 6.40E-06 |
| 200 | 6.70E-06 |
| 300 | 6.90E-06 |
| 400 | 7.10E-06 |
| 500 | 7.30E-06 |
| 600 | 7.40E-06 |
| 650 | 7.60E-06 |

| Temperature (°F) | Lead α (in/in-°F) [51] |
|---|---|
| 70 | 16.07 E-6 |
| 100 | 16.21 E-6 |
| 175 | 16.58 E-6 |
| 250 | 16.95 E-6 |
| 325 | 17.54 E-6 |
| 440 | 18.50 E-6 |
| 620 | 20.39 E-6 |

The density of lead as a function of temperature is listed below.

**Density of Lead**

| Temperature (K) | Density [24] (kg/m3) | Temperature (°F) | Density ($lbm/in^3$) |
|---|---|---|---|
| 50 | 11,570 | -370 | 0.4180 |
| 100 | 11,520 | -280 | 0.4162 |
| 150 | 11,470 | -190 | 0.4144 |
| 200 | 11,430 | -100 | 0.4129 |
| 250 | 11,380 | -10 | 0.4111 |
| 300 | 11,330 | 80 | 0.4093 |
| 400 | 11,230 | 260 | 0.4057 |
| 500 | 11,130 | 440 | 0.4021 |
| 600 | 11,010 | 620 | 0.3978 |

The volume within the "lead cavity" is calculated by determining the cask body dimensions at 620°F. As no gaps will be present between the lead and the cask body, this volume is also equal to the volume of lead at 620°F. The mass of the lead *in the* lead cavity at 620°F is then determined.

The dimensions of the "lead cavity" for operating conditions are calculated based on cask body temperature at NCT. A temperature of 360°F is considered for the cask body. This temperature is lower than the maximum cask inner shell temperature shown in Table A.3–11 for 32 kW heat load. Since the gap size increases at lower temperatures, the above chosen value is conservative. From the mass of the lead and its density at 360°F, the lead volume at NCT is determined.

The length of the gamma shield at the cask body temperature is calculated based on thermal expansion coefficients listed in the above table. The lead volume is used to determine the maximum size of the air gap adjacent to the lead.

**Determination of Lead Mass**

$\alpha_{CS}$ = 7.44 x $10^{-6}$ in/in-°F @ 620°F (via linear interpolation from expansion coefficients table, above)

$\rho_{lead}$ = 0.3978 $lbm/in^3$ @ 620°F (from lead density table, above)

$R_{in}$ = inner radius of lead cavity @ 70°F= 36.50"
$R_{out}$ = outer radius of lead cavity @ 70°F = 39.75"
$L_{cavity}$ = length of lead cavity @ 70°F = 195.75"

$R_{in,\ 620} = (R_{in})(1+(\alpha_{CS})(\Delta T)) = (36.50)[1+(7.44E\text{-}6)(550)] = 36.6494"$

$R_{out,\ 620} = (R_{out})(1+(\alpha_{CS})(\Delta T)) = (39.75)[1+(7.44E\text{-}6)(550)] = 39.9127"$

$L_{cavity,\ 620} = (L_{cavity})(1+(\alpha_{CS})(\Delta T)) = (195.75)[1+(7.44E\text{-}6)(550)] = 196.5510"$

$V_{cavity} = V_{lead} = (\pi)(R_{out,620}^2 - R_{in,620}^2)(L_{cavity,\ 620}) = 154{,}274.9\ in^3$

$M_{lead} = (V_{lead})(\rho_{lead}) = (154{,}274.9\ in^3)(0.3978\ lbm/in^3) = 61{,}363.6\ lbm$

**Determination of Lead Gap**

$\alpha_{CS}$ = 7.02 x $10^{-6}$ in/in-°F @ 360°F (via linear interpolation from expansion coefficients table, above)

$\alpha_{lead,\ 620}$ = 20.39 x $10^{-6}$ in/in-°F @ 620°F (from expansion coefficients table, above)

$\alpha_{lead,\ 360}$ = 17.83 x $10^{-6}$ in/in-°F @ 360°F (via linear interpolation from expansion coefficients table, above)

$\rho_{lead}$ = 0.4037 lbm/$in^3$ at 360°F, via linear interpolation from lead density table, above)

$R_{in,\ cs,\ 360} = (R_{in})(1+(\alpha_{CS})(\Delta T)) = (36.50)[1+(7.02E\text{-}6)(290)] = 36.5743"$

$R_{out,\ cs,\ 360} = (R_{out})(1+(\alpha_{CS})(\Delta T)) = (39.75)[1+(7.02E\text{-}6)(290)] = 39.8309"$

$L_{lead,\ 360} = (L_{cavity,\ 620})/(1+(\alpha_{lead,620})(620 - 70))*(1+(\alpha_{lead,620})(360 - 70)) =$

$(196.5510) / [1+(20.39E\text{-}6)(550)] * [1+(17.83E\text{-}6)(290)] = 195.3764"$

$V_{lead,\ 360} = M_{lead} / \rho_{lead} = 61{,}363.6 / 0.4037 = 152{,}004.6\ in^3$

Since $R_{in,cs,360} = R_{in,lead,360}$, then :

$V_{lead,360} = (\pi)(R_{out,\ lead,360}^2 - R_{in,\ ss,\ 360}^2)(L_{lead,\ 360})$

It gives:

$R_{out,lead,360} = 39.8162"$

Air gap = $R_{out,cs,360} - R_{out,\ lead,360} = 39.8309 - 39.8162 = 0.0147"$

The assumed air gap of 0.025" is larger than the above calculated gap. Therefore, using a gap of 0.025" is conservative to maximize the DSC shell temperature.

A.3.6.7.2 Gap between Finned Aluminum Shell and Cask Shield Shell

An air gap of 0.01" is considered in the model between the cask shield shell (SA-516-70) and the finned aluminum shell (Al 6061) for the MP197HB cask with over 26 kW

heat load. The following calculation shows that the modeled gap of 0.01" is adequate to bound the existing contact resistance between these two shells.

Yovanovich suggests the following approach in [38] to calculate the thermal contact conductance.

$$h_j = h_c + h_g \qquad \text{(A.1)}$$

$h_j$ = total thermal contact conductance ($m^2$-K/W)
$h_c$ = contact conductance ($m^2$-K/W)
$h_g$ = gap conductance ($m^2$-K/W)

The thermal contact resistance is:

$$R_j = 1/h_j \qquad \text{(A.2)}$$

The contact conductance, $h_c$, is given in [38] by:

$$h_c = 1.25\, k_s \frac{m}{\sigma}\left(\frac{P}{H_c}\right)^{0.95} \qquad \text{(A.3)}$$

Where

$k_s = 2k_1 k_2/(k_1 + k_2)$ Harmonic mean thermal conductivity of interface (W/m-K)

$m = \sqrt{m_1^2 + m_2^2}$ Effective mean absolute asperity slope of interface

$\sigma = \sqrt{\sigma_1^2 + \sigma_2^2}$ Effective RMS surface roughness of contacting asperities (m)

P = Contact pressure (MPa)
$H_c$ = Microhardness of the softer of the two contacting solids (MPa) = $H_{C,Al}$ in this evaluation

The mean absolute asperity slope for each plate can be approximated by the following correlation from [38]:

$$m_i = 0.125\left(\sigma_i \times 10^{-6}\right)^{0.402} \quad \text{for } 0.216\,\mu m \le \sigma \le 9.6\,\mu m \qquad \text{(A.4)}$$

As seen in equation (A.3), the contact conductance, $h_c$, depends heavily on the contact pressure, P. Assuming a very small contact pressure of $10^{-6}$ psi, gives a negligible contact conductance, $h_c$ and eliminates this term in calculation of the total thermal contact conductance in equation (A.1).

A contact pressure of $10^{-6}$ psi is equivalent to having no friction between the two shells, which is very conservative.

Due to elimination of $h_c$ in equation (A.1), the conductivities of the contacting plates are not required for this calculation.

The gap conductance, $h_g$, is given in [38] by:

$$h_g = k_g/(Y + M) \qquad \text{(A.5)}$$

Where

$k_g$ = thermal conductivity of the gap substance (W/m-K)

Y = effective gap thickness (m)
M = gas parameter (m)

Based on [38], the effective gap thickness, Y, shown in the figure below, can be calculated as follows:

$$Y = 1.53\,\sigma\,(P/H_c)^{-0.097} \qquad \text{for } 10^{-5} < P/H_c < 2\text{x}10^{-2} \qquad \text{(A.6)}$$

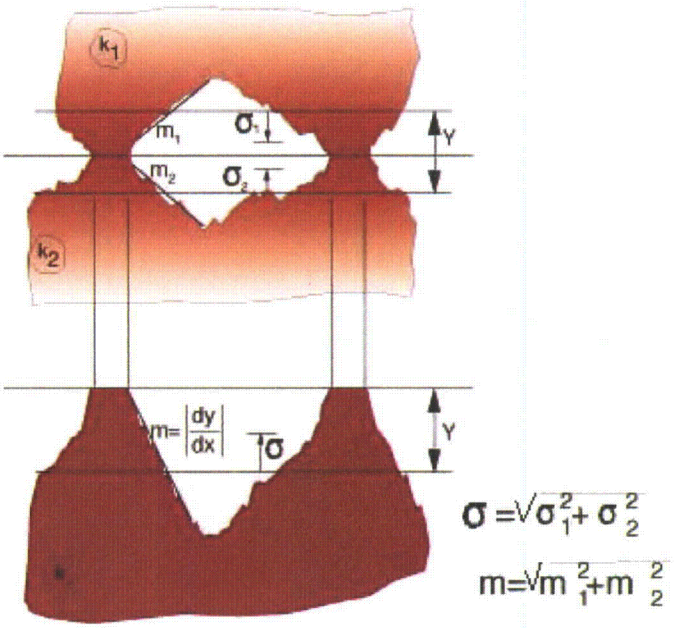


**Conforming Rough Surfaces [38]**

The gas parameter M accounts for the rarefaction effects at high temperatures and low gas pressure. This gas-surface parameter depends on the thermal accommodation coefficients, the ratio of specific heats, the Prandtl number, and the molecular mean free-path of the gas. This complex gas-surface parameter depends on gas pressure and temperature according to the following relationship:

$$M = M_0 \frac{T}{T_0} \frac{P_{g,0}}{P_g} \qquad \text{(A.7)}$$

Where $M_0$ denotes the gas parameter value at the reference values of gas temperature and pressure, $T_0$ and $P_{g,0}$, respectively. T and $P_g$ are temperature and pressure of the contact gas. The gas parameter for air is 0.373x10-6 m at 50°C and 1 atm, as reported in [38].

An operating temperature of 200°F (378K) is considered for T and $k_g$ in equations (A.5) and (A.7). The assumed operating temperature is well below the cask shield shell and the finned aluminum shell temperatures in Table A.3–11 and is therefore conservative.

A pressure of 1 atm is considered for air between the two shells.

Based on data in Section A.3.2.1, material # 16, the air conductivity is 0.0015 Btu/hr-in-°F or 0.031 W/m-K at 200°F.

The following data is considered for roughness and hardness of the shells.

**Surface Properties for Aluminum and Stainless Steel Plates**

| Material | Roughness (μm) | Hardness | Microhardness (1) (MPa) |
|---|---|---|---|
| Aluminum | 0.2 to 6.3 [39] | 25 to 95 Brinell 500kg [40] | 440 to 1079 |
| SA 203, Gr. E | 0.2 to 6.3 [39] | (2) | --- |

Notes:
(1) For conversion of roughness units see reference [42]
(2) Based on [38], the hardness of the softer plate, aluminum here, is taken for evaluation.

Surface roughness is mainly determined by the production method. The roughness values in the above table correspond to average values for cold rolling / drawing process.

The contact resistances are calculated based on the average roughness and hardness are listed below.

$\sigma_{Al}$ = 3.25 μm, $H_{c,Al}$ = 760 MPa
$\sigma_{CS}$ = 3.25 μm

The calculated contact resistance between cask shield shell and finned aluminum shell is 2.7E-3 $m^2$-K/W as listed in the following table.

**Contact Resistances between Shield Shell and Finned Aluminum Shell**

| Contact Type | Al / SA203 |
|---|---|
| σ (μm) | 4.60E-06 |
| P (MPa) | 6.891E-09 |
| $H_c$ (MPa) | 760 |
| $P_g$ (atm) | 1.0 |
| T (K) | 378 |
| $k_g$ (W/m-K) | 0.031 |
| $P/H_c$ | 9.073E-12 |
| Y (μm) | 8.283E-05 |
| M (μm) | 4.361E-07 |
| $h_c$ ($W/m^2$-K) | 0.00 |
| $h_g$ ($W/m^2$-K) | 374 |
| $h_j$ ($W/m^2$-K) | 374 |
| $R_j$ ($m^2$-K/W) | 2.7E-03 |

The equivalent thermal resistance for the air gaps across the shells considered in the MP197HB is:

$$R_{j,model} = \frac{\Delta x_{gap}}{k_g} \qquad \text{(A.8)}$$

$\Delta x_{gap}$ = 0.01" = 2.54E-4 m

$$R_{j,model} = \frac{2.54E-4}{0.031} = 8.2E-3 \text{ m}^2\text{-K/W}$$

The above thermal resistance considered in the model ($R_{j,model}$) is about three times larger than the calculated contact resistances ($R_j$) between cask shield shell and finned aluminum shell. This indicates that the air gap of 0.01" considered in the model is more than adequate to bound the contact resistance between the cask shield shell and the finned aluminum shell.

A.3.6.7.3 Gap between Basket Outer Surface and DSC Shell Inner Surface in the 69BTH DSC Model

Based on the drawings in Chapter A.1, Appendix A.1.4.10, a nominal diametrical cold gap of 0.40" is considered between the basket and the canister shell for the 69BTH DSC. The nominal canister inner diameter (ID) of the 69BTH DSC is 68.75". The nominal basket outer diameter (OD) is then 68.35".

To calculate the minimum gap, the average temperatures for the basket, aluminum rails, and DSC shell at the hottest cross section for NCT at 100°F ambient are required to calculate the thermal expansion at thermal equilibrium. These temperatures are retrieved from the 69BTH DSC/basket model described in Section A.3.3.1.4. These average temperatures are listed in the following table.

**Average Temperatures at Hottest Cross Section for 69BTH Basket**

| Component | HLZC#1, 26kW NCT at 100°F $T_{avg}$ (°F) | HLZC#4, 32kW NCT at 100°F $T_{avg}$ (°F) |
|---|---|---|
| Basket (compartments & wrap plates only) | 547 | 547 |
| Al Rail @ 0 degree | 472 | 504 |
| Al Rail @ 180 degree | 398 | 421 |
| DSC Shell | 388 | 408 |

The hot dimensions of the basket OD and DSC ID are calculated as follows.

The outer diameter of the hot basket is:

$$OD_{B,hot} = OD_B + [L_{SS,B} \times \alpha_{SS,B} (T_{avg,B} - T_{ref})] + L_{Rail} \times [\alpha_{Al,0} (T_{avg,R0} - T_{ref}) + \alpha_{Al,180} (T_{avg,R180} - T_{ref})]$$

Where:

$OD_{B,hot}$ = hot OD of the basket

$OD_B$ = nominal cold OD of the basket
= 68.75" – 0.40" = 68.35"

$L_{SS,B}$ = width of basket at 0-180 direction
= 9 × compartment width +
9 × 2 × compartment plate +
6 × Al/Poison within nine-compartment blocks +
2 × Al/Poison between nine-compartment blocks +
6 × wrap plate

$= 9 \times 6 + 9 \times 2 \times 0.165 + 6 \times 0.25 + 2 \times 0.375 + 6 \times 0.105 = 59.85"$

$L_{Al}$ = width of aluminum rail = $(OD_B - L_{SS,B})/2 = 4.25"$

$\alpha_{SS,B}$ = Average stainless steel axial coefficient of thermal expansion (interpolated using data in [10], in/in-°F)

$\alpha_{Al}$ = Average aluminum coefficient of thermal expansion (interpolated using data in [10], in/in-°F)

$T_{avg,B}$ = Average basket temperature at the hottest cross section, see table above, (°F)

$T_{avg,R0}$ = Average Al rail temperature at the hottest cross section at 0 degree orientation, see table above, (°F )

$T_{avg,R180}$ = Average Al rail temperature at the hottest cross section at 180 degree orientation, see table above, (°F)

$T_{ref}$ = reference temperature for stainless steel and aluminum alloys = 70°F [10]

The inner diameter of the hot DSC shell is:

$ID_{DSC,hot} = ID_{DSC} [1 + \alpha_{SS,DSC} (T_{avg,DSC} - T_{ref})]$

Where:

$ID_{DSC,hot}$ = Hot ID of DSC shell

$ID_{DSC}$ = Cold ID of DSC shell = 68.75"

$\alpha_{SS,DSC}$ = Average stainless steel axial coefficient of thermal expansion (interpolated using data in [10], in/in-°F)

$T_{avg,DSC}$ = Average DSC shell temperature at hottest cross section, see above table, (°F)

$T_{ref}$ = Reference temperature for low alloy steel = 70°F [10]

The diametrical hot gap between the basket and cask inner shell is:

$G_{hot} = ID_{DSC,hot} - OD_{B,hot}$

The diametrical hot gap at the hottest cross section is calculated for 26kW (HLZC#1) and 32 kW ((HLZC#4) heat loads in the 69BTH basket to bound the problem. The calculated hot gaps are listed below.

**Diametrical Hot Gaps for 69BTH Basket**

| 26kW, HLZC # 1 | | | | | |
|---|---|---|---|---|---|
| | Cold dimension | Temp | $\alpha x10^{-6}$ (1) | $\Delta L$ | Hot dimension |
| | (in) | (°F) | (in/in/°F) | (in) | (in) |
| Basket width | 59.85 | 547 | 9.747 | 0.278 | 60.128 |
| Large rail @ 0° | 4.25 | 472 | 13.844 | 0.024 | 4.274 |
| Large rail @ 180° | 4.25 | 398 | 13.592 | 0.019 | 4.269 |
| Basket OD | 68.35 | | | | 68.671 |
| DSC ID | 68.75 | 388 | 9.464 | 0.207 | 68.957 |
| Gap | 0.4 | | | | **0.286** |

| 32kW, HLZC # 4 | | | | | |
|---|---|---|---|---|---|
| | Cold dimension | Temp | $\alpha x10^{-6}$ (1) | $\Delta L$ | Hot dimension |
| | (in) | (°F) | (in/in/°F) | (in) | (in) |
| Basket width | 59.85 | 547 | 9.747 | 0.278 | 60.128 |
| Large rail @ 0° | 4.25 | 504 | 13.916 | 0.026 | 4.276 |
| Large rail @ 180° | 4.25 | 421 | 13.684 | 0.020 | 4.270 |
| Basket OD | 68.35 | | | | 68.674 |
| DSC ID | 68.75 | 408 | 9.516 | 0.221 | 68.971 |
| Gap | 0.4 | | | | **0.297** |

Note:
(1) The average thermal expansion coefficient is calculated by interpolation using data in [10].

A uniform diametrical hot gap of 0.30" is considered in the model between the basket and the DSC shell for the 69BTH DSC. This assumption is conservative since the hot gaps shown in the above table are smaller than the assumed gap of 0.3".

### A.3.6.7.4 Contact Resistance across Paired Aluminum and Poison Plates in 69BTH Basket

The 0.01" gaps considered on both sides of the paired aluminum and poison plates account for all the thermal resistance across the paired plates. Dividing the thermal resistance into three separate resistances would only change the temperature distribution between the two paired plates without changing the overall thermal resistance. The temperature distribution among the paired aluminum and poison plates are of no particular significance.

The following calculation shows that the modeled gaps (0.01") on both sides of the paired aluminum and poison plates are adequate to bound the existing contact resistances.

According to the basket configuration, three contact resistances are recognizable for the paired aluminum/poison plates sandwiched between the fuel compartments or wrap plates:

a) contact resistance between the aluminum plate and the stainless steel fuel compartment or wrap plates

b) contact resistance between the aluminum plate and the poison plate

c) contact resistance between the poison plate and the stainless steel fuel compartment or wrap plate

These contact resistances are shown schematically in the following figure.

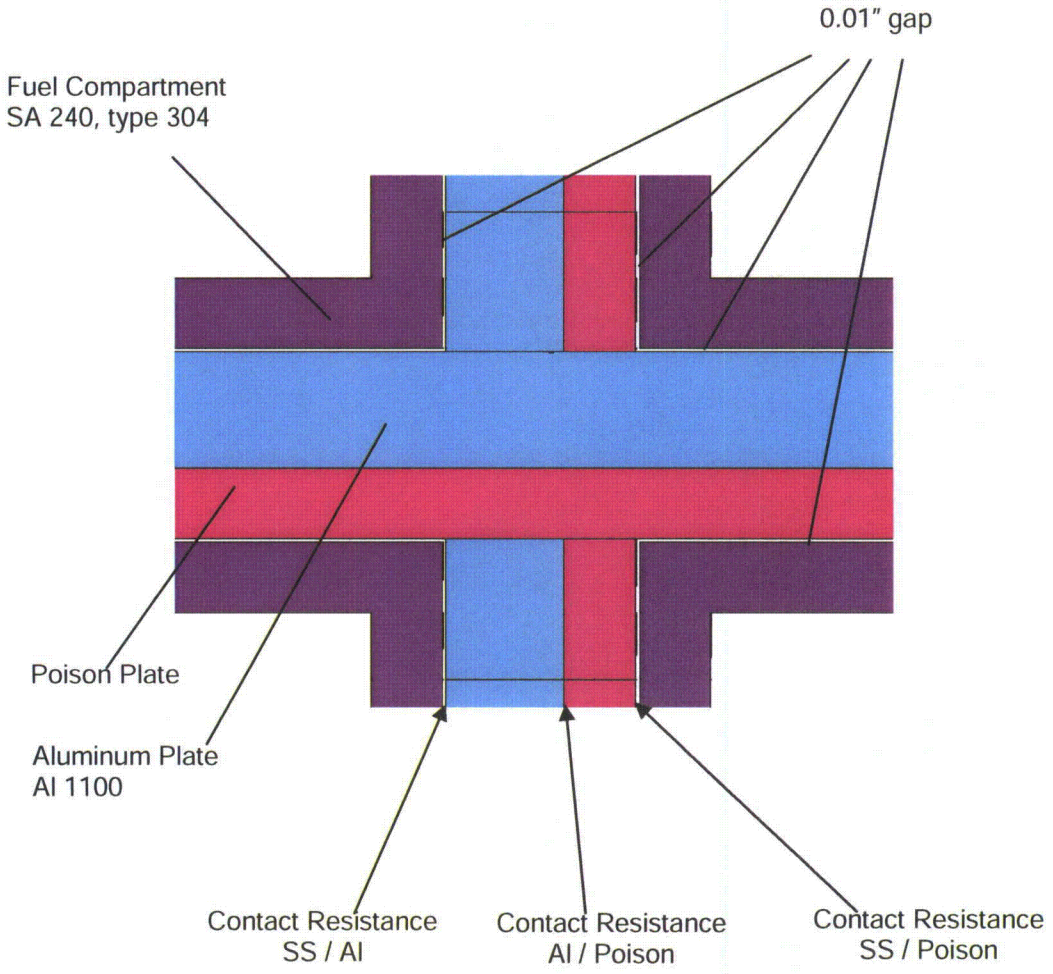


**Location of Contact Resistances**

The contact resistances between the components shown in the above figure are calculated using the same methodology as the one described in Section A.3.6.7.2.

The gas parameter for helium is $2.05 \times 10^{-6}$ m at 50°C and 1 atm, as reported in reference [38].

The thermal contact resistance is:

$$R_j = 1/h_j$$

Based on the location of the contact resistances shown in the above figure, the total thermal contact resistance for the paired plates is:

$$R_{j,plates} = R_{j,SS-Al} + R_{j,Al-Poison} + R_{j,poison-SS}$$

$R_{j,SS-Al}$ = contact resistance between stainless steel and aluminum plates
$R_{j,Al-Poison}$ = contact resistance between aluminum and poison plates
$R_{j,Poison-SSI}$ = contact resistance between poison and stainless steel plates

An operating temperature of 400°F (204°C) is considered for conductivity of helium. The assumed operating temperature is well below the average basket temperature at the hottest cross section shown in Section A.3.6.7.3 and is therefore conservative.

A moderate gas pressure (Pg) of 5 psig (1.34 abs atm), lower than the normal operating pressures listed in Table A.3–23, is considered to evaluate the contact resistances.

Based on data in Section A.3.2.1, material # 15, the helium conductivity is 9.84E-3 Btu/hr-in-°F or 0.204 W/m-K at 400°F. The following data is considered for roughness and hardness of the plates.

**Surface Properties for Aluminum and Stainless Steel Plates**

| Material | Roughness (μm) | Hardness | Microhardness [1] (MPa) |
|---|---|---|---|
| Aluminum 1100/ Poison Plate | 0.2 to 6.3 [39] | 25 to 95 Brinell 500kg [40] | 440 to 1079 |
| SA 240, type 304 | 0.2 to 6.3 [39] | 92 Rockwell B [41], Table 2 | 1960 to 2000 |

Note: [1] For conversion of roughness units see reference [42]

Surface roughness is mainly determined by the production method. The roughness values in the above table correspond to average values for cold rolling / drawing process. The hardness values are collected for aluminum alloys 6063 and 6061, which are the closest to aluminum alloy 1100.

The contact resistances calculated based on the average roughness and hardness are:

$\sigma_{Al}$ = 3.25 μm, $H_{c,Al}$ = 760 MPa
$\sigma_{poison}$ = 3.25 μm, $H_{c,poison}$ = 760 MPa
$\sigma_{SS}$ = 3.25 μm, $H_{c,SS}$ = 1980 MPa

The calculated contact resistances are listed in the following table.

**Contact Resistances between Plates in 69BTH Basket**

| Contact Type | Al / Poison | SS / Al or SS/ Poison |
|---|---|---|
| σ (m) | 4.60E-06 | 4.60E-06 |
| P (MPa) | 6.891E-09 | 6.891E-09 |
| $H_c$ (MPa) | 760 | 760 |
| $P_g$ (atm) | 1.34 | 1.34 |
| T (K) | 478 | 478 |
| $k_g$ (W/m-K) | 0.204 | 0.204 |
| $P/H_c$ | 9.073E-12 | 9.073E-12 |
| Y (m) | 8.283E-05 | 8.283E-05 |
| M (m) | 2.262E-06 | 2.262E-06 |
| $h_c$ (W/m$^2$-K) | 0.00 | 0.00 |
| $h_g$ (W/m$^2$-K) | 2402 | 2402 |
| $h_j$ (W/m$^2$-K) | 2402 | 2402 |
| $R_j$ (m$^2$-K/W) | 4.164E-04 | 4.164E-04 |

The total thermal contact resistance across the plates is:

$$R_{j,total} = 3 \times 4.164E-4 = 1.249E-3 \text{ m}^2\text{-K/W}$$

The equivalent thermal resistance for the helium gaps across the plates considered in the 69BTH basket model is:

$\Delta x_{He}$ = 2 × 0.01" = 0.02" = 5.08E-4 m (total gap thickness across plates)

$$R_{j,model} = \frac{\Delta x_{He}}{k_g}$$

$$R_{j,model} = \frac{5.08E-4}{0.204} = 2.486E-3 \text{ m}^2\text{-K/W}$$

The total thermal resistance considered in the model ($R_{j,model}$) is about two times larger than the calculated contact resistances for the paired plates ($R_{j,total}$). This shows that the gaps considered in the model are more than adequate to bound the contact resistances and the other uncertainties, such as thickness tolerances, surface finishing, etc., involved in fabrication of the basket.

If the poison plate is paired with multiple aluminum plates, the total thermal contact resistance across the plates depends on the number of aluminum plates as follows.

$$R_{j,multiple} = R_{j,SS-Al} + (m-1)R_{j,Al-Al} + R_{j,Al-Poison} + R_{j,poison-SS}$$

m = number of aluminum plates used to pair with poison plate

According to the table of the contact resistances, the contact resistances between Al/SS, Al/Al, and Al/poison plates are equal if the contact pressure nears zero. The total thermal resistance for multiple aluminum plates is therefore:

$$R_{j,multiple} = (n+1)R_{j,Al-Al}$$

n = number of multiple aluminum plates including poison plate

The maximum number of multiple aluminum plates that can be used in 69BTH basket can be calculated by setting $R_{j,multiple}$ in the above equation equal to the total thermal resistance considered in the model, $R_{j,model}$.

$$n_{max} = \frac{R_{j,model}}{R_{j,Al-Al}} - 1$$

$$n_{max} = \frac{2.486E-3}{4.164E-4} - 1 = 4.97$$

This shows that at least four plates, three aluminum plates and one poison plate can be paired together in 69BTH basket without affecting the thermal performance evaluated in this calculation.

### *A.3.6.8 Sensitivity Study for Effects of Fire Emissivity*

*A fire emissivity ($\varepsilon_f$) of 0.9 was considered in Section A.3.4.2 to calculate the fire radiation heat transfer coefficient ($h_{r,fire}$). Assuming conservatively, the fire as a black body, an emissivity of 1.0 can be considered for the fire. The effect of this assumption is enveloped for the MP197HB TC in a sensitivity analysis in this section considering the maximum heat load of 32 kW with the external fins installed on the shield shell. The only change is the increase of the fire emissivity ($\varepsilon_f$) from 0.9 to 1.0 in the input file for running the finned TC under HAC. The maximum component temperatures from the sensitivity run with $\varepsilon_f$=1.0 are shown in the following table.*

**Maximum Component Temperatures for $\varepsilon_f$ = 1.0**

| DSC type | 69BTH DSC, with 32 kW heat load, Finned MP197HB TC, $\varepsilon_f$ = 1.0 | | | |
|---|---|---|---|---|
| Component | Time (hr) | $T_{max}$ (°F) | $T_\infty$ (°F)[2] | Limit (°F) |
| DSC shell | 7.0 | 512 | [3] | --- |
| DSC shell at mid-length[1] | 7.0 | 512 | [3] | --- |
| Cask inner shell | 1.9 | 497 | 400 | --- |
| Gamma shield | 0.5 | 571 | 399 | 621 [5] |
| Outer shell | 0.5 | 720 | 382 | --- |
| Shield shell | 0.5 | 1440 | 335 | --- |
| Cask lid | 13.0 | 315 | 309 | --- |
| Cask bottom plate | 1.0 | 416 | 383 | --- |
| Cask lid seal | 10.0 | 323 | 314 | 400 [18, 19] |
| Vent & test seal at top | 13.0 | 313 | 308 | 400 [18, 19] |
| Ram plate seal | 1.9 | 380 | 377 | 400 [18, 19] |
| Test seal at bottom | 13.0 | 382 | 377 | 400 [18, 19] |
| Drain port seal at bottom | 10.0 | 388 | 381 | 400 [18, 19] |
| Helium in TC cavity | 4.0 | 389 | 380 | --- |

*Notes:*
*[1] This value is the maximum DSC shell temperature in the region where the fuel assemblies have the maximum peaking factor.*
*[2] These values are retrieved from the transient model at 27.0 hrs after the end of the fire accident. Based on the time-temperature histories for the original TC model shown in Figure A.3-40 through Figure A.3-42, the steady state temperatures are bounded by these temperatures.*
*[3] Due to the adiabatic boundary conditions considered conservatively for the steady state cool-down runs (described in Section A.3.4.2), the maximum DSC shell temperature at the end of the transient run remains bounded by the steady state temperature of 537°F reported for the 69BTH DSC with 32kW heat load in Table A.3-17.*

*Since the fire emissivity does not have any effect on the steady state temperatures after cool-down, the maximum DSC shell temperature for the 69BTH with 32 kW heat load remains bounded by 537°F as reported in Table A.3-17.*

*A comparison of the maximum TC component temperatures for $\varepsilon_f$ of 1.0 to those for $\varepsilon_f$ of 0.9 are shown in the following table.*

***Comparison of the Maximum TC Component Temperatures for $\varepsilon_f$ of 1.0 and 0.9***

| | Transient Temperature | | | Steady State Temperature | | |
|---|---|---|---|---|---|---|
| | $\varepsilon_f$ =1.0 | $\varepsilon_f$ = 0.9 | | $\varepsilon_f$ =1.0 | $\varepsilon_f$ = 0.9 | |
| Component | $T_{max}$ (°F) | $T_{max}$ (°F) | $\Delta T_{max}$ (°F) | $T_\infty$ (°F)(2) | $T_\infty$ (°F)(3) | $\Delta T_\infty$ (°F) |
| DSC shell | 512 | 509 | +3 | (4) | (4) | 0 |
| DSC shell at mid-length(1) | 512 | 509 | +3 | --- | --- | N/A |
| Cask inner shell | 497 | 487 | +10 | 400 | 403 | -3 |
| Gamma shield | 571 | 552 | +21 | 399 | 401 | -2 |
| Outer shell | 720 | 690 | +30 | 382 | 383 | -1 |
| Shield shell | 1440 | 1393 | +47 | 335 | 337 | -2 |
| Cask lid | 315 | 314 | +1 | 309 | 311 | -2 |
| Cask bottom plate | 416 | 416 | 0 | 383 | 384 | -1 |
| Cask lid seal | 323 | 321 | +2 | 314 | 316 | -2 |
| Vent & test seal at top | 313 | 311 | +2 | 308 | 310 | -2 |
| Ram plate seal | 380 | 380 | 0 | 377 | 378 | -1 |
| Test seal at bottom | 382 | 380 | +2 | 377 | 379 | -2 |
| Drain port seal at bottom | 388 | 386 | +2 | 381 | 383 | -2 |
| Helium in TC cavity | 389 | 387 | +2 | 380 | 380 | 0 |

*Notes:*
*(1) This value is the maximum DSC shell temperature in the region where the fuel assemblies have the maximum peaking factor.*
*(2) These values are retrieved from the transient model at 27.0 hrs after the end of the fire accident.*
*(3) These values are retrieved from the transient model at 20.0 hrs after the end of the fire accident.*
*(4) Due to the adiabatic boundary conditions considered conservatively for the steady state cool-down runs (described in Section A.3.4.2), the maximum DSC shell temperature at the end of the transient run remains bounded by the steady state temperature of 537°F reported for the 69BTH DSC with 32kW heat load in Table A.3-17.*

*As seen in the above table, the largest effect of increasing the fire emissivity from 0.9 to 1.0 occurs during the short period of the fire at the shield shell, which is directly exposed to the fire. The other components remain shielded from the fire effect so that the cask inner shell temperature increases by only 10°F and the DSC shell temperature increases only by 3°F during the transient run.*

*These temperature increases are relatively small and occur for a short period of time and therefore do not affect the thermal and structural performance of the MP197HB TC.*

*The containment seals are protected from direct fire exposure by the impact limiters. The effect of increasing the fire emissivity from 0.9 to 1.0 on the maximum seal temperatures is limited to 2°F for a short period of time after the fire. The transient and the steady state temperatures of the containment seals remain well below the temperature limit of 400°F [18, 19]. Therefore the containment function of the seals remains unaffected by the increase of the fire emissivity from 0.9 to 1.0.*

*The time temperature histories for the TC shield shell and DSC shell from the sensitivity study with $\varepsilon_f$ of 1.0 are compared to those from the original model with $\varepsilon_f$ of 0.9 in the following figures, respectively.*

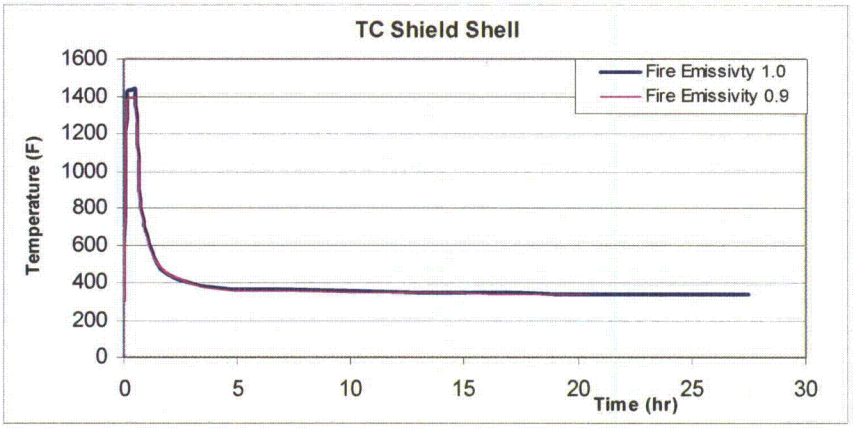


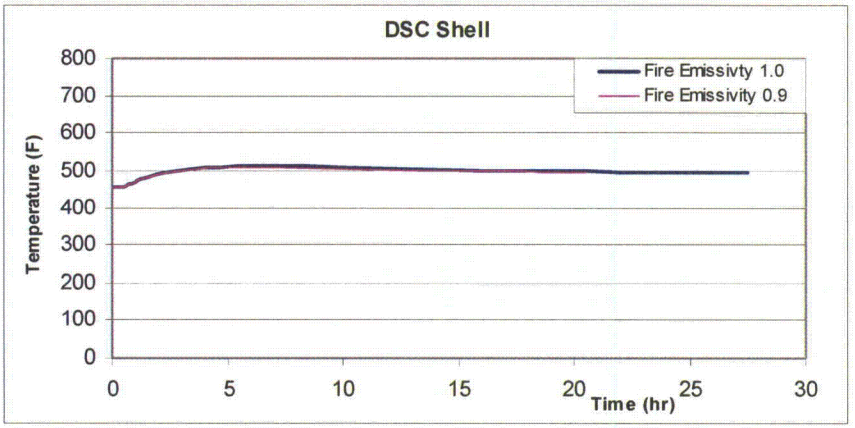


***Results of the Sensitivity Study***

*As seen in Figure A.3-40 through Figure A.3-42, all the TC component temperatures decrease through the cool-down period. The small differences seen in the comparison table between the steady state temperatures are caused by the fact that the transient temperatures at different hours (27.0 hours for sensitivity run and 20.0 hours for the original run) are used to bound the steady state temperatures. Since the TC component temperatures are decreasing, the values at 27.0 hours for the sensitivity run are lower than those for the original run. It is expected that the actual steady state temperatures in both runs achieve the same values and are independent of the fire emissivity.*

*It is evident from the first table in this section that the maximum TC component temperatures remain well below the allowable limits.*

*In conclusion, the effect of increasing the fire emissivity from 0.9 to 1.0 occurs only for a short period of time on the outermost components of the TC exposed to the fire. The function of these TC components remains unaffected by this change in the fire emmissivity.*

### *A.3.6.9 Sensitivity Study for Effects of High Burnup Damaged Fuel Assemblies*

*The cladding of high burnup damaged fuel assemblies can experience further damages during NCT. To bound the effect of these damages, a sensitivity analysis is conducted considering the worst case condition, in which the high burnup damaged fuel assemblies become rubbles. Following the rationale in NUREG/CR-6835 [50], it is assumed that the fuel rods do not shatter into very small pieces and the fuel rubble is not in a tightly compacted mass. Instead, the fuel rubble is assumed to be 50% void by volume. Since the end drop is the most critical condition under NCT and the end caps and the fuel compartment walls constrain the damaged fuel assembly, the fuel rubble is assumed to be contained within the original active fuel volume, albeit in the lower portion of the original volume. Consistent with NUREG/CR-6835, the axial-burnup variation in the rubble is also assumed to be uniform.*

*The height of the fuel rubbles with the assumption of 50% void by volume is determined based on the volume of the fuel rods. The bounding fuel rubble height is 108" for the fuel assemblies.*

*The 69BTH DSC with the bounding heat load of 32 kW is considered for this sensitivity analysis. In the sensitivity run, the heat generation rate corresponding to the damaged fuel assemblies is applied uniformly over the fuel rubble height of 108" concentrated at the rear bottom of the 69BTH DSC with a peaking factor of one.*

*Conductivity of helium is considered for the fuel rubble for conservatism.*

*The DSC shell temperature retrieved from the cask model described in Section A.3.3.1.1 is applied as boundary conditions for the 69BTH DSC model, which is consistent with the approach described in Section A.3.3.1.4.*

*The maximum component temperatures resulting from the sensitivity analysis are compared to the corresponding values for 69BTH with intact fuel assemblies in the following table.*

***Comparison of the Maximum Fuel Temperatures for 69BTH DSC with Intact and Damaged Fuel Assemblies under NCT***

| DSC Type | $T_{max, Fuel}$* (°F) | $T_{max, Comp}$ (°F) | $T_{max, Al/Poison}$ (°F) | $T_{max, Rail}$ (°F) |
|---|---|---|---|---|
| 69BTH, 32 kW w/ intact FAs (see Table A.3-10) | 674.3 | 638.3 | 621.8 | 534.3 |
| 69BTH, 32 kW w/ intact and damaged FAs | 679.6 | 644.3 | 628.0 | 537.1 |
| Difference | + 5.3 | + 6.0 | + 6.2 | + 2.8 |

* Fuel cladding temperature limit is 752° F

*As seen in the above table, the maximum fuel cladding temperature changes approximately by 5°F. Considering the large margin of 78°F for the fuel cladding temperature, this small change does not have any significant effect on the thermal performance of the cask and DSC.*

### *A.3.6.10 Sensitivity Analysis for HAC using Coupled Model*

*The analysis for HAC described in Section A.3.4 is based on a combination of transient calculations of the MP197HB TC (including a homogenized basket) and steady state calculations of the DSC including basket components described in Section A.3.3.1 as separate thermal analyses. These models are used to calculate the component maximum temperatures (including cladding temperatures). To justify the approach considered in the HAC analysis, a coupled transient model is prepared to include the TC, DSC, and basket in one single model assigned here as coupled model.*

*The coupled model is created by introducing the elements and nodes from the 69BTH basket model described in Section A.3.3.1.4 into the TC model with crushed impact limiters described in Section A.3.4. The 69BTH basket and the MP197HB TC thermal models have dissimilar meshes since the mesh density of the 69BTH basket model is much finer than the mesh density of the TC model. The mesh density of the DSC shell is refined to provide adequate interfaces between the TC and the basket meshes. These two dissimilarly meshed models of the TC and 69BTH basket are tied together using the DSC shell nodes and constraint equations via the "CEINTF" command in ANSYS.*

*To ensure the correct application of the constraint equations, the same fine meshed DSC shell used in the coupled model described above was introduced into the coarser meshed model of TC described in Section A.3.3.1.1 and the constrained equations were applied at the intersection of the fine/coarse meshes. The results of this model were compared to the result of the TC model for NCT. The comparison showed that the maximum temperatures of the TC components remain virtually unchanged (the changes are within ±0.1°F) and the maximum DSC shell temperature changes by approximately by 1°F.*

*The coupled model of the TC, DSC, and basket includes the MP197HB TC and the bounding DSC (69BTH with 32 kW heat load) and considers the homogenized fuel assemblies within compartments. All the basket components (including back-filled gas and aluminum transition rails) are explicitly modeled in the coupled model considering the same assumption described in Section A.3.3.1.4 for 69BTH basket. The geometry of the coupled model is shown in Figure A.3-53.*

*Decay heat load is applied as heat generation boundary conditions over the elements representing homogenized fuel assemblies. The base heat generation rate is multiplied by peaking factors along the axial fuel length to represent the axial decay heat profile consistent with the approach described in Section A.3.3.1.4. The peaking factors remain identical to those shown in Table A.3-2.*

*The ambient boundary conditions for the coupled model are identical to those described in Section A.3.4 for the TC model under HAC.*

*The time temperature histories resulting from the coupled model are shown in Figure A.3-54 and Figure A.3-55. The maximum component temperatures from the coupled HAC thermal analysis are compared with the corresponding temperatures from the decoupled HAC analysis described in Sections A.3.4 in the following table.*

***Comparison of Maximum Temperatures of MP197HB TC for HAC with Coupled/Decoupled Models***

| | | | | |
|---|---|---|---|---|
| DSC type | 69BTH | | | |
| Heat Load | 32 kW | | | |
| Inner sleeve | No | | | |
| External fins | Yes (Melted) | | | |
| Component | $T_{max, coupled}$ (°F) | $T_{max, decoupled}$ [1] (°F) | ΔT (°F) | Limit (°F) |
| Fuel Cladding | 680 | 693 | -13 | 1058 [7] |
| Fuel Compartment | 650 | 658 | -8 | |
| Aluminum / Poison Plates | 649 | 657 | -8 | |
| Basket Rails | 548 | 557 | -9 | |
| DSC shell | 521 | 537 | -16 | |
| Cask inner shell | 499 | 497 | 2 | --- |
| Gamma shield | 567 | 571 | -4 | 621 [5] |
| Outer shell | 716 | 720 | -4 | --- |
| Shield shell | 1440 | 1440 | 0 | --- |
| Cask lid | 306 | 315 | -9 | --- |
| Cask bottom plate | 419 | 416 | 3 | --- |
| Cask lid seal | 314 | 323 | -9 | 400 [18], [19] |
| Vent & test seal @ top | 304 | 313 | -9 | |
| Ram plate seal | 387 | 380 | 7 | |
| Test seal @ bottom | 388 | 382 | 6 | |
| Drain port seal @ bottom | 392 | 388 | 4 | |
| Helium in TC Cavity | 387 | 389 | -2 | --- |

[1] For the maximum temperatures of the decoupled HAC analysis fire emissivity of 1.0, see Table A.3-17 and Table A.3-18 for 69BTH DSC (32 kW heat load) and Section A.3.6.8 for MP197HB TC.

*As seen in the above table, all the maximum temperatures remain below the allowable limits in the coupled model.*

*The fuel cladding temperature resulting from the coupled model is 680°F and is lower by 13°F compared to the results from the decoupled models and is well below the accident temperature limit of 1058°F.*

*The maximum seal temperature for fluorocarbon seals is 392°F at drain port resulting from the coupled model. Although the maximum seal temperature increases by 4°F compared to the results from the decoupled models, the maximum seal temperature remains below the long-term limit of 400°F specified for continued seal function. Parker O-ring [18] gives a short term temperature limit of 482°F for fluorocarbon seals. The short term temperature limit was verified in [49] for this seal compound. The maximum seal temperatures resulting from the coupled or decoupled models remain well below the short term limit.*

*The maximum temperature of gamma shield (lead) is 567°F in the coupled model, which is 4°F lower than the corresponding value from the decoupled model and remains well below the lead melting point of 621°F.*

*Based on the above discussion, the differences between the maximum temperatures of critical components resulting from the coupled and decoupled models are limited to a*

*few degrees. This comparison shows that although the decoupled models do not include the axial profile of the decay heat load directly, the approach followed in the decoupled models captures the transient behavior of the TC and DSC during the fire and cool-down stages with adequate accuracy.*

Table A.3–1
DSC Shell Nominal Dimensions

| Parameter [1] | 69BTH | 61BT / 61BTH Type 1 | 61BTH Type 2 | 37PTH[2] | 32PTH / 32PTH1[3] | 32PT[4] | 24PTH[5] | 24PT4 |
|---|---|---|---|---|---|---|---|---|
| Outer Top Cover | 2.00 | 1.25 | 1.50 | 2.00 | 2.00 | 1.50 | 1.50 | 1.25 |
| Inner Top Cover | 2.00 | 0.75 | 1.25 | 2.00 | 2.00 | 1.25 | 1.25 | 6.75 [6] |
| Top Shield Plug | 5.75 | 7.00 | 6.25 | 5.75 | 8.00 | 7.50 | 6.25 | |
| Total Top End | 9.75 | 9.00 | 9.00 | 9.75 | 12.00 | 10.25 | 9.00 | 8.00 |
| Inner Bottom Cover | 2.25 [8] | 0.75 | 1.75 | 2.25 [8] | 2.25 | 1.75 | 1.75 | 2.00 |
| Bottom Shield Plug | 3.00 [8] | 5.00 | 4.00 | 3.00 [8] | 4.50 | 5.25 | 4.00 | 4.75 [6] |
| Outer Bottom Cover | 2.00 | 1.75 | 1.75 | 2.00 | 2.00 | 1.75 | 1.75 | |
| Total Bottom End | 7.25 | 7.50 | 7.50 | 7.25 | 8.75 | 8.75 | 7.50 | 6.75 |
| Cavity Length | 178.41 | 179.50 | 179.50 | 164.38 | 164.38 | 167.10 | 169.60 | 180.20 |
| DSC Length (w/o grapple) [7] | 195.41 | 196.00 | 196.00 | 181.38 | 185.13 | 186.10 | 186.10 | 194.95 |
| Basket height | 164 | 164 | 164 | 162 | 162.00 | 166.10 | 168.60 | 179.13 |

Note:
[1] 61BTHF and 24PTHF *DSCs* have the same dimensions as DSC types 61BTH and 24PTH, respectively.
[2] The shortest cavity length for 37PTH baskets belongs to 37PTH-S.
[3] The shortest cavity length for 32PTH, 32PTH, type 1 and 32PTH1 Type 1 & 2 baskets belongs to 32PTH1-S.
[4] The shortest cavity length for 32PT baskets belongs to 32PT-S125.
[5] The shortest cavity length for 24PTH baskets belongs to 24PTH-S.
[6] Shield plugs of the 24PT4 DSC are lead encapsulated in plates of stainless steel 316, see [2].
[7] The canister length in the model is the sum of total top end, total bottom end, and cavity length.
[8] The thicknesses of inner bottom cover plate and bottom shield plug for 69BTH and 37PTH DSCs are designed as 1.75" and 3.5", respectively. Since the bottom shield plug (carbon steel) has a higher conductivity than the inner bottom cover plate (stainless steel), considering a smaller thickness of 3" for bottom shield plug and higher thickness of 2.25" for inner bottom cover plate is conservative which increases the thermal resistance across these two plates.

Table A.3–2
Peaking Factors for Fuel Assemblies in the 69BTH DSC Model

| Region # | Fuel Model Z-Coord (in) from | to | Average Height from Bottom (in) | Peaking Factor | Area under Curve |
|---|---|---|---|---|---|
| 1 | 7.375 | 11.80 | 2.213 | 0.166 | 0.733 |
| 2 | 11.80 | 19.60 | 8.325 | 0.641 | 5.001 |
| 3 | 19.60 | 27.40 | 16.125 | 0.984 | 7.678 |
| 4 | 27.40 | 35.20 | 23.925 | 1.115 | 8.700 |
| 5 | 35.20 | 43.00 | 31.725 | 1.168 | 9.114 |
| 6 | 43.00 | 50.80 | 39.525 | 1.188 | 9.266 |
| 7 | 50.80 | 58.60 | 47.325 | 1.196 | 9.326 |
| 8 | 58.60 | 66.40 | 55.125 | 1.200 | 9.360 |
| 9 | 66.40 | 74.20 | 62.925 | 1.200 | 9.360 |
| 10 | 74.20 | 82.00 | 70.725 | 1.199 | 9.356 |
| 11 | 82.00 | 89.80 | 78.525 | 1.197 | 9.339 |
| 12 | 89.80 | 97.60 | 86.325 | 1.178 | 9.186 |
| 13 | 97.60 | 105.40 | 94.125 | 1.151 | 8.981 |
| 14 | 105.40 | 113.20 | 101.925 | 1.116 | 8.704 |
| 15 | 113.20 | 121.00 | 109.725 | 1.070 | 8.348 |
| 16 | 121.00 | 128.80 | 117.525 | 0.994 | 7.752 |
| 17 | 128.80 | 136.60 | 125.325 | 0.840 | 6.548 |
| 18 | 136.60 | 144.40 | 133.125 | 0.596 | 4.646 |
| 19 | 144.40 | 151.375 | 140.513 | 0.230 | 1.604 |
| | | | | Sum | 143.003 |
| | | | | Normalized | 0.99308 |
| | | | | Corr. Factor | 1.00697 |

Table A.3–3
Effective Density for the 69BTH Basket

| **Basket** | | |
|---|---|---|
| Components | Material | Total Weight (lbm) |
| Fuel Assembly | | 48,645 |
| Fuel Compartment | SS304 | 13,174 |
| Poison Plate + Alum | Aluminum | 2,169 |
| Sub-Assy. Wrap | SS304 | 3,484 |
| Aluminum Plates | Aluminum | 1,434 |
| Rail 90 | Aluminum | 6,204 |
| Rail 45 | Aluminum | 3,508 |
| Total | | 78,618 |
| | | |
| $D_{basket}$ | 68.75 | in |
| $L_{basket}$ | 164.0 | in |
| $V_{basket}$ | 608,806 | $in^3$ |
| $\rho_{eff\ basket}$ | 0.129 | $lbm/in^3$ |

| **Top Grid Assembly** | | |
|---|---|---|
| Components | Material | Total Weight (lbm) |
| Plates | SA182 | 2,123 |
| | | |
| $D_{topgrid}$ | 68.75 | in |
| $L_{topgrid}$ | 14.4 | in |
| $V_{topgrid}$ | 53,493 | $in^3$ |
| $\rho_{eff\ topgrid}$ | 0.040 | $lbm/in^3$ |

Table A.3–4
Effective Specific Heat for the 69BTH Basket

| **69BTH Basket** | | | | | | | | | |
|---|---|---|---|---|---|---|---|---|---|
| Components | Fuel Assembly | Fuel compartments | Poison Plates | Sub-Assy. Wrap | Aluminum Plates | Rail 90 | Rail 45 | Total | |
| Material | --- | Stainless Steel | Al | St. Steel | Al | Al | Al | --- | |
| Weight (lbm) | 48,645 | 13,174 | 2,169 | 3,484 | 1,434 | 6,204 | 3,508 | 78,618 | |
| Temperature | m.Cp | m.Cp | m.Cp | m.Cp | m.Cp | m.Cp | m.Cp | Σ m.Cp | $Cp_{eff}$ |
| (°F) | (Btu/°F) | (Btu/°F) | (Btu/°F) | (Btu/°F) | (Btu/°F) | (Btu/°F) | (Btu/°F) | (Btu/°F) | (Btu/lbm-°F) |
| 70 | 2,797 | 1,529 | 462 | 404 | 305 | 1,322 | 747 | 7,566 | 0.096 |
| 100 | 2,797 | 1,536 | 466 | 406 | 308 | 1,334 | 754 | 7,603 | 0.097 |
| 200 | 2,797 | 1,600 | 479 | 423 | 317 | 1,371 | 775 | 7,763 | 0.099 |
| 300 | 2,797 | 1,644 | 490 | 435 | 324 | 1,402 | 793 | 7,885 | 0.100 |
| 400 | 2,797 | 1,692 | 499 | 447 | 330 | 1,427 | 807 | 7,999 | 0.102 |
| 500 | 2,797 | 1,731 | 499 | 458 | 330 | 1,427 | 807 | 8,049 | 0.102 |
| 600 | 2,797 | 1,743 | 499 | 461 | 330 | 1,427 | 807 | 8,064 | 0.103 |
| 700 | 2,797 | 1,770 | 499 | 468 | 330 | 1,427 | 807 | 8,097 | 0.103 |
| 800 | 2,797 | 1,794 | 499 | 475 | 330 | 1,427 | 807 | 8,129 | 0.103 |
| 900 | 2,797 | 1,804 | 499 | 477 | 330 | 1,427 | 807 | 8,140 | 0.104 |
| 1000 | 2,797 | 1,813 | 499 | 479 | 330 | 1,427 | 807 | 8,152 | 0.104 |
| 1100 | 2,797 | 1,844 | 499 | 488 | 330 | 1,427 | 807 | 8,192 | 0.104 |

| **Top Grid Assembly (SA 240, Type 304)** | | | |
|---|---|---|---|
| Temp | $Cp_{eff}$ | Temp | $Cp_{eff}$ |
| (°F) | (Btu/lbm-°F) | (°F) | (Btu/lbm-°F) |
| 70 | 0.116 | 600 | 0.132 |
| 100 | 0.117 | 700 | 0.134 |
| 200 | 0.121 | 800 | 0.136 |
| 300 | 0.125 | 900 | 0.137 |
| 400 | 0.128 | 1000 | 0.138 |
| 500 | 0.131 | 1100 | 0.140 |

Table A.3–5
Effective Axial Conductivity for the 69BTH Basket

| **Basket** | | | | |
|---|---|---|---|---|
| T2 ($T_{top}$) | T1 ($T_{bottom}$) | $Q_{axl}$ | $T_{avg}$ | $k_{basket, axl}$ |
| (°F) | (°F) | (Btu/hr) | (°F) | (Btu/hr-in-°F) |
| 50 | 0 | 6319.4 | 25 | 1.682 |
| 150 | 100 | 6389.7 | 125 | 1.701 |
| 250 | 200 | 6479.2 | 225 | 1.724 |
| 350 | 300 | 6559.4 | 325 | 1.746 |
| 450 | 400 | 6613.1 | 425 | 1.760 |
| 550 | 500 | 6615.9 | 525 | 1.761 |
| 650 | 600 | 6615.7 | 625 | 1.761 |
| 750 | 700 | 6630.8 | 725 | 1.765 |
| 850 | 800 | 6649.5 | 825 | 1.770 |
| 950 | 900 | 6665.5 | 925 | 1.774 |
| 1050 | 1000 | 6681.8 | 1025 | 1.778 |
| 1150 | 1100 | 6698.7 | 1125 | 1.783 |

| **Top Grid Assembly** | | | |
|---|---|---|---|
| D_topgrid | 68.5 | in | |
| L_topgrid | 14.4 | in | |
| Plate Thickness | 0.25 | in | |
| | Length (in) | No. of Plates | Area ($in^2$) |
| L1 | 44.17 | 16 | 176.7 |
| L2 | 18.71 | 4 | 18.7 |
| L3 | 6.25 | 16 | 25.0 |
| Total | | | 220.4 |
| A_model | 3712 | $in^2$ | |
| A_plates | 220.4 | $in^2$ | |
| Temp | $k_{SS304}$ | $k_{topgrid, axl}$ | |
| (°F) | (Btu/hr-in-°F) | (Btu/hr-in-°F) | |
| 70 | 0.717 | 0.043 | |
| 100 | 0.725 | 0.043 | |
| 200 | 0.775 | 0.046 | |
| 300 | 0.817 | 0.048 | |
| 400 | 0.867 | 0.051 | |
| 500 | 0.908 | 0.054 | |
| 600 | 0.942 | 0.056 | |
| 700 | 0.983 | 0.058 | |
| 800 | 1.025 | 0.061 | |
| 900 | 1.058 | 0.063 | |
| 1000 | 1.092 | 0.065 | |
| 1100 | 1.133 | 0.067 | |

Table A.3–6
Effective Radial Conductivity for the 69BTH Basket

| **69BTH Basket** | | | | |
|---|---|---|---|---|
| $T_{max}$ (°F) | $T_o$ (°F) | $Q_{rad}$ (Btu/hr) | $T_{avg}$ (°F) | $k_{basket\_rad}$ (Btu/hr-in-°F) |
| 336 | 0 | 9678 | 168 | 0.167 |
| 429 | 100 | 9678 | 264 | 0.171 |
| 519 | 200 | 9678 | 360 | 0.176 |
| 603 | 300 | 9678 | 451 | 0.186 |
| 688 | 400 | 9678 | 544 | 0.195 |
| 776 | 500 | 9678 | 638 | 0.204 |
| 866 | 600 | 9678 | 733 | 0.211 |
| 959 | 700 | 9678 | 830 | 0.217 |
| 1054 | 800 | 9678 | 927 | 0.222 |
| 1148 | 900 | 9678 | 1024 | 0.227 |
| 1243 | 1000 | 9678 | 1122 | 0.231 |
| 1339 | 1100 | 9678 | 1219 | 0.236 |

Table A.3–7
Peaking Factors for Fuel Assemblies in the 37PTH DSC Model

| Region # | Fuel Model Z-Coord (in) from | to | Average Height from Bottom (in) | Peaking Factor | Area under Curve |
|---|---|---|---|---|---|
| 1 | 11.350 | 20.350 | 4.500 | 0.672 | 6.044 |
| 2 | 20.350 | 29.350 | 13.500 | 0.987 | 8.884 |
| 3 | 29.350 | 38.350 | 22.500 | 1.083 | 9.748 |
| 4 | 38.350 | 47.350 | 31.500 | 1.105 | 9.947 |
| 5 | 47.350 | 47.475 | 36.063 | 1.108 | 0.138 |
| 6 | 47.475 | 56.558 | 40.667 | 1.108 | 10.061 |
| 7 | 56.558 | 65.642 | 49.750 | 1.103 | 10.021 |
| 8 | 65.642 | 74.725 | 58.834 | 1.098 | 9.971 |
| 9 | 74.725 | 83.808 | 67.917 | 1.094 | 9.937 |
| 10 | 83.808 | 92.892 | 77.000 | 1.094 | 9.939 |
| 11 | 92.892 | 101.970 | 86.081 | 1.095 | 9.943 |
| 12 | 101.970 | 111.060 | 95.165 | 1.096 | 9.959 |
| 13 | 111.060 | 120.140 | 104.250 | 1.090 | 9.899 |
| 14 | 120.140 | 129.220 | 113.330 | 1.068 | 9.698 |
| 15 | 129.220 | 129.350 | 117.935 | 1.038 | 0.135 |
| 16 | 129.350 | 138.020 | 122.335 | 0.989 | 8.577 |
| 17 | 138.020 | 146.680 | 131.000 | 0.767 | 6.644 |
| 18 | 146.680 | 155.350 | 139.665 | 0.473 | 4.105 |
| | | | | Sum | 143.650 |
| | | | | Normalized | 0.998 |
| | | | | Corr. Factor | 1.002 |

Table A.3–8
Maximum TC Component and DSC Shell Temperatures for NCT
(100°F and Insolation), BWR DSCs

| DSC type | | 69BTH | | | 61BTH/61BTHF Type 1 | 61BTH/61BTHF Type 2 | 61BT | |
|---|---|---|---|---|---|---|---|---|
| Heat Load | 32 kW | 32 kW | 29.2 kW | 26 kW | 22 kW | 24 kW | 18.3 kW | |
| Internal sleeve | No | No | No | No | Yes | Yes | Yes | |
| External fins | No | Yes | Yes | No | No | No | No | |
| Component | $T_{max}$ (°F) | $T_{max}$ (°F) | $T_{max}$ (°F) | $T_{max}$ (°F) | $T_{max}$ (°F) | $T_{max}$ (°F) | $T_{max}$ (°F) | Limit (°F) |
| DSC shell ($T_{Max}/T_{Min}$) | 510 | 484/266 | 458/255 | 451/266 | 414/250 | 435/260 | 372/229 | --- |
| DSC shell @ mid-length[1] | 496 | 470 | 445 | 440 | 406 | 427 | 365 | --- |
| Internal sleeve | N/A | N/A | N/A | N/A | 317 | 333 | 286 | --- |
| Cask inner shell | 398 | 367 | 347 | 351 | 315 | 331 | 284 | --- |
| Gamma shield | 397 | 366 | 345 | 349 | 314 | 330 | 283 | 621 [5] |
| Outer shell | 382 | 352 | 332 | 337 | 306 | 321 | 276 | --- |
| Shield shell | 335 | 305 | 289 | 299 | 272 | 285 | 248 | --- |
| Finned Shell | N/A | 229 | 220 | N/A | N/A | N/A | N/A | --- |
| Cask lid | 295 | 267 | 254 | 265 | 248 | 259 | 228 | --- |
| Cask bottom plate | 383 | 353 | 334 | 338 | 307 | 322 | 277 | --- |
| Neutron Shield Resin[2] | 276 | 290 | 276 | 288 | 264 | 276 | 241 | 320 [17] |
| Trunnion Plug Resin[2] | 303 | 277 | 263 | 272 | 249 | 260 | 229 | 445 [25] |
| Cask lid seal | 296 | 268 | 256 | 266 | 249 | 260 | 229 | 400 [18, 19] |
| Ram plate seal | 382 | 352 | 332 | 337 | 306 | 321 | 277 | 400 [18, 19] |
| Drain port seal @ bottom | 381 | 351 | 332 | 337 | 306 | 321 | 276 | 400 [18, 19] |
| Test seal @ bottom | 379 | 349 | 330 | 335 | 305 | 320 | 276 | 400 [18, 19] |
| Vent & test seal @ top | 295 | 267 | 254 | 265 | 248 | 259 | 228 | 400 [18, 19] |
| Wood in Impact limiter | 208 | 302 | 287 | 291 | 265 | 278 | 242 | 320 |

Notes
(1) This value is the maximum DSC shell temperature in the region where the fuel assemblies have the maximum peaking factor.
(2) This temperature is the volumetric, average temperature of the elements located at hottest cross section of the neutron shield resin/the trunnion plug resin.

Table A.3–9
Maximum TC Component and DSC Shell Temperatures for NCT
(100°F and Insolation), PWR DSCs

| DSC type | 37PTH | 32PTH / 32PTH Type1 / 32PTH1 Type 1 | 32PTH1 Type 2 | 32PT | 24PTH or 24PTHF (all types) | 24PT4 | |
|---|---|---|---|---|---|---|---|
| Heat Load | 22.0 kW | 26 kW | 24 kW | 24 kW | 26 kW | 24 kW | |
| Internal sleeve | No | No | No | Yes | Yes | Yes | |
| External fins | No | No | No | No | No | No | |
| Component | $T_{max}$ (°F) | $T_{max}$ (°F) | $T_{max}$ (°F) | $T_{max}$ (°F) | $T_{max}$ (°F) | $T_{max}$ (°F) | Limit (°F) |
| DSC shell ($T_{Max}/T_{Min}$) | 408/261 | 444/289 | 423/278 | 443/283 | 464/299 | 428/313 | --- |
| DSC shell @ mid-length[1] | 395 | 434 | 414 | 430 | 447 | 421 | |
| Internal sleeve | N/A | N/A | N/A | 329 | 347 | 319 | --- |
| Cask inner shell | 314 | 337 | 322 | 326 | 344 | 317 | --- |
| Gamma shield | 313 | 336 | 321 | 325 | 343 | 316 | 621 [5] |
| Outer shell | 301 | 320 | 306 | 316 | 335 | 308 | --- |
| Shield shell | 271 | 290 | 278 | 281 | 295 | 274 | --- |
| Cask lid | 301 | 319 | 305 | 318 | 336 | 306 | --- |
| Cask bottom plate | 246 | 276 | 265 | 268 | 282 | 309 | --- |
| Neutron Shield Resin[2] | 263 | 280 | 268 | 273 | 285 | 265 | 320 [17] |
| Trunnion Plug Resin[2] | 249 | 264 | 254 | 257 | 268 | 250 | 445 [25] |
| Cask lid seal | 301 | 319 | 305 | 317 | 336 | 307 | 400 [18, 19] |
| Ram plate seal | 244 | 274 | 263 | 267 | 280 | 308 | 400 [18, 19] |
| Drain port seal @ bottom | 245 | 275 | 264 | 267 | 281 | 308 | 400 [18, 19] |
| Test seal @ bottom | 243 | 272 | 262 | 265 | 279 | 307 | 400 [18, 19] |
| Vent & test seal @ top | 300 | 318 | 305 | 317 | 336 | 306 | 400 [18, 19] |
| Wood in Impact limiter | 262 | 278 | 266 | 274 | 289 | 267 | 320 [20] |

Notes
[1] This value is the maximum DSC shell temperature in the region where the fuel assemblies have the maximum peaking factor.
[2] This temperature is the volumetric, average temperature of the elements located at hottest cross section of the neutron shield resin / the trunnion plug resin.

Table A.3–10
Maximum Fuel Cladding and Basket Component Temperatures for NCT

| DSC Type | $T_{max,\ Fuel}$ (°F) | Reference for bounding fuel cladding temperature | $T_{max,\ Comp}$ (°F) | $T_{max,\ Al/Poison}$ (°F) | $T_{max,\ Rail}$ (°F) | Reference for bounding basket component temperatures |
|---|---|---|---|---|---|---|
| 69BTH, 32 kW[3] | 674 | – | 638 | 622 | 534 | – |
| | 650 | – | 612 | 612 | 507 | – |
| 69BTH, 29.2 kW | 651 | – | 622 | 621 | 481 | – |
| 69BTH, 26 kW | 658 | – | 643 | 643 | 475 | – |
| 61BTH Type 1 | < 706 | [3], Table T.4-12 | < 683 | < 682 | < 565 | [3], Table T.4-13 |
| 61BTH Type 2 | < *721* | [3], Table T.4-12[4] | < *692* | < *692* | < 549 | [3], Table T.4-14[4] |
| 61BT | < 638 | [1], Table K.4-2 | < 615 | < 615 | < 493 | [1], Table K.4-2 |
| 37PTH | 660 | – | 649 | 648 | 443 | – |
| 32PTH, 32PTH Type 1 | < 723 | [4], Table 4-1 | < 697 | < 696 | < 561 | [4], Table 4-1 |
| 32PTH1 Type 1 | < 713 | [3], Table U.4-15 | < 677 | < 676 | < 520 | [3], Table U.4-16 |
| 32PTH1 Type 2 | < 728 | [3], Table U.4-15 | < 648 | < 648 | < 529 | [3], Table U.4-17 |
| 32PT | < 720 | [1], Table M.4-2 | < 705 | < 705 | < 471 | [1], Table M.4-3 |
| 24PTH-S or –L w/ Al Inserts | < 733 | [1], Table P.4-14 | < 680 | < 679 | < 576 (1) | [1], Table P.4-16 |
| 24PTH-S or –L w/o Al Inserts | < 733 | [1], Table P.4-14 | < 682 | < 681 | < 576 (1) | [1], Table P.4-16 |
| 24PTH-S-LC | < 714 | [1], Table P.4-14 | < 674 | < 673 | < 500 (1) | [1], Table P.4-17 |
| 24PT4 | < 707 | [2], Table A4.4-7 | < 670 | < 670 | (2) | [2], Table A4.4-6 |

Notes:
(1) This value is the maximum rail temperature for rail R90 taken from evaluations of 24PTH DSC under normal transfer conditions.
(2) Based on [2], Table A.4.4-6, the maximum spacer disc and support rod temperatures for 24PT4 DSC under normal transfer conditions are 663°F and 574°F. These temperatures are the bounding values for NCT.
(3) The maximum temperatures for TC without external fins are presented in the first row and the maximum temperatures for TC with external fins are presented in the second row.
(4) *The maximum temperatures for 61BTH Type 2 DSC are increased from values in [3] due to allowance of six shims between the basket and the rails per note 5 of Drawing NUH61BTH-71-1102 in Appendix A.1.4.10.9.*

Table A.3–11
Maximum/Minimum Component Temperatures for NCT

| Conditions | 100°F with Insolation [1] | | | | -40°F No Insolation [2] | |
|---|---|---|---|---|---|---|
| Heat load | 26 < Q ≤ 32 kW | | Q ≤ 26 kW | | 0 | |
| Inner sleeve | No | No | No | Yes | N/A | |
| External fins | No | Yes | No | No | N/A | |
| Component | $T_{max}$ (°F) | $T_{max}$ (°F) | $T_{max}$ (°F) | $T_{max}$ (°F) | $T_{min}$ (°F) | Allowable Range (°F) |
| Fuel Cladding | 674 | 651 | < 728 | < 733 | -40 | 752 max. [7] |
| Fuel Compartment | 638 | 622 | < 697 | < 692 | -40 | [4] |
| Al/Poison Plates | 622 | 621 | < 696 | < 692 | -40 | [4] |
| Basket Rails | 534 | 507 | < 561 | < 576 | -40 | [4] |
| DSC shell | 510 | 484 | 451 | 464 | -40 | [4] |
| Inner sleeve | N/A | N/A | N/A | 347 | -40 | [4] |
| Cask inner shell | 398 | 367 | 351 | 344 | -40 | [4] |
| Gamma shield | 397 | 366 | 349 | 343 | -40 | 621 max. [5] |
| Outer shell | 382 | 352 | 337 | 335 | -40 | [4] |
| Shield shell | 335 | 305 | 299 | 295 | -40 | [4] |
| Finned Shell | N/A | 229 | N/A | N/A | -40 | [4] |
| Cask lid [5] | 295 | 267 | 319 | 336 | -40 | [4] |
| Cask bottom plate | 383 | 353 | 338 | 322 | -40 | [4] |
| Neutron Shield Resin[3] | 276 | 290 | 288 | 285 | -40 | 320 max. [17] |
| Trunnion Plug Resin[3] | 303 | 277 | 272 | 268 | -40 | 445 max. [25] |
| Seals | 382 | 352 | 337 | 336 | -40 | 400 max. [18, 19] |
| Wood in Impact limiter | 208 | 302 | 291 | 289 | -40 | 320 max. [20] |

Notes:
[1] These temperatures are the highest values taken from Table A.3–8, Table A.3–9, and Table A.3–10.
[2] These temperatures are based on assuming no credit for decay heat and a daily average ambient temperature of -40°F.
[3] The resin temperature is the volumetric, average temperature at the hottest cross section.
[4] The components perform their intended safety function within the operating range.
[5] The maximum cask lid temperatures for 26 kW < Q ≤ 32 kW and Q ≤ 26 kW belong to DSCs loaded with BWR and PWR fuel assemblies, respectively. Since a spacer is used for PWR DSCs, the heat load of the PWR fuel assemblies is closer to the cask lid. Due to this configuration, the maximum cask lid temperature for Q ≤ 26 kW is higher than for 26 kW < Q ≤ 32 kW. See Table A.3-8 and Table A.3-9 for details.

Table A.3–12
Maximum TC Component and 69BTH DSC Temperatures for Cold NCT
(32 kW, No insolation)

| Ambient Temperature | -20°F | -40°F |
|---|---|---|
| Component | $T_{max}$ (°F) | $T_{max}$ (°F) |
| Fuel Cladding | 582 | 570 |
| Basket (compartment) | 537 | 524 |
| Al / Poison Plate | 536 | 524 |
| Basket Rails | 431 | 419 |
| DSC shell | 405 | 392 |
| Cask inner shell | 267 | 250 |
| Gamma shield | 265 | 248 |
| Outer shell | 250 | 233 |
| Shield shell | 202 | 184 |
| Finned Shell | 124 | 105 |
| Cask lid | 162 | 145 |
| Cask bottom plate | 252 | 235 |
| Neutron Shield Resin (1) | 187 | 169 |
| Trunnion Plug Resin (1) | 169 | 151 |
| Wood in Impact limiter | 193 | 175 |

Note: (1) This temperature is the volumetric, average temperature of the elements located at hottest cross section of the neutron shield resin/the trunnion plug resin.

Table A.3–13
Maximum TC Component and 37PTH DSC Temperatures for Cold NCT
(22 kW, No insolation)

| Ambient Temperature | -20°F | -40°F |
|---|---|---|
| Component | $T_{max}$ (°F) | $T_{max}$ (°F) |
| Fuel Cladding | 593 | 582 |
| Basket (compartment) | 580 | 569 |
| Al / Poison Plate | 580 | 569 |
| Basket Rails | 365 | 353 |
| DSC shell | 328 | 315 |
| Cask inner shell | 219 | 203 |
| Gamma shield | 217 | 202 |
| Outer shell | 204 | 188 |
| Shield shell | 173 | 157 |
| Cask lid | 204 | 188 |
| Cask bottom plate | 146 | 130 |
| Neutron Shield Resin [1] | 164 | 148 |
| Trunnion Plug Resin [1] | 145 | 128 |
| Wood in Impact limiter | 157 | 140 |

Note: [1] This temperature is the volumetric, average temperature of the elements located at hottest cross section of the neutron shield resin/the trunnion plug resin.

Table A.3–14
Average Component Temperatures for NCT and HAC

| DSC Type | 69BTH | 61BTH/ 61BTHF Type 1 | 61BTH/ 61BTHF Type 2 | 61BT | 37PTH |
|---|---|---|---|---|---|
| Heat load | 32 kW | 22 kW | 24 kW | 18.3 kW | 22.0 kW |
| Component | $T_{avg}$ (°F) | $T_{avg}$ (°F) | $T_{avg}$ (°F) | $T_{avg}$ (°F) | $T_{avg}$ (°F) |
| Helium in TC cavity @ NCT | 339 | 301 | 316 | 273 | 269 |
| Helium in TC cavity @ HAC[1] | 387 | [2] | [2] | [2] | [2] |

| DSC Type | 32PTH / 32PTH Type1 / 32PTH1 Type 1 | 32PTH1 Type 2 | 32PT | 24PTH/ 24PTHF (all types) | 24PT4 |
|---|---|---|---|---|---|
| Heat load | 26 kW | 24 kW | 24 kW | 26 kW | 24 kW |
| Component | $T_{avg}$ (°F) | $T_{avg}$ (°F) | $T_{avg}$ (°F) | $T_{avg}$ (°F) | $T_{avg}$ (°F) |
| Helium in TC cavity @ NCT | 301 | 288 | 281 | 297 | 313 |
| Helium in TC cavity @ HAC[1] | [2] | [2] | [2] | 333 | [2] |

| Basket Type | 69BTH | 69BTH | 69BTH | 69BTH | 37PTH |
|---|---|---|---|---|---|
| Heat Load | 26 KW | 26 kW | 29.2 kW | 32 kW | 22 kW |
| Configuration | HLZC # 1 | HLZC # 2 | HLZC # 3 | HLZC # 4 | HLZC # 1 |
| Component | $T_{avg}$ (°F) | $T_{avg}$ (°F) | $T_{avg}$ (°F) | $T_{avg}$ (°F) | $T_{avg}$ (°F) |
| ***Normal Conditions of Transport*** | | | | | |
| Fuel Assemblies | 534 | 525 | 535 | 547 | 517 |
| Helium Elements[3] | 398 | 404 | 404 | 432 | 406 |
| Aluminum Rail | 457 | 457 | 464 | 490 | 436 |
| ***Hypothetical Accident Conditions*** | | | | | |
| Fuel Assemblies | 544 | 535 | 579 | 592 | 530 |
| Helium Elements[3] | 411 | 417 | 453 | 482 | 426 |
| Aluminum Rail | 470 | 470 | 511 | 538 | 454 |

Note:
[1] This value is the highest average helium temperature for the transient run.
[2] The average helium temperature for this case is bounded by 69BTH or 24PTH cases.
[3] This value is the volumetric, average temperature of the elements with helium properties in the basket model. In addition to the gaps, helium properties are considered for the elements within the fuel compartments located beyond the active fuel length and for the empty compartments.

Table A.3–15
List of the Gaps and Thermal Properties for HAC Analysis

| | Gap Size (in) | Location | Initial / Cool-down Properties | Properties during Fire |
|---|---|---|---|---|
| 1 | 0.01[1] | Axial gap between aluminum blocks of thermal shield and impact limiter case | Air | SA-240, type 304 (Impact Limiter Shell) |
| 2 | 0.01[1] | Axial gap between thermal shield plates and cask top or bottom end surfaces | Air | Al 6061 (Thermal shield) |
| 3 | 0.01 | Axial gap between cask lid and cask flange | Helium | SA-350-LF3/SA-203, Gr. E (Cask lid) |
| 4 | 0.01 | Axial gap between ram closure plate and cask bottom plate | Helium | SA-240, type 304 (Ram Closure Plate) [2] |
| 5 | 0.01 | Radial gaps between neutron shield boxes and surrounding shells | Air | Al 6063 (Neutron shield boxes) |
| 6 | 0.01 | Gaps between trunnion replacement plugs and the trunnion attachment blocks | Air | SA-182-F6NM (Trunnion block) |
| 7 | 0.025 | Radial gap between gamma shield and cask outer shell | Air | ASTM B-29 (Gamma shield) |
| 8 | 0.01 | Radial gaps between the cask inner shell and aluminum sleeve | Helium | Al 6061 (Inner sleeve w/o gaps) |
| 9 | 0.01 | Radial gap between the finned aluminum shell and the cask shield shell | Air | Al 6061 (Finned shell) |
| 10 | 0.0625 | Axial gaps between the DSC bottom shield plug and bottom cover plates | Air[3] | A36 (DSC bottom shield plug) |
| 11 | 0.0625 | Axial gaps between the DSC top inner cover and the adjacent plates | Air[3] | SA-240, type 304 (DSC top inner cover plate) |

Notes:
[1] The size of this axial gap is 0.0625" for initial conditions.
[2] A stainless steel weld is overlaid on the ram closure surfaces in contact with the cask bottom plate. For conservatism, ram closure plate is considered as SA-240, type 304 in this analysis.
[3] These gaps are incorporated into corresponding plates as effective conductivities in Section A.3.3.1.3

Table A.3–16
Maximum Temperatures of TC Components / DSC Shell for HAC

| DSC type | 69BTH | | | 69BTH | | | 24PTH | | | |
|---|---|---|---|---|---|---|---|---|---|---|
| Heat Load | 32 kW | | | 26 kW | | | 26 kW | | | |
| Internal sleeve | No | | | No | | | Yes | | | |
| External fins | Yes (Melted) | | | No | | | No | | | |
| Component | Time (hr) | $T_{max}$ (°F) | $T_{\infty}$ (°F) [2] | Time (hr) | $T_{max}$ (°F) | $T_{\infty}$ (°F) [2] | Time (hr) | $T_{max}$ (°F) | $T_{\infty}$ (°F) [2] | Limit (°F) |
| DSC shell | 7.2 | 509 | 496 | 4.7 | 451 | 443 | 7.6 | 473 | 467 | --- |
| DSC shell @ mid-length [1] | 7.2 | 509 | 496 | 4.7 | 451 | 442 | 7.6 | 464 | 453 | --- |
| Internal sleeve | N/A | N/A | N/A | N/A | N/A | N/A | 2.3 | 409 | 366 | --- |
| Cask inner shell | 2.0 | 487 | 403 | 0.5 | 441 | 363 | 0.5 | 413 | 363 | --- |
| Gamma shield | 0.5 | 552 | 401 | 0.5 | 521 | 362 | 0.5 | 508 | 361 | 621 [5] |
| Outer shell | 0.5 | 690 | 383 | 0.5 | 651 | 352 | 0.5 | 645 | 352 | --- |
| Shield shell | 0.5 | 1393 | 337 | 0.5 | 1072 | 306 | 0.5 | 1071 | 303 | --- |
| Cask lid | 13.2 | 314 | 311 | 10.7 | 299 | 292 | 4.6 | 367 | 352 | --- |
| Cask bottom plate | 1.0 | 416 | 384 | 1.0 | 404 | 353 | 7.6 | 309 | 300 | --- |
| Cask lid seal | 10.2 | 321 | 316 | 7.7 | 304 | 295 | 4.6 | 373 | 351 | 400 [18, 19] |
| Vent & test seal @ top | 13.2 | 311 | 310 | 10.7 | 298 | 291 | 4.6 | 366 | 351 | 400 [18, 19] |
| Ram plate seal | 2.0 | 380 | 378 | 2.3 | 366 | 350 | 10.6 | 302 | 297 | 400 [18, 19] |
| Test seal @ bottom | 13.2 | 380 | 379 | 1.3 | 364 | 350 | 10.6 | 303 | 297 | 400 [18, 19] |
| Drain port seal @ bottom | 10.2 | 386 | 383 | 7.7 | 362 | 352 | 7.6 | 308 | 299 | 400 [18, 19] |
| Helium in TC Cavity | 4.2 | 387 | 380 | 4.7 | 356 | 347 | 7.6 | 333 | 327 | --- |

Notes:
[1] This value is the maximum DSC shell temperature in the region where the fuel assemblies have the maximum peaking factor. See Appendix A.3.6.3 for discussion.
[2] These values are retrieved from the transient model at 20 hrs after fire accident. Based on the time-temperature histories shown in Figure A.3–40 through Figure A.3–42, the steady state temperatures are bounded by the temperatures at 20 hr transient.

Table A.3–17
Maximum DSC Shell Temperatures for Steady State Cool-Down

| DSC type | 69BTH | 69BTH | 69BTH | 61BTH/ 61BTHF Type 1 | 61BTH/ 61BTHF Type 2 | 61BT |
|---|---|---|---|---|---|---|
| Heat Load | 32 kW | 29.2 kW | 26 kW | 22 kW | 24 kW | 18.3 kW |
| Internal sleeve | No | No | No | Yes | Yes | Yes |
| External fins | Yes (Melted) | Yes (Melted) | No | No | No | No |
| $T_{max}$ DSC shell (°F) | 537 | 509 | 469 | 441 | 464 | 397 |

| DSC type | 37PTH | 32PTH/ 32PTH Type1/ 32PTH1 Type 1 | 32PTH1 Type 2 | 32PT | 24PTH / 24PTHF (all types) | 24PT4 |
|---|---|---|---|---|---|---|
| Heat Load | 22.0 kW | 26 kW | 24 kW | 24 kW | 26 kW | 24 kW |
| Inner sleeve | No | No | No | Yes | Yes | Yes |
| External fins | No | No | No | No | No | No |
| $T_{max}$ DSC shell (°F) | 438 | 473 | 452 | 470 | 480 | 454 |

Table A.3–18
Maximum Fuel Cladding and Basket Component Temperatures for HAC

| DSC Type | $T_{max, Fuel}$ (°F) | Reference for bounding fuel cladding temperature | $T_{max, Comp}$ (°F) | $T_{max, Al/Poison}$ (°F) | $T_{max, Rail}$ (°F) | Reference for bounding basket component temperatures |
|---|---|---|---|---|---|---|
| 69BTH, 32 kW | 693 | – | 658 | 657 | 557 | – |
| 69BTH, 29.2 kW | 693 | – | 667 | 666 | 529 | – |
| 69BTH, 26 kW | 668 | – | 653 | 653 | 487 | – |
| 61BTH Type 1 | < 749 | [3], Table T.4-21 | < 727 | < 727 | < 609 | [3], Table T.4-22 |
| 61BTH Type 2 | *< 830* | [3], Table T.4-21[6] | *< 805* | *< 804* | *< 650* | [3], Table T.4-23[6] |
| 61BT | < 809 | [1], Section K.4.6.4 | < 787 | < 787 | < 772 | [1], Table K.4-1[3] |
| 37PTH | 671 | – | 661 | 660 | 459 | – |
| 32PTH, 32PTH Type 1 | < 1036 | [4], Table 4-5 | < 1021 | < 1021 | < 878 | [4], Table 4-5 |
| 32PTH1 Type 1[1] | < 796 | [3], Table U.4-24 | < 766 | < 766 | < 609 | [3], Table U.4-25 |
| 32PTH1 Type 2[2] | < 858 | [3], Table U.4-24 | < 831 | < 830 | <689 | [3], Table U.4-26 |
| 32PT | < 863 | [1], Table M.4-13 | < 852 | < 852 | < 631 | [1], Table M.4-14 |
| 24PTH-S or –L w/ Al inserts | < 843 | [1], Table P.4-25 | < 802 | < 801 | < 716[4] | [1], Table P.4-27 |
| 24PTH-S or –L w/o Al inserts | < 843 | [1], Table P.4-25 | < 802 | < 801 | < 716[4] | [1], Table P.4-27 |
| 24PTH-S-LC | < 747 | [1], Table P.4-25 | < 709 | < 708 | < 716[4] | [1], Table P.4-28 |
| 24PT4 | < 805 | [2], Table A4.4-7 | < 768 | < 768 | [5] | [2], Table A4.4-6 |

Notes:
[1] This value is the maximum fuel cladding temperature for 32PTH1 Type 1 DSC with 31.2 kW heat load under transfer accident conditions.
[2] This value is the maximum fuel cladding temperature for 32PTH1 Type 2 DSC with 31.2 kW heat load under transfer accident condition.
[3] Based on discussion in [1], Appendix K, Section K.4.6.5, the maximum temperatures for transfer accident conditions are bounded by the maximum temperatures for blocked vent accident conditions.
[4] This value is the maximum rail, R90, temperature for transfer accident conditions with 40.8 kW heat load.
[5] Based on [2], Table A.4.4-6, the maximum spacer disc and support rod temperatures for 24PT4 DSC under accident transfer conditions (loss of sunshade and neutron shield) are 761°F and 673°F. These temperatures are the bounding values for transport HAC.
[6] *The maximum temperatures for 61BTH Type 2 DSC are increased from values in [3] due to allowance of six shims between the basket and the rails per note 5 of Drawing NUH61BTH-71-1102 in Appendix A.1.4.10.9.*

Table A.3–19
Summary of the Maximum Temperatures for HAC

| Heat load | 26 < Q ≤ 32 kW [2] | | | Q ≤ 26 kW [2] | | | | | | |
|---|---|---|---|---|---|---|---|---|---|---|
| Internal sleeve | No | | | No | | | Yes | | | |
| External fins | Yes (Melted) | | | No | | | No | | | |
| Component[1] | Time (hr) | $T_{max}$ (°F) | $T_{\infty}$ (°F) | Time (hr) | $T_{max}$ (°F) | $T_{\infty}$ (°F) | Time (hr) | $T_{max}$ (°F) | $T_{\infty}$ (°F) | Limit (°F) |
| Fuel Cladding | ∞ | 693 | 693 | ∞ | <1036 | <1036 | ∞ | <863 | <863 | 1058 [7] |
| Fuel Compartment | ∞ | 667 | 667 | ∞ | <1021 | <1021 | ∞ | <852 | <852 | --- |
| Al/Poison Plates | ∞ | 666 | 666 | ∞ | <1021 | <1021 | ∞ | <852 | <852 | --- |
| Basket Rails | ∞ | 557 | 557 | ∞ | <878 | <878 | ∞ | <772 | <772 | --- |
| DSC shell | ∞ | 537 | 537 | ∞ | 469 | 469 | ∞ | 480 | 480 | --- |
| Internal sleeve | N/A | N/A | N/A | N/A | N/A | N/A | 2.3 | 409 | 366 | --- |
| Cask inner shell | 2.0 | 487 | 403 | 0.5 | 441 | 363 | 0.5 | 413 | 363 | --- |
| Gamma shield | 0.5 | 552 | 401 | 0.5 | 521 | 362 | 0.5 | 508 | 361 | 621 [5] |
| Outer shell | 0.5 | 690 | 383 | 0.5 | 651 | 352 | 0.5 | 645 | 352 | --- |
| Shield shell | 0.5 | 1393 | 337 | 0.5 | 1072 | 306 | 0.5 | 1071 | 303 | --- |
| Cask lid | 13.2 | 314 | 311 | 10.7 | 299 | 292 | 4.6 | 367 | 352 | --- |
| Cask bottom plate | 1.0 | 416 | 384 | 1.0 | 404 | 353 | 7.6 | 309 | 300 | --- |
| Seals at TC Lid | 10.2 | 321 | 316 | 7.7 | 304 | 295 | 4.6 | 373 | 351 | 400 [18], [19] |
| Seals at TC Bottom Plate | 10.2 | 386 | 383 | 2.3 | 366 | 352 | 7.6 | 308 | 299 | 400 [18], [19] |

Notes:
[1] The maximum fuel cladding, basket component, and DSC shell temperatures are based on the conservative steady state cool-down period runs.
[2] These values are the highest temperatures taken from Table A.3–16 through Table A.3–18.

Table A.3–20
MP197HB TC Cavity Pressure for NCT

| | Heat Load | $V_{free,cc}$ [1] | $n_{he\text{-}initial}$ | $T_{avg,\ he,NCT}$ | $P_{NCT}$ |
|---|---|---|---|---|---|
| | kW | $in^3$ | g-moles | °F | psig |
| 69BTH | 32 | 19914 | 16.73 | 339 | 12.7 |
| 37PTH | 22 | 19876 | 16.70 | 269 | 10.3 |
| 32PTH | 26 | 19876 | 16.70 | 301 | 11.4 |
| 32PTH, Type 1 | 26 | 19876 | 16.70 | 301 | 11.4 |
| 32PTH1, Type 1 | 26 | 18940 | 15.91 | 301 | 11.4 |
| 32PTH1, Type 2 | 24 | 18940 | 15.91 | 288 | 11.0 |
| 61BTH, Type 1 | 22 | 19072 | 16.02 | 301 | 11.4 |
| 61BTH, Type 2 | 24 | 19072 | 16.02 | 316 | 11.9 |
| 61BT | 18.3 | 19072 | 16.02 | 273 | 10.5 |
| 32PT | 24 | 20233 | 17.00 | 281 | 10.7 |
| 24PTH (all types) | 26 | 19779 | 16.61 | 297 | 11.3 |
| 24PT4 | 24 | 19386 | 16.28 | 313 | 11.8 |

Note: [1] 98% of the TC cavity free volume is conservatively used in calculating the maximum pressures.

Table A.3–21
Volume and Average Helium Temperatures in 69BTH and 37PTH DSCs
for NCT and HAC

| | | | | | | |
|---|---|---|---|---|---|---|
| ***Normal Conditions of Transport*** | | | | | | |
| DSC | | 69BTH | | | | 37PTH |
| Thermally bounding FA | | FANP9x9 | | | | BW15x15[5] |
| Heat Loading Zoning Configuration (HLZC) | | #1 | #2 | #3 | #4 | --- |
| Number of FAs | | 69 | 61 | 61 | 52 | 37 |
| Temperature of Fas along active fuel [Table A.3–21] | °F | 534 | 525 | 535 | 547 | 517 |
| Volume of helium in Fas along active fuel [1] | $in^3$ | 244059 | 215763 | 215763 | 183929 | 231507 |
| Number of dummy fuel assemblies (DA) | | 0 | 8 | 8 | 16 | 0 |
| Temperature of Das along active fuel [Table A.3–21] | °F | n/a | 559 | 568 | 558 | n/a |
| Volume of helium outside Das along active fuel[2] | $in^3$ | n/a | 1710 | 1710 | 3420 | n/a |
| Free helium volume in DSC[3] | $in^3$ | 263687 | 232756 | 232756 | 204051 | 273058 |
| Temperature of helium in cavity outside Fas and Das along active fuel [Table A.3–21] | °F | 398 | 404 | 404 | 432 | 406 |
| Rest of helium volume in DSC outside Fas and Das along active fuel[4] | $in^3$ | 19628 | 15283 | 15283 | 16702 | 41551 |
| Temperature of helium in DSC | °F | 524 | 517 | 527 | 538 | 500 |
| ***Hypothetical Accident Conditions*** | | | | | | |
| DSC | | 69BTH | | | | 37PTH |
| Thermally bounding FA | | FANP9x9 | | | | BW15x15[5] |
| HLZC | | #1 | #2 | #3 | #4 | --- |
| Number of FAs | | 69 | 61 | 61 | 52 | 37 |
| Temperature of FAs along active fuel [Table A.3–21] | °F | 541 | 532 | 576 | 589 | 530 |
| Volume of helium in FAs along active fuel[1] | $in^3$ | 244059 | 215763 | 215763 | 183929 | 231507 |
| Number of dummy FAs | | 0 | 8 | 8 | 16 | 0 |
| Temperature of DAs along active fuel [Table A.3–21] | °F | 0 | 567 | 610 | 601 | 0 |
| Volume of helium outside DAs along active fuel[2] | $in^3$ | 0 | 1710 | 1710 | 3420 | 0 |
| Free Helium volume in DSC[3] | $in^3$ | 263687 | 232756 | 232756 | 204051 | 273058 |
| Temperature of helium in cavity outside FAs, DAs along active fuel [Table A.3–21] | °F | 415 | 421 | 457 | 486 | 426 |
| Rest of helium volume in DSC outside FAs and DAs along active fuel[4] | $in^3$ | 19628 | 15283 | 15283 | 16702 | 41551 |
| Temperature of helium in DSC | °F | 532 | 525 | 568 | 581 | 514 |

Notes:
(1) Calculated based on compartment dimensions and total fuel rods' volume along active fuel,
(2) Calculated based on compartment and assumed dummy fuel assembly dimensions along active fuel,
(3) Calculated using weight calculation results for DSC cavity helium volume without 69 FAs volume from Chapter A.2. FAs volume from Chapter A.2, dummy FAs volume as $V_{He\_DSC} = V_{He\_DSC\_w/o\_FA} - V_{FAs} - V_{DAs}$,
(4) Calculated as $V_{He\_DSC\_out\_FA/DA\_act\_fuel} = V_{He\_DSC} - V_{He\_in\_FA\_act\_fuel} - V_{He\_in\_DA\_act\_fuel}$.
(5) BW 15x15 is not allowed in the 37PTH DSC but is used in this analysis for conservatism.

Table A.3–22
Maximum Internal Pressures of 69BTH and 37PTH DSCs in MP197HB TC

***Maximum Pressures for Normal Conditions of Transport***

| DSC | HLZC # | DSC cavity volume | Helium fill amount | Plenum volume | Plenum helium amount | CC gas amount | Fission products amount | Total gas amount | $T_{av\ He}$ | *Calculated* Pressure | *Design* Pressure |
|---|---|---|---|---|---|---|---|---|---|---|---|
| | | $in^3$ | g-moles | $in^3$ | g-moles | g-moles | g-moles | g-moles | °F | psig | psig |
| 69BTH | 1 | 258,413 | 134.4 | 442.2 | 3.3 | 0.0 | 14.16 | 151.82 | 524 | 8.89 | 15 |
| | 2 | 228,101 | 118.6 | 390.9 | 2.9 | 0.0 | 12.52 | 134.03 | 517 | 8.74 | |
| | 3 | 228,101 | 118.6 | 390.9 | 2.9 | 0.0 | 12.52 | 134.03 | 527 | 8.96 | |
| | 4 | 199,970 | 104.0 | 333.2 | 2.5 | 0.0 | 10.67 | 117.13 | 538 | 9.15 | |
| | | | | | | | | | | | |
| 37PTH | 37 FAs w/CC | 257,646 | 138.1 | 306.1 | 17.0 | 2.5 | 0.0 | 157.6 | 500 | 9.28 | 15 |

***Maximum Pressures for Hypothetical Accident Conditions***

| DSC | HLZC # | DSC cavity volume | Helium fill amount | Plenum volume | Plenum helium amount | CC gas amount | Fission products amount | Total gas amount | $T_{av\ He}$ | *Calculated* Pressure | *Design* Pressure |
|---|---|---|---|---|---|---|---|---|---|---|---|
| | | $in^3$ | g-moles | $in^3$ | g-moles | g-moles | g-moles | g-moles | °F | psig | psig |
| 69BTH | 1 | 258,413 | 134.4 | 14,738.4 | 108.9 | 0.0 | 472.09 | 715.39 | 532 | 91.47 | 140 |
| | 2 | 228,101 | 118.6 | 13,029.6 | 96.3 | 0.0 | 417.36 | 632.26 | 525 | 90.88 | |
| | 3 | 228,101 | 118.6 | 13,029.6 | 96.3 | 0.0 | 417.36 | 632.26 | 568 | 95.54 | |
| | 4 | 199,970 | 104.0 | 11,107.2 | 82.1 | 0.0 | 355.78 | 541.85 | 581 | 94.52 | |
| | | | | | | | | | | | |
| 37PTH | 37 FAs w/CC | 257,646 | 138.1 | 10,204.9 | 568.1 | 82.9 | 0.0 | 789.2 | 514 | 102.64 | 140 |

Table A.3–23
Maximum Internal Pressure in DSCs for Transport in MP197HB TC

| DSC | Operating conditions | *Design* Pressure psig | *Calculated* Pressure psig |
|---|---|---|---|
| 69BTH | NCT | 15 | 9.15 |
| | HAC | 140 | 95.54 |
| 61BTH/61BTHF Type 1 | NCT | 10 | 8.10 |
| | HAC | 65 | 56.10 |
| 61BTH Type 2 | NCT | 15 | 8.60 |
| | HAC | 120 | 68.70 |
| 61BT | NCT | 10 | 9.56 |
| | HAC | 65 | 46.00 |
| 37PTH | NCT | 15 | 9.28 |
| | HAC | 140 | 102.64 |
| 32PTH/32PTH Type 1 | NCT | 15 | 7.47 |
| | HAC | 120 | 91.00 |
| 32PTH1 Type 1/Type 2 | NCT | 15 | 10.74 |
| | HAC | 140 | 126.34 |
| 32PT | NCT | 15 | 8.04 |
| | HAC | 105 | 101.68 |
| 24PTH/24PTHF (all types) | NCT | 15 | 8.57 |
| | HAC | 120 | 97.20 |
| 24PT4 | NCT | 20 | 18.57 |
| | HAC | 100 | 80.70 |

Table A.3–24
Comparison of Maximum DSC Shell Temperatures

| For Normal Conditions of Transport | | | | | |
|---|---|---|---|---|---|
| DSC type | 10 CFR 71 DSC Shell Temp [1] (°F) | 10 CFR 71 Heat Load (kW) | 10 CFR 72 Bounding DSC Shell Temp [2] (°F) | 10 CFR 72 Model Reference | 10 CFR 72 Heat Load (kW) |
| 61BTH Type 1 | 414/406 | 22.0 | 418 [3], Table T.4-7 [3] | [3], Section T.4.5.1 | 22.0 |
| 61BTH Type 2 | 435/427 | 24.0 | 441 [3], Table T.4-8 [3] | [3], Section T.4.5.1 | 31.2 |
| 61BT | 372/365 | 18.3 | 378 [1], Table K.4-2 | [1], Section K.4.4.1 | 18.3 |
| 32PTH / 32PTH Type 1 | 444/436 | 26.0 | 475 [4], Table 4-1 | [4], Section 4.3.1.1 | 34.8 |
| 32PTH1 Type 1 | 444/436 | 26.0 | 485 [3], Table U.4-11 | [3], Section U.4.5.2 | 40.8 |
| 32PTH1 Type 2 | 423/416 | 24.0 | 485 [3], Table U.4-11 | [3], Section U.4.5.2 | 31.2 |
| 32PT | 443/432 | 24.0 | 445 [1], Table M.4-3 | [1], Section M.4.4.1.6 | 24.0 |
| 24PTH-S or –L w/ Al inserts | 464/449 | 26.0 | 551 [1], Table P.4-11 [3] | [1], Section P.4.5.2 | 40.8 |
| 24PTH-S or –L w/o Al inserts | 464/449 | 26.0 | 475 [1], Table P.4-10 [3] | [1], Section P.4.5.2 | 31.2 |
| 24PTH-S-LC | 464/449 [4] | 24.0 | 475 [1], Table P.4-10 [4] | [1], Section P.4.5.2 | 24.0 |
| 24PT4 | 428/424 | 24.0 | 439 [2], Table A.4.4-4 | [2], Section 4.4.3.1 | 24.0 |

| For Hypothetical Accident Conditions | | | | | |
|---|---|---|---|---|---|
| DSC type | 10 CFR 71 DSC Shell Temp [5] (°F) | 10 CFR 71 Heat Load (kW) | 10 CFR 72 Bounding DSC Shell Temp [2] (°F) | 10 CFR 72 Model Reference | 10 CFR 72 Heat Load (kW) |
| 61BTH Type 1 | 441 | 22.0 | 484 [3], Table T.4-10 | [3], Section T.4.5.3.3 | 22.0 |
| 61BTH Type 2 | 464 | 24.0 | 544 [3], Table T.4-10 | [3], Section T.4.5.3.3 | 31.2 |
| 61BT | 397 | 18.3 | 499 [1], Table K.4-6 | [1], Section K.4.6.5 | 18.3 |
| 32PTH / 32PTH Type 1 | 473 | 26.0 | 790 [4], Table 4-5 | [4], Section 4.4.1.1 | 34.8 |
| 32PTH1 Type 1 | 473 | 26.0 | 578 [3], Table U.4-14 | [3], Section U.4.5.4.2 | 40.8 |
| 32PTH1 Type 2 | 452 | 24.0 | 578 [3], Table U.4-14 | [3], Section U.4.5.4.2 | 31.2 |
| 32PT | 470 | 24.0 | 600 [1], Table M.4-14 | [1], Section M.4.6.2 | 24.0 |
| 24PTH-S or –L w/ Al inserts | 480 | 26.0 | 685 [1], Table P.4-26 | [1], Section P.4.5.5.3 | 40.8 |
| 24PTH-S or –L w/o Al inserts | 480 | 26.0 | 610 [1], Table P.4-27 | [1], Section P.4.5.5.3 | 31.2 |
| 24PTH-S-LC | 480 [4] | 24.0 | 487 [1], Table P.4-28 | [1], Section P.4.5.5.3 | 24.0 |
| 24PT4 | 454 | 24.0 | 536 [2], Table A.4.4-5 | [2], Section 4.4.3.1 | 24.0 |

Notes:
[1] The first value is the absolute maximum DSC shell temperature and the second value is the maximum DSC shell temperature where the fuel has the maximum peaking factor. These values are taken fromTable A.3–8 and Table A.3–9.
[2] These values are the maximum DSC shell temperatures taken from evaluations under 10 CFR 72.
[3] The small differences between the maximum DSC shell temperatures in this table and those shown in Figure A.3-51 and Figure A.3-52 are caused by imperfections in the nodal temperature transfer from TC to DSC models for 61BTH and 24PTH DSCs in [3] and [1].
[4] The maximum DSC shell temperature for 24PTH-S or -L DSC (without aluminum inserts) with 26 kW heat load is bounding for use with the 24PTH-S-LC with 24 kW heat load.
[5] These values are taken from Table A.3–17.

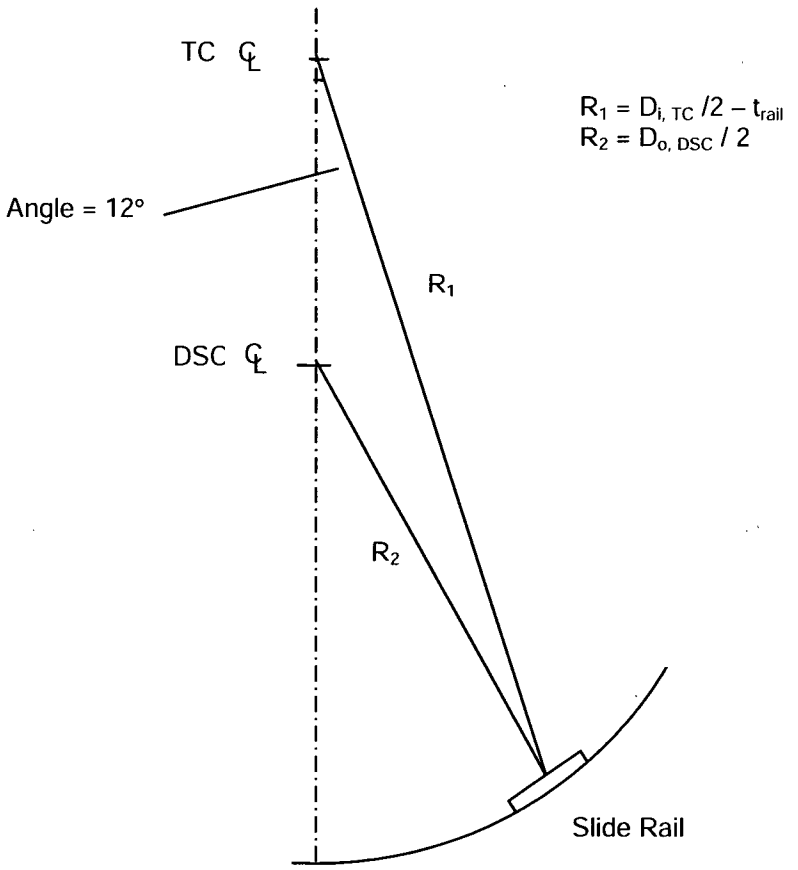


Figure A.3–1
Location of DSC within the MP197HB TC

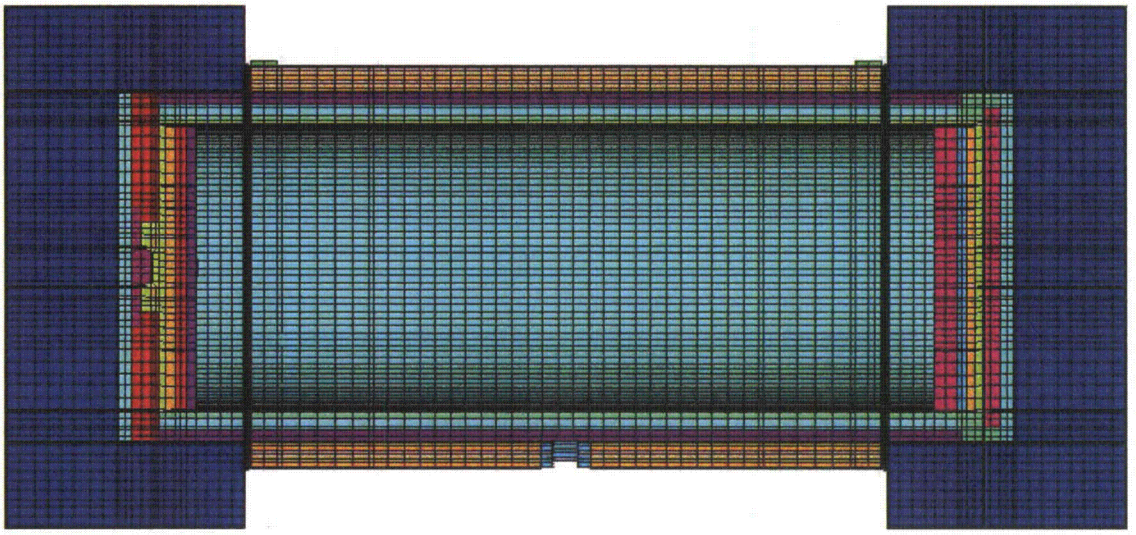

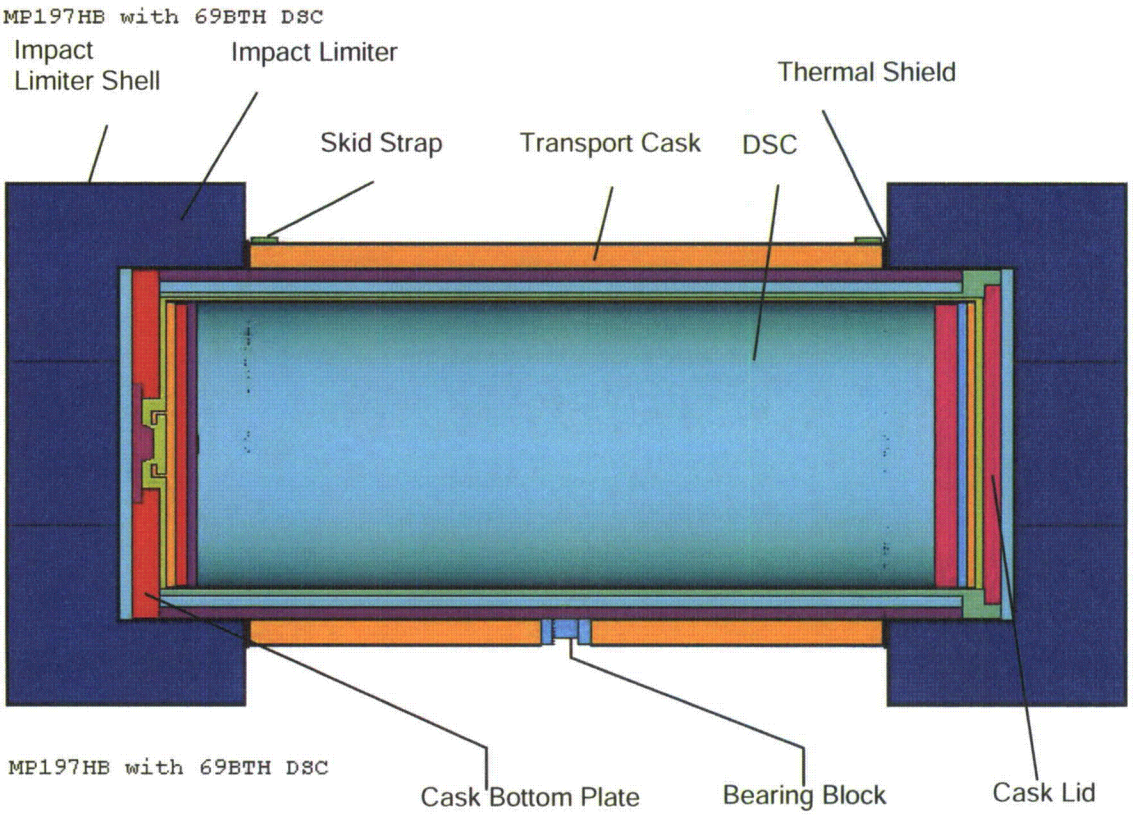


Figure A.3–2
Finite Element Model of the MP197HB with the 69BTH DSC

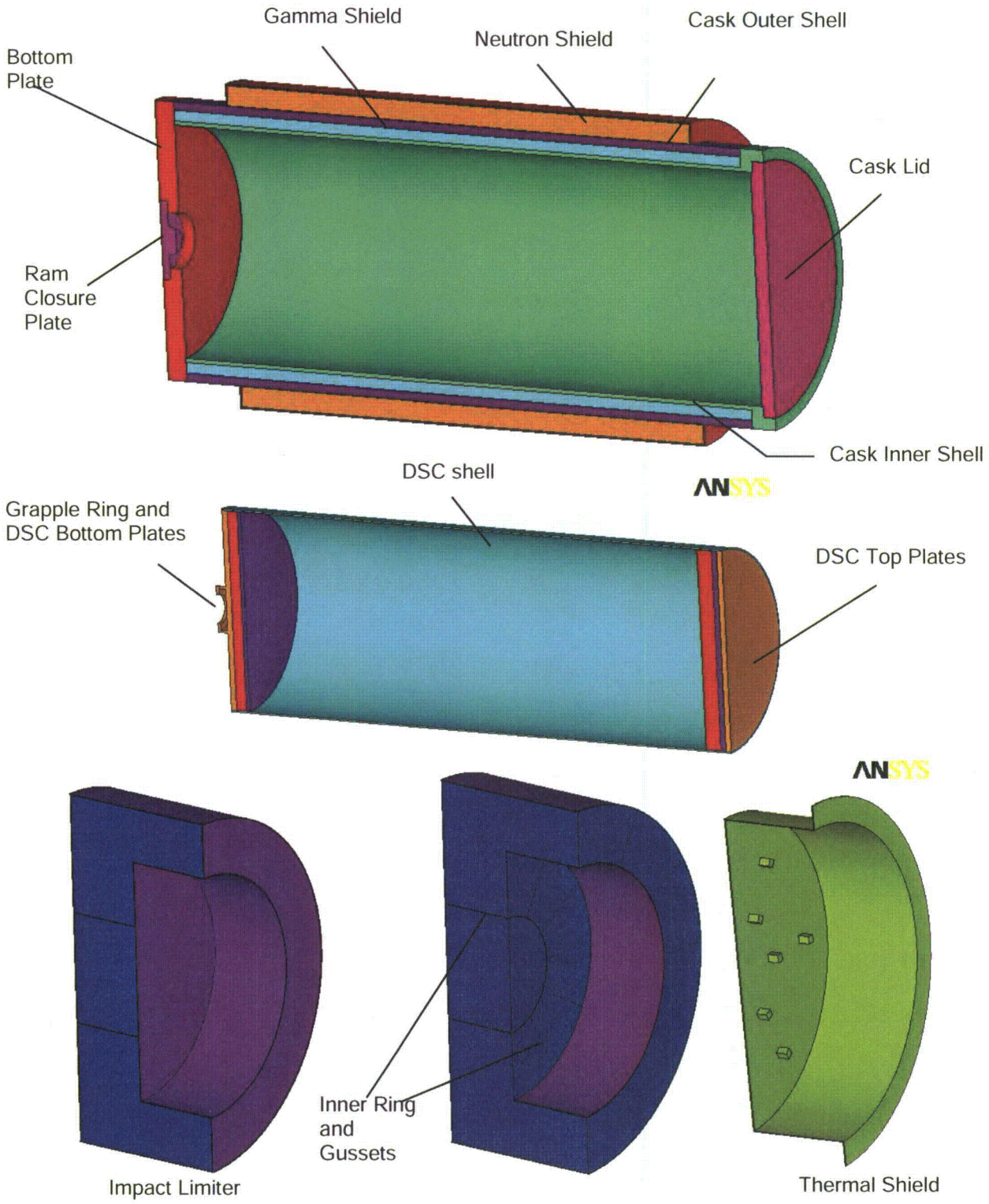


Figure A.3–3
Components of the MP197HB TC Model

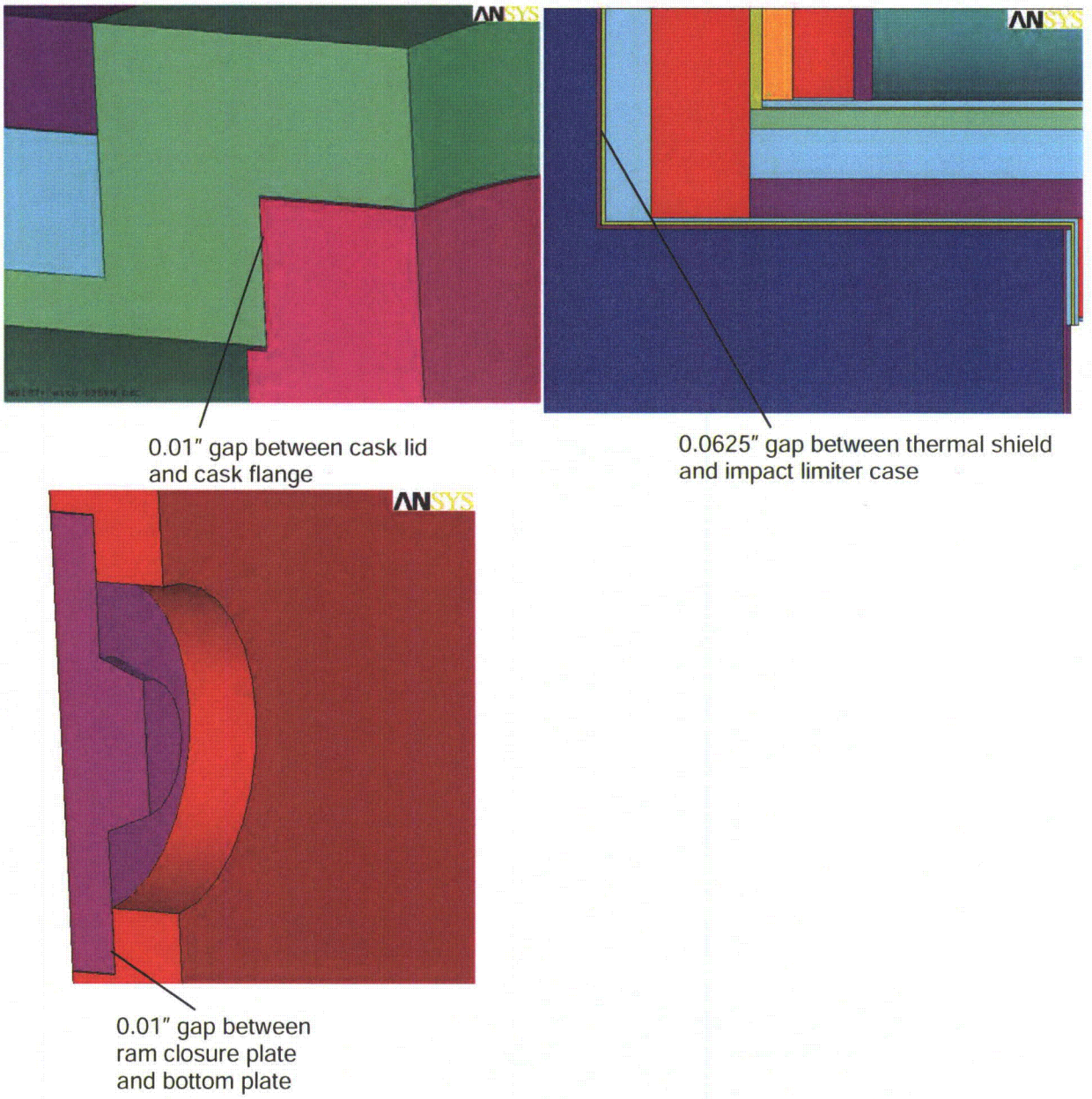


Figure A.3–4
Gaps in the MP197HB TC Model

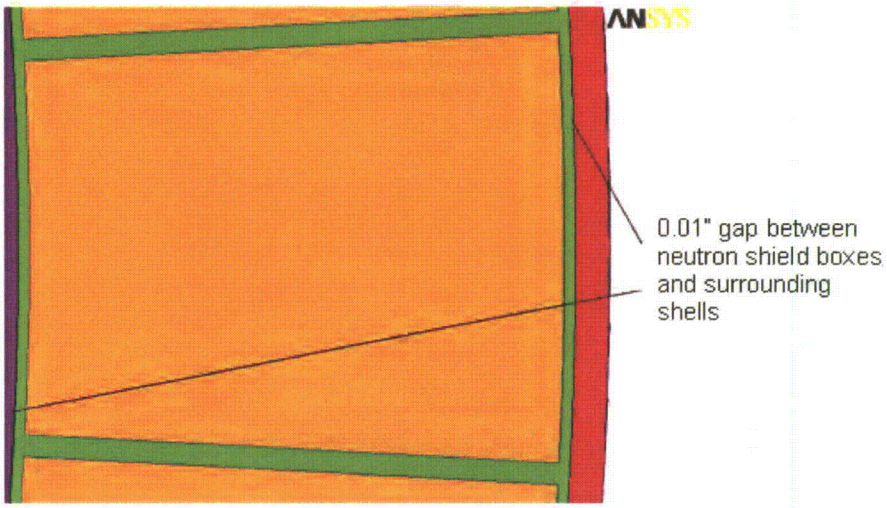


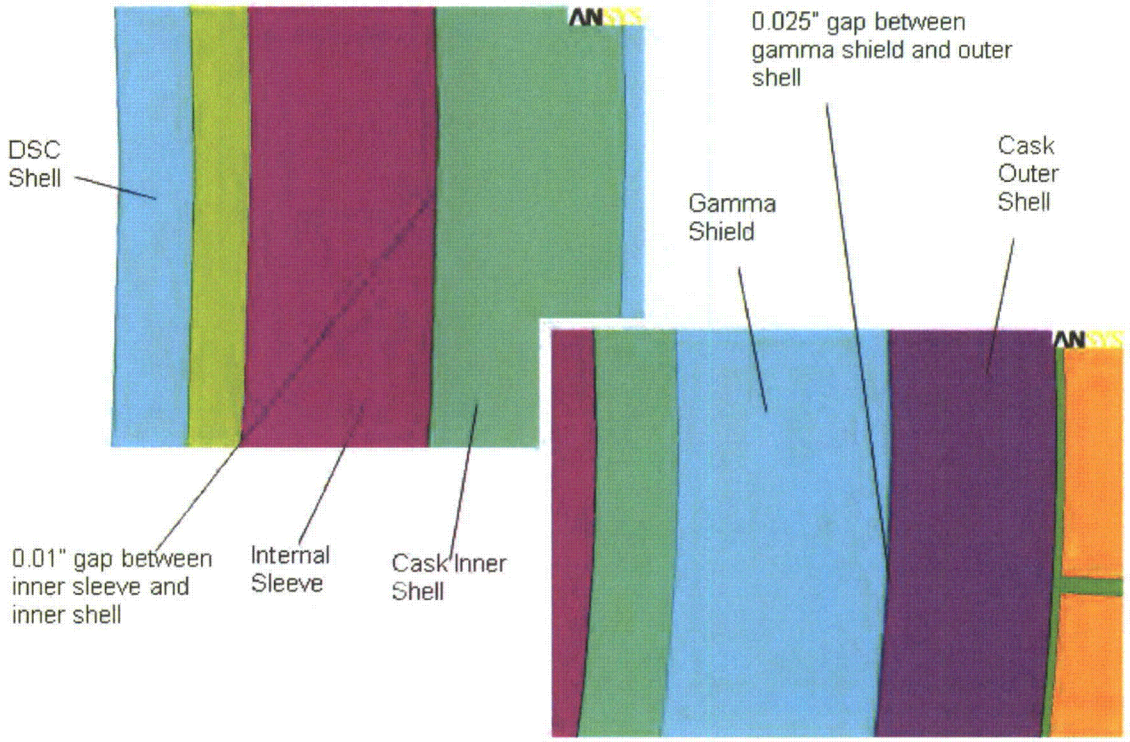


Figure A.3–5
Gaps in the MP197HB TC Cross Section

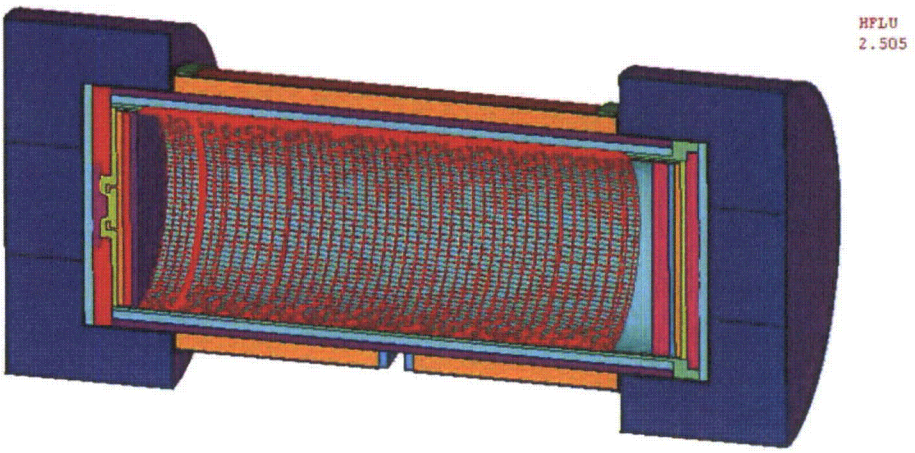


Decay Heat Boundary Conditions for 69BTH DSC, 26 kW

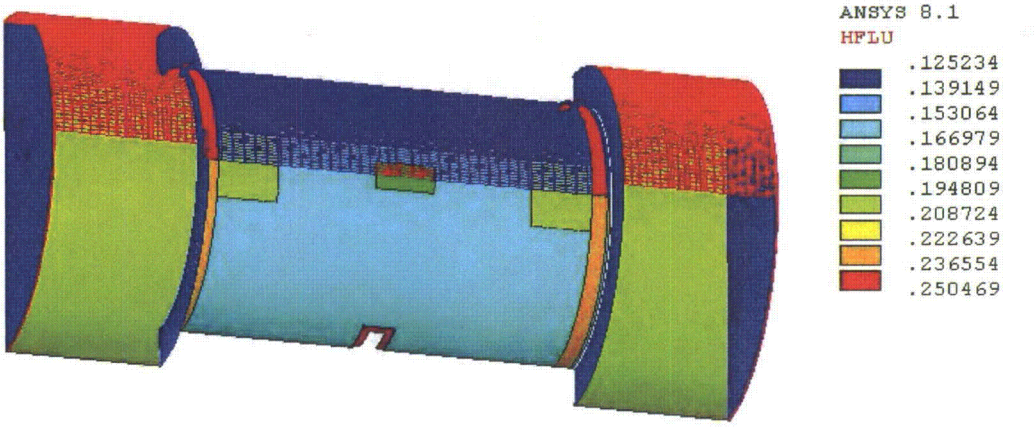


Insolance Boundary Conditions

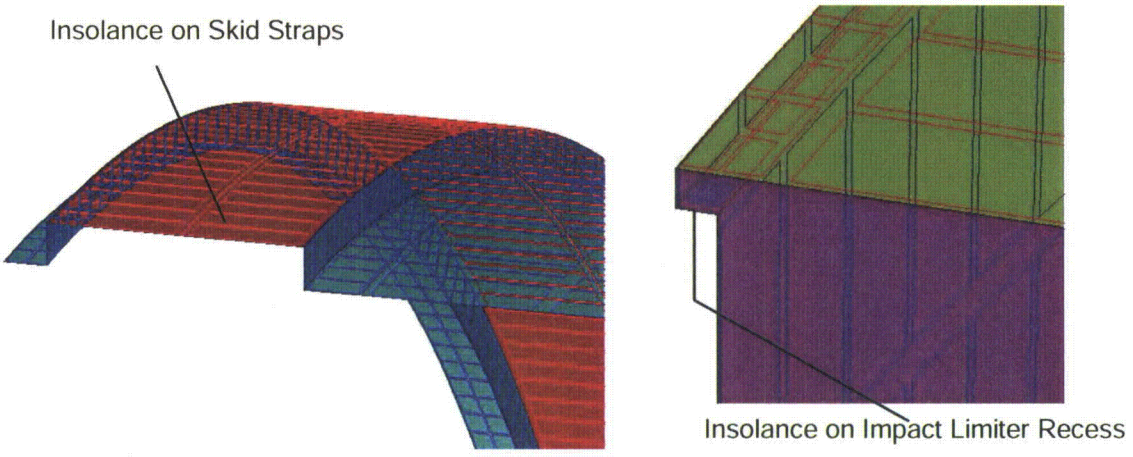


Figure A.3–6
Typical Decay Heat and Insolance Boundary Conditions

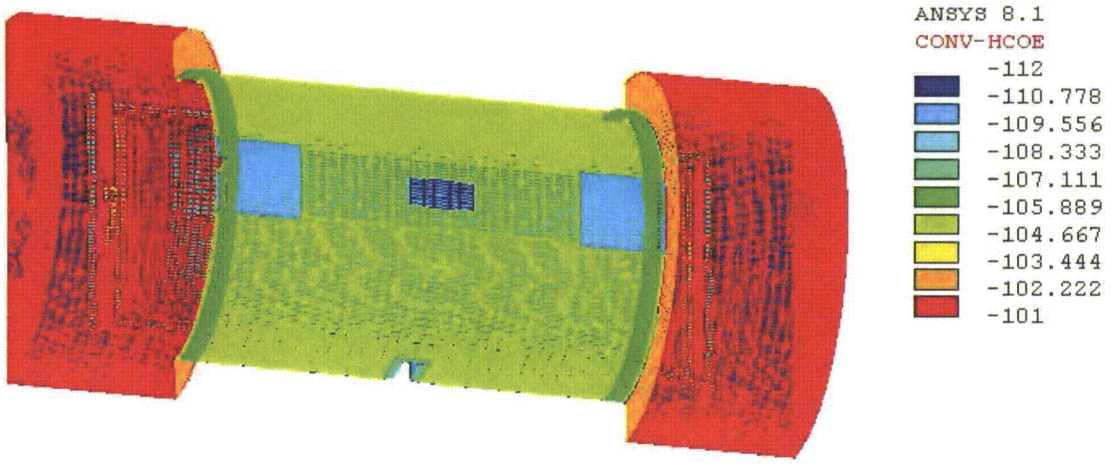


Convection and Radiation Boundary Conditions for MP197HB w/o External Fins

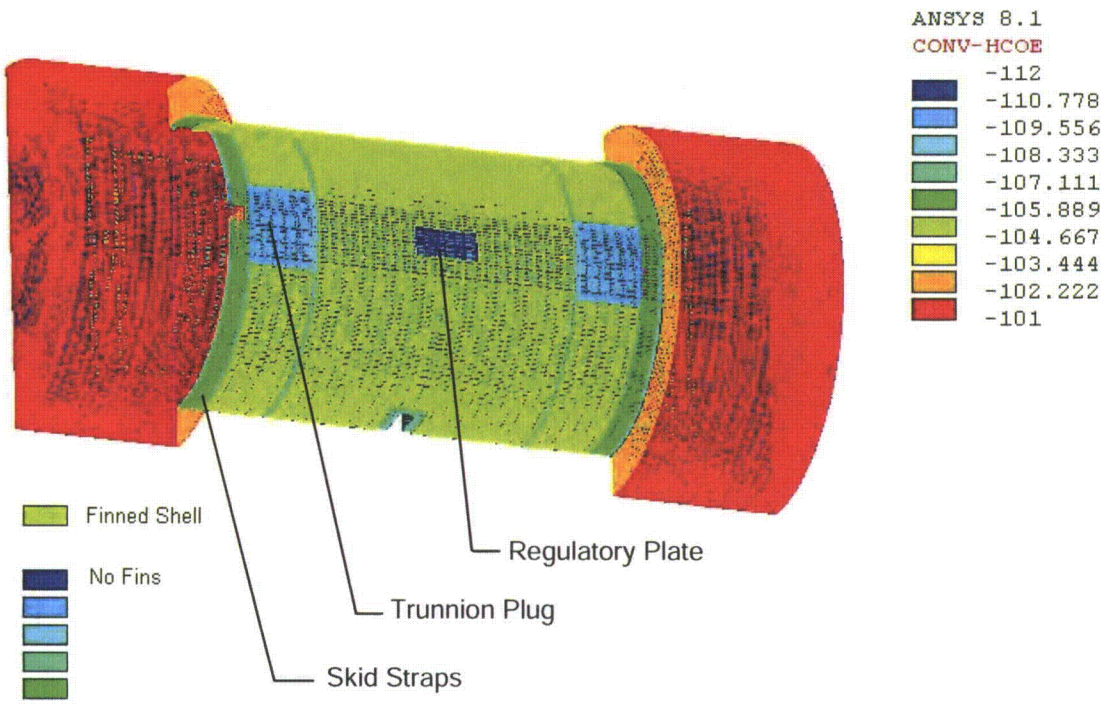


Convection and Radiation Boundary Conditions for MP197HB with External Fins

Figure A.3–7
Typical Convection and Radiation Boundary Conditions

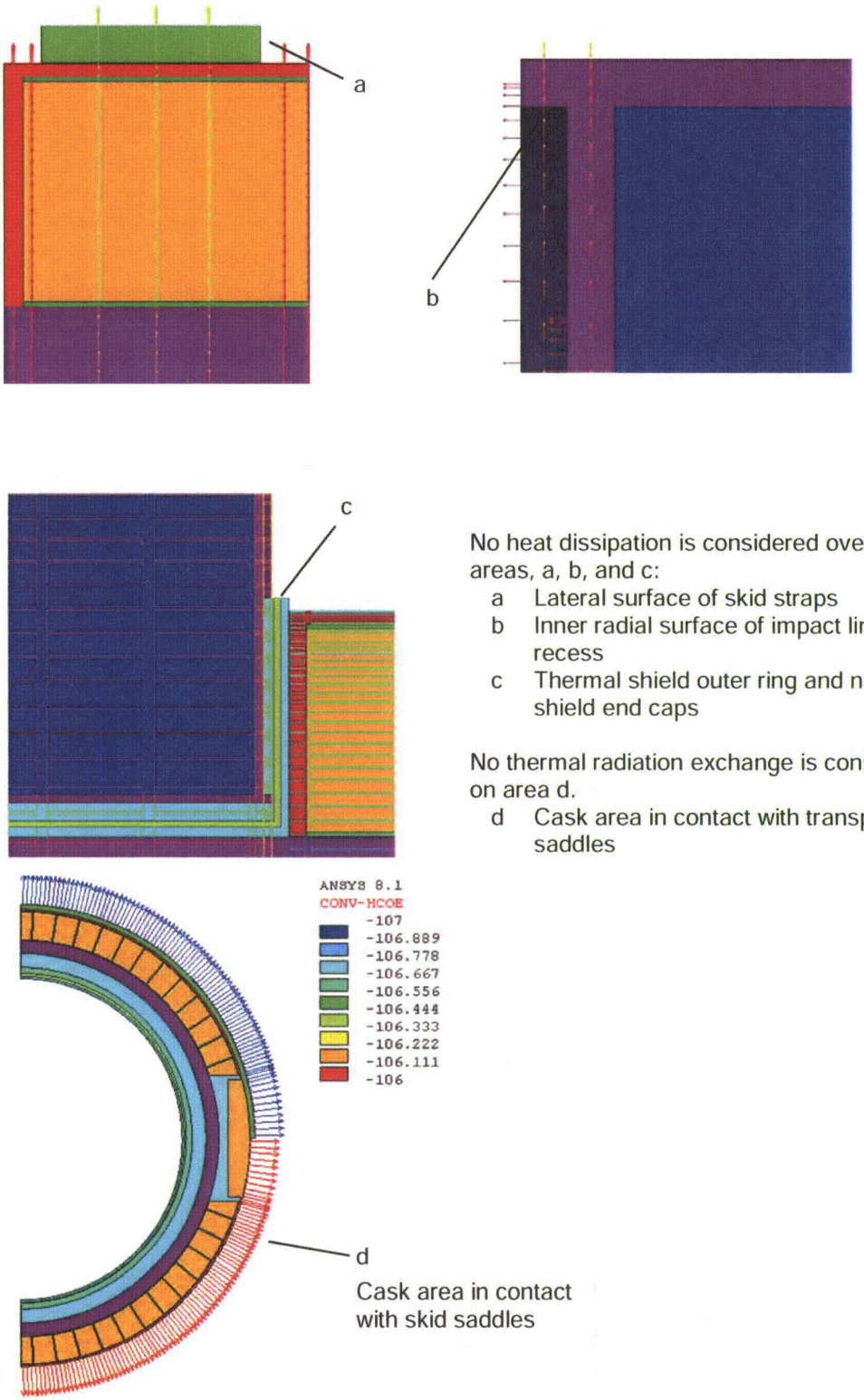


No heat dissipation is considered over marked areas, a, b, and c:

- a Lateral surface of skid straps
- b Inner radial surface of impact limiter recess
- c Thermal shield outer ring and neutron shield end caps

No thermal radiation exchange is considered on area d.

- d Cask area in contact with transport skid saddles

Figure A.3–8
Typical Convection and Radiation Boundary Conditions – Details

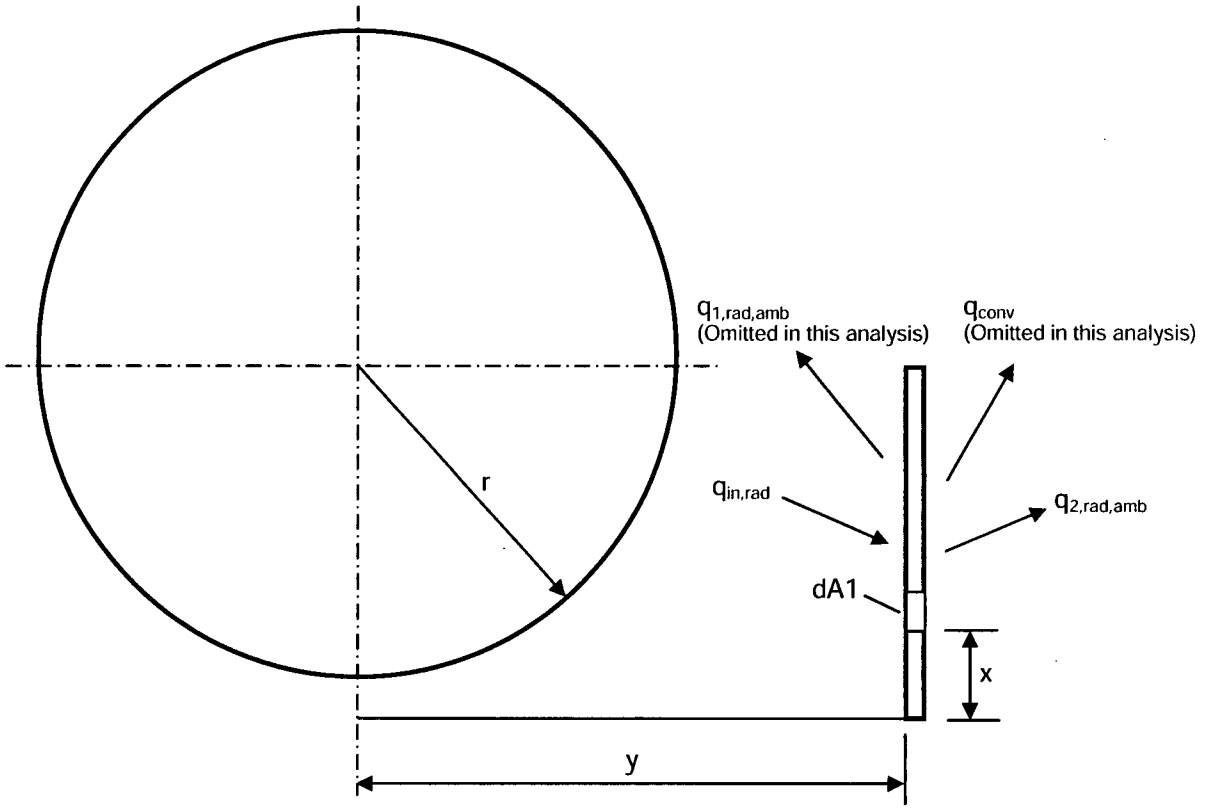


Figure A.3–9
Schematic View of Cask and Personnel Barrier

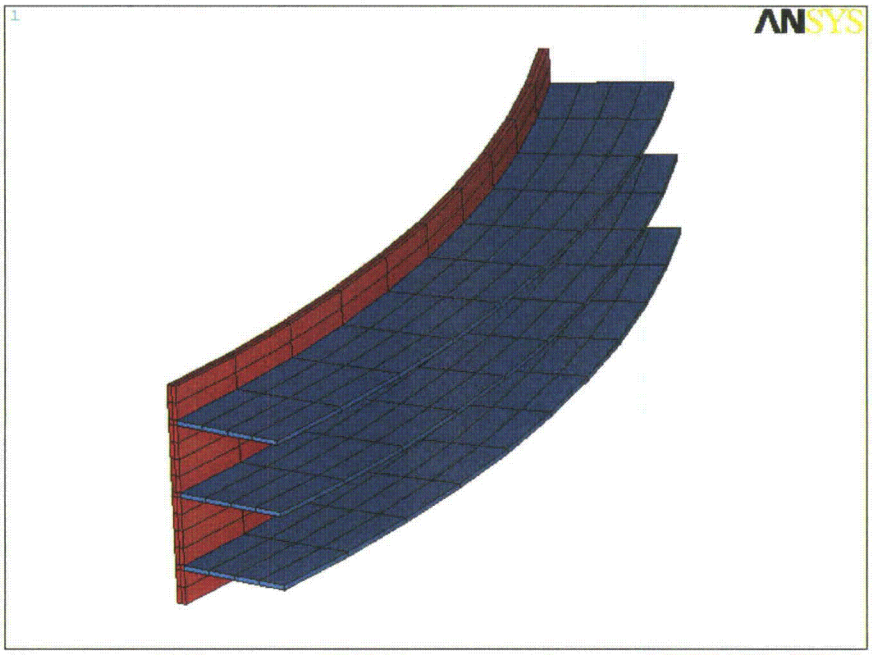


Solid Elements

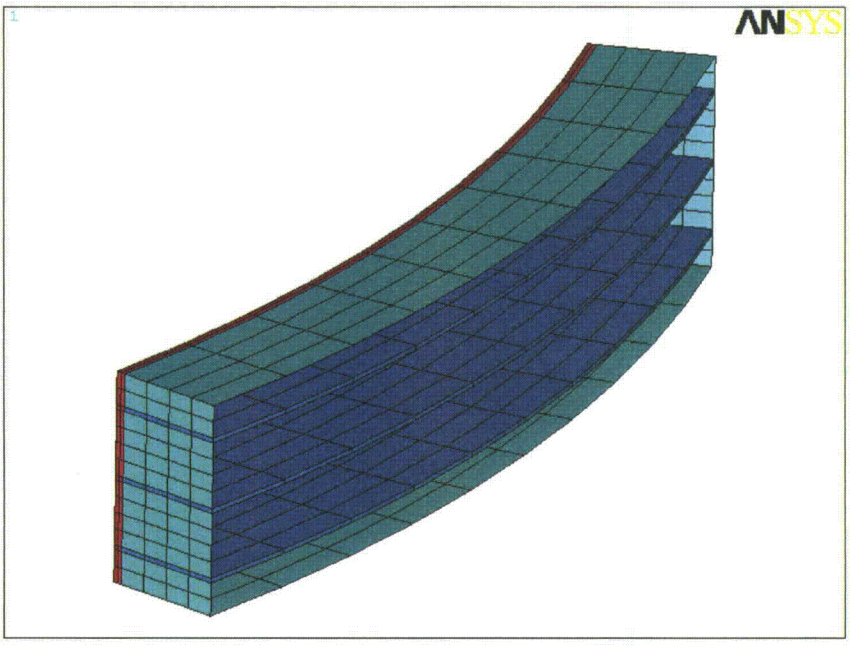


Shell Elements for Radiation

Figure A.3–10
Sub-Model of the External Fins for MP197HB TC

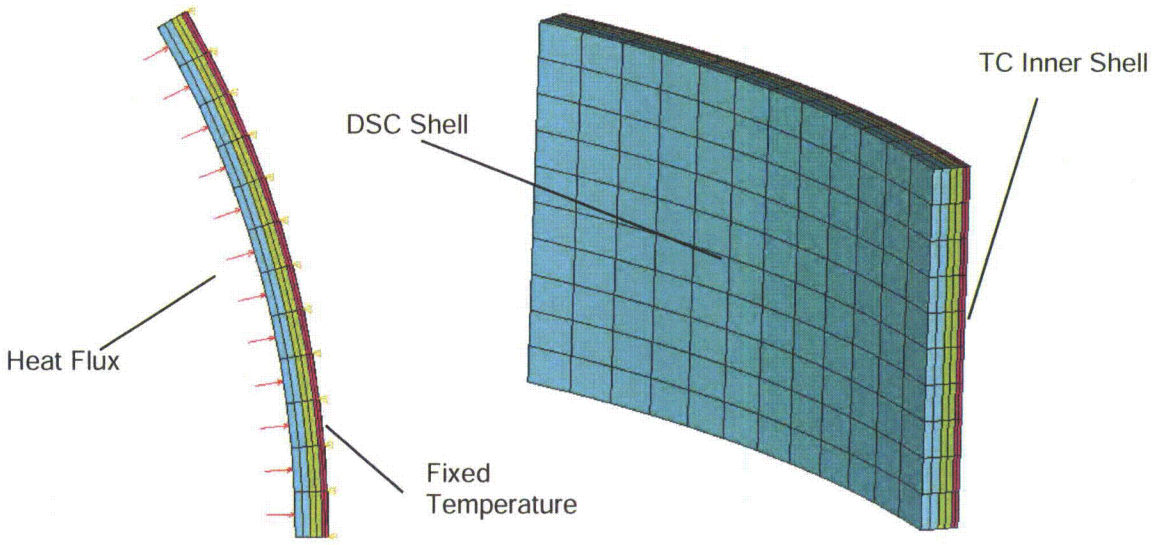


Figure A.3–11
Sub-Model for Helium Gap Effective Conductivity Calculation

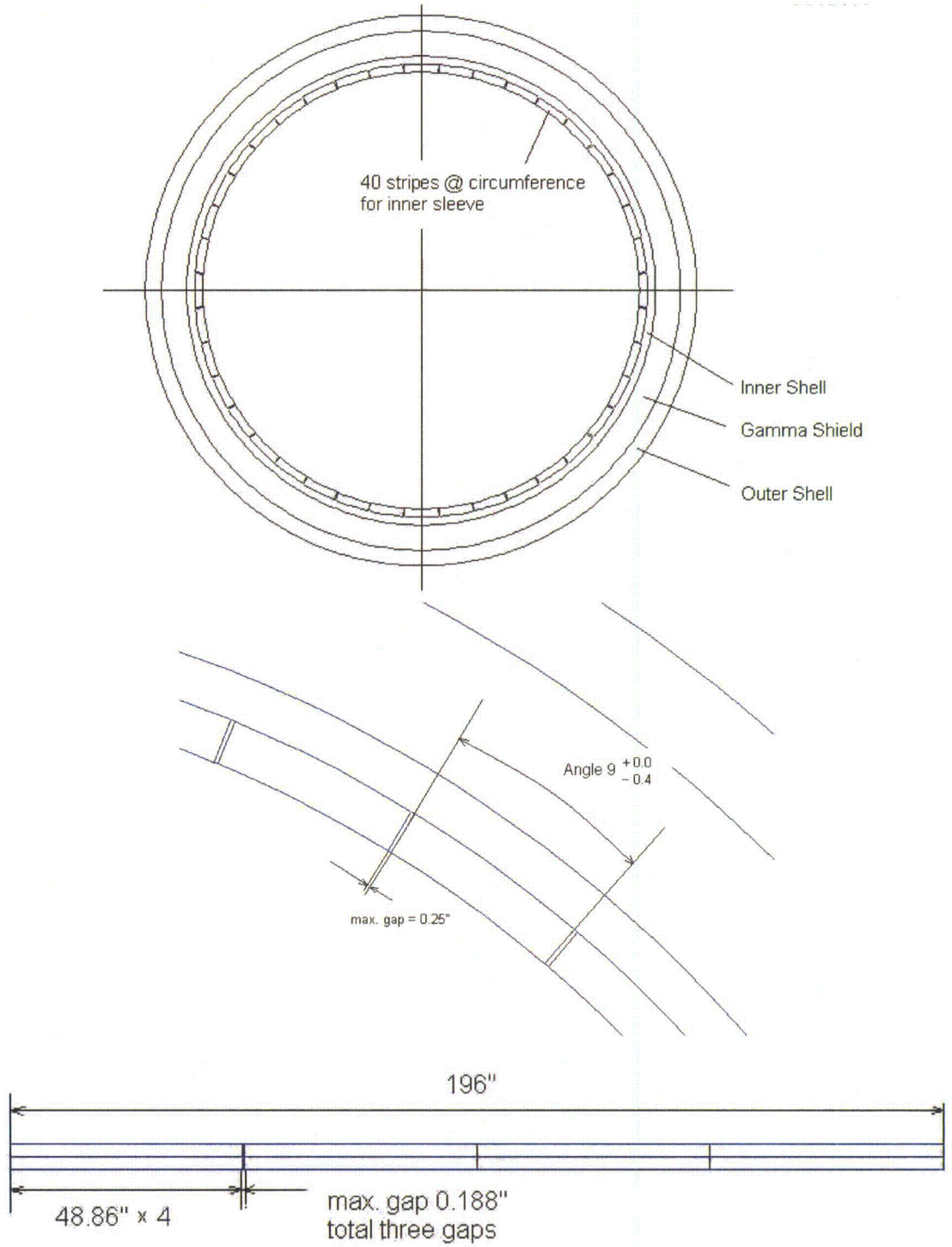


Figure A.3–12
Assumed Geometry of Internal Sleeve in Thermal Model

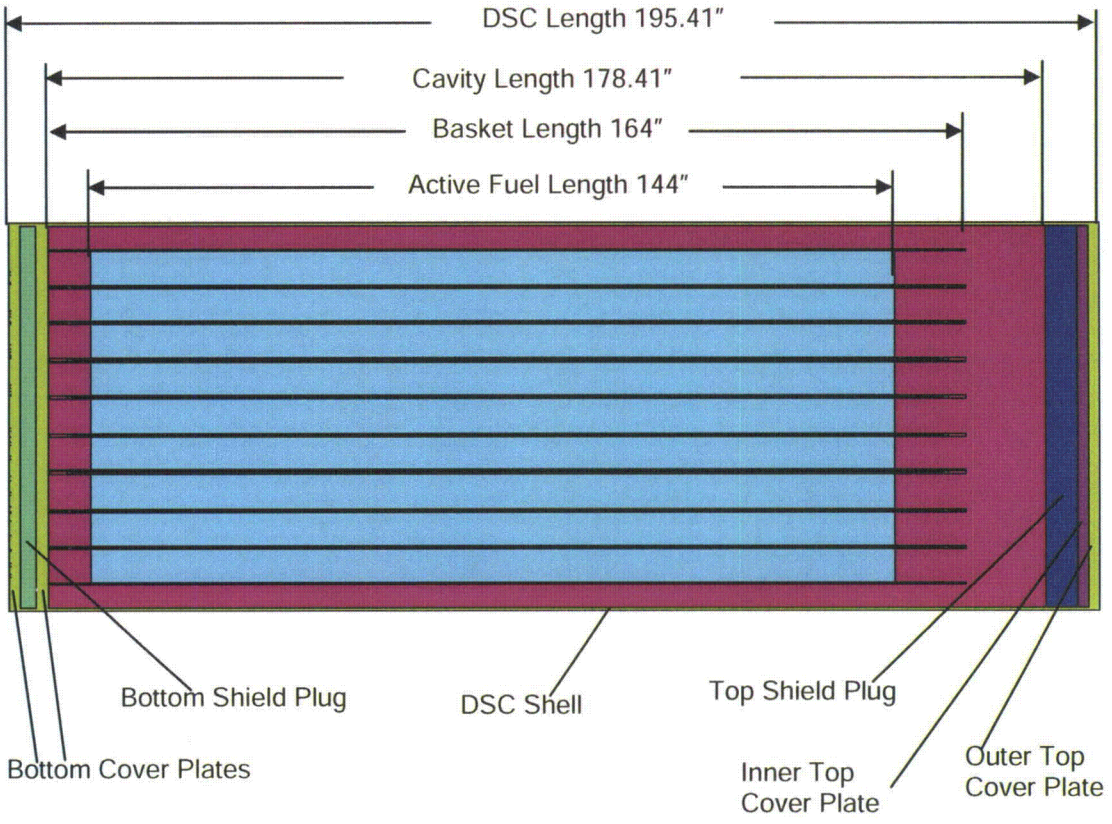


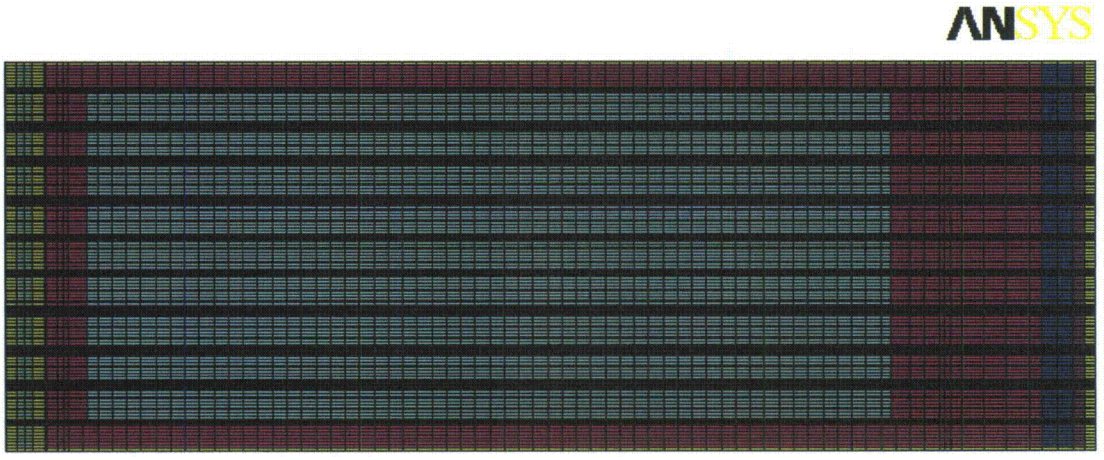


Figure A.3–13
Finite Element Model of 69BTH DSC/Basket

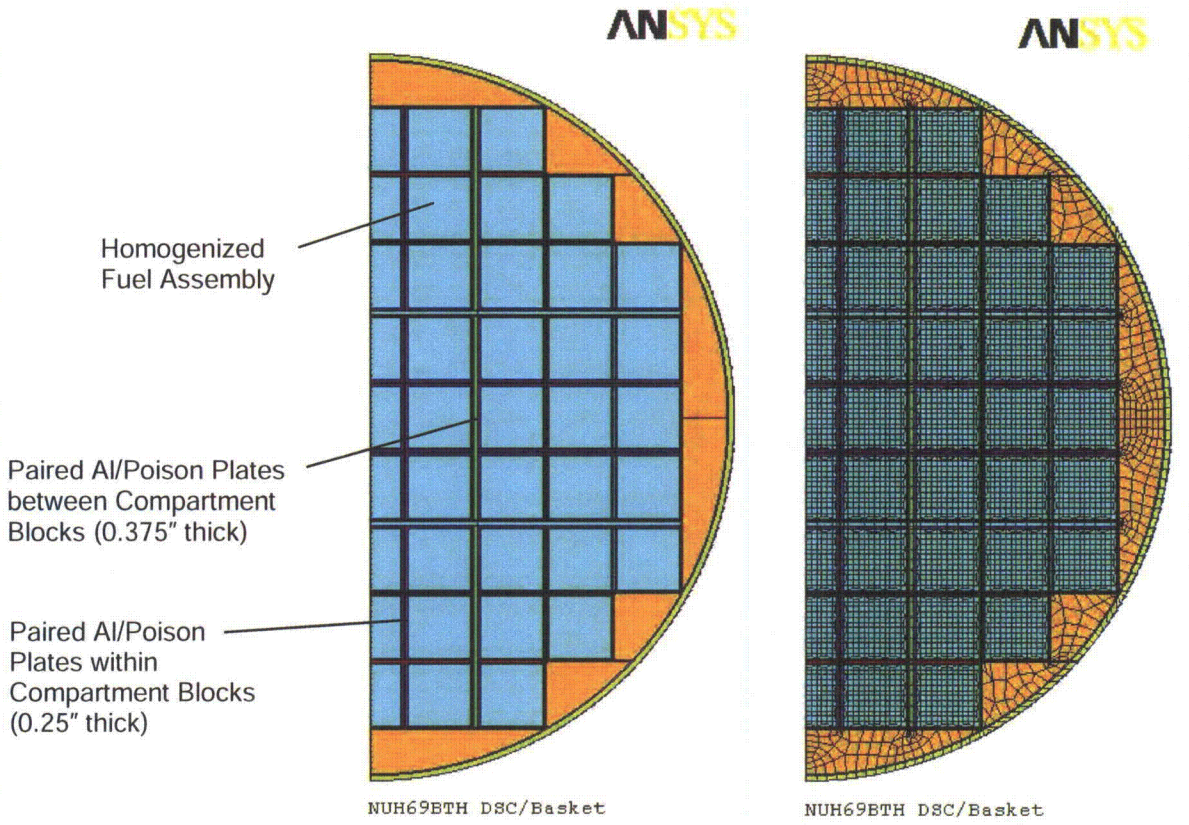


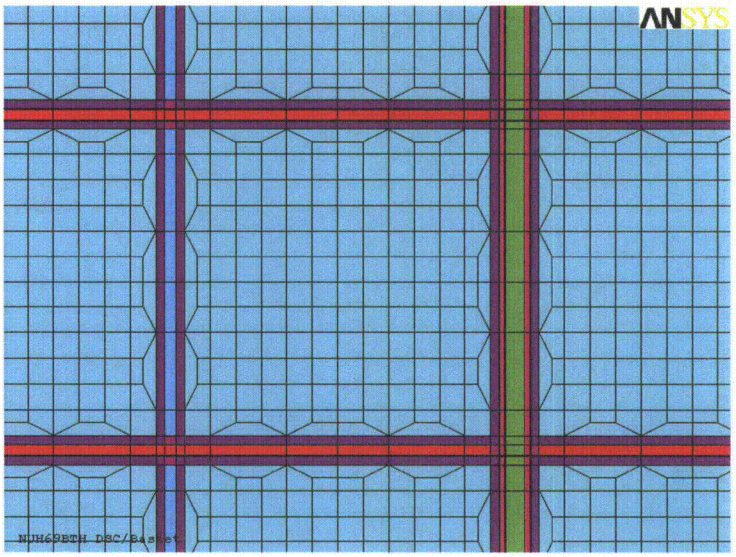


Mesh Density

Figure A.3–14
69BTH DSC/Basket – Cross Section

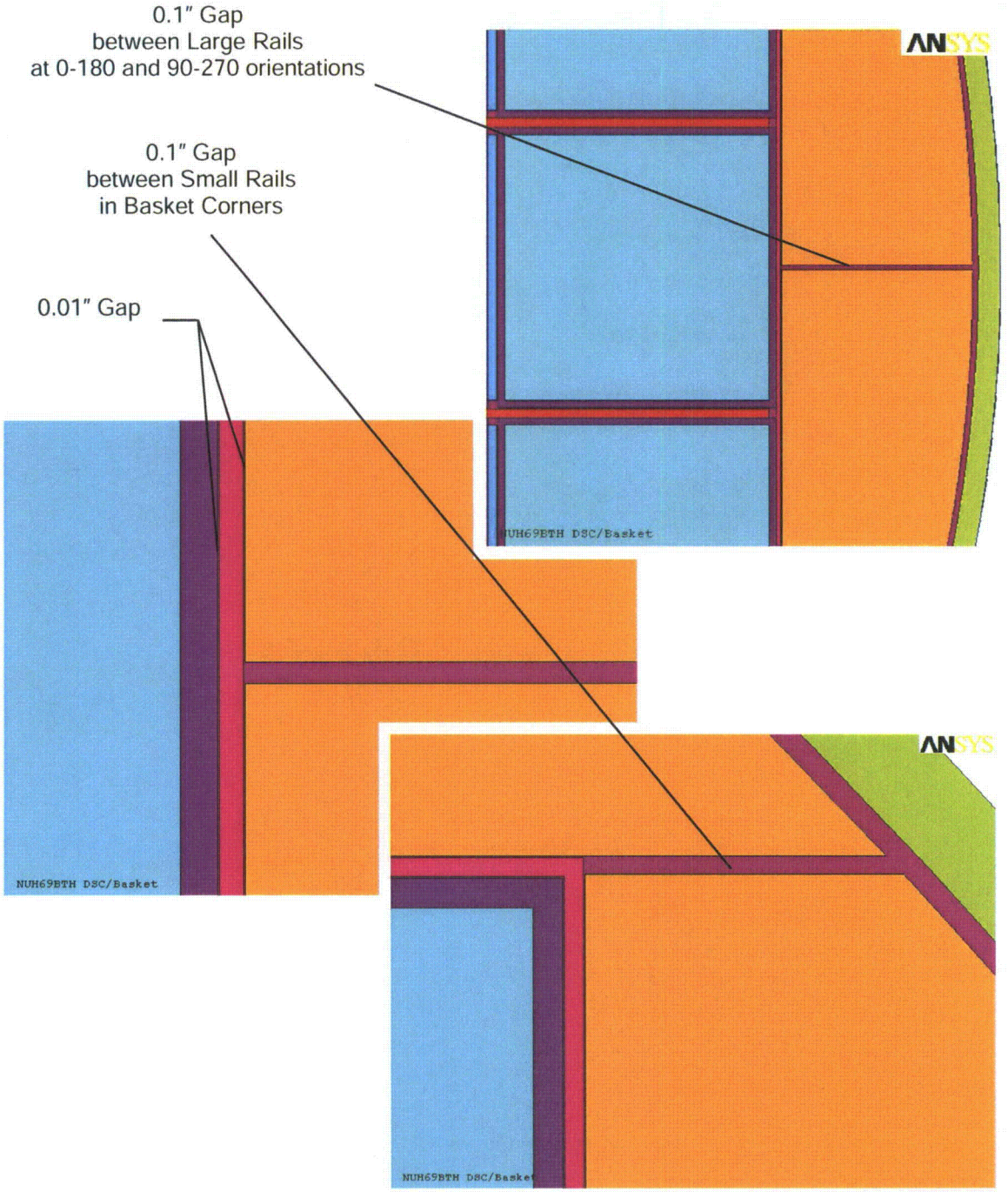


Figure A.3–15
69BTH DSC/Basket – Gaps between Rail Sections at Cross Section

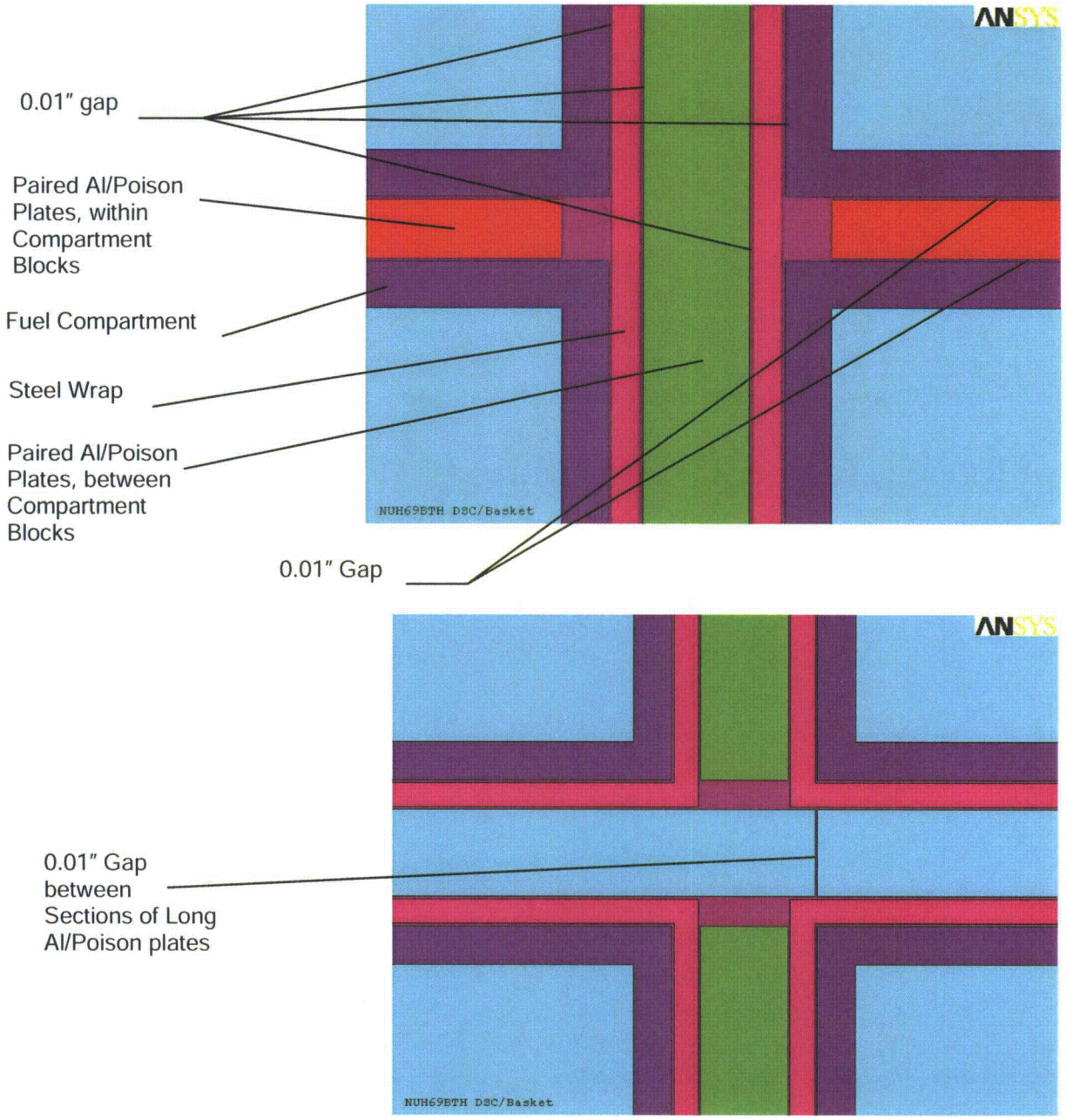


Figure A.3–16
69BTH DSC/Basket – Gaps between Basket Plates at Cross Section

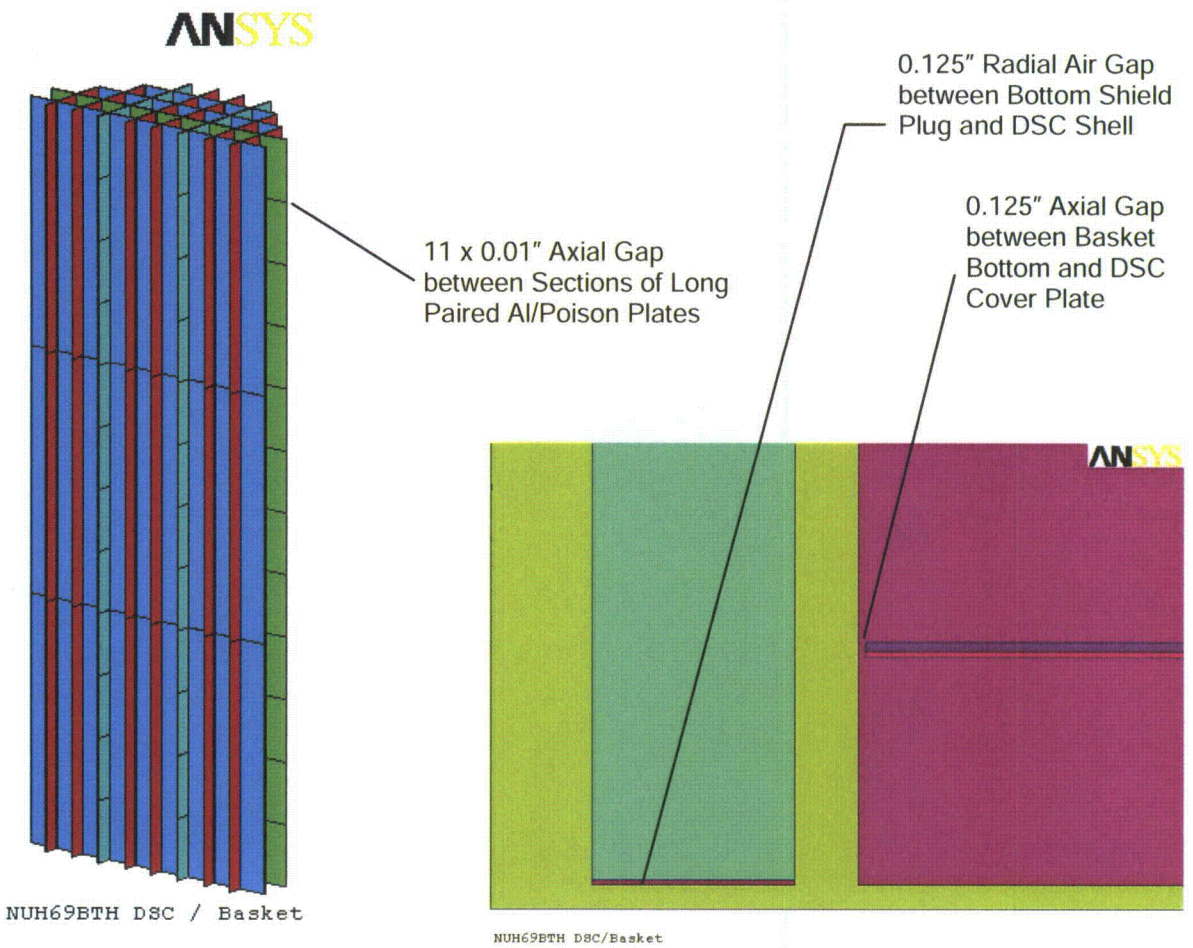


0.01" Axial Gap between Sections of Short Paired Al/Poison Plates

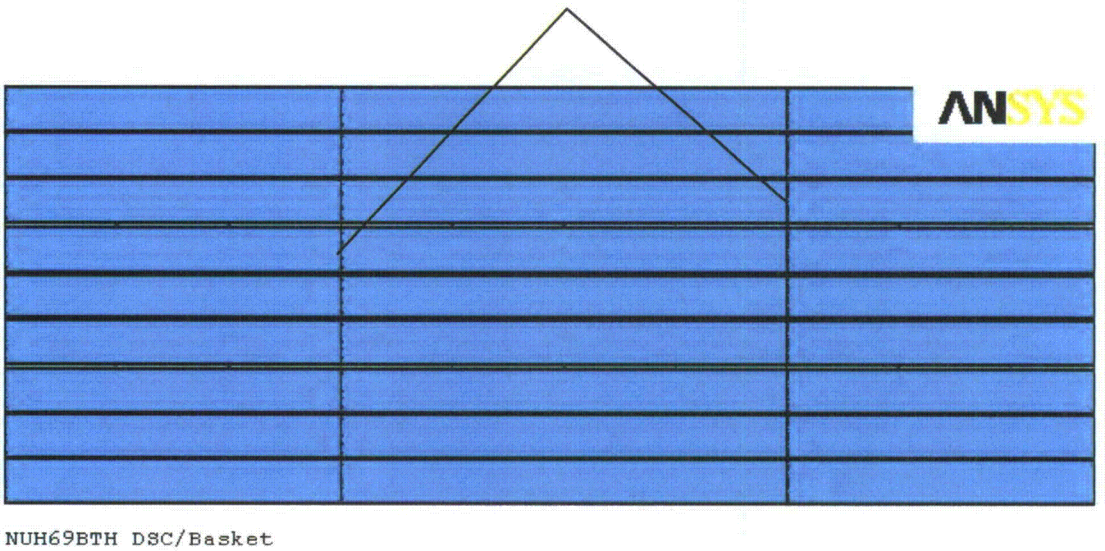


Figure A.3–17
69BTH DSC/Basket – Axial Gaps

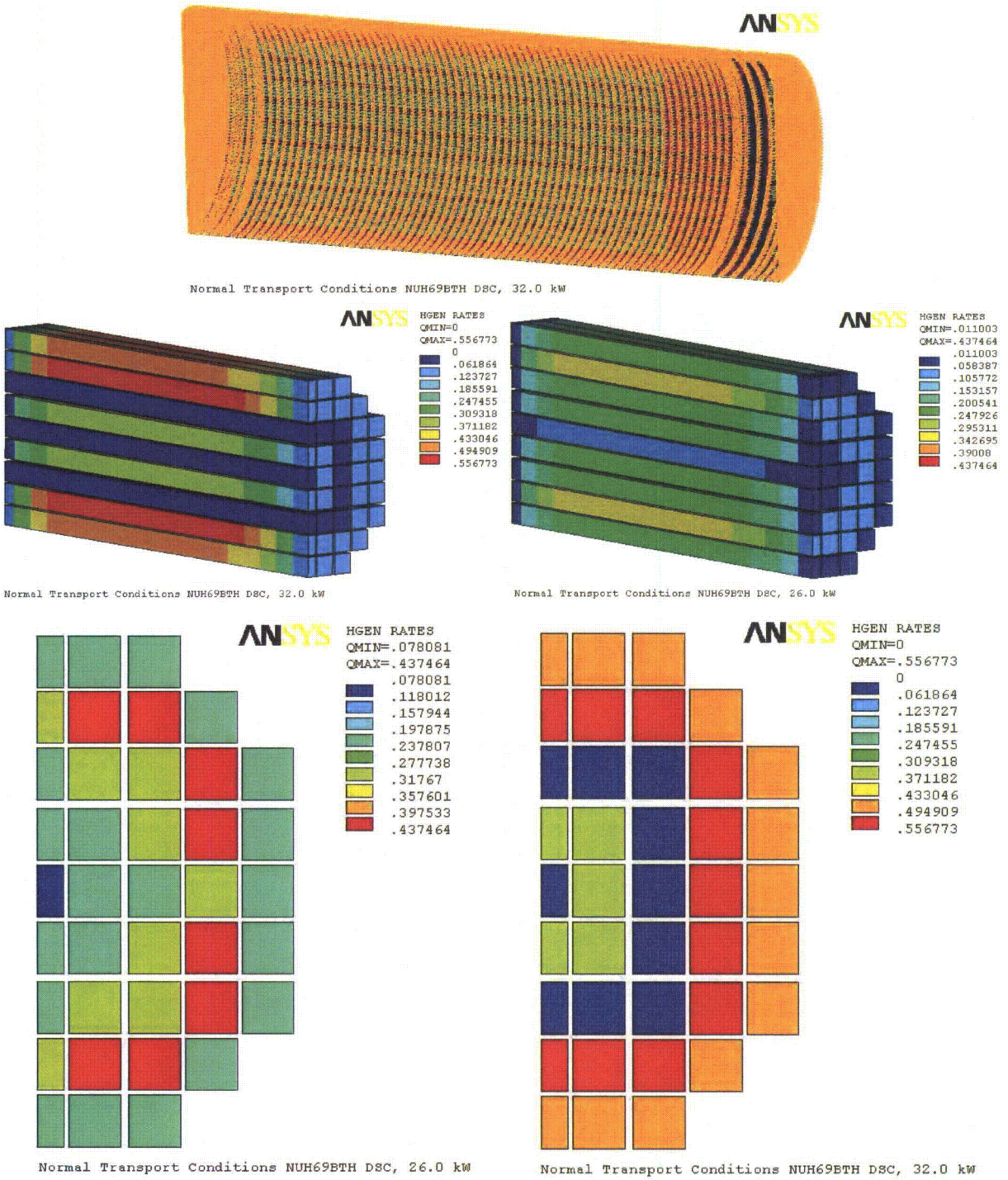


Figure A.3–18
Typical Boundary Conditions for the 69BTH Basket

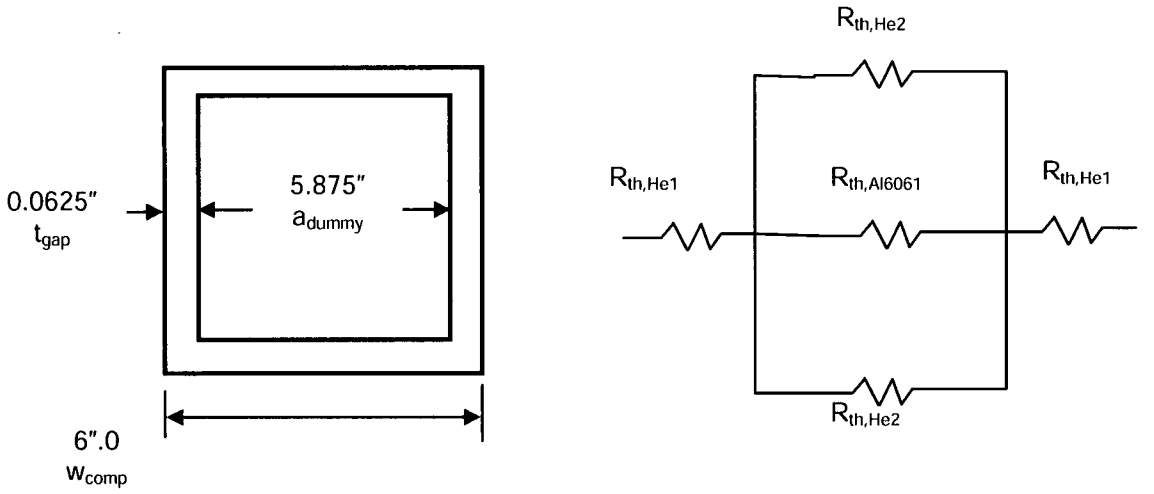


Figure A.3–19
Thermal Resistances for Aluminum Dummy Assembly

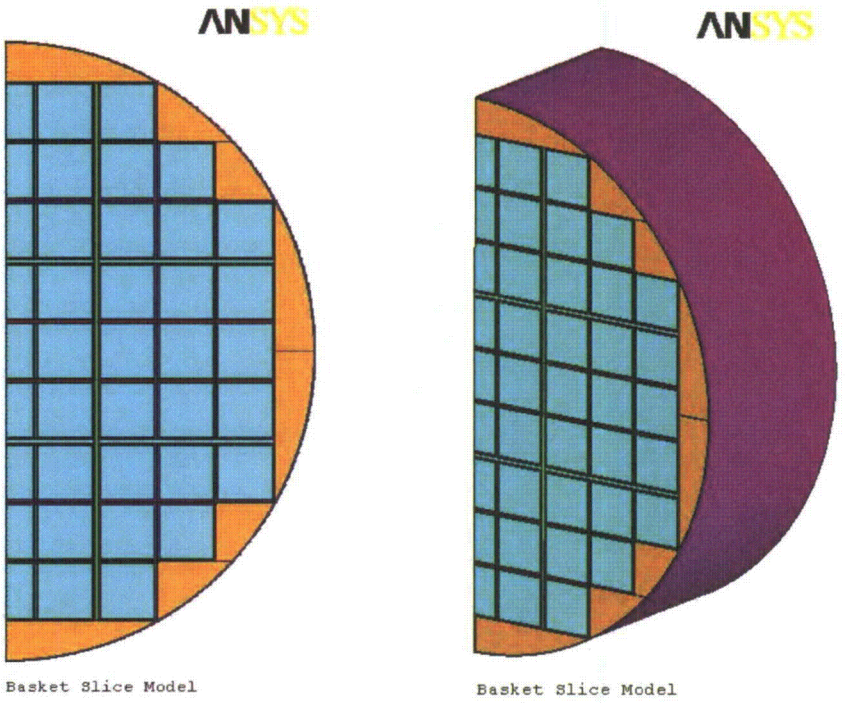


For 69BTH DSC

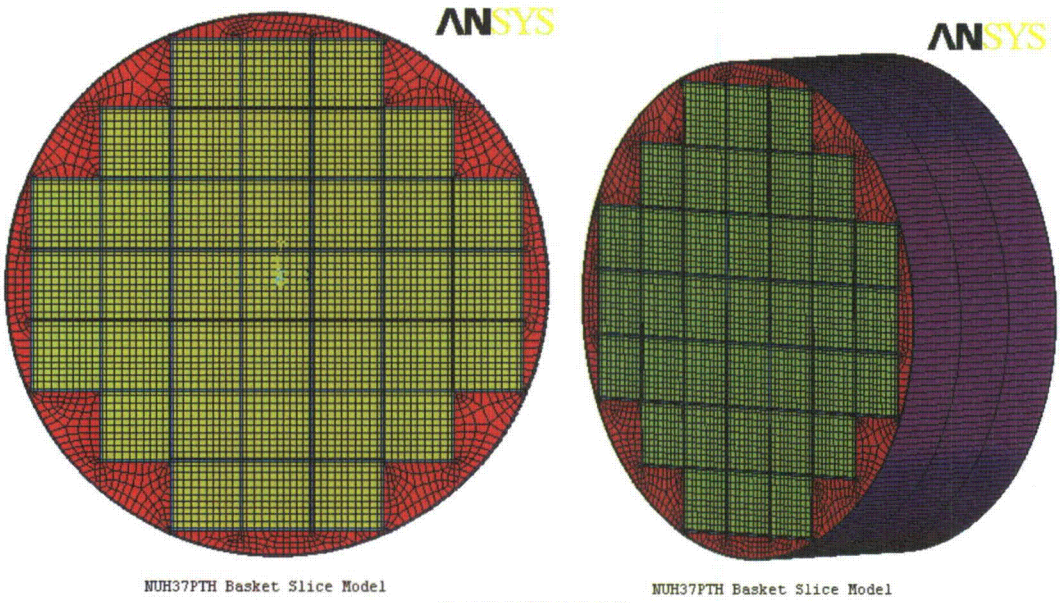


For 37PTH DSC

Figure A.3–20
Basket Slice Models

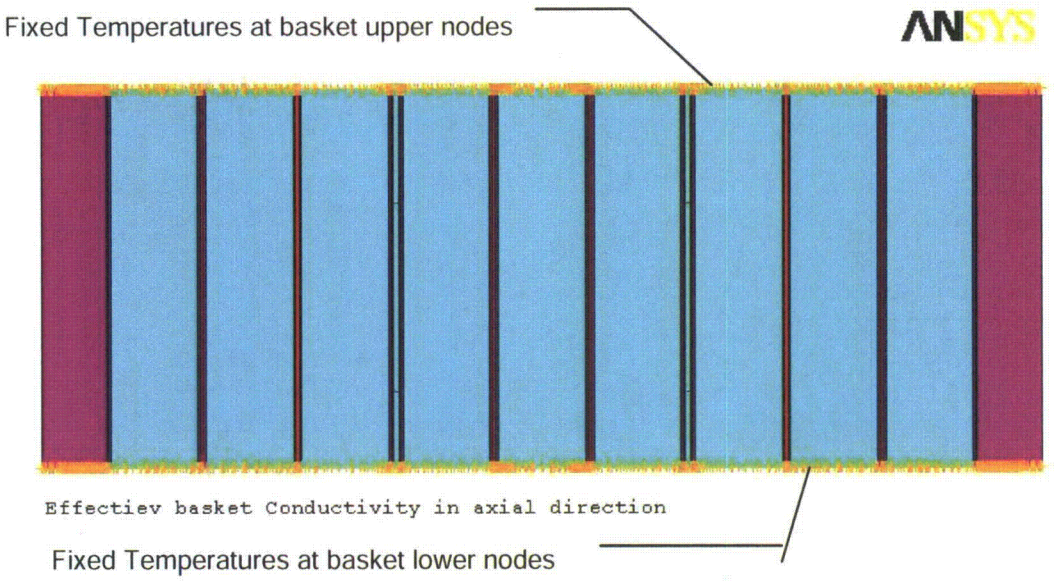


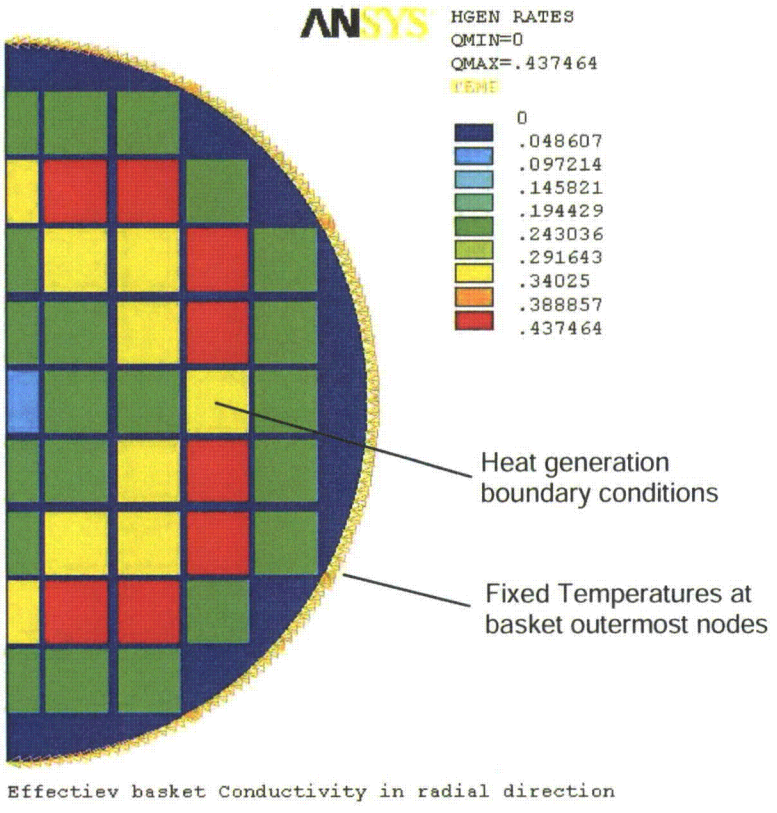


Figure A.3–21
Typical Boundary Conditions for the Basket Slice Model

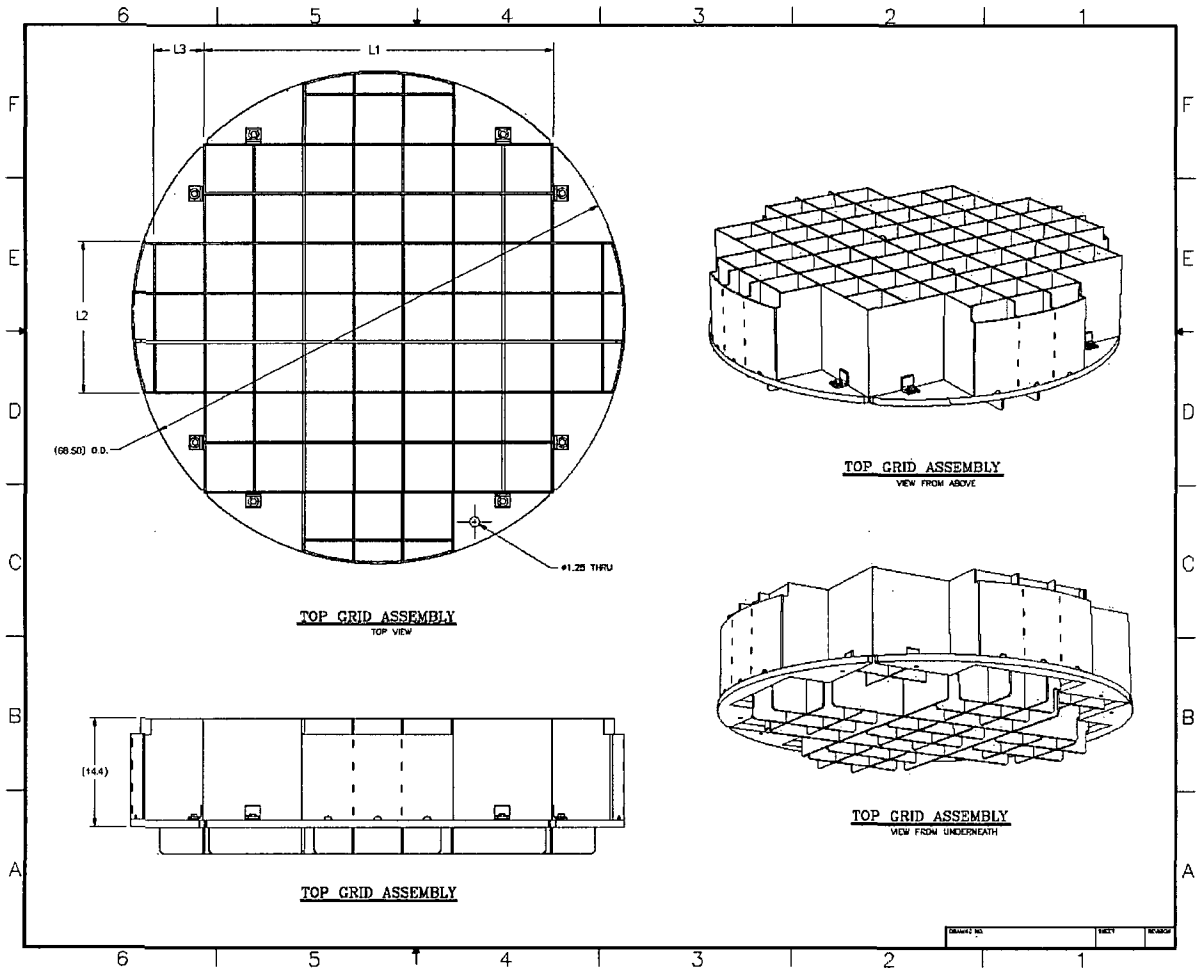


Figure A.3–22
Schematic View of Top Grid Assembly (Hold-Down Ring)

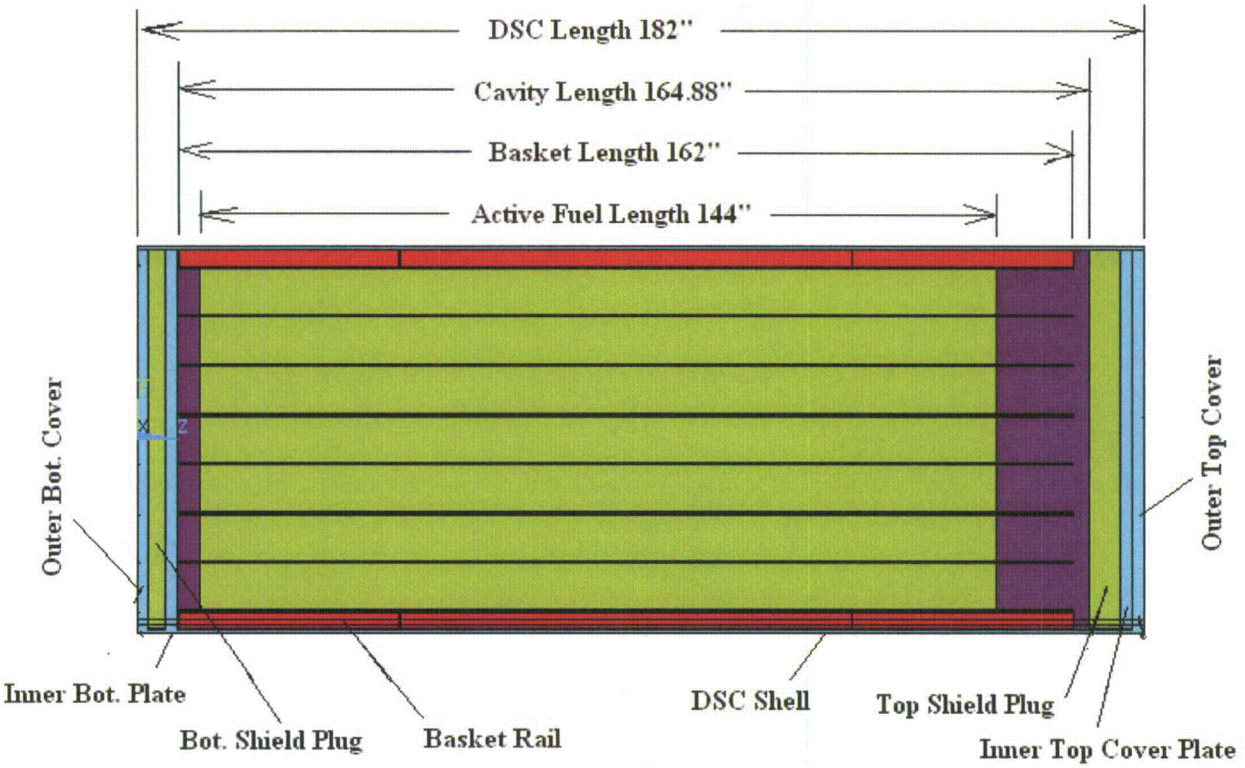


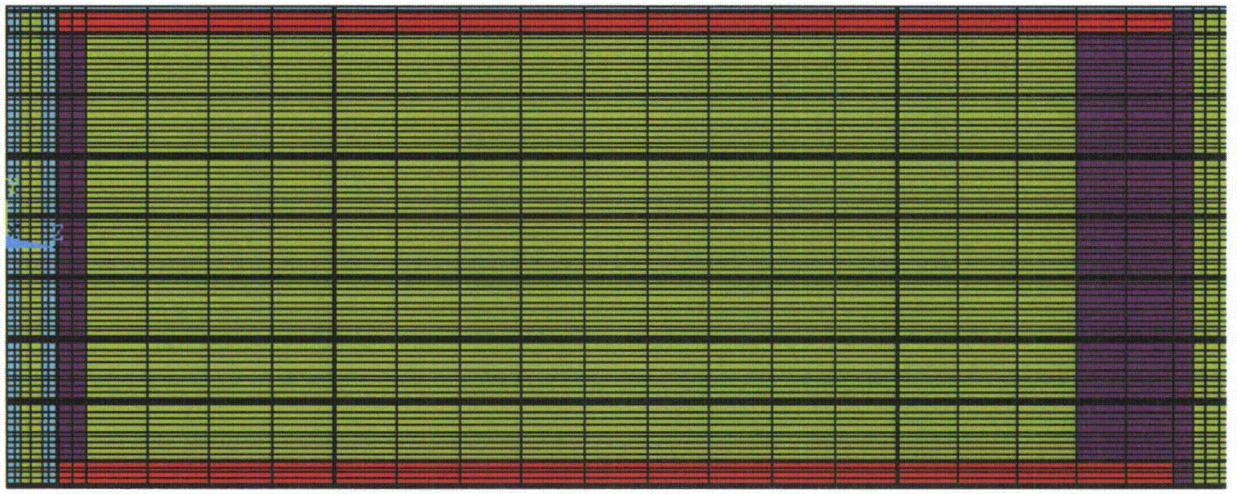

NUH37PTH DSC/Basket

**Mesh Density**

Figure A.3–23
Finite Element Model of the 37PTH DSC/Basket

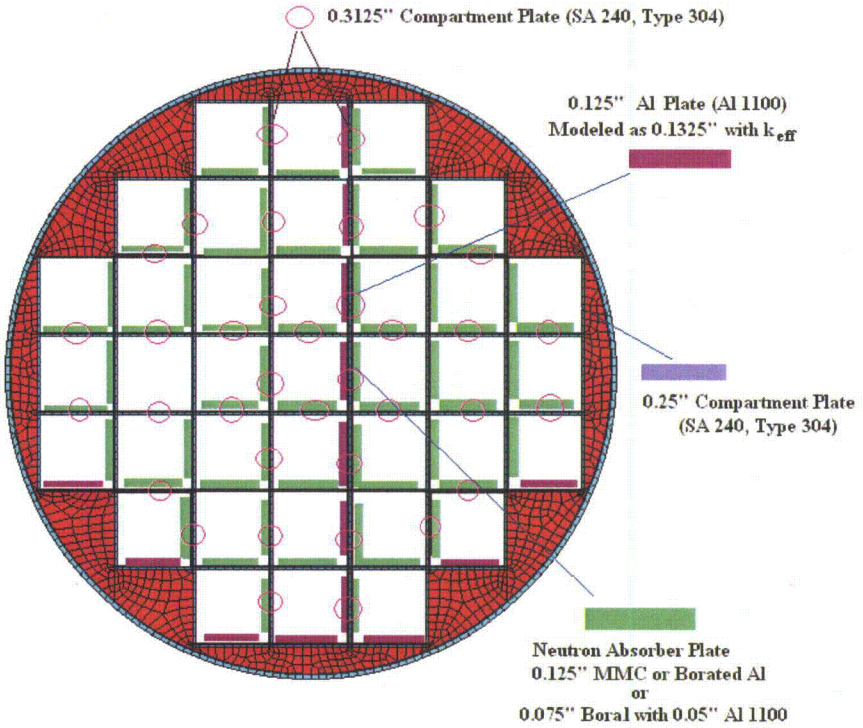


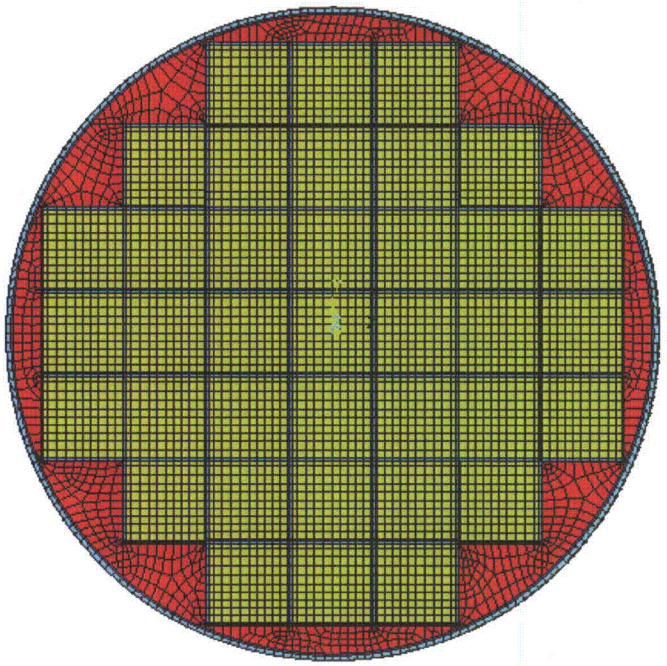

**Mesh Density**

Figure A.3–24
37PTH DSC/Basket – Cross Section and Details

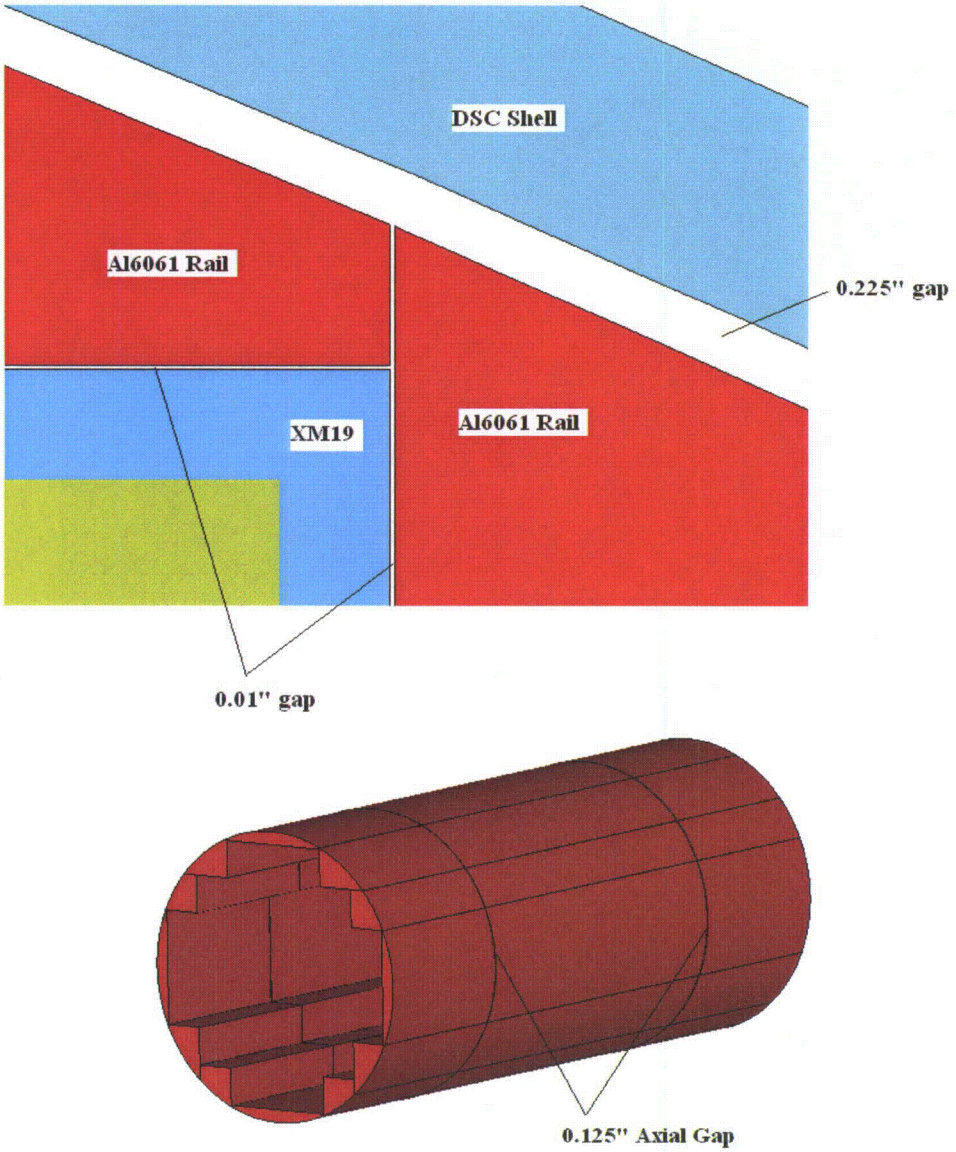


Figure A.3–25
37PTH DSC/Basket – Gaps between Rail Sections

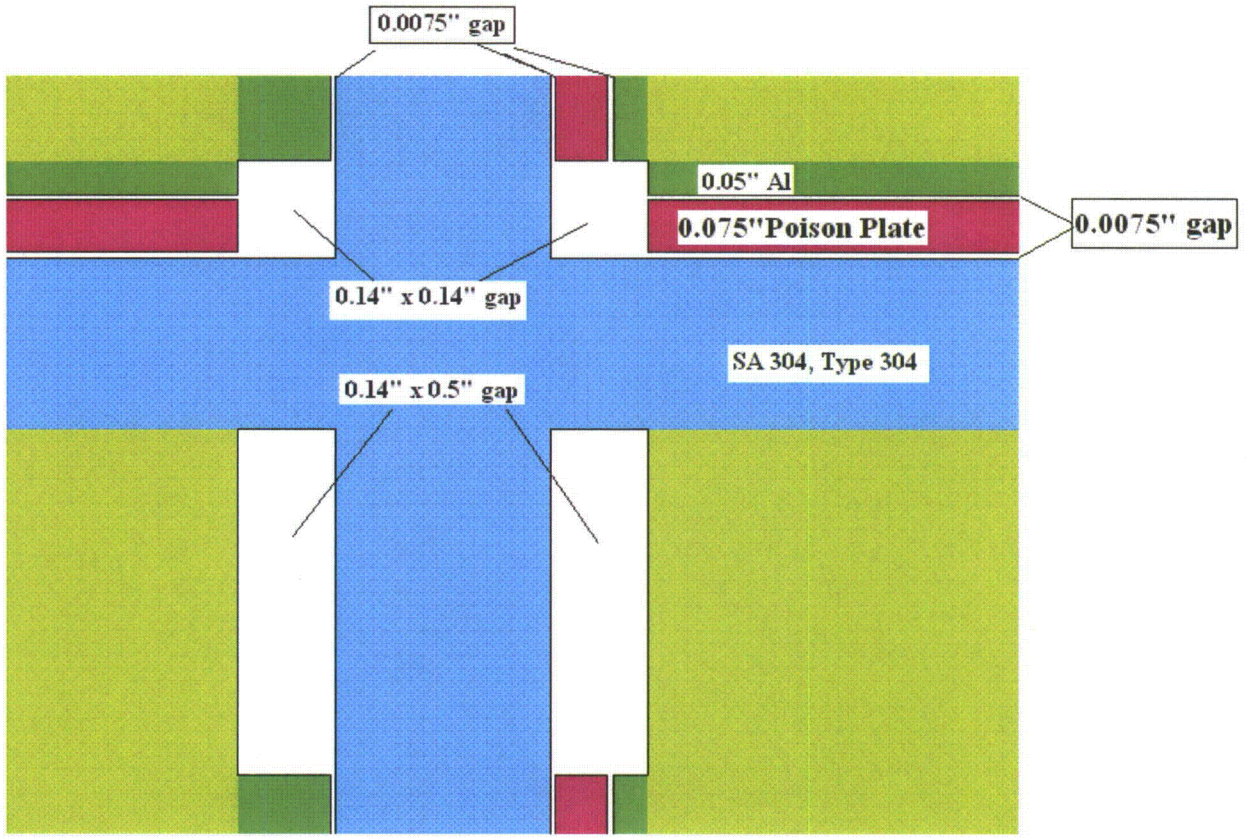


Figure A.3–26
37PTH DSC/Basket – Gaps between Basket Plates at Cross Section

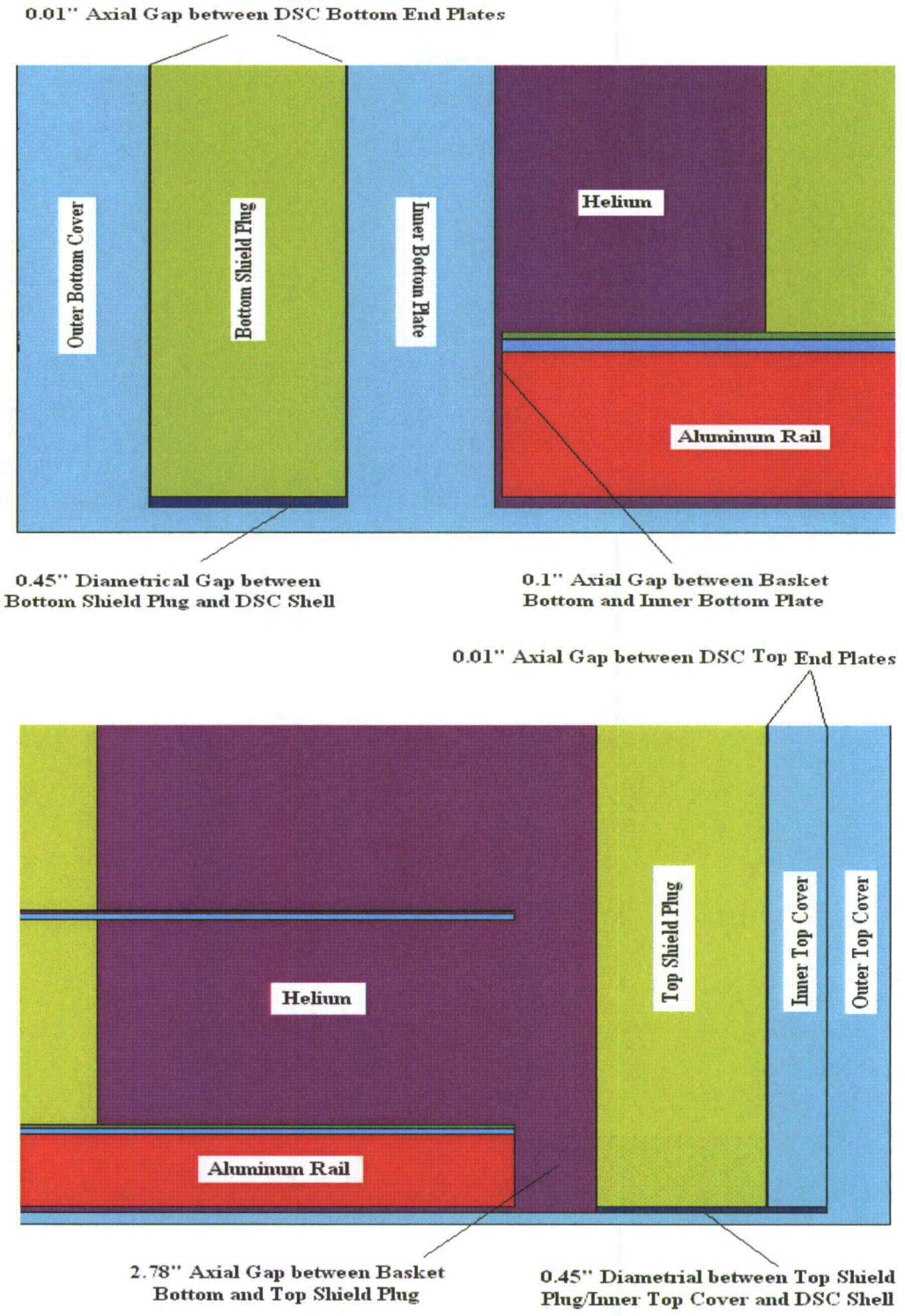


Figure A.3–27
37PTH DSC/Basket – Axial Gaps

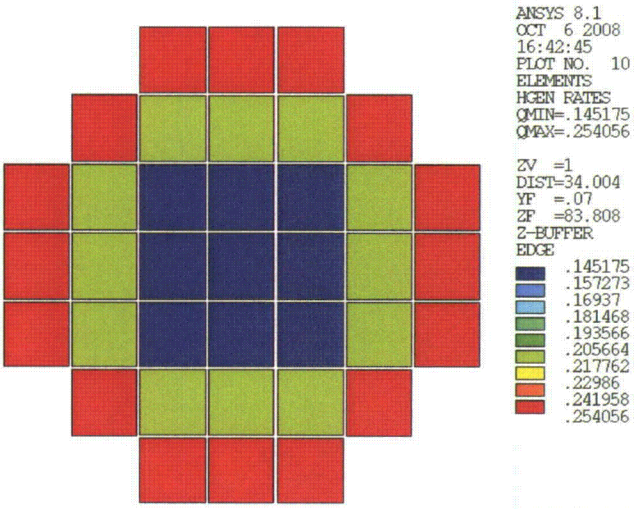


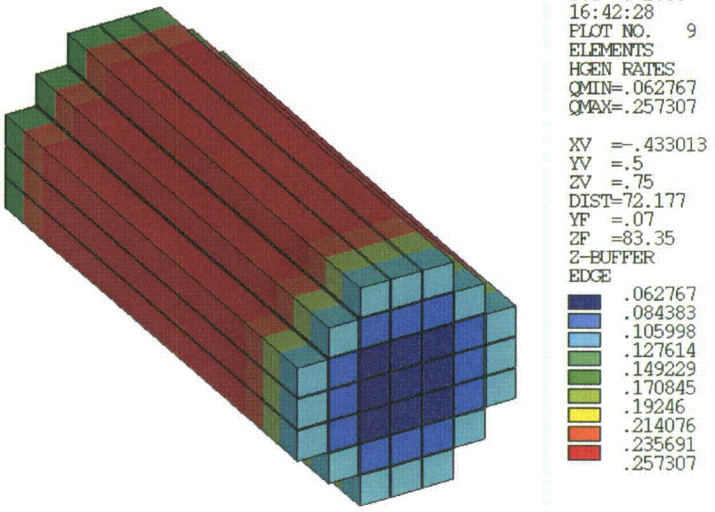


Heat Generation Boundary Conditions, 37PTH DSC, 22.0 kW

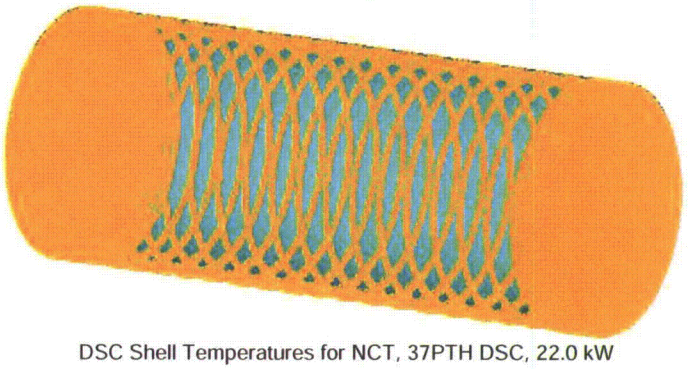

DSC Shell Temperatures for NCT, 37PTH DSC, 22.0 kW

Figure A.3–28
Typical Boundary Conditions for the 37PTH Basket

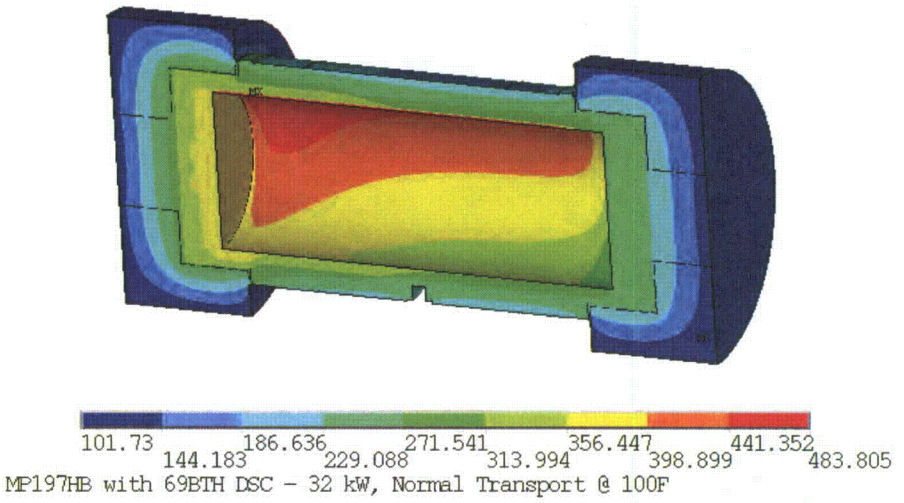


Figure A.3–29
Temperature Profiles for MP197HB Transport Cask
NCT, 100°F, Insolation, 69BTH DSC, 32 kW

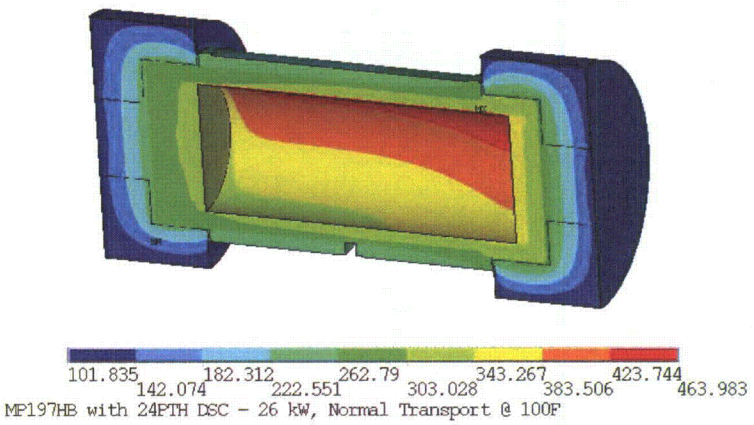


Figure A.3–30
Temperature Profiles for MP197HB Transport Cask
NCT, 100°F, Insolation, 24PTH DSC, 26 kW

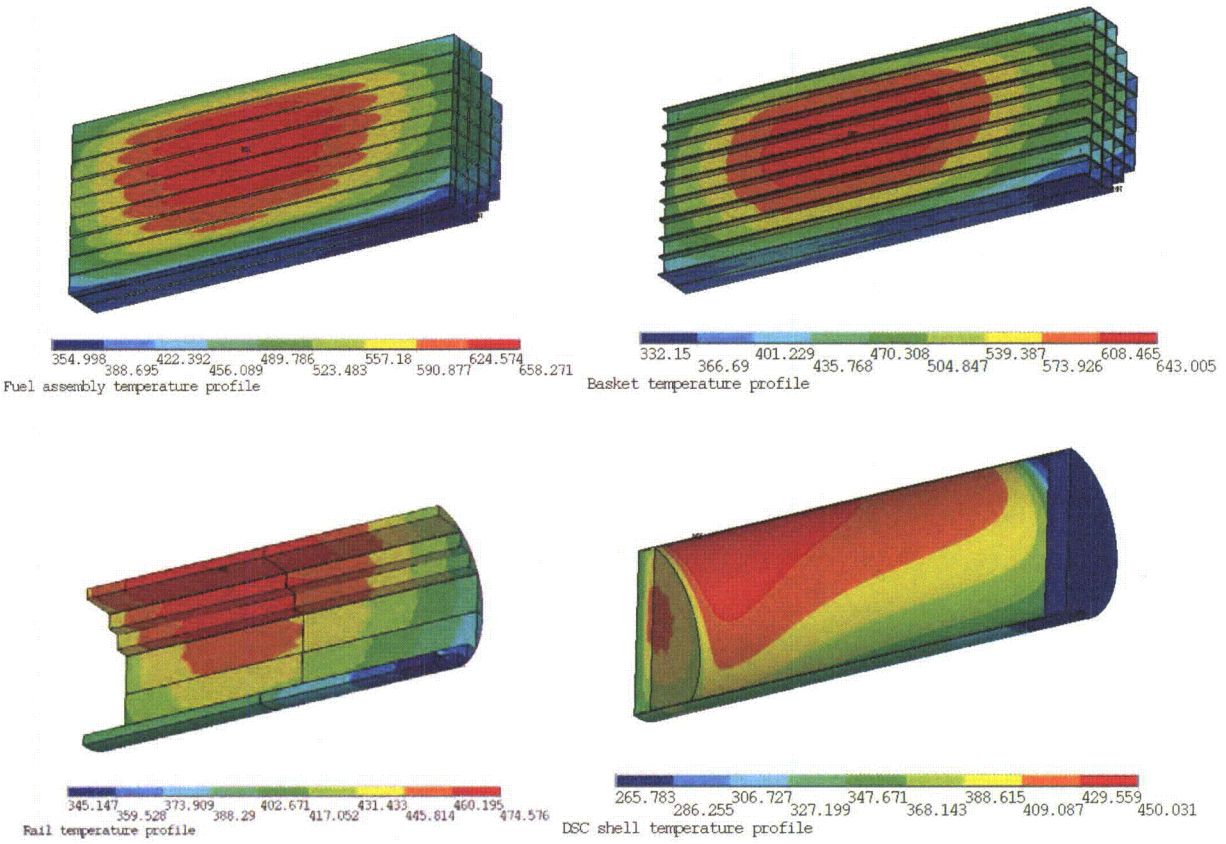


Figure A.3–31
Typical Temperature Distributions for 69BTH Basket
(NCT @ 100°F, HLZC#1, 26kW)

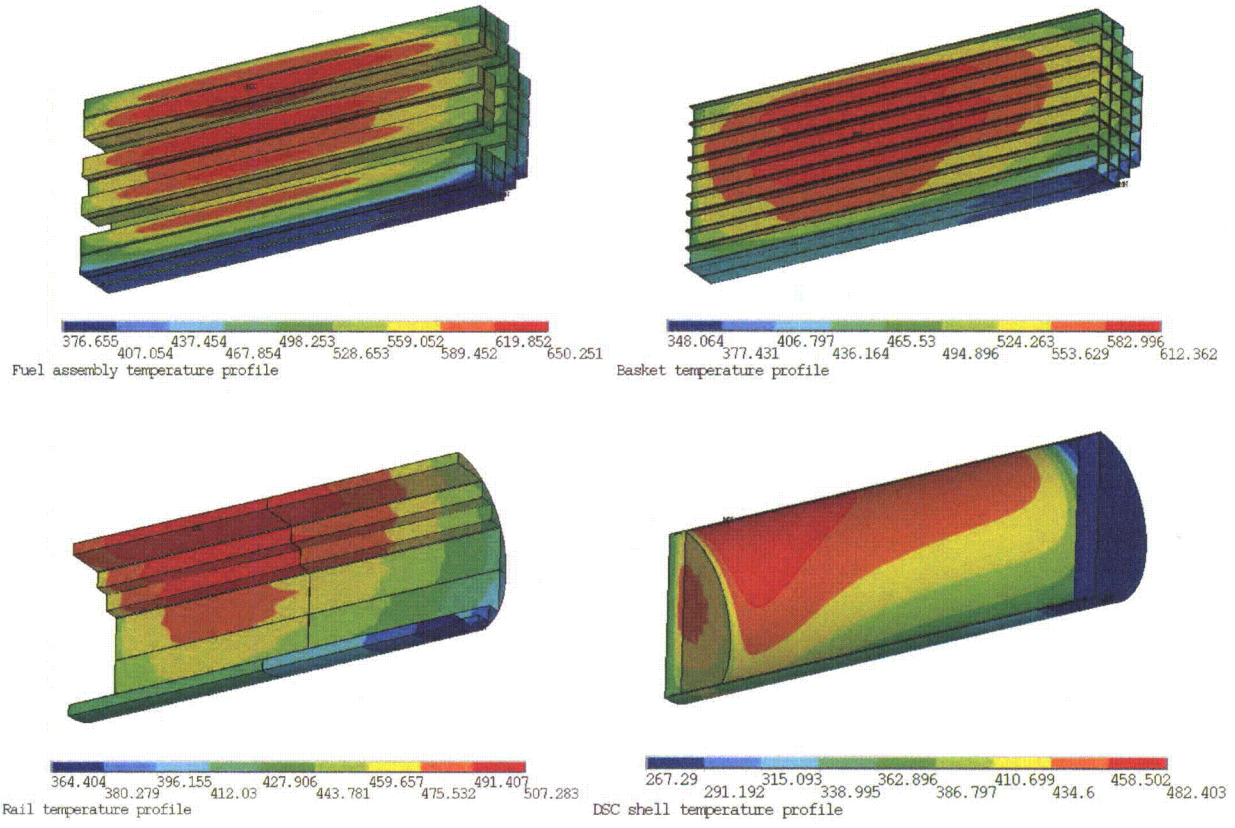


Figure A.3–32
Typical Temperature Distributions for 69BTH Basket
(NCT @ 100°F, HLZC#4, 32kW)

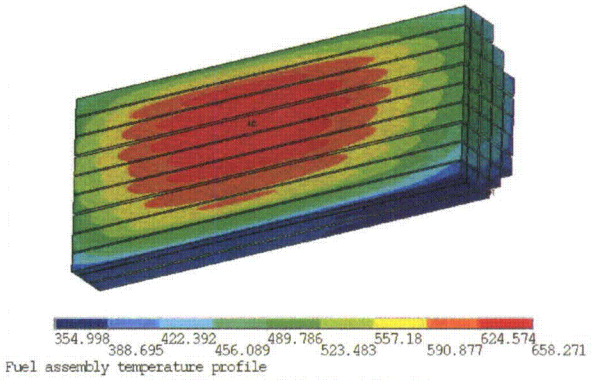


69BTH, HLZC#1, 26kW

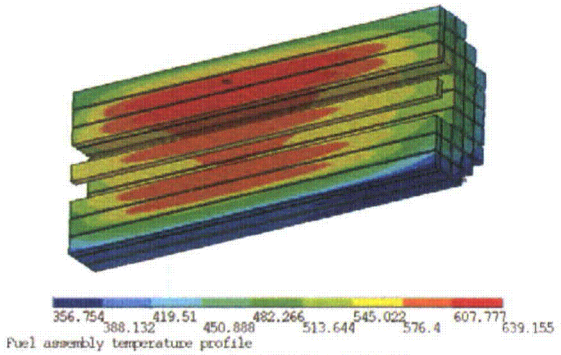


69BTH, HLZC#2, 26kW

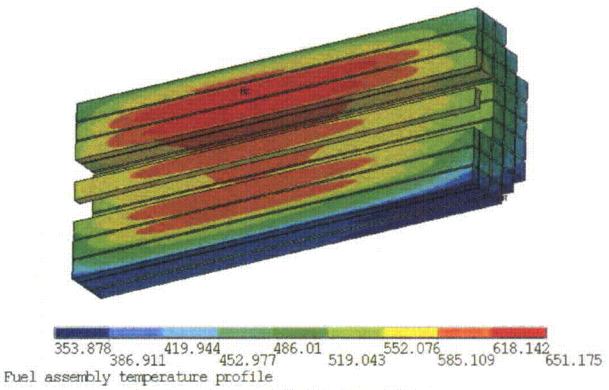


69BTH, HLZC#3, 29.2kW

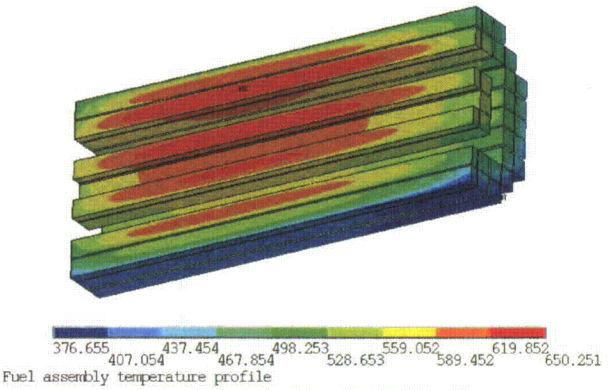


69BTH, HLZC#4, 32kW

Figure A.3–33
Temperature Distributions for Fuel Assemblies in 69BTH Basket
(NCT @ 100°F)

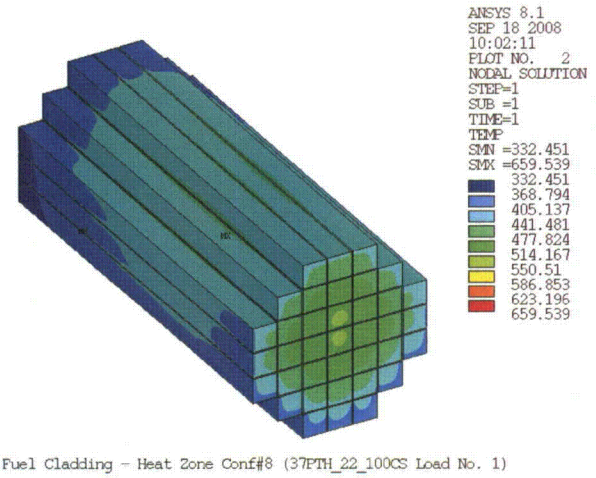


Fuel Cladding - Heat Zone Conf#8 (37PTH_22_100CS Load No. 1)

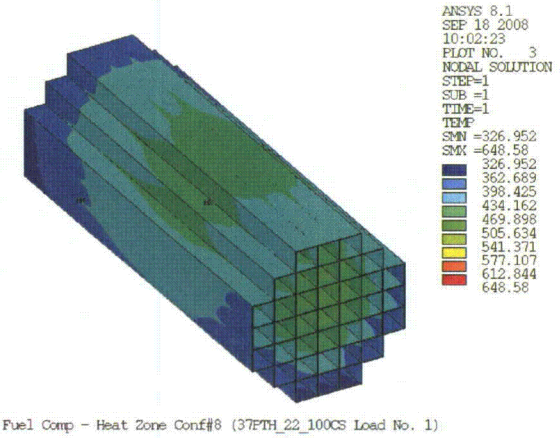


Fuel Comp - Heat Zone Conf#8 (37PTH_22_100CS Load No. 1)

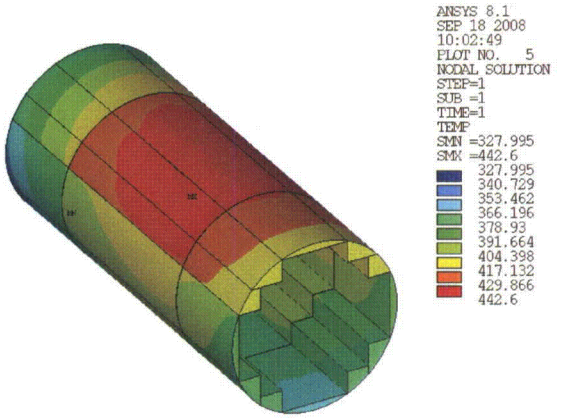


Rails - Heat Zone Conf#8 (37PTH_22_100CS Load No. 1)

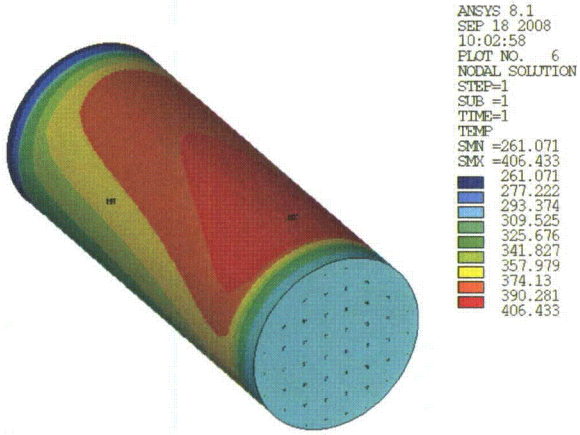


DSC Shell - Heat Zone Conf#8 (37PTH_22_100CS Load No. 1)

Figure A.3–34
Typical Temperature Distributions for 37PTH Basket
(NCT @ 100°F, 22 kW)

The shortest distance between TC and crushed impact limiter for end drop is 20.3".

**End Drop**

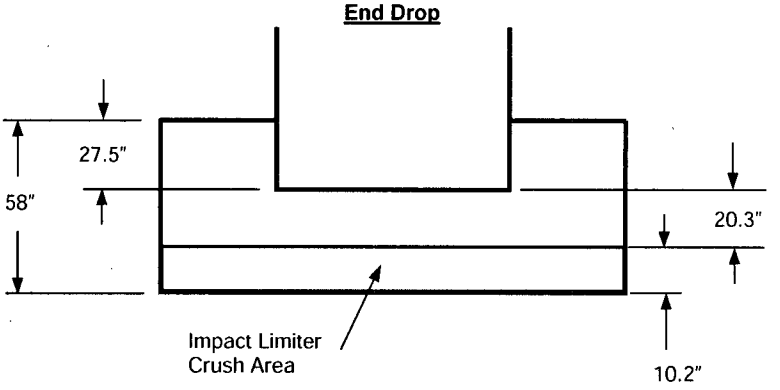


**Corner Drop**

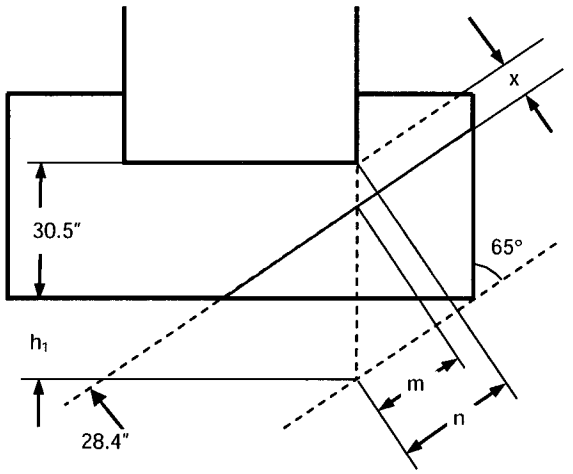


$OD_{IL}$ = Impact limiter OD = 126"
$OD_{TC}$ = Cask OD = 84.5"
$h_1 = [(OD_{IL}-OD_{TC}) / 2] / \tan 65 = 9.7"$
$n = (30.5 + h_1) \cos 65 = 17.0"$
$m = 28.4 / \tan 65 = 13.2"$

The shortest distance between TC and crushed impact limiter for corner drop is:

$x = (n - m) \tan 65 = 8.0"$

Figure A.3–35
Impact Limiter Crush Areas for MP197HB
(Side, End, and Corner Drop)

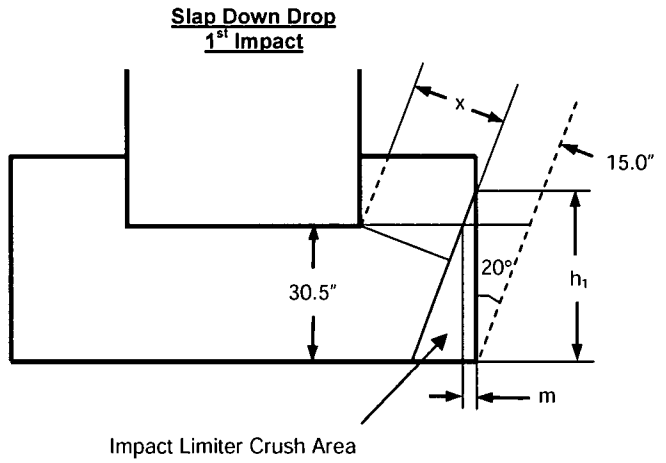


$OD_{IL}$ = Impact limiter OD = 126"

$OD_{TC}$ = Cask OD = 84.5"

$h_1$ = 15 / sin 20 = 43.9"

m = ($h_1$ – 30.5) tan 20 = 4.9"

The shortest distance between TC and crushed impact limiter for slap down drop, 1st impact is:

x = [($OD_{IL}$ – $OD_{TC}$) /2 – m] cos 20 = 14.9"

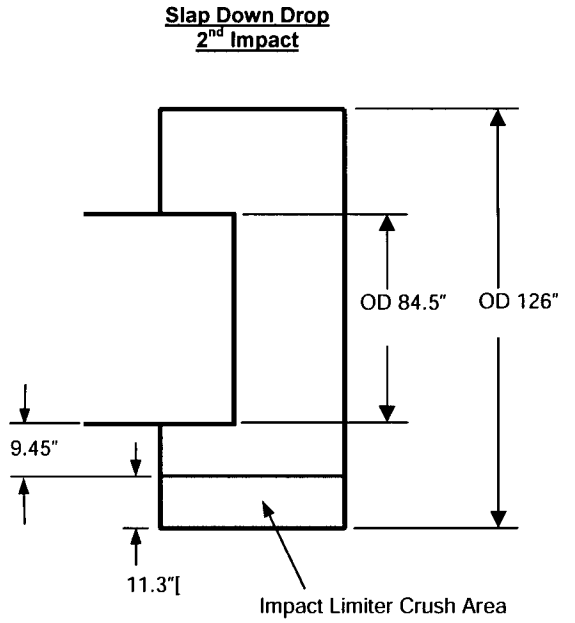


The shortest distance between TC and crushed impact limiter for slap down drop, 2nd impact is 9.45"

Figure A.3–36
Impact Limiter Crush Areas for MP197HB
(Slap Down)

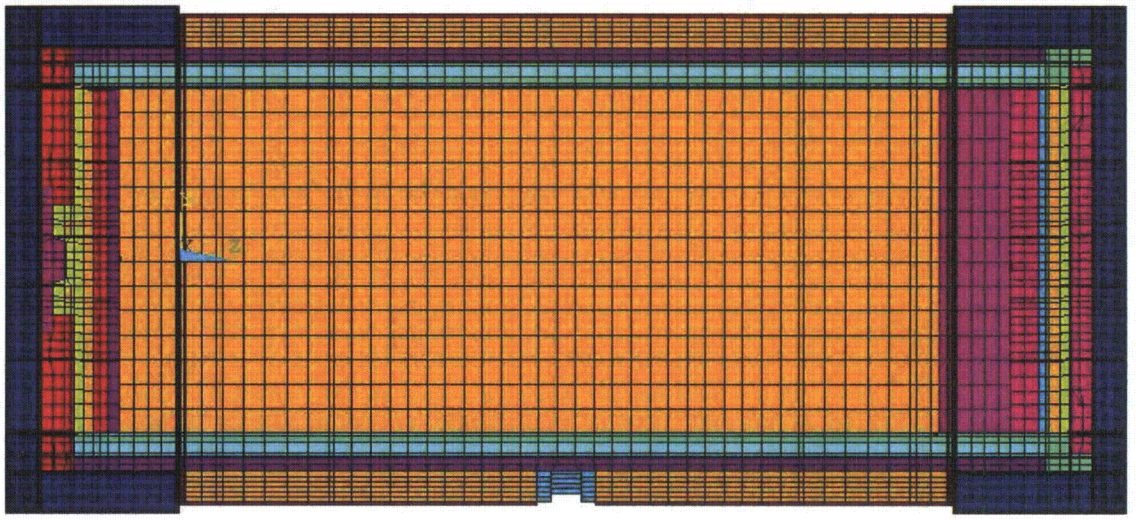

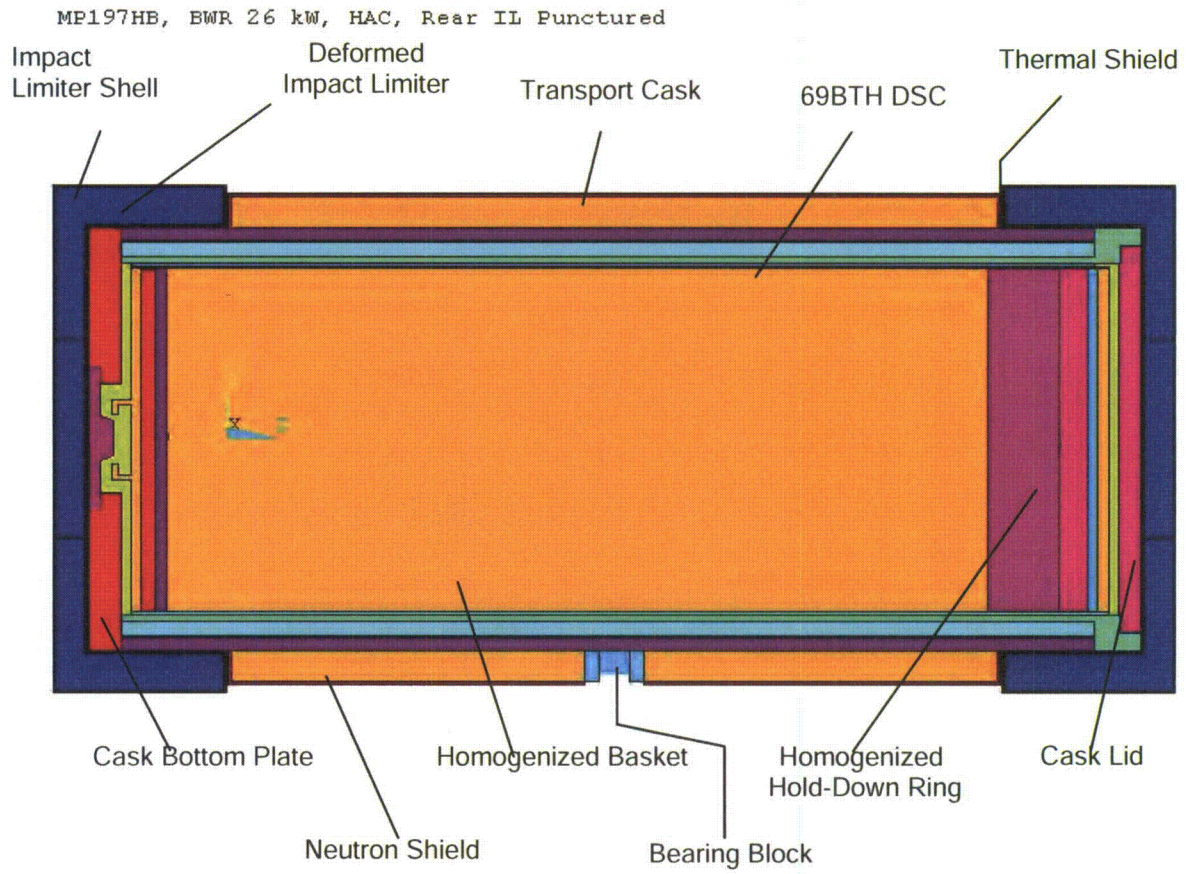


Figure A.3–37
Finite Element Model of TC with Deformed Impact Limiters

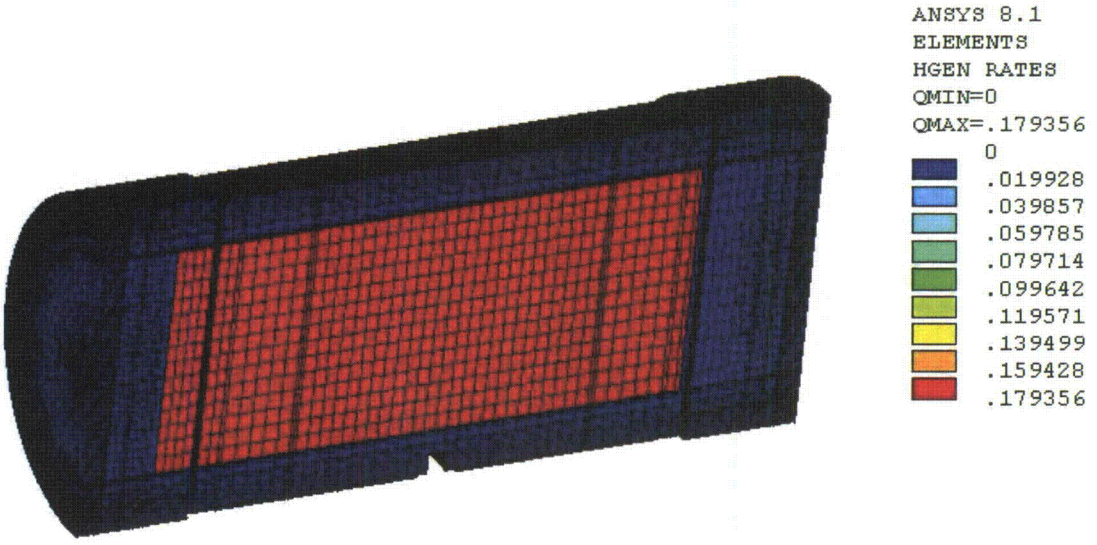


Heat Generation Boundary Conditions for MP197HB + 69BTH DSC, 32 kW, HAC

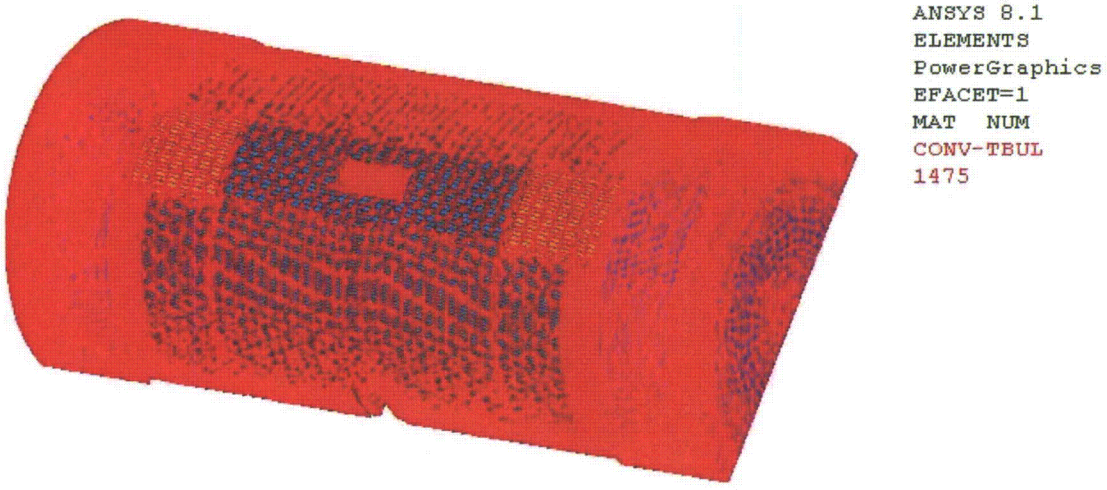


Convection & Radiation from Fire to MP197HB + 69BTH DSC, 32 kW

Figure A.3–38
Typical Boundary Conditions during Fire Conditions

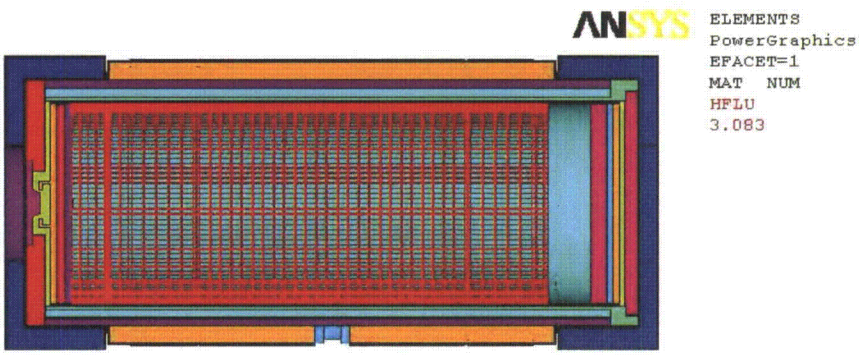


Decay Heat Flux for Cool-Down Conditions

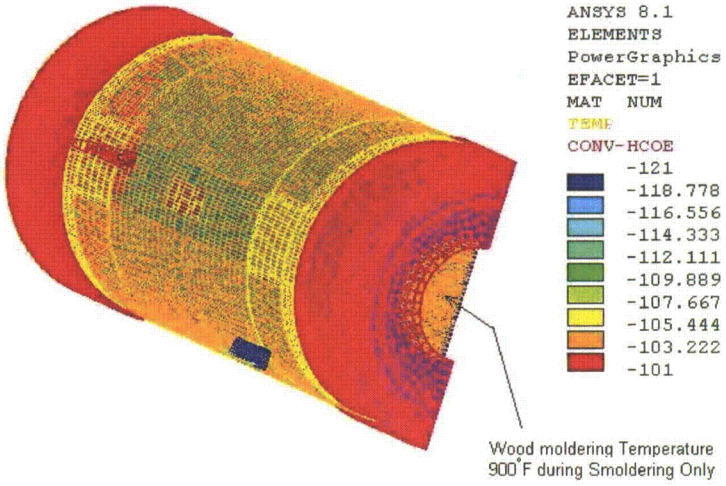


Convection & Radiation to Ambient, MP197HB + 69BTH DSC, 32 kW, Smoldering/Cool-Down

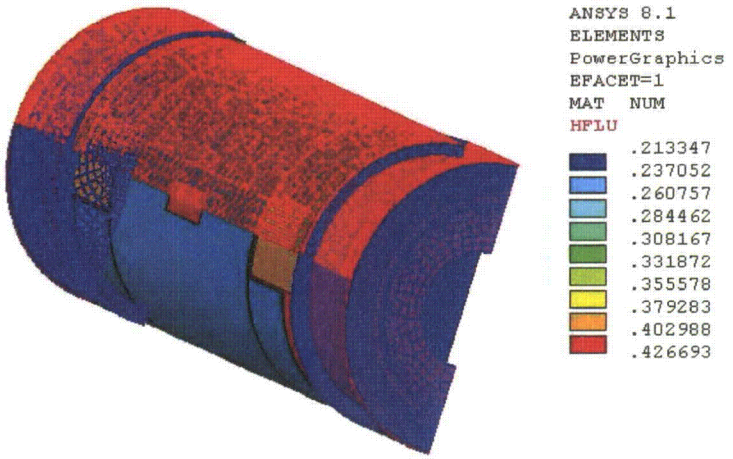


Insolance, MP197HB + 69BTH DSC, 32 kW, Smoldering/Cool-Down

Figure A.3–39
Typical Boundary Conditions for Smoldering/Cool-Down Periods

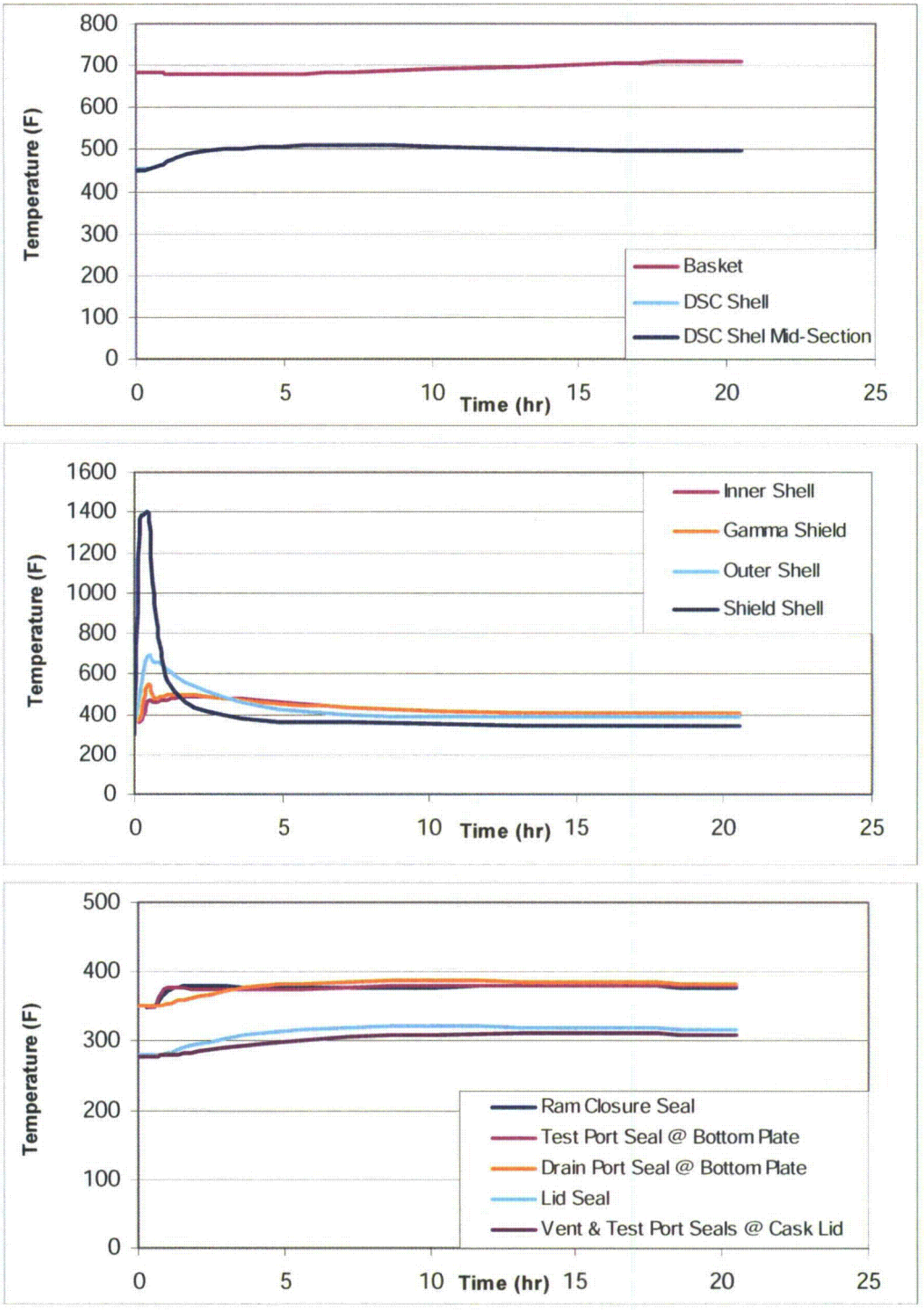


Figure A.3–40
Time-Temperature Histories for TC/DSC Shell
HAC, with External Fins (Melted after Fire), 69BTH DSC, 32 kW

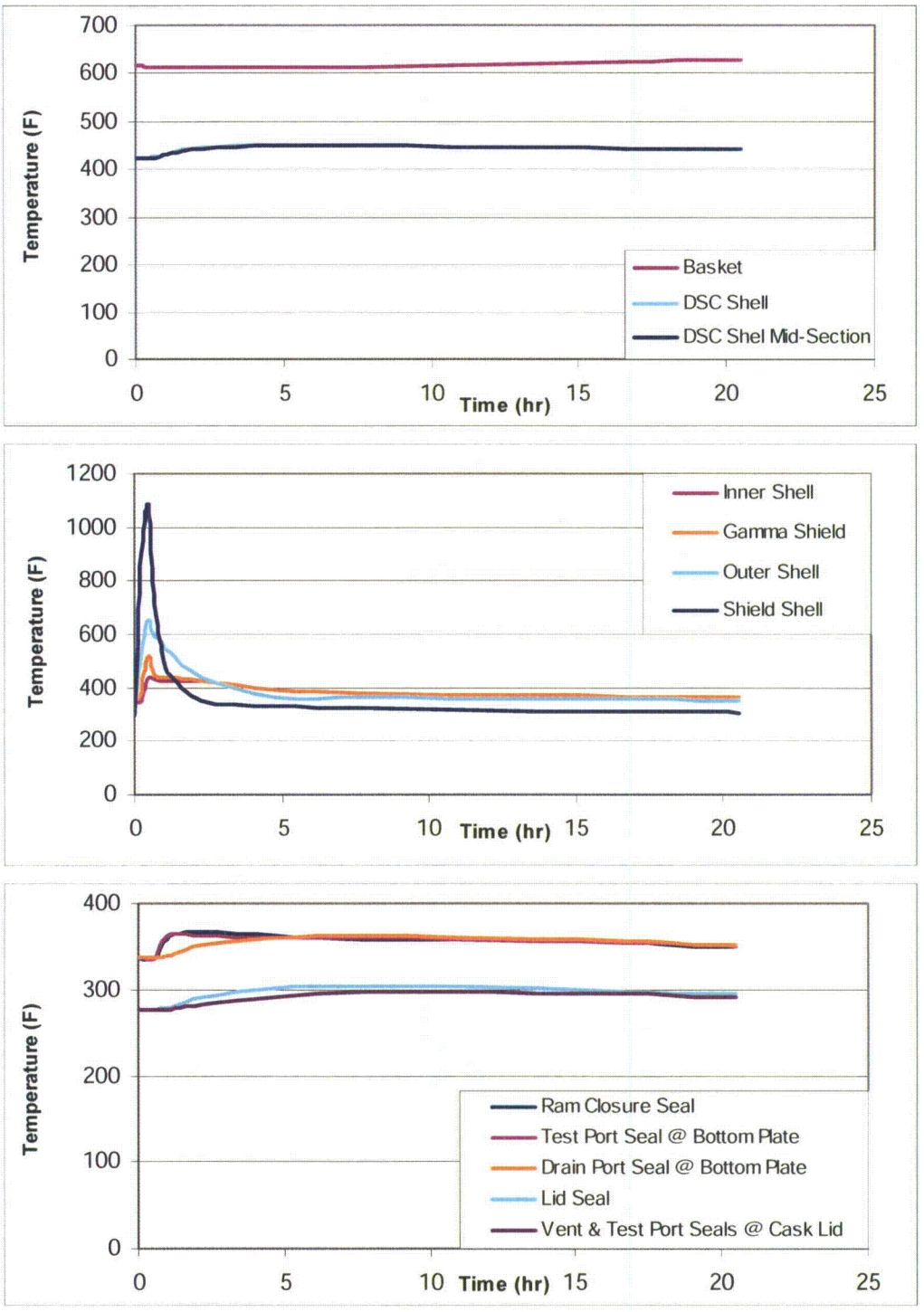


Figure A.3–41
Time-Temperature Histories for TC/DSC Shell
HAC, w/o Fins, 69BTH DSC, 26 kW

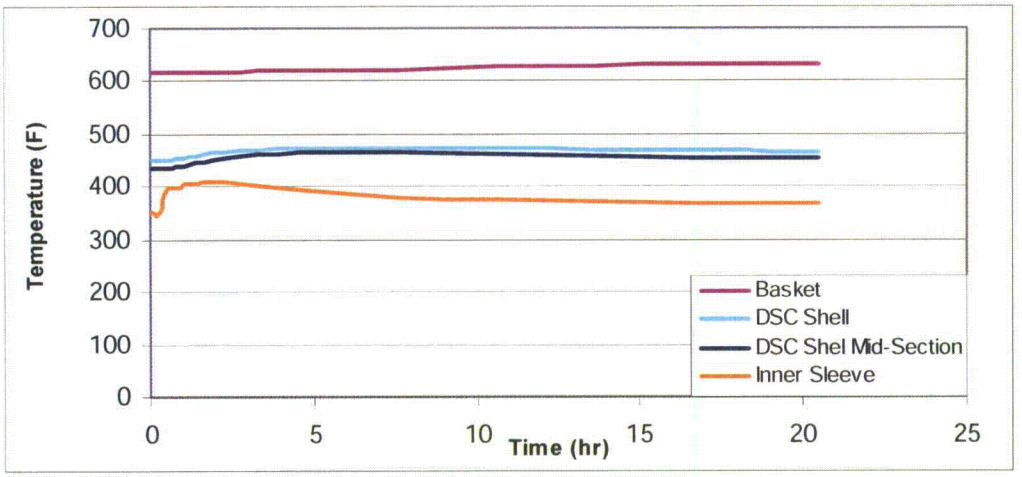


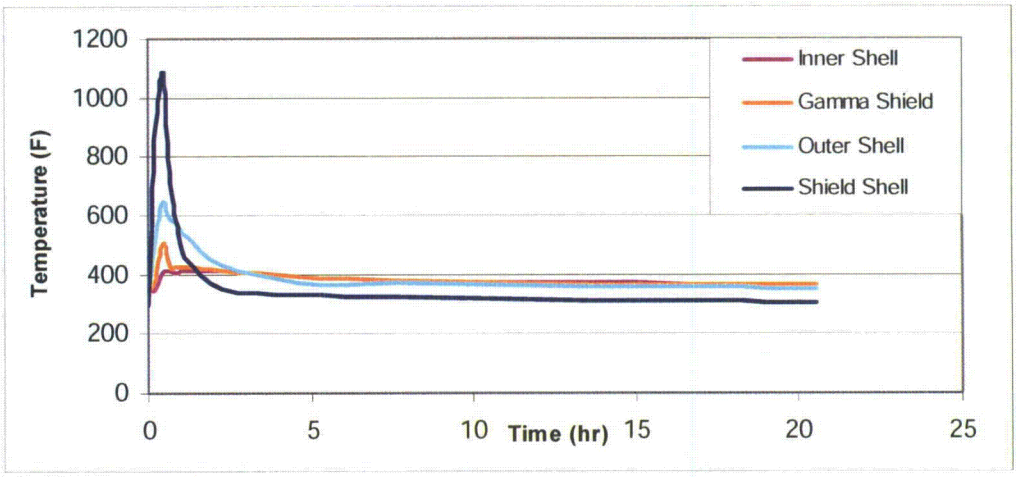


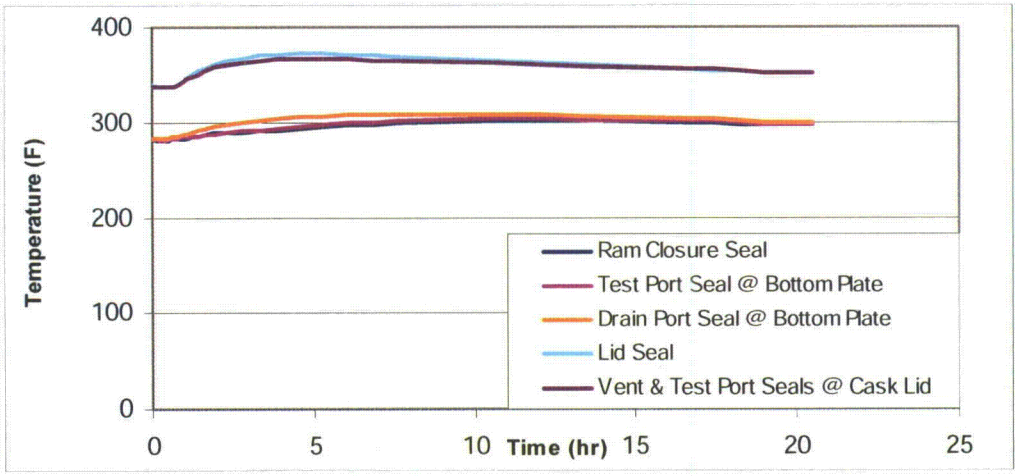


Figure A.3–42
Time-Temperature Histories for TC/DSC Shell
HAC, w/o Fins, 24PTH DSC, 26 kW

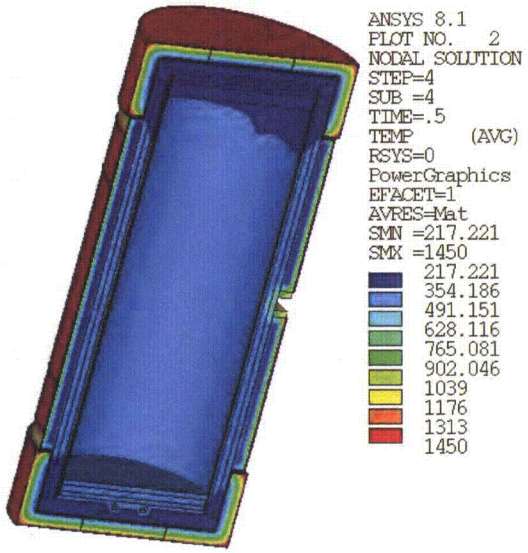


MP197HB w/ Fins, BWR 32 kW, End of Fire

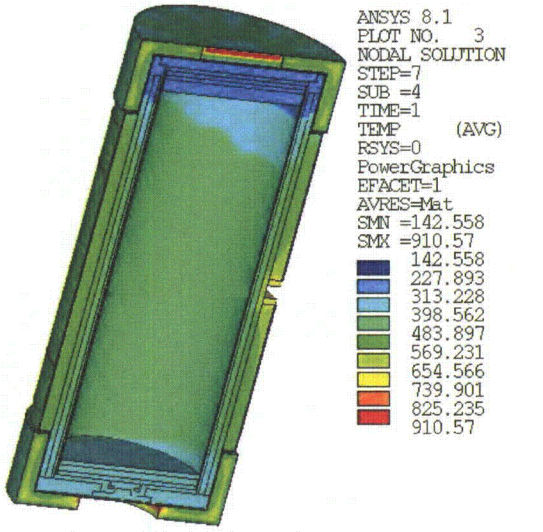


MP197HB w/ Fins, BWR 32 kW, Smoldering Wood after Fire

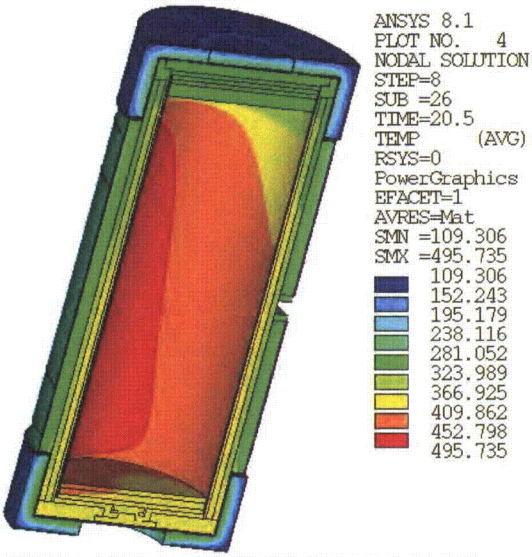


MP197HB w/ Fins, BWR 32 kW, Puncture Rear IL, 20 hrs after Fire

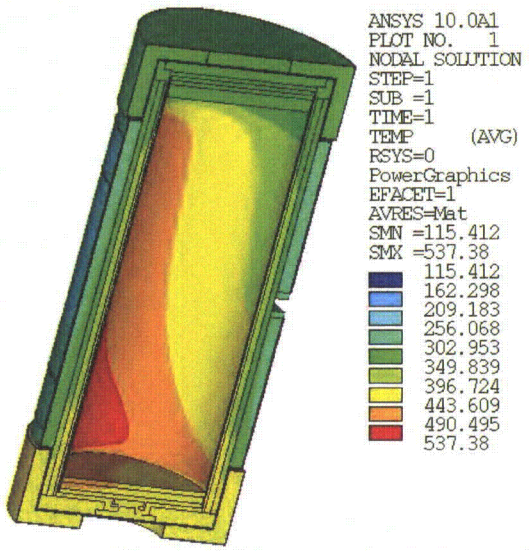


Finned MP197HB, BWR 32 kW, CD, Rear IL Punctured

Figure A.3–43
Temperature Profiles for MP197HB Transport Cask
HAC, 69BTH DSC, 32 kW, with External Fins
(Melted after Fire)

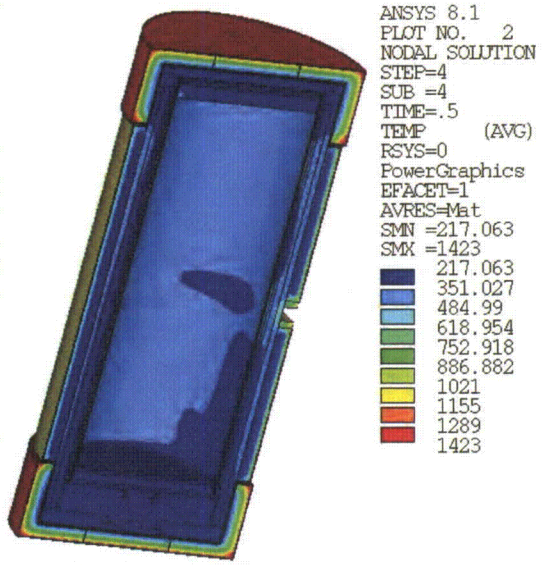


MP197HB, PWR 26 kW, End of Fire

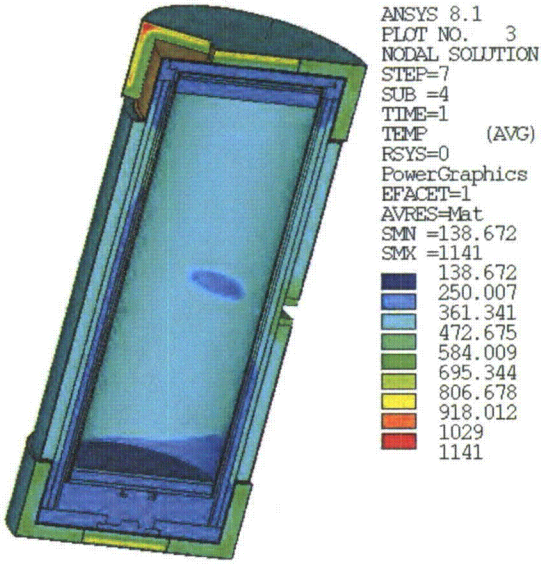


MP197HB, PWR 26 kW, Smoldering Wood after Fire

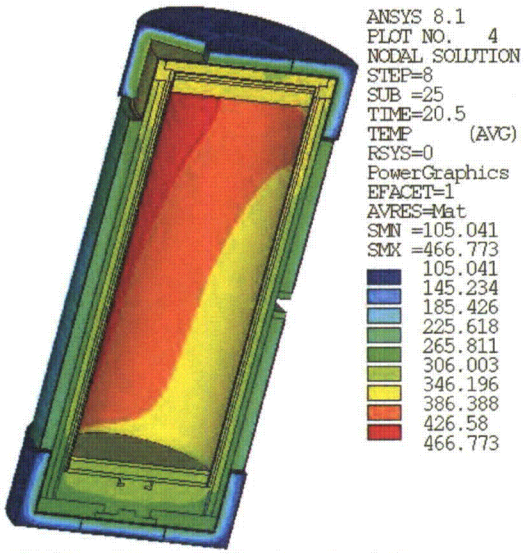


MP197HB, PWR 26 kW, Puncture Front IL,
20 hrs after Fire

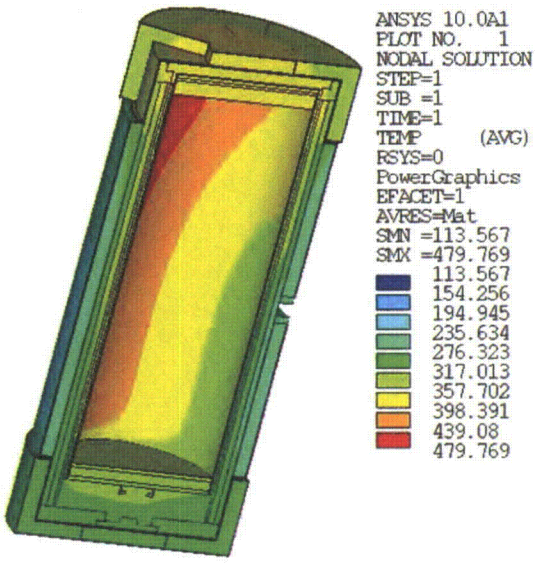


MP197HB, PWR 26 kW, CD, Front IL Punctured

Figure A.3–44
Temperature Profiles for MP197HB Transport Cask
HAC, 24PTH DSC, 26 kW, without External Fins

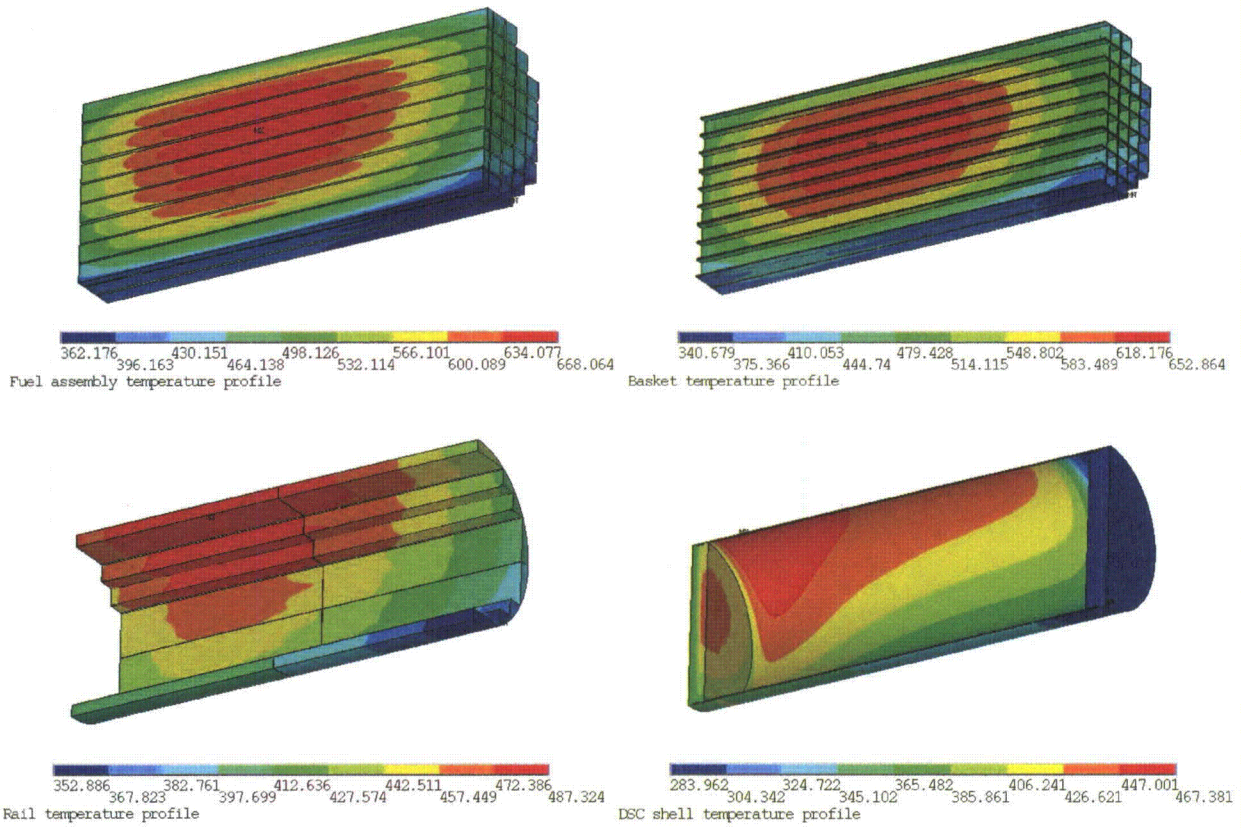


Figure A.3–45
Typical Temperature Distributions for 69BTH DSC
(HAC Post Fire Cool-Down, HLZC#1, 26kW)

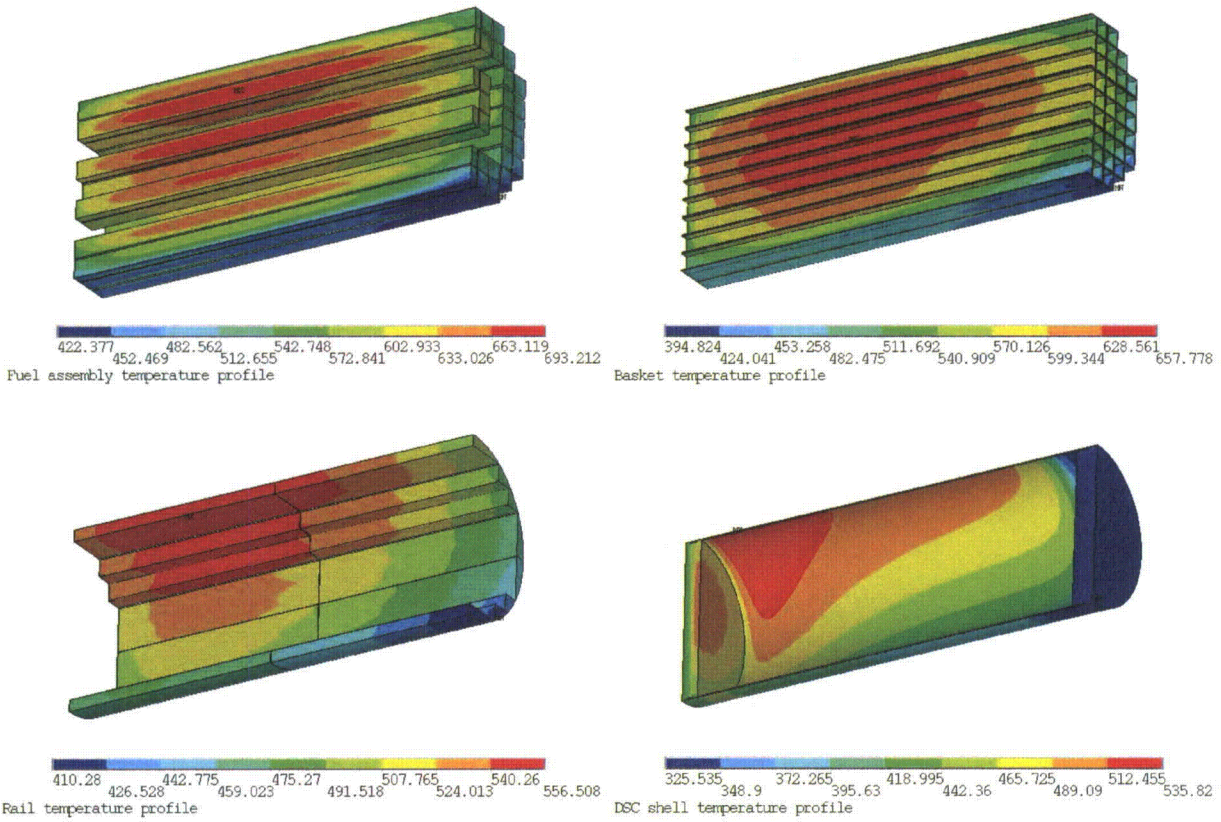


Figure A.3–46
Typical Temperature Distributions for 69BTH DSC
(HAC Post Fire Cool-Down, HLZC#4, 32kW)

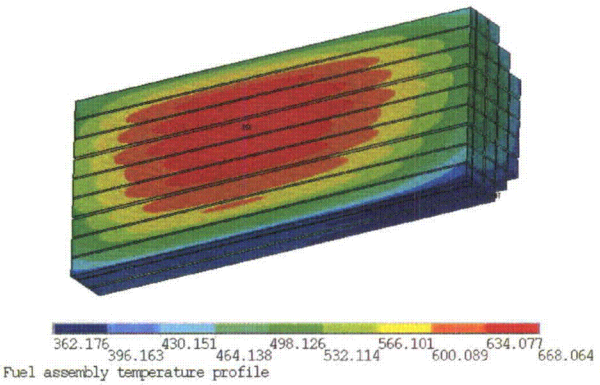


69BTH, HLZC#1, 26kW

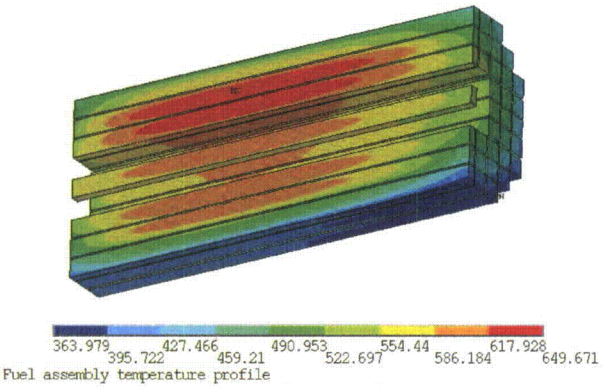


69BTH, HLZC#2, 26kW

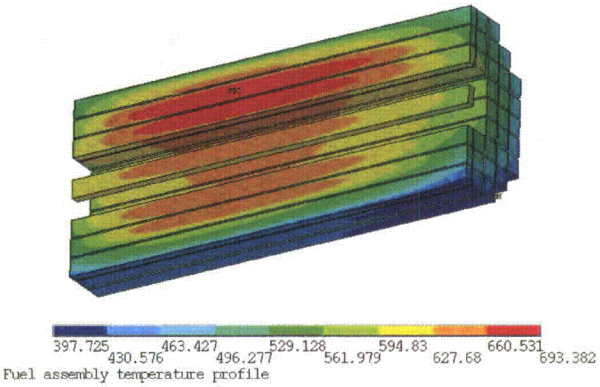


69BTH, HLZC#3, 29.2kW

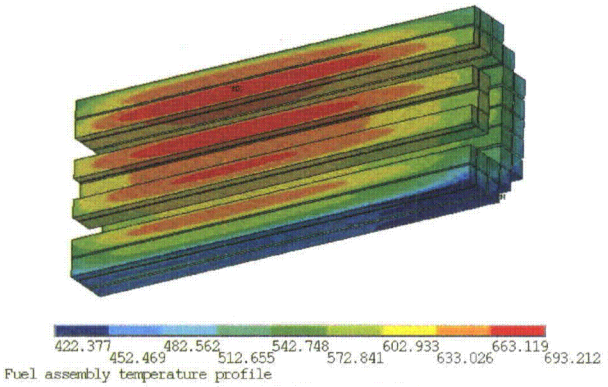


69BTH, HLZC#4, 32kW

Figure A.3–47
Temperature Distributions for Fuel Assemblies in 69BTH DSC
(HAC Post Fire Cool-Down)

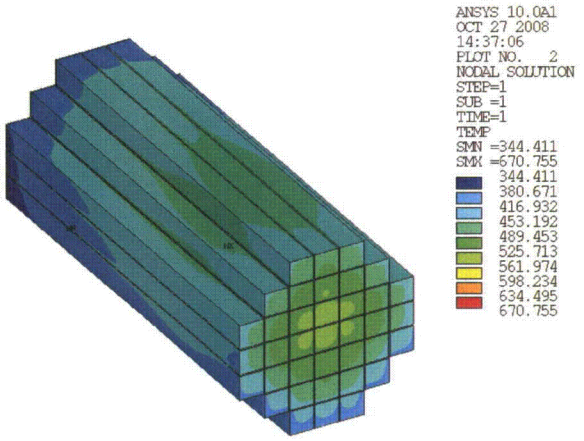


Fuel Cladding - Heat Zone Conf#8 (37PTH_22CD_B Load No. 1)

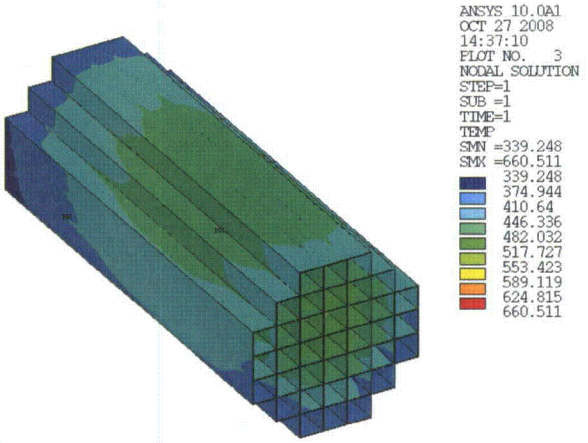


Fuel Comp - Heat Zone Conf#8 (37PTH_22CD_B Load No. 1)

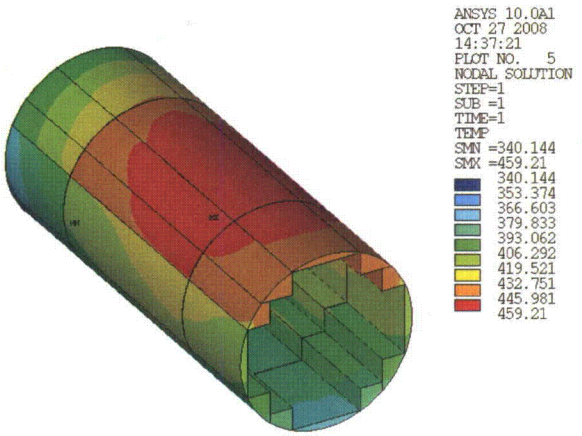


Rails - Heat Zone Conf#8 (37PTH_22CD_B Load No. 1)

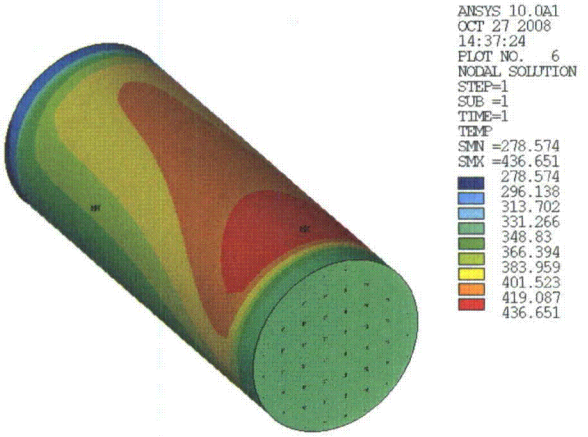


DSC Shell - Heat Zone Conf#8 (37PTH_22CD_B Load No. 1)

Figure A.3–48
Typical Temperature Distributions for 37PTH DSC
(HAC Post Fire Cool-Down, 22 kW, Boral Plates)

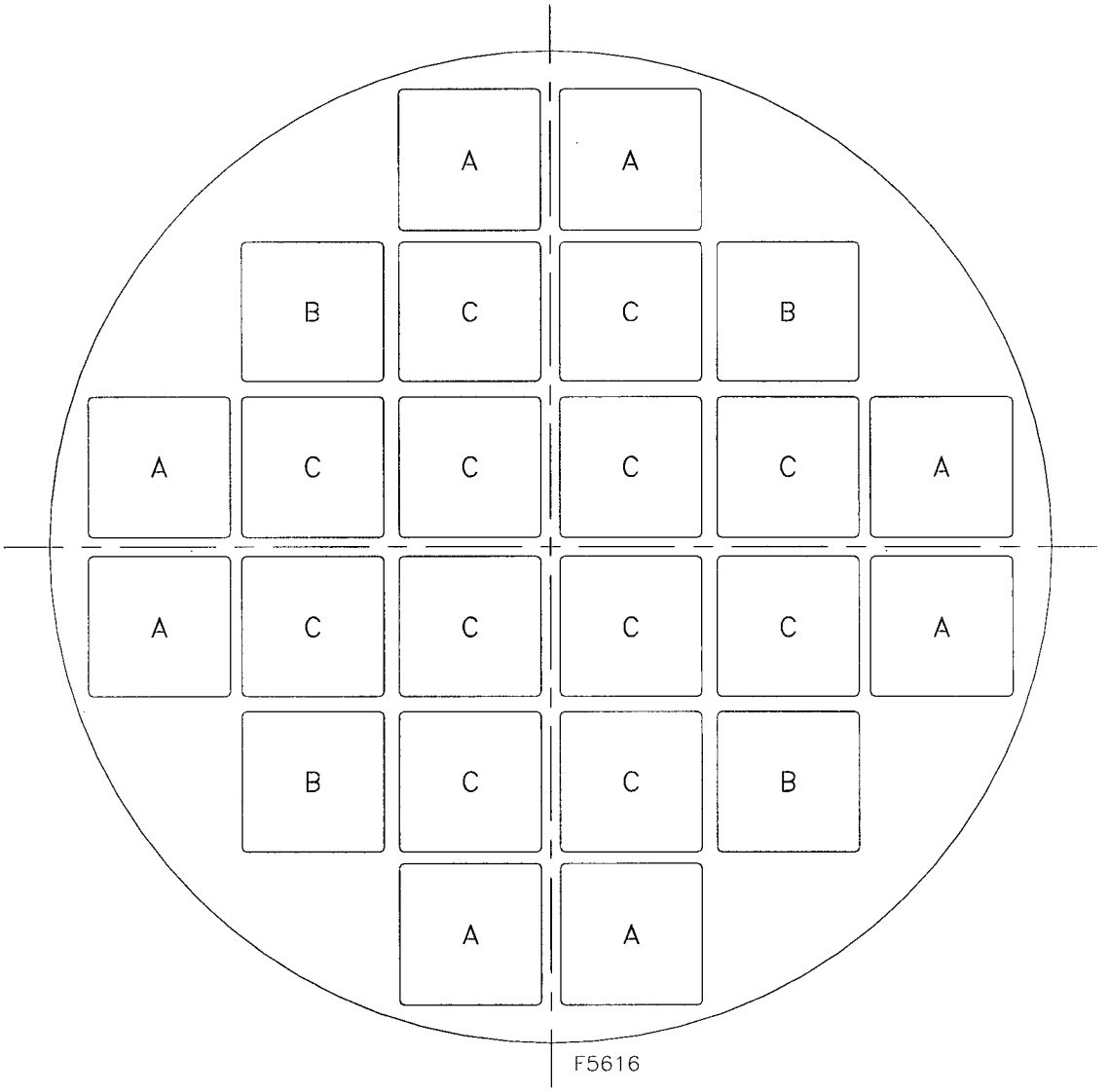


Notes:

1. Locations identified as "A" are for placement of up to 8 damaged or failed fuel assemblies (balance intact).
2. Locations identified as "B" are for placement of up to 4 additional damaged fuel assemblies (Maximum of 12 damaged fuel assemblies allowed, Locations "A" and "B" combined) (balance intact).
3. Locations identified as "C" are for placement of up to 12 intact fuel assemblies, including 4 empty slots in the center as shown in Chapter A.1, Appendix A.1.4.3, Figure A.1.4.3-2.

Figure A.3–49
Location of Damaged/Failed Fuel inside 24PTHF DSC

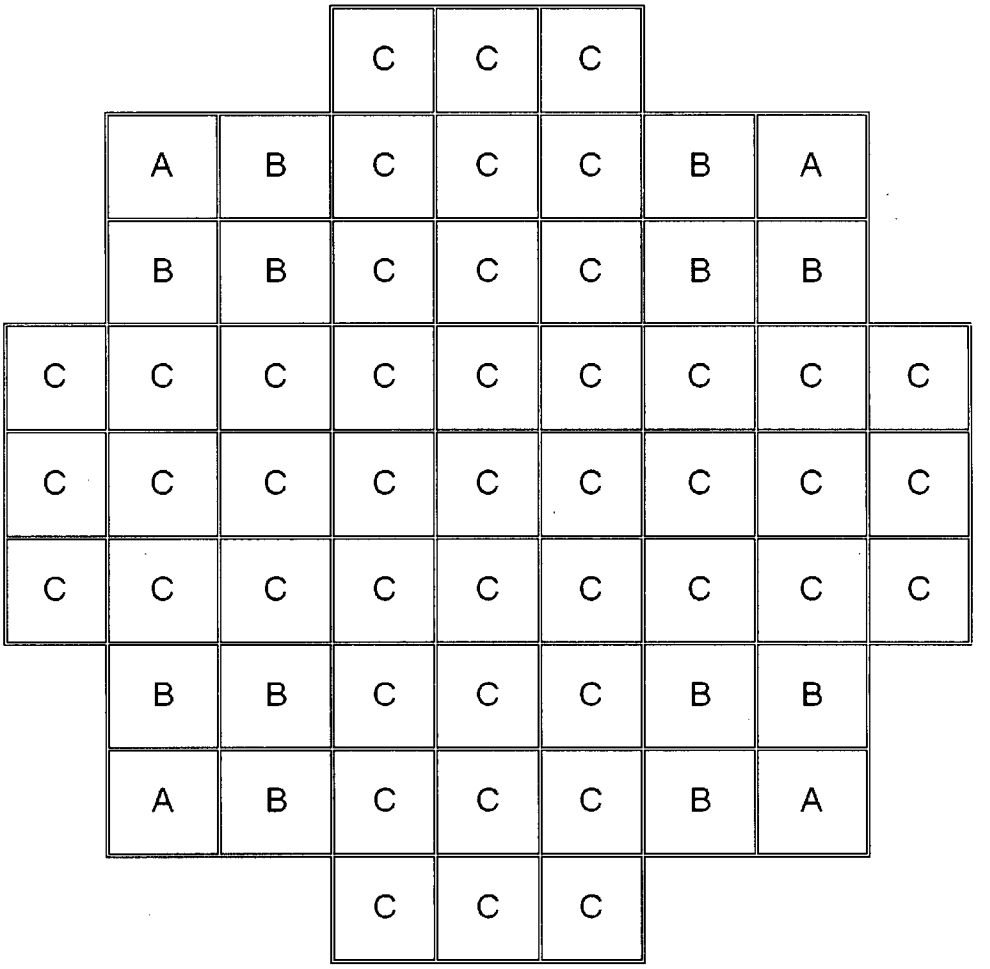


Notes:

1. Corner locations identified as "A" are for placement of up to 4 failed or damaged fuel assemblies with balance intact.
2. Locations identified as "B" are for placement of up to 12 additional damaged fuel assemblies (Maximum of 16 damaged fuel assemblies allowed in locations "A" and "B" combined with balance intact)
3. Locations identified as "C" are only for placement of additional 45 intact fuel assemblies.

Figure A.3–50
Location of Damaged/Failed Fuel inside 61BTHF DSC

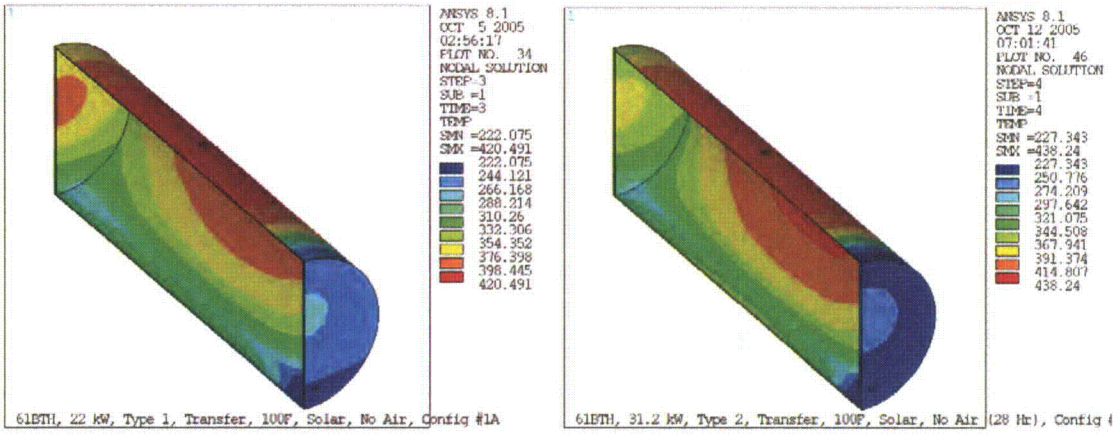


Transfer Conditions
61BTH Type 1, 22.0 kW, 100°F

Transfer Conditions
61BTH Type 2, 31.2 kW, 100°F

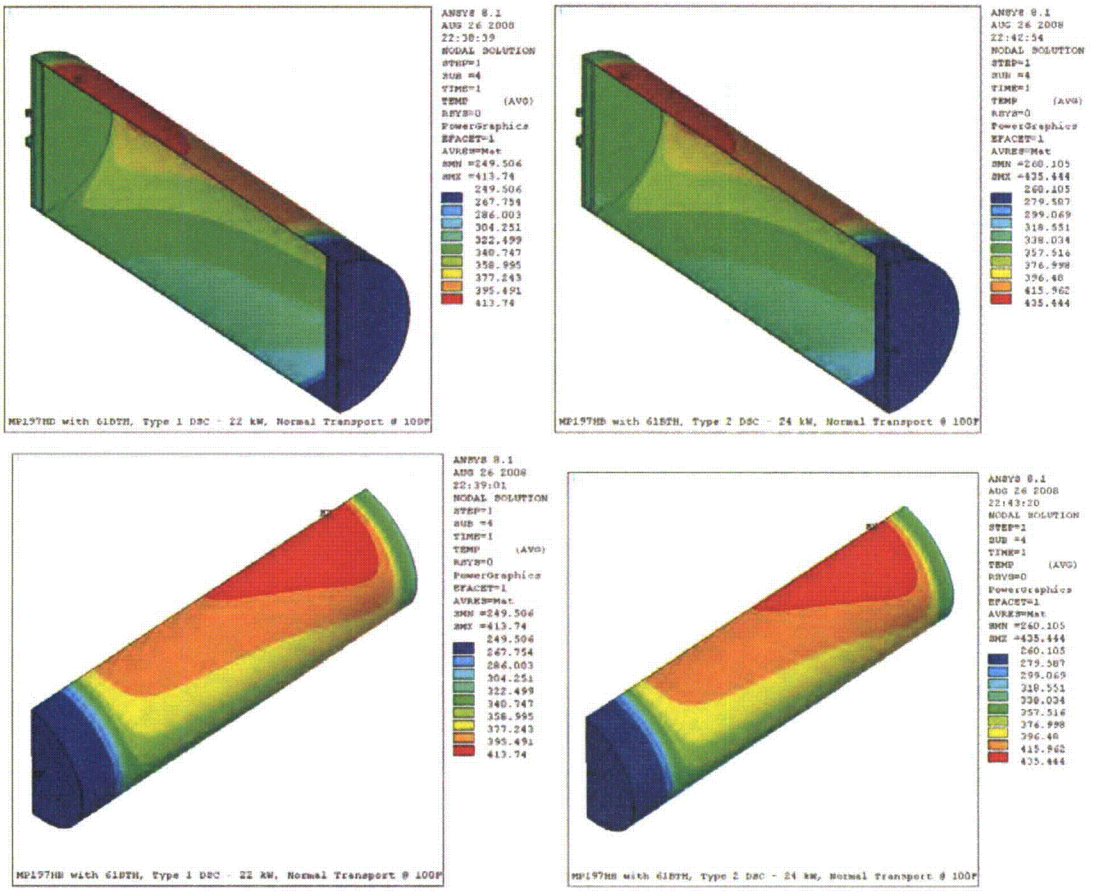


NCT, 61BTH Type 1, 22.0 kW, 100°F

NCT, 61BTH Type 2, 24.0 kW, 100°F

Figure A.3–51
Comparison of DSC Shell Temperature Profiles for 61BTH DSC

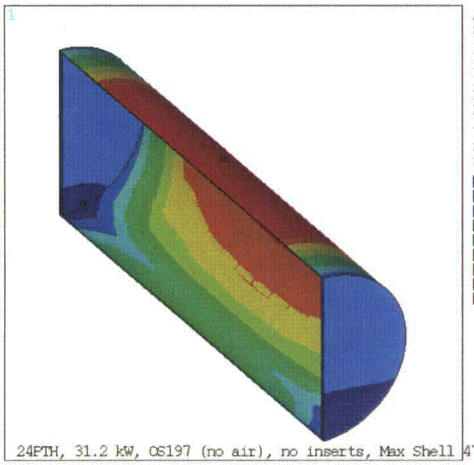


Transfer Conditions
24PTH-S or -L (w/o Al inserts), 31.2 kW, 100°F

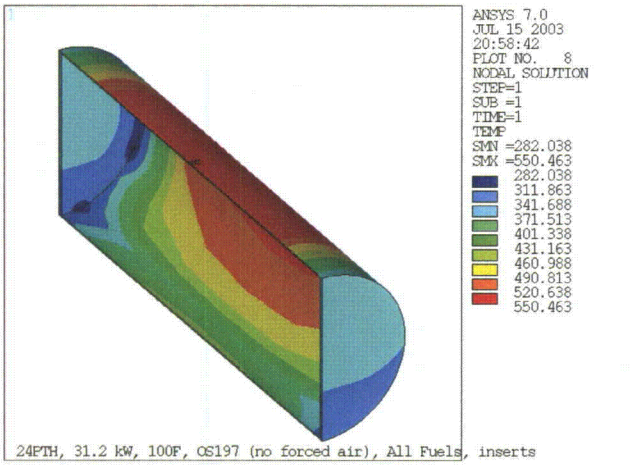


Transfer Conditions
24PTH-S or -L (w/ Al inserts), 31.2 kW, 100°F

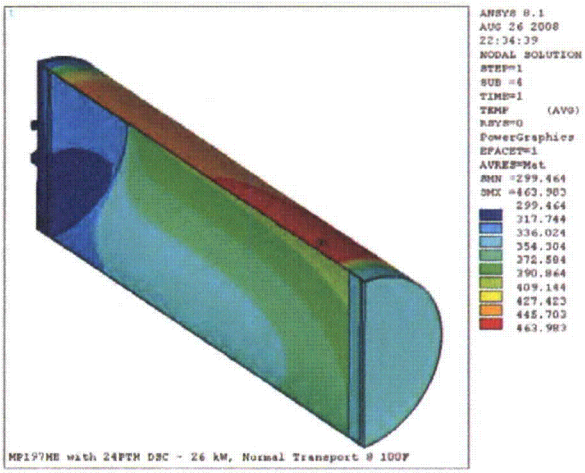


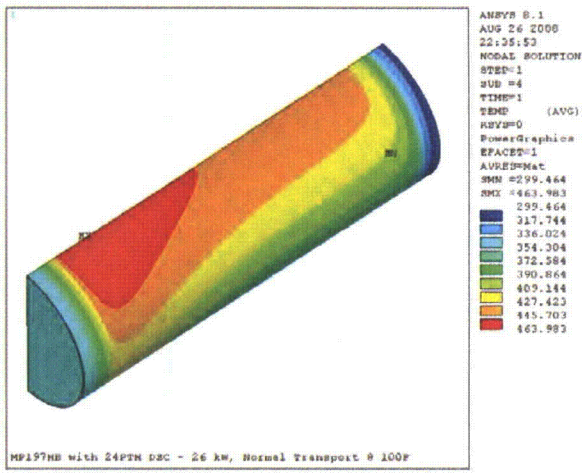


NCT, 24PTH, 26.0 kW, 100°F

Figure A.3–52
Comparison of DSC Shell Temperature Profiles for 24PTH DSC

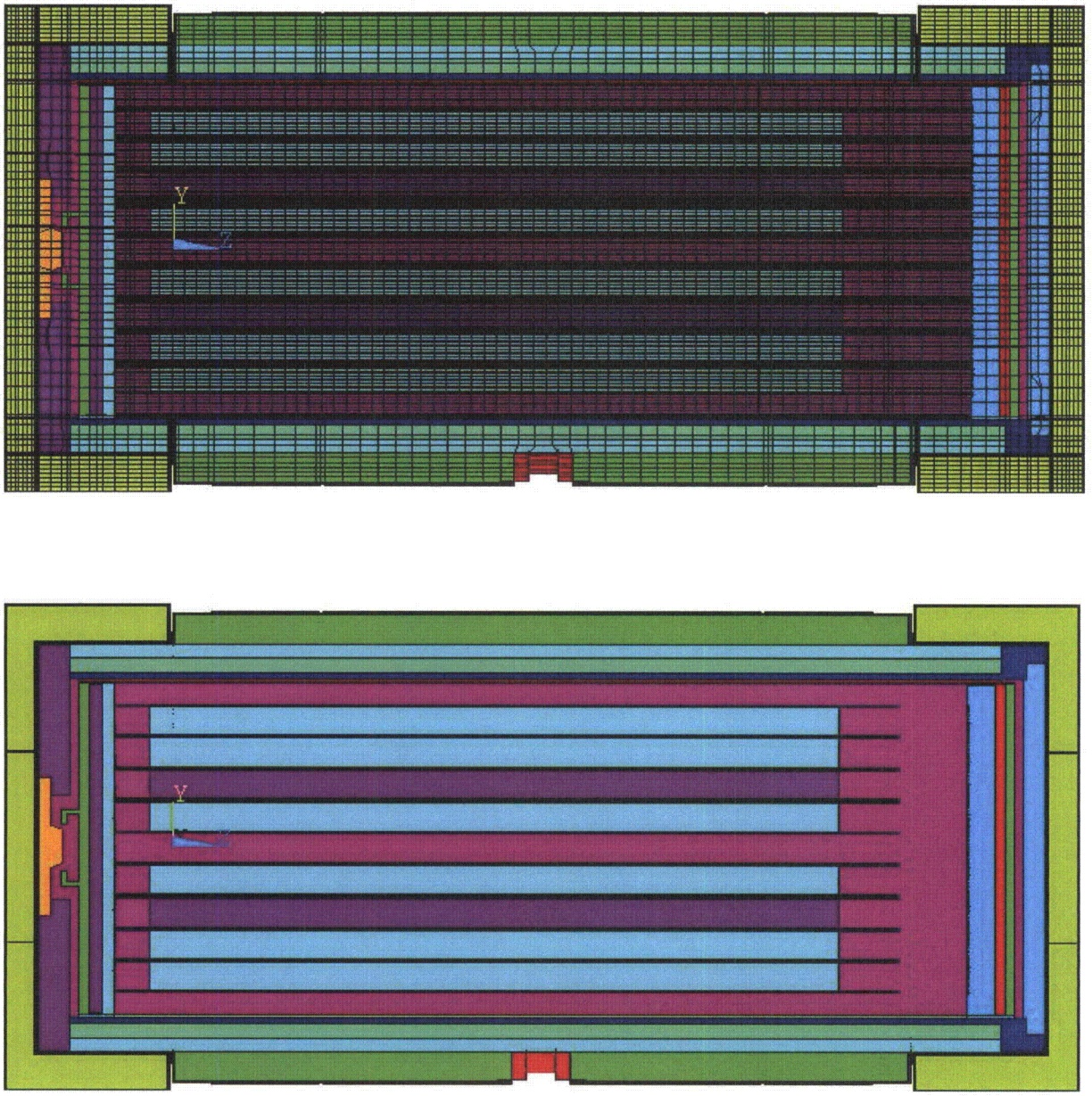

*Figure A.3-53*
*Coupled Model of MP197HB TC and 69BTH DSC*

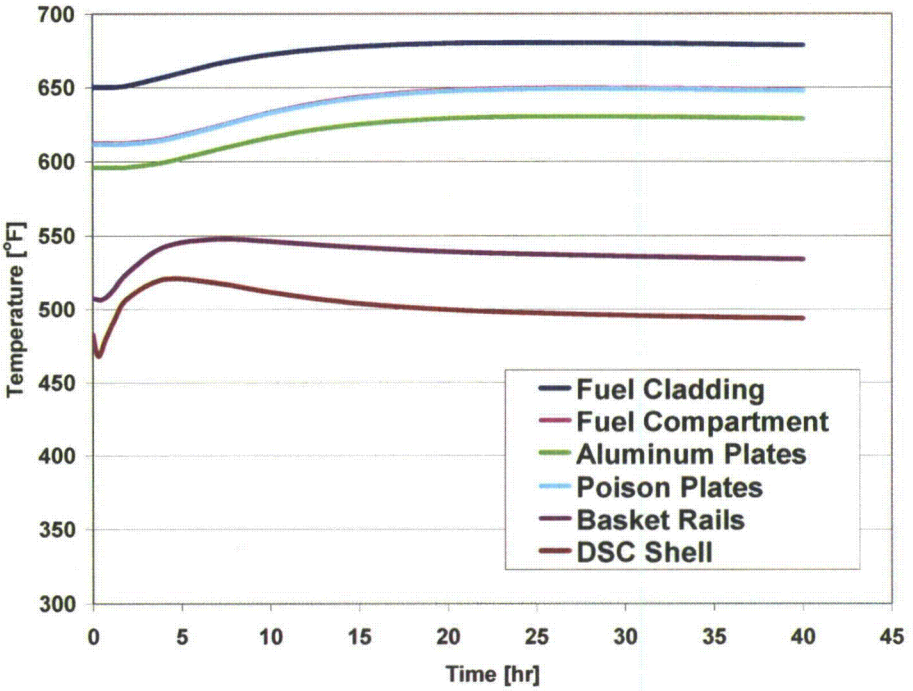


*Figure A.3-54*
*Temperature Time Histories for Coupled Model, 69BTH DSC Components*

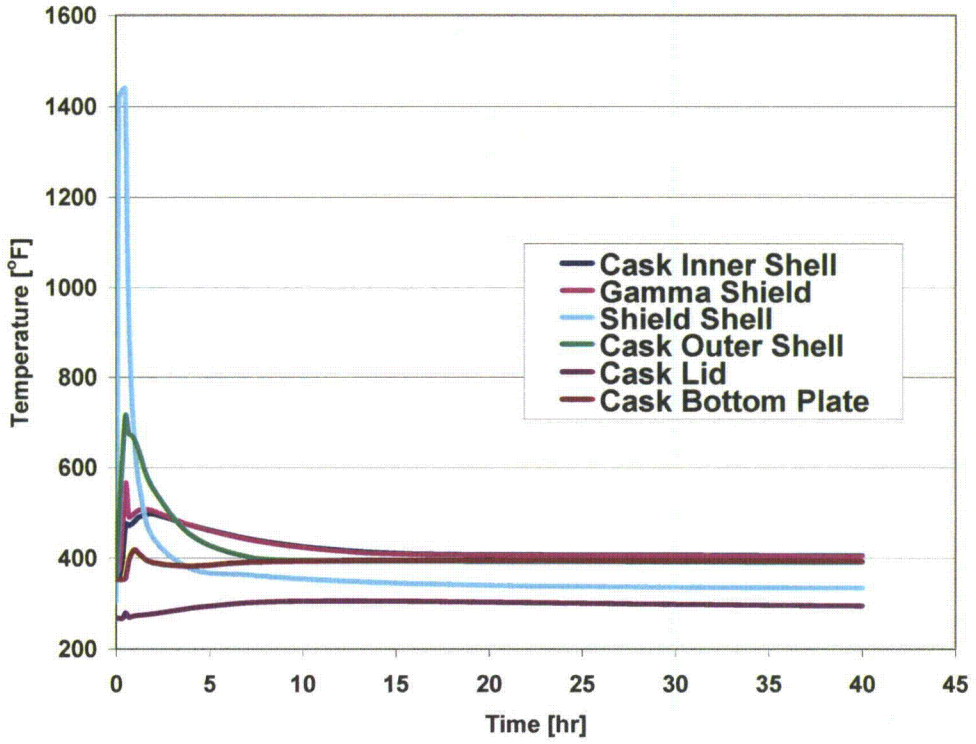


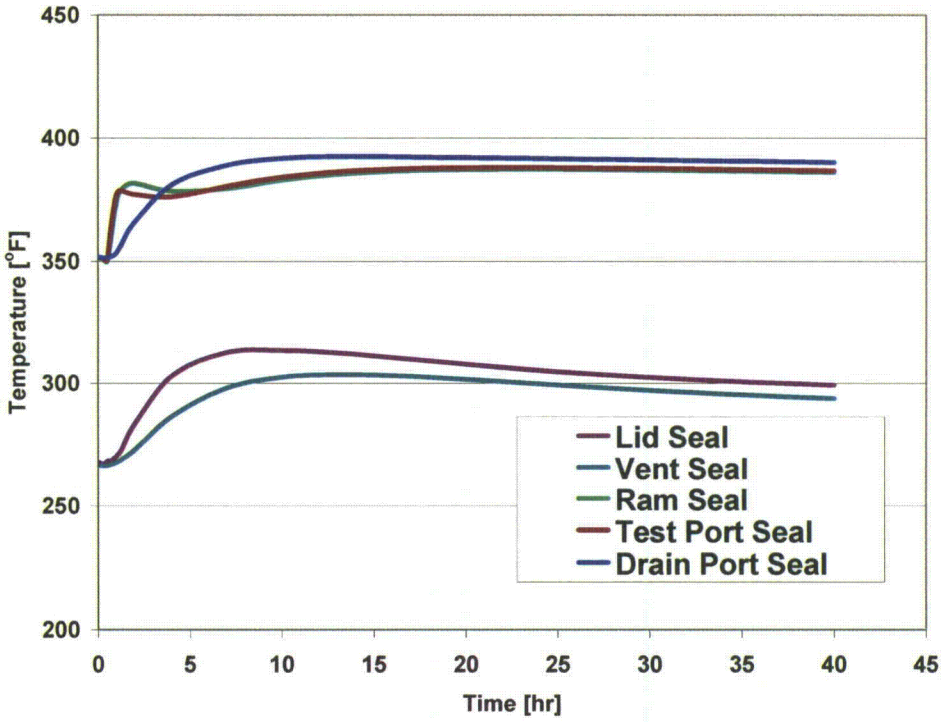


*Figure A.3-55*
*Temperature Time Histories for Coupled Model, MP197HB TC Components*